Université catholique de Louvain
Secteur des Sciences de la Santé
Louvain Drug Research Institute

Lipid nanocapsules as a delivery platform to tackle colorectal cancer microenvironment

Thibaut Fourniols

Thèse présentée en vue de l'obtention du grade
de docteur en Sciences biomédicales et pharmaceutiques

2020

Director: Professor Véronique Préat

REMERCIEMENTS

Ma thèse fut un long chemin de plus de quatre ans, parsemé de multiples rencontres. Sans ces interactions et les coopérations qui en découlèrent, ma volonté n'aurait sans doute pas été capable de venir au bout de ce travail, et la qualité globale en aurait été très affectée. Un tout grand merci à tous. Merci...

Tout d'abord au Pr Véronique Préat pour avoir supervisé de près mon travail, sans jamais céder face aux résultats décourageants. Sa grande disponibilité, son calme et son pragmatisme ont accompagné avec une grande bienveillance mon parcours en gardant toujours l'objectif de thèse en tête. Merci de m'avoir laissé une grande liberté pour poursuivre mes idées de collaborations ou d'expériences.

Au Dr Fabienne Danhier, pour m'avoir accompagné la première moitié de ma thèse, avec énergie et amitié.

Au Dr Diego Arago, qui m'a supervisé durant mon séjour au Vall d'Hebron, puis pour avoir co-dirigé l'étude sur le JQ1. Cela m'a permis de découvrir d'autres méthodes de travail et de management. Merci également aux autres membres de l'équipe à Barcelone : Agueda pour son professionnalisme et son humour, Jose Higinio, Lee Jin, Priscilla, Estefania, Rocio, et Valentina. J'ai beaucoup profité de mon séjour à l'étranger et me suis senti tout de suite accueilli.

Au Pr Anne des Rieux qui, sans tutelle officielle, a grandement participé à encadrer de nombreuses expériences, à me donner de multiples conseils, à discuter librement durant et hors les repas. Sa franchise et son professionnalisme m'ont beaucoup aidé.

Aux autres membres de mon comité d'accompagnement, pour avoir fait de chacun de mes comités un moment scientifique précieux qui me permettait ensuite de fixer un cap plus clair sur la suite, tout en conservant une atmosphère très agréable : au Pr Pierre Sonveaux pour ses questions périlleuses et sa jovialité, au Pr Olivier Feron pour ses questions profondes et sa collaboration sur les sphéroïdes, et au Pr Nathalie Delzenne pour sa gentillesse et ses questions de côté bien utile.

Aux membres extérieurs de mon jury de thèse, les Pr Frédéric Lagarce et Jay Prakash, pour avoir accepté de juger mon travail et avoir pris le temps de le discuter en profondeur durant la défense privée. Au Pr Olivier De Wever, pour sa collaboration qui a sauvé ma thèse en lui fournissant un modèle solide de CAFs, pour ses conseils associés, pour avoir rejoint mon comité d'accompagnement et m'avoir accueilli dans son laboratoire plusieurs fois.

À toute l'unité ADDB. À la fantastique équipe de techniciens dont chaque doctorant aimerait les avoir pour lui tout seul tellement ils sont précieux, avec en particulier Bernard, râleur et dont la franchise et l'honnêteté font tellement de bien, et Kevin, jongleur multitâche infatigable et (presque) toujours de bonne humeur. À Murielle Callier, la secrétaire la plus investie et mystérieuse jamais rencontrée.

À tous ces moments de camaraderie durant ces 4 années avec les doctorants et docteurs. À mes collègues plus expérimentés, dont j'ai de nombreuses fois sollicité l'assistance et qui m'ont inspiré: Alessandra, Chiara, Dario, et Valentina. À Nikos, mon frère de thèse qui a réussi plus rapidement, sa folie et sa joie remplissaient de vie les plus mornes bureaux. À mes collègues que j'ai pu à mon tour aider et qui m'ont fait ressentir mon utilité et mes compétences : en particuliers Yasmine et Aristote, ainsi que mes stagiaires Juliette et Ariana. À Elia, Mathilde, Ariane, et tous les autres !

À Nicolas Dauguet et Caroline Bouzin, dont l'expertise, la gentillesse et le sens du service rendent accessible à tous les techniques les plus pointues de cytométrie et d'histologie. À Estelle Bastien pour la grosse collaboration réussie avec ses sphéroides et tous les moments où je la cherchais désespérément à travers FATH.

À Luc, cet ami unique toujours intéressé par mes sujets de discussion, toujours motivé pour les activités les plus décalées, dont chaque rencontre me fait réfléchir profondément, dont chaque bière St-Thibaluc brassée laissera plus de souvenirs loufoques que gustatifs. Pour ton soutien indéfectible et le temps passé à me coacher, je te salue très bas.

À mes colocataires du Kot-à-côte puis du koté jardin, pour m'avoir rendu bien belge, pour avoir constitué des familles d'adoption, pour tous les projets réalisés ensemble qui m'ont transformé autant que la thèse en me faisant gagner en organisation, en leadership, en résolution de conflit, en cuisine pour famille nombreuse, et pour continuer à me faire croire en la vie communautaire. À Pierre-Olivier en particulier pour l'amitié construite au-delà. Plus largement aux fraternités du bon pasteur dont le lieu de vie idéal a pu m'accueillir trois années. Ce sera sans doute le plus difficile à quitter de Belgique.

À la Bees Coop et à EDIW, les 2 associations dans lesquelles je me suis engagées avec beaucoup d'énergie et de plaisir, dont les résultats rapides compensaient l'attente laborieuse de la thèse. Elles m'ont apportées tant de belles rencontres.

À ma famille, mes parents qui malgré la distance n'ont pas cessé d'être là lorsque j'avais un problème, et qui continuent de me laisser libre d'accomplir mes rêves. À Alexia, pour être venue plusieurs fois me rendre visite, pour oser me contredire avec franchise, pour son engagement complètement différent et sans doute complémentaire.

Enfin, à la plus belle rencontre de ma thèse, Irene, qui a su si vite devenir indispensable dans ma vie, qui m'a rempli d'énergie positive depuis trois ans, dont la patience envers moi n'a été égalée que par ma capacité à étendre le temps de thèse. Les sacrifices que tu as consentis te seront rendus avec intérêt mon amour.

ABBREVIATIONS

(LNC-)ACF	:	Acriflavine(-loaded LNCs)
APC	:	Adenomatous polyposis coli
ATRA	:	All-trans retinoic acid
BCA	:	Bicinchoninic acid
BET(i)	:	Bromodomain and extraterminal domain (protein inhibitor)
BMP	:	Bone morphogenetic protein
BRD	:	Bromodomain-containing protein
CAF	:	Cancer-associated fibroblast
CapeOX	:	Combination of capecitabine + oxaliplatin
CAR-T	:	Chimeric antigen receptor T
CBQCA	:	3-(4-Carboxybenzoyl)quinoline-2-carboxaldehyde
CCL	:	C-C motif ligand
CIMP	:	CpG island methylator phenotype
CIN	:	Chromosomal instability
CM	:	Conditioned medium
CMS	:	Consensus molecular subtype
CPP	:	Cell-penetrating peptide
CRC	:	Colorectal cancer
CTL(A-4)	:	Cytotoxic T lymphocytes (antigen-4)
CXCL	:	C-X-C motif ligand
CXCR	:	C-X-C motif receptor
DC	:	Dendritic cell
DiR	:	1,1'-Dioctadecyl-3,3,3',3'-tetramethylindotricarbocyanine iodide
DLS	:	Dynamic light scattering
DMEM	:	Dulbecco/Vogt modified Eagle's minimal essential medium
DMSO	:	Dimethylsulfoxide
DOX	:	Doxorubicin
(DS)PE	:	(1,2-distearoyl-sn-glycero-3-)phosphoethanolamine
EC_{50}	:	Concentration corresponding to 50% of the maximal effect
ECM	:	Extracellular matrix
EGF(R)	:	Epidermal growth factor (receptor)
EMT	:	Epithelial-to-mesenchymal transition
EPR	:	Enhanced permeation and retention

ERK	:	Extracellular signal-regulated kinase
Fab	:	Fragment antigen-binding
FACS	:	Flow cytometry, fluorescence activated cell sorting
FAP	:	Alpha fibroblast activation protein
(h)FGF(R)	:	(Human) Fibroblast growth factor (receptor)
FOLFOX	:	Combination of 5-FU/LV + oxaliplatin
FOLFIRI	:	Combination of 5-FU/LV + irinotecan
FRET	:	Förster resonance energy transfer
5-FU	:	5-Fluorouracil
FSP1 (S100A4)	:	Fibroblast specific protein
HA	:	Hyaluronic acid
HDAC	:	Histone deacetylase
HGF	:	Hepatocyte growth factor
HIF	:	Hypoxia-inducible factor
His-tag	:	Polyhistidine-tag
HPLC	:	High-performance liquid chromatography
IC_{50}	:	Concentration inducing a half complete inhibition
ICI	:	Immune checkpoint inhibitor
IFP	:	Interstitial fluid pressure
IFNγ	:	Interferon gamma
IGF	:	Insulin-like growth factor
IL	:	Interleukine
i.p.	:	Intraperitoneal or intraperitoneally
IRI	:	Irinotecan
i.v.	:	Intravenous or intravenously
LNC	:	Lipid nanocapsule
LNP	:	Lipidic nanoparticle
LV	:	Leucovorin
MDSC	:	Myeloid derived suppressor cell
MHC	:	Major histocompatibility complex (= HLA)
miRNA or miR-x	:	Micro-RNA x
MMP	:	Matrix metalloproteinase
MMR	:	Mismatch repair
MRT	:	Mean residence time

MSC	:	Mesenchymal stem (stromal) cell
MSS	:	Microsatellite stability
MSI	:	Microsatellite instability
NIF	:	Normal inactivated fibroblast
NK	:	Natural killer lymphocytes
(L)NP	:	(Lipidic) nanoparticle
NTA	:	Nitrilotriacetic acid
PD-(L)1	:	Programmed cell death protein (ligand)-1
PDAC	:	Pancreatic ductal adenocarcinoma
PDGF(R)	:	Platelet-derived growth factor (receptor)
PDPN	:	Podoplanin
PEG	:	Poly(ethylene glycol)
PFA	:	Para-formaldehyde
P-gp	:	P-glycoprotein
PI	:	Propidium iodide
PI3K	:	Phosphoinositide 3-kinase
PIT	:	Phase inversion temperature
PK	:	Pharmacokinetic
PLGA	:	Poly(lactic-co-glycolic acid)
PM	:	Polymeric micelle
pNP	:	Para-nitrophenylcarbonyl
PSC	:	Pancreatic stellate cell
(nab-)PTX	:	(Albumin-bound) Paclitaxel
RGD	:	Arginine-glycine-aspartate peptide
ROS	:	Reactive oxygen species
RTK	:	Receptor tyrosine kinase
s.c.	:	Subcutaneous or subcutaneously
scFv	:	Single-chain variable fragment
SCNA	:	Somatic copy number alteration
SEC	:	Size-exclusion chromatography
sHDL	:	Synthetic high-density lipoprotein–like
SHH	:	Sonic hedgehog
SLN	:	Solid lipid nanoparticle
SMA	:	Alpha smooth muscle actin

TAM	:	Tumor-associated macrophage
TEM	:	Transmission electron microscopy
TGFβ(R)	:	Transforming growth factor β (receptor)
Th	:	T helper lymphocytes
TIL	:	Tumor-infiltrated lymphocytes
TNC	:	Tenascin C
TNF	:	Tumor necrosis factor
TNM	:	Tumor, node, metastasis classification
TRAIL	:	TNF-related apoptosis-inducing ligand
VEGF(R)	:	Vascular endothelial growth factor (receptor)
WB	:	Western Blot
WT	:	Wild type

CHAPTER I
INTRODUCTION

Partly adapted from:

Nanotechnology is an important strategy for combinational innovative chemo-immunotherapies against colorectal cancer, Ana I. Matos, Barbara Carreira, Carina Peres, Liane I.F. Moura, João Conniot, Thibaut Fourniols, Anna Scomparin, Águeda Martinez-Barriocanal, Diego Arango, João P. Conde, Véronique Préat, Ronit Satchi-Fainaro, Helena H. Florindo, *Journal of Controlled Release* 307, 108–138 (2019).

TABLE OF CONTENTS

I. CLINICAL CLASSIFICATION AND STANDARD THERAPY OF COLORECTAL CANCER

Colorectal cancer (CRC) is a high-impact disease at the world level. It was ranked in 2018 as the third most frequent cancer with almost 1.8 million new cases, and the second-most killer with around 880,000 deaths[1]. Males have been more at risk than females with a cumulative life incidence risk of 2.7 vs 1.8%, respectively. CRC world distribution reflects socio-economic development, with a 3-fold higher incidence rate in transitioned versus transitioning countries. Developing countries have encountered a parallel growth of CRC incidence and mortality, whereas CRC lethality in developed countries has been decreasing. The main individual risk factors include a diet rich in red or processed meat, alcohol consumption, high body fatness, and low physical activity[1].

I.1. THE TNM CLASSIFICATION

In the current clinical practice, medical care is based on the tumor, node, and metastasis (TNM) classification of CRC[2] (Table 1 and Figure 1). The "T" factor describes the tumor localization, depending on the tissues invaded by the tumor: T1) submucosa, T2) the muscularis propria, T3) beyond the muscularis propria, into the outermost layers of the colon or rectum, and T4) growth through the colorectal wall.

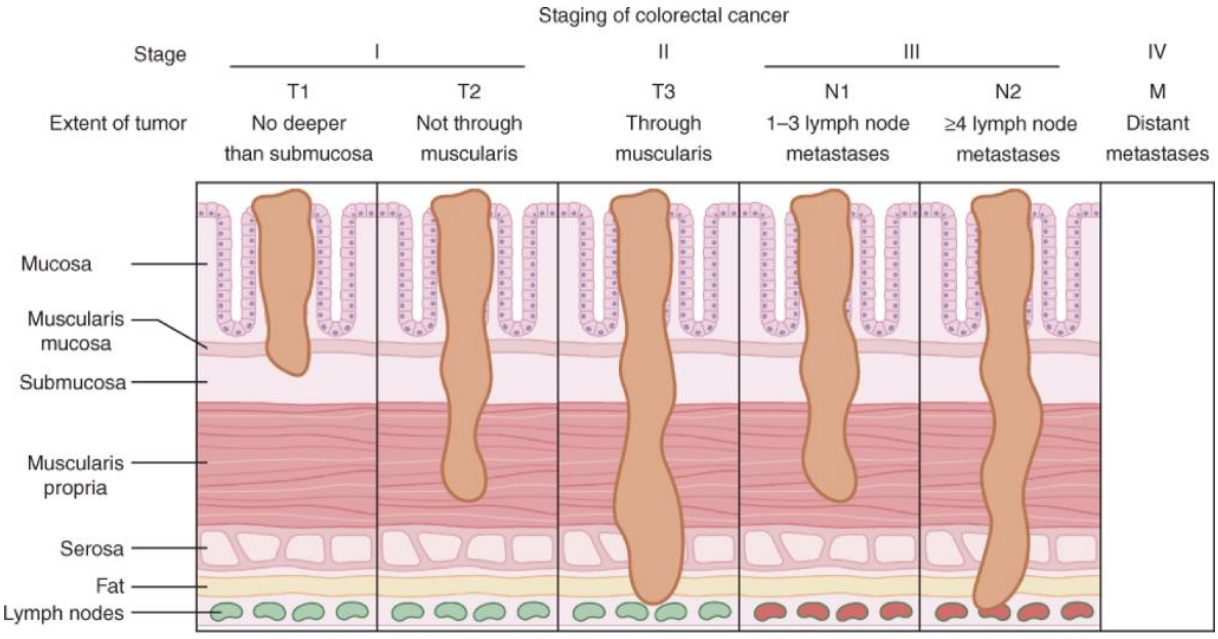

Figure 1. The TNM classification of CRC. Reproduced[3]

The "N" factor is related to the nearby lymph node invasion: N1c) growth into areas of fat near the lymph nodes but not the nodes themselves, N1a or b) spread to 1 to 3 nearby lymph node, and N2) spread to more than 3 nearby lymph nodes. Finally, the "M" factor describes the presence of metastasis in distant organs: M1a) spread to 1 distant organ, most often the liver or the lung, M1b) spread to more than 1 distant organ, and M1c) spread to distant parts of the peritoneum.

Table 1. Summary of CRC stages. Adapted[3–5]

Stage	Definition	5-year relative survival rate	Adjuvant therapy to surgery
Stage 0: Tis, N0, M0	Carcinoma in situ, tumor limited to the colon epithelium	-	Observation
Stage I: T1/T2, N0, M0	Into the submucosa (T1) or muscularis propria (T2)	92%	Observation
Stage II: T3/T4, N0, M0	Outermost layers of the colon (T3), or beyond the wall (T4) and potential reached nearby tissues or organs	63%-87%	Observation OR Capecitabine or 5FU/LV OR FOLFOX or CapeOX
Stage III: T1-T4, N1/N2, M0	Spread to lymph node	53-89%	FOLFOX or CapeOX
Stage IV: T1-T4, N0-N4, M1	Spread to distant organs: liver, lung, peritoneum,…	10-15%	Cf Table 4

FOLFOX: combination of 5-FU/LV + oxaliplatin; CapeOX: capecitabine + oxaliplatin.

The CRC stage, determined from the TNM status, is directly associated to the disease advancement, prognostic, and therapy regimen (Table 1). A global 5-year relative survival rate of 65% is associated with CRC, but stage IV survival is dramatically reduced to 14%[6].

I.2. CONSENSUS MOLECULAR CLASSIFICATION OF CRC

A global classification of CRC called the consensus molecular subtype (CMS) classification has been proposed in 2015, establishing four molecular subtypes from transcriptomic data of thousands of human tumor samples[7]. The advantage of this classification based on the whole tumor gene expression is that it gathered genetic alterations, microenvironment characteristics, and the driving oncogenic pathways (Table 2). The most important molecular features of CRC are described below. In repartition, canonical CMS2 is the most frequent subtype with 37% of whole CRC, then mesenchymal CMS4 presents a frequency of 23%, immune CMS1 represents 14%, and metabolic CMS3 13%. Out of the 4 CMS groups, 6% of the tumors are considered as a mix of at least 2 subtypes, and 7% cannot be determined.

Table 2. Summary of consensus molecular subtypes (CMS) features. Adapted[8,9]

CRC subtype	%	Clinical and prognostic associations	Molecular features	Pathways involved	Micro-environment composition	Potential target therapy
CMS1 MSI-Immune	14	Good prognosis Poor survival after relapse Higher histo-pathological grade	MSI (76%) Hypermutation (94%) SCNA low, CIMP high Enriched BRAF-mut	RTK and MAPK pathways activation	HIGH immune INTERMEDIATE stromal	Immune checkpoint inhibitors in MSI patients
CMS2 Canonical	37	Better survival rates after relapse	MSS (99%) SCNA high, CIMP low	Wnt and MYC hyper-activation Low EMT, TGF activation, Low mesenchymal	LOW immune LOW stromal	Enhanced tumors immunogenicity, cancer vaccines, Adoptive T cells therapy, β-catenin inhibitors, Anti-macrophages
CMS3 Metabolic	13		MSI (16%) Hypermutation (28%) SCNA intermediate, CIMP intermediate Enriched KRAS-mut	Metabolic burst RTK and MAPK-activation Low VEGF/VEGFR Low EMT, TGF activation, Low mesenchymal	LOW immune LOW stromal	Enhanced tumors immunogenicity Cancer vaccines Adoptive T cells therapy Metabolism targeting
CMS4 Mesenchymal	23	Worse relapse-free and overall survival Diagnosed at more advanced stages (III & IV)	MSS (92%) SCNA high, CIMP low	Angiogenic signature (High VEGF/VEGFR) Immunosuppressive signature Inflammatory signature High EMT, TGF activation, High Mesenchymal	INTERMEDIATE immune HIGH stromal	Anti-angiogenic Anti-inflammatory Immune checkpoint inhibitors Anti-fibrotic or anti-TGFβ Anti-macrophages

CIMP: CpG island methylator phenotype; EMT: epithelial-to-mesenchymal transition; MSS: Microsatellite stability; MSI: Microsatellite instability; RTK: Receptor tyrosine kinase; SCNA: somatic copy number alterations; TGF: Transforming growth factor; VEGF: Vascular endothelial growth factor

I.2.1. Genomic alterations define different CRC diseases

Cancer, including CRC, is always due and associated to genetic alterations. Three molecular features have been considered as major oncogenic drivers in CRC: (i) mutations in DNA mismatch repair (MMR) genes, leading to a DNA microsatellite instability (MSI) phenotype, (ii) mutations in adenomatous polyposis coli (*APC*) and other genes that activate Wnt pathway, characterized by chromosomal instability (CIN) with a high rate of somatic copy number alterations (SCNAs) phenotype, and (iii) global genome hypermethylation, resulting in switch off of tumor suppressor genes, indicated as CpG island methylator phenotype (CIMP)[10]. CMS1 gathers most of MSI phenotypes and CIMP high, whereas CMS2 & 4 are associated to CIN phenotype, and CMS3 being intermediate.

The MSI phenotype is associated to 15-20% of CRCs and 75% of CMS1 tumors[11]. It is due to the MMR deficiency, a highly conserved gene family including MutL homolog 1. MMR proteins are responsible for DNA error recognition and reparation after each replication to keep genome integrity. Its inactivation leads to the accumulation of DNA errors and is characterized by a high frequency of frameshift mutations in microsatellite DNA, referred as to MSI [11]. MSI phenotype can be induced by germinal mutations in MMR genes, leading to the familial CRC Lynch syndrome, an autosomal-dominant hereditary disease, counting for 5% of all CRC. Most of the time, MSI CRC is sporadic and caused by epigenetic silencing of the MutL homolog 1 gene promoter by hypermethylation, joining the CIMP high tumors into the CMS1. Finally, some remaining sporadic cases can be characterized by multiple somatic mutations in MMR genes

In opposition to MSI, CRCs with microsatellite stability (MSS) are often into the CIN phenotype. It means mainly SCNAs, aneuploidy, and loss of heterozygosity[12]. These chromosomal abnormalities lead to tumor suppressor genes inactivation and oncogene activation.

I.2.2. Main alterations of gene and signalization pathway

This wide picture at the genome-scale must be zoomed into some gene and signalization pathways highly mutated in CRC (Figure 2). The cancer genome atlas study on 276 tumor samples has led to precise cartography of mutations that have been then associated to CMS classification: APC/Wnt pathway with 93% of alteration, common to all groups, RTK-RAS with 63%, P53 signaling with 61%, PI3K 51%, and TGFβ 39%. Wnt/β-catenin signaling pathway is a genetic alteration closely related to CRC. Wnt ligand binds to its receptors FZD and LRP5/6 and this interaction destabilizes the APC/AXIN1/CK1/GSK3β complex responsible for β-catenin phosphorylation and proteasome direction. When the Wnt pathway is activated, or the APC complex mutated, β-catenin

translocates into the nucleus, where it can associate with coactivators and promotes the transcription of target genes, including *MYC* [13]. APC alone plays additional regulation roles in cell adhesion, differentiation, migration, and apoptosis, and it could explain why it is the main mutated gene of the Wnt pathway in CRC[14].

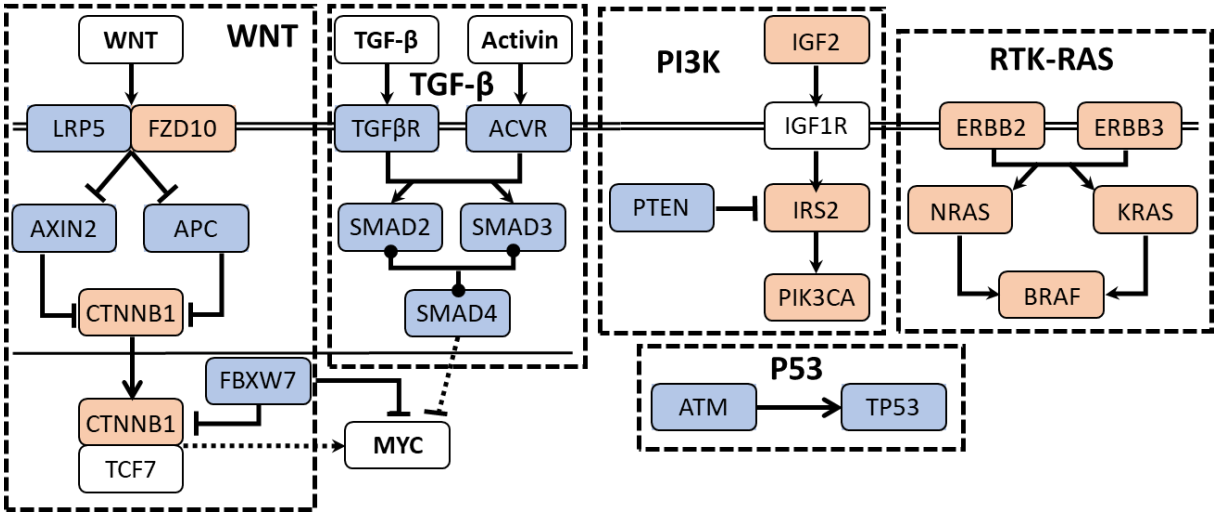

Figure 2. Main signalization pathways altered in CRC. Tumor suppressor genes are represented in blue and oncogenes in red. The double line represents the cell membrane and single line the nucleus membrane.

Another MYC related signaling pathway is the TGFβ one[15]. At the early stage, TGFβ and its receptors TGFβ-RI/II exert an antitumor role by its downstream effectors of the SMAD family. This is why the pathway is negatively altered in 39% of CRCs. SMAD are transcription factors that turn off *MYC* transcription, among many targets. But some SMAD mutations, or other mediators of the pathway, lead to a shift from an antitumor to a malignant role of TGFβ implying tumor growth, invasion and metastasis through the activation of SMAD-independent pathways like Ras-MAPK and PI3K-AKT, and a stromal compartment involvement characteristic of CMS4 tumors.

The RTK-RAS and PI3K signaling pathways are both leading to MAPKs activation, proliferation, and cell survival. Many genes from these 2 pathways present a high mutation rate, such as KRAS (from 60% in CMS3 to 20% in CMS1), BRAF (from 57% in CMS1 to <1% in CMS2), NRAS (10%), PIK3CA (15% for MSS and 37% for MSI) or can be just upregulated such as insulin-like growth factor 2 (IGF2) (22% for MSS)[16,17].

All these genetic alterations have been observed at different tumor stages and have been associate in a carcinogenesis history of CRC development from first polyps to adenocarcinoma: a loss-of-function in APC gene would be the early event at the stage of adenoma development, then a gain-of-function of KRAS oncogene may direct progression to large adenoma, and finally, loss-of-function of tumor suppressor genes like TP53 could allow the transition from large adenoma to

adenocarcinoma. A metastatic lesion can also gain additional genetic alterations. But the accumulation of gene defect is more important than the order[14,18].

I.2.3. MYC, a key oncogene in CRC molecular alterations

MYC codes for c-myc, a transcription factor involved in the control of normal cellular functions. Its expression is closely related to cell cycle activation[19]. Its downstream effectors also include glycolytic pathway and mitochondrial function, and therefore the cell metabolism[20,21]. *MYC* dysregulation leads to genome instability and multiple protumorigenic roles like uncontrolled cell proliferation, cell immortalization, metastasis, escape from immunity, or uncontrolled angiogenesis[19]. In CRC, *MYC* alteration is prompted by Wnt activation, SMAD inactivation, or also by Notch, sonic hedgehog (SHH)/GLI-1 or CEMIP-dependent pathway through ERK-1/2 signaling, making *MYC* and its target genes involved in almost 100% of CRC, with a central role in CMS2[17,19,22]. Its oncogenicity has been demonstrated by *in vitro* and *in vivo* studies where its inactivation was able to stop cancer development[23]. C-myc has also been associated with chemotherapy resistance, by genomic instability leading to DNA-damaging agent resistance, by increasing expression of ATP-binding cassette and multidrug resistance proteins, and by maintaining stemness in some cancer cells[19,24].

MYC has also been related to microenvironment changes. In a pan-cancer view, MYC-dependent cancers were considered to be related to angiogenesis and immunosuppression[25]. In CRC, MYC has been associated to hypoxia-inducible factor-1α (HIF-1α) stabilization, responsible for further angiogenesis[26]. In KRAS mutant lung cancer, MYC expression in cancer cells induced IL-23, responsible for natural killer lymphocytes (NK) and B cell suppression, and CCL-9 attracting M2 macrophages with VEGF-production associated to angiogenesis and PD-L1 production associated to T cell anergy and suppression[27]. But there is no data over MYC expression by the non-cancer cells in the tumor microenvironment (TME) in our knowledge.

Due to the evidence about c-myc potential as a therapeutic target in cancer, several strategies have been developed to inhibit its actions (Figure 3)[19]. Among them, bromodomain and extraterminal domain protein inhibition (BETi) has attracted attention to negatively regulate *MYC*[28]. BET is a family of chromatin regulator proteins, including bromodomain containing 2 (BRD2), BRD3 and BRD4. These proteins associate with acetylated chromatin and facilitate transcriptional activation. BRD4 binds to many gene enhancer regions, together with other co-activators. BRD4 inhibition reduces selectively gene expression in some super-enhancer regions, more sensitive to transcription factor concentration. This is the case of *MYC* oncogene[29]. JQ1 has been the first-in-class BETi,

and it has demonstrated *MYC* downregulation and cell proliferation inhibition at submicromolar concentrations in vitro in many CRC cell lines[30,31].

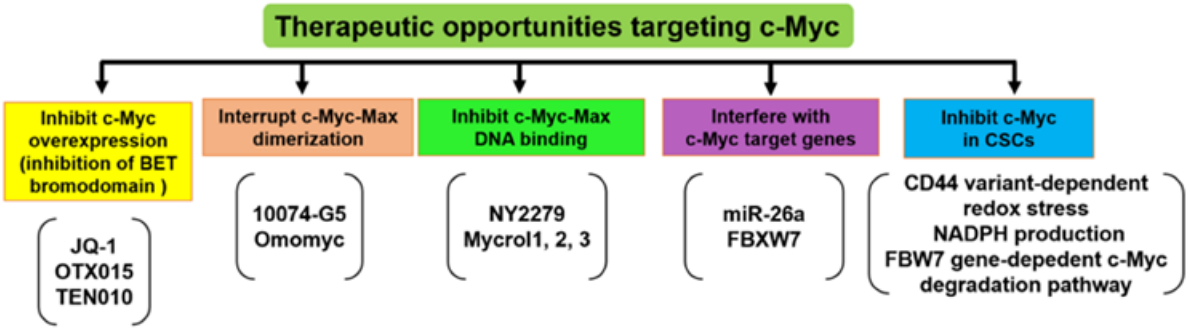

Figure 3. Strategies for targeting *MYC*. Reproduced[19]

I.3. STANDARD TREATMENT OF CRC

Localized CRC (Stage 0 to III) is treated by surgery. The surgical resection of the tumor should correspond to the lymphovascular drainage of the tumor site[32]. Adjuvant chemotherapy, following resection, is advised in high-risk stage II and in all stage III CRC, to treat micro-metastasis risk and prevent a recurrence. Despite the recognized advances in the screening methods, surgical procedures, and chemotherapeutic treatments currently available, 30% of CRC patients, and approximately 20% from the time of the first diagnosis (synchronous metastasis), are diagnosed with the metastatic disease[33]. These patients with metastatic CRC present a median survival time lower than 8 months in the absence of treatment.

Chemotherapy has been the best therapeutic ally of surgery for high-grade CRC. It can be administered before or after surgical resection in the neoadjuvant or adjuvant setting therapy, respectively. The most active cytotoxic drugs to control tumor growth and to improve the life expectancy of CRC patients include 5-fluorouracil (5-FU), irinotecan (IRI), oxaliplatin, and capecitabine[5].

5-FU has been the first approved chemotherapy for CRC and the only one until 1996[34]. It is metabolized in 5-fluorodeoxy-uridine monophosphate, a suicide substrate of the thymidylate synthase, essential for pyrimidine DNA bases synthesis. Its action is potentiated by leucovorin (LV), a reduced form of folate which acts after metabolization as a co-enzyme of the thymidylate synthase[35]. 5-FU also inhibits RNA synthesis by ending RNA elongation under its triphosphate form. Administered as an intravenous (i.v.) bolus, 5-FU has excellent diffusion and acts in rapidly growing tissues like tumors. Capecitabine, a 5-FU prodrug, is bioavailable by oral administration and has shown better tolerability for the same antitumor efficacy than 5-FU/LV[36].

Oxaliplatin, the most used platinum derivative, is an alkylating agent creating mostly intra-strand DNA crosslinking, leading to cytotoxicity. In CRC, it is used in combination with infusional 5-FU/LV in the FOLFOX regimen or with Capecitabine in the CapeOX regimen, as the first-line therapy for stage III. The FOLFOX regimen can overcome resistance to 5-FU[37].

IRI is a derivative of natural camptothecin, an inhibitor of the topoisomerase I. It is metabolized by the liver in the active form SN38. It is administered by slow i.v. infusion. FOLFIRI combination associates IRI to infusional 5-FU/LV, and is the standard of care like FOLFOX since 2000 for mCRC[38].

Multiple clinical trials have tested all combinations between these 4 drugs, leading to current evidence-based protocols (Table 3). Unresectable metachronous metastasis, defined as a metastasis occurrence after a period of three months postoperatively, has benefited from detailed guidelines (Table 4). The details of standard-of-care regimens are available on cancertherapyadvisor.com[39].

Most of the described genetic mutations have prognostic and therapeutic consequences. Anti-EGFR antibodies, mainly cetuximab and panitumumab, have been approved to inhibit the RTK-RAS pathway. They are used in combination with chemotherapy, including in the mCRC first-line. In the case of the downstream activation of the pathway by positive mutation of one *RAS* or *BRAF*, the tumor becomes insensitive to EGFR inhibitors. CRC tumors with at least one mutation among KRAS, NRAS, BRAF or PIK3CA have demonstrated a reduced efficacy to FOLFIRI plus cetuximab or FOLFOX plus panitumumab[40]. These mutations are normally screened in routine and anti-RTK antibodies are limited to the wild-type tumors. Also, the specific V600E mutation on BRAF, accounting for over 90% of BRAF total mutation, is an indication of vemurafenib inhibitor use in primary treatment[5].

Table 3. Summary of current CRC chemotherapy with key clinical trial data. Adapted[41]

Cytotoxic drug(s)	Biological effect	Ref.
5-FU adjuvant therapy	Improved OS rate of patients within stage III or high-risk stage II disease.	42
High / low-dose 5-FU / LV	Enhanced 5-FU cytotoxicity, RR (18.8–48 vs. 10–12%), and OS (11.7–12 vs. 7.7–10.5 months) for mCRC patients using high/ low-dose 5-FU/LV, when compared to 5-FU alone.	35,43–46
Capecitabine	Similar efficacy to 5-FU/LV in mCRC, less myelosuppression, and stomatitis.	36,47
IFL regimen (IRI plus i.v. bolus 5-FU/LV)	Improved RR (35–49 vs. 22–31%), PFS (7 vs. 4.3 months) and OS (14.8–17.4 vs. 12.6–14.1 months) in mCRC patients compared to 5-FU/LV alone.	48,49
FOLFIRI (IRI plus infusional 5-FU/LV)	Offered as second-line chemotherapy for patients with a good status and organ function; improved PFS and OS.	50,51
FOLFOX or CapeOX	Decrease of several chemotherapy-derived side effects (diarrhea, nausea, vomiting, dehydration) and improved OS (19.5 vs. 15 months), TTP (8.7 vs. 6.9 months), and RR (45 vs. 31%) compared to IFL regimen. Improved PFS (9 vs. 6.2 months) and RR (50.7 vs. 22.3%) compared with 5-FU/LV or oxaliplatin	52,53
FOLFIRI & FOLFOX	Similar efficacy in terms of RR (31 vs. 34%), OS (14 vs. 15 months), and TTP (7 months). Similar efficacy of FOLFIRI followed by FOLFOX vs. FOLFOX followed by FOLFIRI in terms of RR (56% vs. 54%), OS (21.5 vs. 20.6 months) and PFS (8.6 vs. 8 months).	54,55
FOLFOXIRI	2 phase III trials showed increased toxicities. Greater RR (60 or 43 vs. 34%), PFS (9.8 or 8.4 vs. 6.9 months), and OS (23 or 22 vs. 17 or 20 months) for mCRC patients treated with FOLFOXIRI compared to the FOLFIRI regimen. One trial concluded to non-significative superiority, while the other, with increased dose, concluded to significant superiority	56,57

RR: response rate; OS: overall survival; PFS: progression-free survival; TTP: time to progression

Table 4. Treatment of unresectable metachronous CRC metastasis in function of the protocol applied to the primary tumor. Adapted from the National Comprehensive Cancer Network® guidelines[5]

Previous treatment of the primary tumor	Treatment of the unresectable metachronous metastasis	Conversion to resectable
Adjuvant FOLFOX/CapeOX within past 12 months	Standard: FOLFIRI or IRI ± bevacizumab (preferred) or ziv-aflibercept or ramucirumab	Yes: resection followed by systemic therapy ± biologic therapy
	KRAS/NRAS-wt gene: FOLFIRI or IRI ± cetuximab or panitumumab	
	dMMR/MSI-H: nivolumab or pembrolizumab	
	BRAF V600E mutation: IRI + vemurafenib ± cetuximab or panitumumab	No: Systemic therapy
Adjuvant FOLFOX/CapeOX >12 months	Systemic therapy	
5-FU/LV or capecitabine	Systemic therapy	
No previous chemotherapy	Systemic therapy	

II. CURRENT CHALLENGES OF COLORECTAL CANCER MICROENVIRONMENT

Even if tumor cells have attracted the main focus of cancer investigation and understanding, the TME is now considered as a critical element in tumor survival, progression, and metastatic process[58]. In most of the solid tumors, the TME constitutes the majority of cells and tumor mass. According to Paget's theory described in 1889, cancer cells are like seeds that would need appropriate soil to grow and survive in primary and metastatic niches[59]. TME includes many cancer-associated cellular actors, such as endothelial cells, fibroblasts, lymphoid or myeloid immune cells, mesenchymal stem/stromal cells (MSCs), pericytes, adipocytes, and other organized structures such as blood vessels, extracellular matrix (ECM), lymphatics vessels and nodes.

TME is a complex network of interactions with no obvious functional classification. The present description of CRC TME will be divided into three compartments, associated to specific cell types, tumor impact, relations to the whole TME, and targeted therapies: the vascular compartment, the immune compartment, and the stromal compartment. The CMS classification of CRC is directly related to the TME organization. CMS1 is associated to a high immune compartment, whereas CMS4 is characterized by a high proportion of the stromal, vascular, and immune compartments together. CMS2 and CMS3 are characterized by poor infiltration[8,9].

II.1. VASCULAR COMPARTMENT

The tumor growth is accompanied by the development of a new vasculature, which presents many differences with normal vascularization. At some point in the tumor development, when cells begin to suffer from hypoxia and starvation due to the remoteness of blood vessels, an angiogenic switch occurs[60]. The main actors of the vascular TME are endothelial cells and pericytes, forming two layers around the blood vessels lumen. Endothelial cells play a key role in the development and function of blood and lymph vessels. Pericytes are cells of mesenchymal origin that provide important support for blood vessel formation and function. Lymphangiogenesis also occurs in and around tumors, comparably with blood vasculature[61].

At a molecular level, the neoangiogenesis process is initiated by hypoxic conditions promoting the maintenance of O_2-regulated HIF-1α in cancer cells[62,63]. HIF-1α translocates into the cell nucleus, and act as a heterodimer with HIF-1β to promote transcription of hundreds of target genes. The angiogenic balance is then switched on by the production of numerous growth factors like the vascular endothelial growth factor (VEGF) family with mainly VEGF-A, fibroblast growth factor

(FGF), hepatocyte growth factor (HGF), platelet-derived growth factor (PDGF), and epidermal growth factor (EGF)[60,62]. These factors attract endothelial cells and pericytes.

Continuous growth factors presence leads to the fast development of new blood vessels sprouting from pre-existing neighboring vessels. Infiltrated new vessels are in the tumor core as the invasive margin, and differ from normal vasculature. New tumor vessels are often disorganized, tortuous, and dysfunctional, without the normal hierarchical branching pattern of arteries, veins, and capillaries[61]. It creates a chaotic vascular network, with heterogeneous distribution of the nutrients and oxygen, unable to stop hypoxia signaling. Tumor-associated endothelial cells change their phenotype compared to normal endothelial cells. In CRC, it has been shown that endothelial cells over-activated HIF-1, PI3K/AKT, and epithelial-to-mesenchymal transition (EMT) signaling pathways[64]. In addition, pericyte coverage may be too high or too low, which creates together with leaky cell-adhesion a hyperpermeability phenotype allowing passage of cancer cells, promoting metastasis[62,65,66].

Antitumor therapy resistance is also induced by angiogenesis. The heterogeneous vascularization leads to heterogeneous drug diffusion. Besides, the leaky vasculature increases the interstitial fluid pressure (IFP) and leads to impaired perfusion, reducing drug diffusion into tissues[67]. On the contrary, a high pericyte coverage of well-constituted vessels shields tumors from circulating therapies. The hypoxia signaling pathway also leads to tumor resistance. HIF-1α/TGFβ2/GLI2 pathway has been described to increase CRC stemness and dedifferentiation, giving intrinsic resistance to chemotherapy, while HIF-1α/micro-RNA-338 (miR-338)-5p/IL-6 feedback loop has reduced antitumor effect of several chemotherapies[68,69].

Antiangiogenic therapies have been the first class of drug targeting the TME instead of the cancer cells. A clinical trial brought the demonstration in mCRC of anti-VEGF-A antibody bevacizumab efficacy in association with FOLFIRI[70,71]. Approved anti-angiogenic include bevacizumab, anti-VEGFR-2 ramucirumab, anti-EGFR cetuximab and panitumumab as EGF signaling is pro-angiogenic, multi-kinase inhibitor regorafenib, and VEGF receptor fusion protein aflibercept[72]. These therapies exhibit a more complex mechanism of action than predicted by their design (Figure 4). At high dose or in prolonged treatment, a vessel depletion is achieved, hypoxia increases and adverse reactions occur, such as metastasis promotion, stroma and tumor cell mechanisms of resistance, or alternative pro-angiogenic signaling. After a quick tumor growth shrinkage, a higher incidence of relapses and deaths has been observed in adjuvant bevacizumab treated mCRC patients by the AVANT trial[72]. Therefore, anti-VEGFRs are used with limited time and doses to not stop completely tumor angiogenesis but to induce a selective pruning of immature vessels[73].

This vasculature normalization, with decreased vessel diameter, density, and permeability, has been described to prevent metastasis, increase oxygenation, decrease tumor growth, and optimize Starling forces to decrease IFP to help deliver cancer cell-directed therapies[66,67]. Vasculature normalization is not stable and constituted a short therapeutic window for combining therapies. The angiogenesis inhibitors have not been associated to specific efficacy depending on CMS classification, and robust biomarkers to predict their efficacy are still lacking[61].

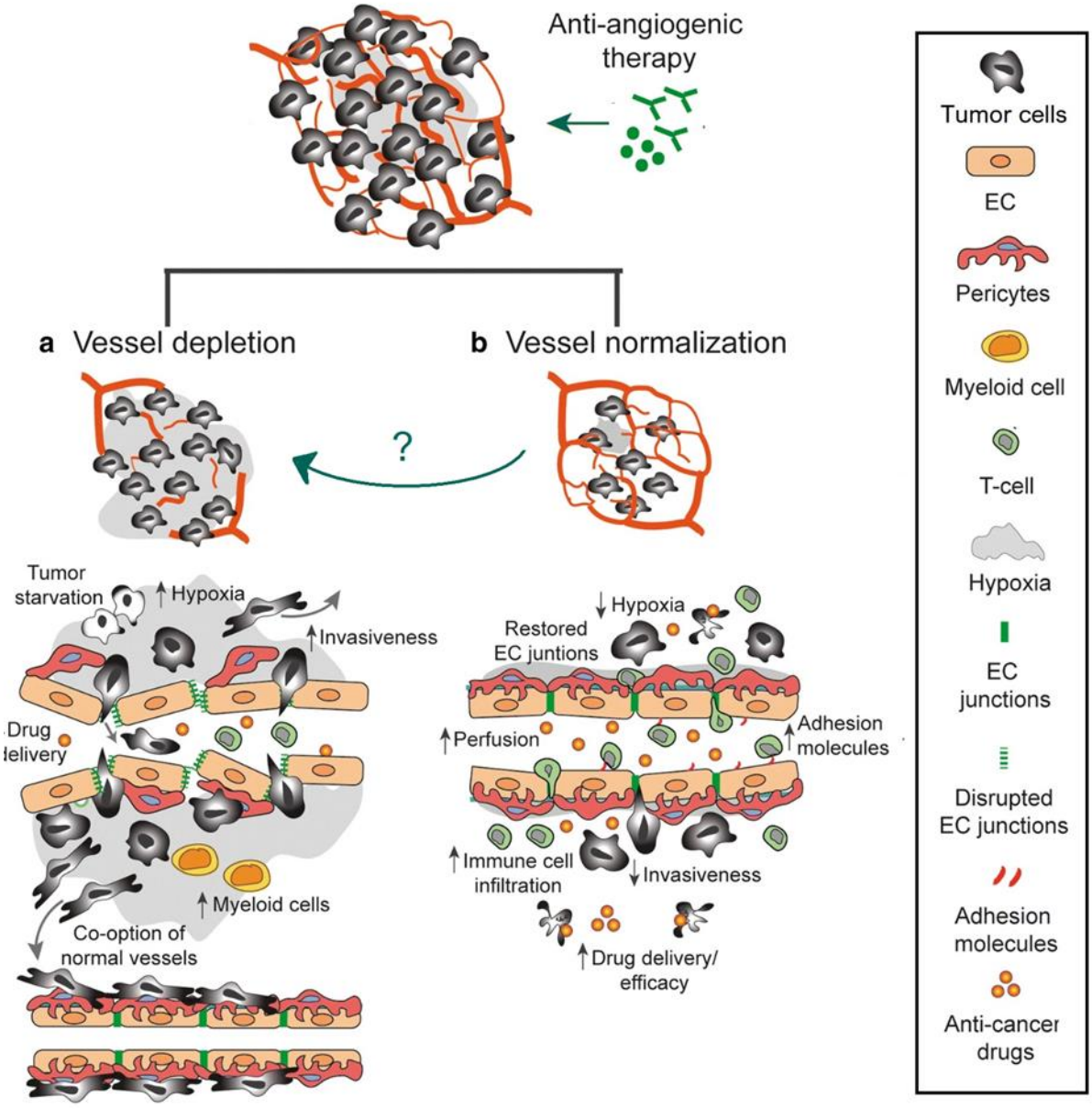

Figure 4. Effects of anti-angiogenic therapy. Angiogenesis inhibitors can induce two vascularization phenotypes. **a)** vessel depletion; **b)** vessel normalization. Adapted[72].

II.2. IMMUNE COMPARTMENT

II.2.1. Immuno-editing, the evolution of immune TME over cancer progression

The immune compartment importance has been discovered since the 1950s with the concept of immune surveillance[74]. Immunoediting is the central theory describing the tumor-immunity interaction and also its evolution along with cancer progress[74]. All along with human life, multiple genetic mutations in somatic cells occur, creating precursors of cancer cells. Initial cancer cells are characterized by tumor antigens presentation through the major histocompatibility complex class I (MHC-I) and the expression of Fas and tumor necrosis factor (TNF)-related apoptosis-inducing ligand (TRAIL) receptors. Most of them will be spotted and eliminated by cytotoxic T lymphocytes (CTL) and NK, supported by T helper (Th) lymphocytes. This is the elimination phase. The selective pressure on cancer cells will promote escape mechanisms such as downregulation of the antigen processing and presentation by cancer cells, expression of non-canonical MHC molecule HLA-G, and expression of proteins such as disintegrin or ADAM10 to cleave presented antigens. These phenomenons lead to the cancer equilibrium phase, where some cancer clones survive and coexist with the host activated immune system, without systemic symptoms. At this step, the adaptative immune system gets the main role, with cytotoxic and memory tumor-infiltrating lymphocytes that sustain tumor dormancy. After a long time with an occult tumor, the expansion of immune-invisible selected tumor clones, an increased inflammation, and the massive infiltration of myeloid cells lead to the escape phase. The tumor growth attains the cancer disease stage. At this stage, the immune environment switches to immunosuppression. Immunosuppressive cells become the majority. Myeloid-derived suppressor cells (MDSCs), M2 tumor-associated macrophages (TAM), N2 tumor-associated neutrophils, regulatory T lymphocytes (Treg), regulatory B lymphocytes, and dendritic cells drive the apoptosis or the anergy of CTLs and other immunoreactive cells. The immunoediting process evolves also by a cytokine equilibrium going progressively from interferon gamma (IFNγ) / TNFα at the elimination phase, IL-23 / IL-12 at the equilibrium phase and TGFβ / IL-10 at the escape phase, for the main cytokines. A list of all immune cells with their function and prognostic impact on CRC is listed in Table 5. The diversity of cell populations reflects the complexity of the immune TME.

Table 5. Key immune players of the CRC TME and their major roles. Green and red backgrounds indicate anti-tumor and protumor impacts, respectively. Adapted[41]

Cell type	Role within the TME	Ref
Cytotoxic T lymphocyte	CD8+ **CTL** promotes the apoptotic death of recognized target cells, by releasing cytotoxins, such as perforins and granzyme B, or through the engagement of the Fas/Fas-ligand, which activate different pathways leading to apoptosis and target cell death. CTL also employs nonlytic effector mechanisms including the production of IFNγ, a cytokine with several direct and indirect anti-tumor properties. A high density of CTL in the CRC TME, measured by the immunoscore, predicts better patient survival.	75,76
T helper cell	**CD4+ T cells** act as helper cells and modulate the activation of CTL. Depending on the amount and type of cytokines present in the environment, Th cells may differentiate into four main classes: Th1, Th2, Th17, and regulatory T cells.	77,78
	Th1 cells' response is associated with the anti-tumor activity through the IFNγ secretion and the recruitment and activation of TAMs. IFNγ can also remarkably induce the IL-12 production by mature dendritic cells, which, in turn, triggers the polarization of more naïve T cells into the Th1 phenotype, contributing to their own growth and maintenance. CRC patients displaying high levels of Th1-associated gene expression in tumor tissues have a better prognosis.	
	Th2 cells favor tumor growth and may be the predominant subpopulation among the infiltrating lymphocytes of some tumors. The Th2-type cytokines in the CRC microenvironment have no prognostic significance for patient survival. **Th17** cells' role in the TME is controversial since they can either promote or prevent cancer cell growth and metastasis. However, a poor prognosis has been reported for CRC patients with high expression of the Th17 cluster. **Treg cells** suppress the activation, proliferation, and effector functions of a wide range of immune cells, including CD4+ and CD8+ T cells, NK, B cells, and antigen-presenting cells. Treg can regulate the immune response by different mechanisms: i) secretion of immunosuppressive molecules, as IL-10, and TGFβ; ii) cytolytic functions via a variety of mediators like granzyme B, TRAIL pathway and galectin-1; iii) IL-2 deprivation-mediated apoptosis of effector CD4+ T cells. Treg prevents effector T cells activation through the inhibition of co-stimulatory molecules or suppression of dendritic cell maturation via IL-10/TGFβ signaling. The accumulation of Treg at TME has also been associated with faster angiogenesis.	
γδ T cell	**γδ T cells** do not bind to the antigens presented by the MHC. They are capable of directly killing tumor cells and performing indirect anti-tumor functions through the secretion of IFNγ. However, their production of IL-17 is associated with pro-tumor functions. The prognosis associated with their tumor infiltration is debated for colorectal cancer.	79–81
B cell	**B cells** were shown to promote anti-tumor T cell-mediated immune responses, but also presented a highly cytotoxic activity mediated by the immunoglobulin G2b. B and plasma cell infiltration correlates with the patient's clinical course and appears to have a beneficial prognostic impact.	82–84
	Regulatory B cells are a newly designated subset of B cells, identified both in murine and human tumor samples. B regulatory cells have been shown to promote tumor progression by attenuating the anti-tumor immunity via the suppression of the T cell immune response through the secretion of anti-inflammatory mediators, such as IL-10, TGFβ, and IL-35, and by facilitating the generation of Treg.	

Natural killer lymphocytes	**NKs** have cytotoxic functions and shape a proinflammatory microenvironment. NKs can recognize the altered expression of tumor cell surface ligands through the activation of specific receptors. Moreover, the downregulation or lack of MHC-I molecules on tumor cell surfaces promotes NK activation and induces their cytotoxic activity through granzyme B- and perforin-mediated apoptosis, Fas-ligand-associated apoptosis or via TRAIL. Recently, NKs have been shown to stimulate the recruitment of conventional dendritic cells into the TME, which is critical for an anti-tumor immunity, but also to prevent metastasis by controlling tumor architecture.	85,86
NKT cell	**NKT cells** recognize lipid antigens presented through CD1d molecules. They show cytotoxic activity and release cytokines. High NKT cell infiltration has been considered a beneficial prognostic factor	87,88
Tumor-associated macrophage	**TAM** activity depends on their differentiation type (M1 or M2) and of their localization within the tumor mass.	89,90
	M1-TAM secrete high levels of IL-12 and Th1 cell-attracting chemokines. They display a tumoricidal capacity and their infiltration stands as an independent prognostic factor	
	M2-TAM down-regulate the MHC-II expression, promote tumor progression through the secretion of immunosuppressive cytokines, and promotion of Treg differentiation, angiogenesis, wound healing and therapeutic resistance via several mediators. A strong infiltration of M2-TAM is associated with poor prognosis	
Myeloid-derived suppressor cell	**MDSCs** exhibit remarkable immunosuppressive and tumorigenic activities. MDSCs mediate the suppression of T cell functions through the upregulation of immune suppressive factors, such as arginase and nitric oxide synthase isoform, and the increased production of reactive oxygen species (ROS), promotion of Treg functions through the secretion of IL-10 and TGFβ, as well as the regulation of NK functions.	91
Mast cell	Although **mast cells** consistently infiltrate tumors, their role as pro- or anti-tumorigenic players is controversial. While some studies have shown a protective role, recent evidence indicates that mast cells enhance blood and lymphatic vessel formation, which results from their degranulation and release of pro-angiogenic and growth stimulatory factors. In CRC, high mast cell density has been related to tumor aggressiveness and reduced survival.	92
Tumor-associated neutrophil	Anti-tumor and pro-inflammatory **N1-neutrophils** effects result from the expression of immunoreactive cytokines and chemokines, the generation of oxidative damage caused by ROS and the induction of Fas-ligand-associated apoptosis.	93
	Tumor-progressive and immunosuppressive **N2-neutrophils** secrete pro-tumorigenic factors and affect other immune cells in an immunosuppressive manner, for example, by inducing T cell tolerance.	
Dendritic cell	**Stimulatory dendritic cells**, exposed to proinflammatory signals, promote the stimulation of T cell proliferation and impairment of Treg function.	94,95
	In contrast, **Regulatory dendritic cells**, induced by tolerogenic signals, such as TGFβ, IL-10, and prostaglandins, suppress T cell activation and proliferation and provide signals that enable Treg differentiation and expansion.	

II.2.2. Immune TME and CRC

The immune TME has a major impact on CRC prognostic. CMS1 CRCs have a better prognostic because their high mutation rate induces neo-antigens creation that activates tumor-infiltrated lymphocytes. On the contrary, CMS4 is associated to a strong infiltrate of immunosuppressive M2-TAMs and MDSCs, leading to an unfavorable outcome[61]. However, CMS classification has limited clinical usefulness. Instead, the immunoscore has been developed and validated through world-level cohorts of CRC at all stages[96]. It consists of the immunohistochemical staining of CD3 for tumor-infiltrating lymphocytes, CD8 for CTLs, and their density measurement in the tumor core and the invasive margin of the tumor. From the 4 densities are calculated a score translated into three categories, IS-high, IS-intermediate, and IS-low, directly correlated with survival, as a high number of infiltrative CTLs gives a higher probability of effective antitumor immune response[97]. The immunoscore has demonstrated a better predictive performance than MSS/MSI distinction or all other pathological-assessed evaluations in stage I-III CRC[98], and better than tumor regression grade after treatment in mCRC[99].

Immunotherapies share the objective to shift the local TME from immunosuppressive to anti-tumor immunoreactive. Several strategies have been developed, and they can be divided between the T cell activators, T-cell therapies, immunosuppression elimination, and cancer vaccines. The immunotherapy field has reached the clinical practice thanks to the immune checkpoint inhibitors. Anti-programmed cell death protein-1 (PD-1) pembrolizumab and nivolumab, or anti-CTLA-4 ipilimumab are targeting key immunosuppressive molecules responsible for the CTL inhibition[74]. Both CMS1 and CMS4 CRCs have high CTLA-4 and PD-1 expression, indicating their potential sensitivity to immune checkpoint inhibitors. Anti-PD-1 is part of the first-line treatment of MSI mCRC only and has recently demonstrated its superiority as monotherapy against standard chemotherapy and antibodies, but the study is still ongoing[100]. Moreover, all antitumor therapies have some effect on the immune system. It has been found that IRI has increased immunosuppression in treated CRC patients, whereas 5-FU and oxaliplatin have a beneficial effect on immune activation, as they can induce immunogenic cell death leading to CTL infiltration in CRC[101,102]. Besides, anti-angiogenics help T cell infiltration and immune activation by restoring adhesion molecules at the endothelium[72]. Immunotherapy has many new compounds and strategies under clinical trials, and new progress is expected in the short term.

II.3. STROMAL COMPARTMENT

II.3.1. Cancer-associated fibroblasts into the CRC stroma

Tumor stroma is a generic term used to qualify the whole TME, the non-immune TME, or the non-immune and non-vascular TME. The third option will be used in this thesis. In a healthy colon, the stroma contains resting MSCs and normal inactivated fibroblasts (NIFs), with a low metabolism and proliferation rate. They regulate tissue homeostasis and prevent tumorigenesis[103]. Normal stroma can be activated during wound healing, fibrosis, or tissue inflammation. The myofibroblast population is characteristic of an activated stroma. Tumor stroma contains the so-called cancer-associated fibroblasts (CAFs), and other actors such as MSCs, that could help CAFs in many of their roles[104]. In solid tumors, NIFs and pericryptal myofibroblasts are recruited and activated to form the majority of CAFs, but other cell lineage origins have been described, such as endothelial or epithelial cells, circulating fibrocytes or MSCs, pericytes, smooth muscle cells, or adipocytes[105,106]. CAFs express a very distinct phenotype from NIFs, closer to myofibroblasts. They are often larger, more proliferative, prone to migrate, and do express a wide range of growth factors, cytokines, chemokines, and other paracrine factors [107].

CAF programming can be driven by different pathways (Figure 5)[103,108]. The TGFβ/SMAD pathway is considered the canonical activation of CAF in colon cancer[109]. Other cancer cells derived factors include growth factors, such as PDGFα/β or FGF. SHH pathway would also activate CAFs via GLI1 and GLI2 expression in colon stromal cells[110,111]. Inflammation, through interleukin-6 (IL-6) or leukemia inhibitory factor, for instance, activates the JAK/STAT signaling pathway responsible for CAF promotion, at least in several non-CRC[112113]. The inflammation is sometimes induced or increased by chemotherapy treatment. For instance, FOLFOX therapy has demonstrated a significant increase in CRC-CAFs, related to the NF-kB signaling pathway[114,115]. Other physicochemical stimuli prone fibroblasts transformation, such as hypoxia, oxidative stress, and matrix stiffness, all of them being frequents in TME. This transformation appeared to be irreversible, as CAFs seem to maintain their activated phenotype when they are cultured[103]. CAFs are genetically stable, even if epigenetic alterations have been considered at the origin of their conversion[107].

CAF heterogeneity between the different organ stroma and into a single tumor is far to be understood. The link between their precursor origin, their way of activation, their specific markers and a specific phenotype is still impossible to draw. Nevertheless, it should be assumed that CAFs populations are heterogeneous, and that all the following descriptions of this chapter could belong

to only a subpart of CAFs. In several cancers, CAF subtypes have been identified using single-cell RNA clustering. Two CAF populations different from colon NIFs have been described in CRC[116]. CAF-A subtype over-expresses ECM related genes such as FAP, matrix metalloproteinase (MMP)2, collagen 1A2, and also podoplanin. They are related to FAP^+/$podoplanin^+$ CAFs found in breast cancer, associated to tumor-specific CTL motility and localization[107]. CAF-B subtype is more distant from NIFs and expresses myofibroblast markers such as SMA, PDGFRα, decorin, and transgelin. A precise attribution of functional roles to the different fibroblasts is not yet clear. Some hypotheses suggest that pro-tumorigenic or anti-tumorigenic roles could be associated to distinct subtypes. FAP^+ and SMA^+ fibroblasts having shown both negative prognostic values in CRC, they are still considered as markers of foes fibroblasts, whereas FSP1 expression in CAF is linked with better survival[117–119].

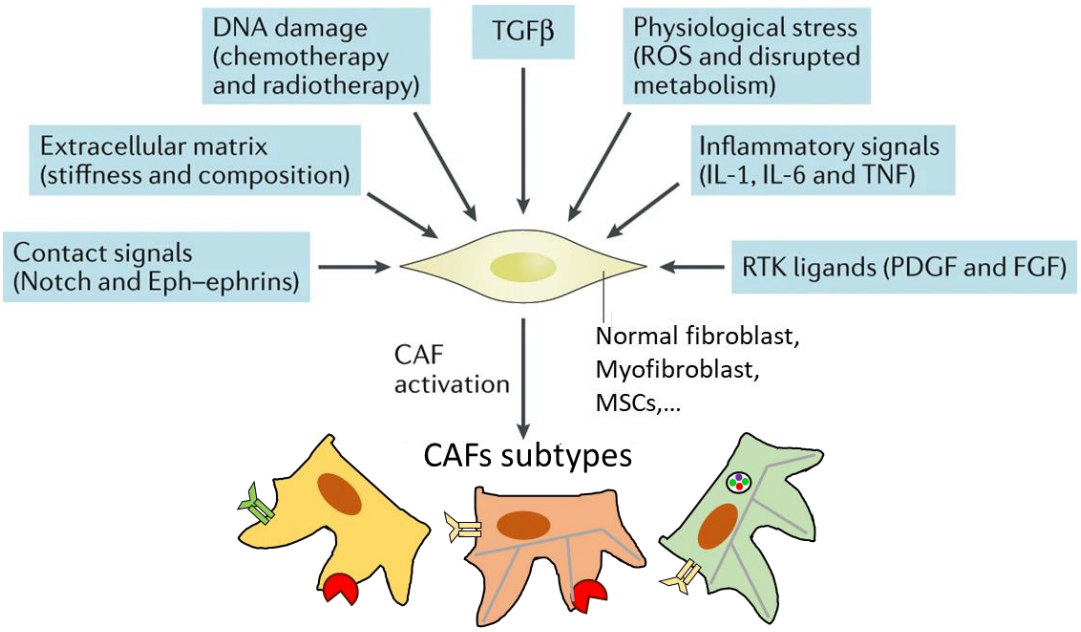

Figure 5. Diverse mechanisms of CAF activation. Adapted[106].

Neither CAFs nor NIFs have a unique marker that is not expressed in any other cell type. Therefore, their characterization is relatively tricky, mixing multiple positive and negative markers. Several molecular markers have been described and associated with CAFs (Table 6). Alpha smooth muscle actin (SMA, *ACTA2* gene) is the characterization marker of activated myofibroblasts. It is part of the cytoskeleton and forms stress fibers with contractility potential. SMA^+ CAFs have been associated with elongated collagen fiber regions[108]. It was the first and still the main CAF marker, as it is expressed by most of CAFs. However, SMA has been observed in NIFs in some studies, and in multiple other cell populations[120].

Table 6. Main CAF markers[105,121,122].

CAF marker	Protein role	Other positive populations
SMA	contractility	Myofibroblasts, smooth muscle cells, pericytes
FAP	ECM remodeling, not fully understood	Wound-associated fibroblasts
Vimentin	Cell motility, structure, and integrity	NIFs, endothelial cells, epithelial cells undergoing EMT
FSP1 (S100A4)	Cell motility, collagen induction, tissue fibrosis	EMT-undergoing epithelial cells, macrophages, quiescent fibroblasts
PDGFRα/β	Growth factor receptor	Myofibroblasts, pericytes, vascular smooth muscle cells

Fibroblast activation protein α (FAP) has been described as a serine protease from the dipeptidyl peptidase IV family, with a dual activity of dipeptidyl peptidase and endopeptidase, but the list of its substrate and its physiological role remain unclear[123]. In adults, FAP should be physiologically expressed by α cells of pancreatic Langerhans islets, and by bone marrow MSC. In mice, controversial literature described FAP in many organs and functions, including uterus or fibroblastic reticular cells in the lymph nodes, but the similarity in its appearance and function with dipeptidyl-peptidase IV makes confusion easy. In diseases, FAP expression is present in wound healing, liver cirrhosis, lung fibrosis, or osteo- and rheumatoid arthritis. In each case, activated MSCs are considered as the source of its expression. In CRC, FAP is more expressed in earlier stages, and a high FAP expression at any stage is associated to a worse prognostic, suggesting that FAP would have a malignant role or would be present on malignant cells[123]. FAP was considered as the best CAF marker as it was thought to be extracellular and specific in the TME. In immunofluorescent staining on stage III CRC patients, FAP has been the only marker that was not confounded with other cell populations[121]. But further studies have described a FAP expression in other cells of the TME, including endothelial cells, TAMs, osteoclasts in multiple myeloma, and some cases by the tumor cells[123].

Vimentin is an MSC marker expressed at a high level in CAFs, at a lower level in NIFs and not by epithelial cancer cells before EMT[108]. It is widely used as a co-marker, as it stains easily all fibroblasts and therefore CAFs. However, macrophages and adipocytes can also be vimentin-positive. Vimentin belongs to the intermediate filament protein family, with a role in the cytoskeleton network[122]. Fibroblast specific protein (FSP1), alternatively called S100A4, has been described as another CAF marker. However, its expression is strongly variable between CAF. In pancreatic ductal adenocarcinoma (PDAC) tissue, FSP1 expression was not correlated with other CAF-associated markers, suggesting its expression in a distinct fibroblast subtype, considered as quiescent fibroblasts[107]. Both PDGFRα and PDGFRβ are used as general markers of fibroblasts

and pericytes, with a recognized expression across all CAF[122]. However, they may be expressed by different CAF subtypes, at least in breast cancer[107]. In CRC, PDGFRβ is more used, as it was not found expressed in several cancer cell lines and would be more CAF selective. Contrary to other CAF markers, PDGFRs roles are better understood: PDGF is expressed by cancer cells for paracrine signaling recruiting and activating fibroblasts[124]. Finally, other CAF markers have been described but not yet used commonly, such as MFAP5, COL11A1, tenascin C, podoplanin, integrin α11β1, or neural/glial antigen 2[122].

II.3.2. CAFs are associated to diverse functions in the tumor

CAF populations have plenty of actions through the TME (Figure 6). Most of the experimental evidence from patients, animal models, and cell co-cultures have shown a detrimental effect of CAFs, contrary to the antitumor activity of NIFs. CAF proteome and secretome have shown over-expression versus NIF of factors belonging to the migration/ adhesion/ cytoskeleton pathways, lipid metabolism, myofibroblast-like activation, oxidation-reduction processes, ECM/ ECM modifiers/ proteases, heat-shock/ stress, and signaling regulators[108].

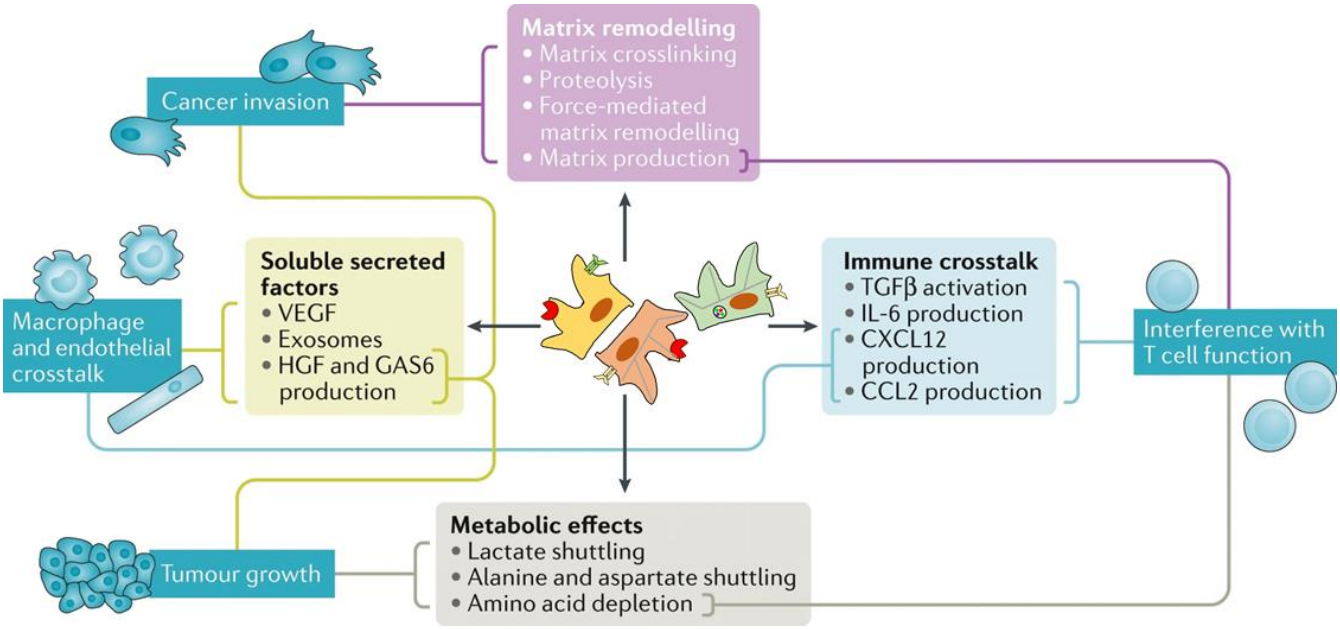

Figure 6. Summary of CAFs functions and the mechanisms by which they are achieved. Adapted[106].

II.3.2.1. CAF activity on cancer cells

CAFs have been associated to most of the canonical oncogenic pathways in CRC. Indeed, CAFs act directly on cancer cells by paracrine secretion of growth factors, such as EGF, HGF, IGF1/2, PGE-2, PDGF, FGF1, and VEGF[125]. This signaling message contributes to the proliferative state of tumor cells, their cell death resistance, and their escape from circulating growth factors. All of

these hormones activate pathways like MAPK or PI3K/AKT. Moreover, TGFβ signaling is the object of a cross-talk between cancer and fibroblast cells. TGFβ is the main driver of CAF activation and is then produced by CAF for an autocrine and a paracrine effect. TGFβ overexpression is deeply correlated with stromal CRC. P53 signaling may also be impaired in CAF by tumor cell action[126]. Another paracrine factor is C-X-C motif ligand 12 (CXCL-12 or SDF-1), binding to cancer cell receptor C-X-C motif receptor 4 (CXCR-4) to promote cancer proliferation[125]. Finally, bone morphogenetic protein (BMP) signaling has been less investigated than TGFβ but a recent illustration of this cross-talk was the BMP2 expression of CAF in response of TRAIL signaling by SMAD4-deficient CRC cells, driving in the end tumor migration, invasion, and metastasis via the EMT[127].

CAF metabolism is reprogrammed depending on the TME. CAF proliferation rate is reduced compared to NIFs, due to their subordination to cancer cell energy needs[128]. Catabolic cancer cells, mostly anaerobic and glucose-dependent described by the classical "Warburg effect", produce a lot of ROS, responsible for CAF oxidative stress, mitochondrial dysfunction, Caveolin-1 degradation, and HIF-1 downstream genes promotion. This promotes CAF metabolic switch towards a catabolic and glycolytic metabolism[128]. They will thus feed the surrounding cancer cells by releasing lactate, pyruvate, glutamine, and ketone bodies to allowing an anabolic metabolism, based on oxidative phosphorylation and much more efficient for producing ATP[128]. This is the described "reverse Warburg effect", not specifically investigated in CRC (Figure 7). However, this metabolic remodeling is more adaptative to the state of the environment, particularly to the oxygen, glucose, and glutamine levels. For instance, if these nutrient levels are low and metabolic by-products accumulate, CAFs can uptake it and promote autophagy and mitophagy to generate more lactate and pyruvate in this harsh environment[129]. This reprogramming was obtained in breast cancer by miR-105 in exosomes in a MYC-dependent manner[130].

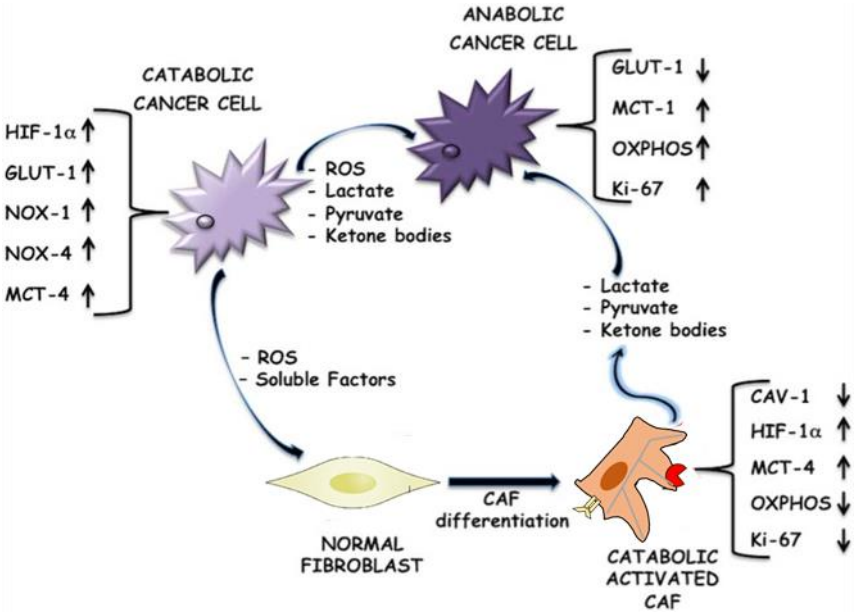

Figure 7. Metabolic reprogramming of tumour microenvironment. Tumour growth and progression are sustained by a metabolic interplay between catabolic tumour cells, ii) normal fibroblasts, and catabolic activated CAFs that contribute to the anabolic reprogramming of cancer cells. Adapted[128]

The stromal TME includes some essential non-cellular elements gathered in ECM. ECM fills the space between cells. It is constituted with a complex network of macromolecules like collagens, laminins, glycoproteins, proteoglycans, and polysaccharides[108]. A constant ECM remodeling occurs by simultaneous synthesis and degradation. Many molecules such as growth factors are bound to the ECM, creating a reservoir available during ECM remodeling. ECM has multiple functions: it is a barrier, an anchorage site, a movement track, and it regulates signaling events by biologic interaction with integrins, syndecans, and discoidin domain proteins[114]. Tumor ECM is altered by dysregulation of the ECM remodeling enzymes, leading to excessive deposition of fibers and their reduced turnover, together with higher stiffness, important for the physical force-induced signaling in all cells[108]. CAFs are the most effective cell population in ECM modification, even if immune cells, MSC, and cancer cells have also some ECM-related actions. CAFs change the collagens proportions and produce matrix-crosslinking enzymes, responsible for tumor stiffening. The resultant mechanical stress can collapse blood vessels, reducing oxygen and drug delivery. CAFs also degrade the ECM through the production of numerous MMPs and proteases like urokinase, increasing the release of growth factors trapped into the ECM[114]. Another example is tenascin C, a matricellular glycoprotein and a non-structural part of the ECM, secreted by CAF and not by NIF in the ECM and extracellular vesicles[108]. Tenascin C is a pro-invasive factor, acting through the inactivation of RhoA[131]. The gelatinolytic activity of FAP also contributes to ECM degradation.

Metastasis is a key cancer phenomenon, leading to most of CRC lethality. It is multi-step, starting with cancer cell migration, invasion of the surrounding tissues, followed by cell intravasation into the bloodstream, dissemination, and extravasation into potential metastatic niches. Metastasis steps have been associated to CAF presence. At first, EMT in cancer cells reduces adhesion while enhances their migratory and invasive capacity[108]. CAF induces cancer cells EMT by multiple pathways depending on the cancer type, such as TGFβ1, HGF/cMET, IL-6, Galectin-1/β1 integrin, or in an MMP-dependent manner[114]. EMT is correlated with CAF presence and expression of several markers. For instance, CAFs express stanniocalcin-1 in response to PDGFβ activation, and stanniocalcin-1 increases migration, invasion, intravasation, and metastasis in CRC, correlated with EMT[124]. Another pro-metastatic activity of CAFs is associated to physical interactions[108,114]. CAFs have been shown to create heterophilic cell contact with cancer cells, through N-cadherin/E-cadherin interactions for instance, and to collectively migrate into the tissue, over the bloodstream, establishing together the metastatic niche. Moreover, ECM digestion can create a path helping cancer cells to migrate, with a direction given by chemotactic attractants secreted by CAFs on the way. Finally, CAF can transmit a physical force to ECM driven by Myo II-contractility, creating a fibronectin-rich fibers orientation in parallel, capable of guiding cancer cells on their migration. CAFs expressing FSP1 have also been shown to prepare the pre-metastatic niche to cancer cell venue. They create a fibronectin-rich environment, producing cancer cells chemoattractant CXCL-12, being pro-angiogenic with VEGF-A and anti-apoptotic with tenascin C[105].

Among the heterogeneity of CAFs subtypes and functions, some anti-tumor activities have been described. However, their anti-tumor function is even less understood than their protumorigenic roles. NIFs are generally recognized as tumor-suppressing. They could prevent tumor development and metastasis before the reprogramming of the TME[132]. Some antitumor factors expressed at a higher level in NIFs include WFDC1, gap junction-mediated transfer of several miRNAs targeting CXCL12, or TGFβ inhibitor asporin in different contexts[132]. Some other anti-tumor factors can be expressed by CAFs and NIFs, such as follistatin-related protein 1, transgelin, or SPARC[120]. CAFs themselves have demonstrated organ-specific anti-tumor properties. In pancreatic cancer, several models and clinical evidence have indicated that proliferating SMA^+ CAFs have globally a protective role, as their depletion leads to more invasiveness, tumor hypoxia, and immunosuppression[133]. In oral carcinoma, SMA^{low} CAFs have shown *in vitro* stem-like cancer cell self-renewal suppression by a BMP4 secretion[129]. In a luminal breast cancer setting, $CD146^+$ CAFs specifically maintain the cancer cells in an estrogen-dependency, increasing the anti-tumor efficacy of tamoxifen[105]. In CRC, the investigations are quite scarce. In human samples, podoplanin was expressed by CAFs but not at the invasive front and correlated with reduced invasion *in vitro*.

Podoplanin was thus considered as a marker of anti-tumor CAFs, and responsible for their anti-invasive properties in advanced CRC[134]. SHH signaling has demonstrated downstream activation in CAFs. Following disappointing anti-SHH clinical trials in pancreatic and CRC, an *in vivo* CRC model confirmed the anti-tumor actions of SHH signaling, fostering epithelial and anti-stem differentiation and being pro-apoptotic through FoxL1 and BMP[111]. To summary the anti-tumor activity of CAFs, it looks that each tumor localization may face specific CAFs or NIFs subtypes protecting their tissue from tumor development, balancing the protumorigenic CAF activity. The mapping of CAF markers heterogeneity could help to better understand and characterize these cell populations.

II.3.2.2. CAFs activity on non-cancer cells

CAFs have key interactions not only with cancer cells but also with the other TME compartments. Stromal cells are an important producer of pro-angiogenic factors. CAFs are driven by HIF-1α-dependant hypoxia, or by PDGF signaling from cancer cells, and IL-6 in a paracrine and autocrine activation. CAFs produce VEGF-A, FGF2, and osteopontin that stimulate angiogenesis, and CXCL-12 that recruits endothelial progenitor cells[103,105,108]. They are helped by stromal MSC in this task[104].

The immune compartment is also targeted by CAFs signalization. They are considered as a key actor in the immunosuppressive environment orchestration[107,135]. Indeed, CAFs interact with most of the infiltrated immune cells from both the innate or adaptative systems (Figure 8). Approximately 1/5 of all CAF-selective-to-NIF secreted proteins are implicated in the immune system, immune response, or immune-related pathways, such as IFNγ signaling and chemokine response[125]. The most important to quote are TGFβ, IL-6, IL-8, IL-13, CXCL-9, CXCL-12, CXCL-14, and VEGF-A. The functional heterogeneity is not fully understood, but a division has been made between SMA^+ CAFs and FAP^+ CAFs[107].

Myeloid cells, such as neutrophils, immature dendritic cells, monocytes, and early myeloid progenitors can be attracted into the TME by chemokines such as IL-8, CXCL-8, or CCL-2, produced by CAFs via myeloid receptor CXCR-2, by adhesion with CRC cells through Vcam-1 induced by CAF IL-6, or directly by adhesion with CAF through Icam-1[105,125,136,137]. By the same cytokines, FAP^+ CAFs upregulate S100A8 and S100A9, promoting myeloid differentiation into either immunosuppressive M2-TAMs or MDSCs.

CAFs are acting synergistically with M2-TAM to inhibit NKs[136]. Indeed, FAP^+ CRC CAFs, via PGE-2, IDO, or IL-6 suppressed the expression of the NK receptors, of their perforin and

granzyme B production, and their TNF-α and IFNγ secretion[107,125]. SMA^+ CAFs-derived TGFβ and MMP2 are considered as major down regulators of NKs activation and cytotoxic activity, as MMP2 cleaves two ligands of the NK-activating receptor at the surface of tumor cells.

CAFs can also modulate the adaptative immunity. Dendritic cell function and maturation are modulated by TGFβ and IL-6 produced from CAFs. CTLs are inhibited by CAFs[105,107]. As NKs and dendritic cells, CTLs are sensitive to TGFβ, which inhibits its perforin, granzymes A/B, Fas-ligand, and IFNγ production. SMA^+ CAF metabolism also produces reprogramming factors, such as IDO1, Arg2, and galectin, that induce T cell anergy and inhibit CD8+ T cell proliferation. CAFs have also been shown to capture and eliminate CTL in the stromal part of the tumor instead of the part containing tumor cells. To do so, CAFs capture tumor antigens from dead cells, processed and cross-present it within the MHC-I to infiltrated CTLs. In parallel, they express at their surface PD-L1/2, inducing CTL anergy, and Fas-ligand, responsible for CTLs apoptosis[138]. The CXCR-4 ligand CXCL-12 is predominantly produced by CAFs in breast, pancreatic, and CRC carcinomas, shielding tumor cells from tumor-infiltrating lymphocytes[139–141]. The ECM stiffness increased by CAFs is also able to reduce the infiltration of effector T cells[107]. On the contrary of CTLs, Treg recruitment and differentiation from CD4+CD25+ T cells are favored by TGFβ, CXCL-12, and VEGF.

At the same time, CAF immunosuppression regulation could be considered as more balanced, as their IL-10, TGFβs, IFNγ, and IL-6 expression participate to the recruitment and polarization of macrophages, NK cells and T cells, which promote an immune control of cancer cells[142].

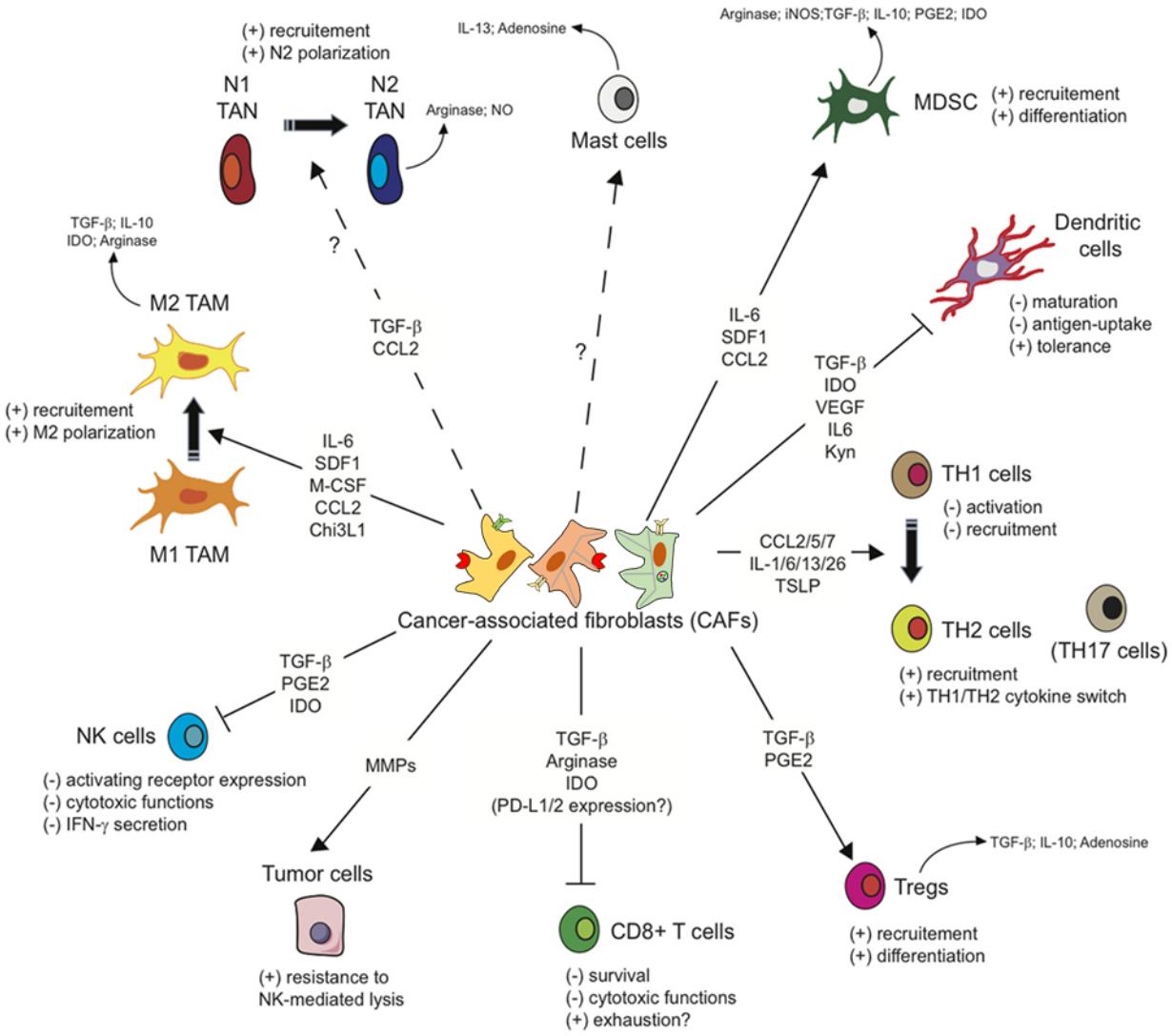

Figure 8. Interactions of CAFs with tumor infiltrated immune cells. Reproduced[143]

II.3.2.3. Resistance to treatments related to CAFs

During anti-tumor therapy, CAFs promote resistance. In CRC, the impact of FOLFOX therapy has been investigated. CAFs promote cancer stem cells, a subpopulation resistant to classical chemotherapy due to their quiescent phenotype. CAFs could help cancer stem cells survival and proliferation through their exosomes-containing miR-92a-3p, inducing Wnt/β-cat pathway[144,145], or by IL-17A and TGFβ secretion[115]. TGFβ2 activates SHH transcription factor GLI2 in stem cells, associated to FOLFOX resistance[69]. Another direct action of CAFs on cancer cells involves AKT, p38 MAPK, and survivin signaling pathways, providing DNA reparation and protection from cell death by apoptosis[146]. Immune checkpoint inhibitors activity has also been canceled by FAP^+ CAFs, up-regulating CCL-2 secretion, recruiting myeloid cells, and decreasing T-cell activity[137]. Finally, high-dose radiotherapy can activate CAF and promote tumor cells radioresistance through IGF[147].

II.3.3. Multi-scale modelization and culture of CAFs

Therefore, CAFs are an obvious target of oncology research for understanding their mechanism and develop new therapeutic strategies. This drives a need to develop research tools and models of tumor including CAFs. Due to the heterogeneity of CAFs, their study into models, out of the human tumors, presents a risk of bias toward a selection or phenotypic reprogramming of some CAF subtypes, not reflecting their whole actions[142].

II.3.3.1. CAF obtention

By nature, CAFs are not an isolated population in tissue, as they need close contact with tumor cells and the TME. However, the need for an isolated CAF cell line, able to be grown in culture, has driven the development of CAF-like cell lines as well as the purification of CAFs from whole tumor extracts.

Several commercial cell lines have been used to model NIFs or CAFs. CCD-18Co is a human infant colon NIF and can serve as NIF control or CAF after activation. CCD-18Co cells can express vimentin, SMA, and PDGFRα, with a demonstrated inhibition capacity of CRC cell proliferation[120]. In other studies, CCD-18Co has been able to prime cancer stem cells for drug resistance[145], or to increase invasion of cancer cells via BMP2 secretion[127]. They have been activated in CAF-like by TGFβ, increasing migration of epithelial cells via activin A secretion[148]. Its co-culture with cancer cells induces FAP production, similar to the other commercial fetal lung fibroblast cell line MRC-5[149].

The most described murine fibroblast cell line is the immortalized embryo fibroblast NIH-3T3. In co-culture with human tumor cell lines, NIH-3T3 expresses FAP[150]. L929 is another commercial immortalized murine fibroblast, derived from adult subcutaneous (s.c.) connective tissue. In co-culture with several murine tumor cell lines, NIH-3T3 or L929 showed different effects on cell proliferation and irradiation resistance, which were not reproducible from a cancer cell line to another[151]. Their CAF markers were inconsistently expressed, therefore these murine immortalized fibroblasts cannot be considered as trustworthy CAF-like sources.

The skin constitutes a simple source for primary NIFs. Human fetal foreskin fibroblasts have been activated in SMA^+ myofibroblast with a deep analysis of the transdifferentiation mechanism[152]. Full myofibroblast phenotype can be obtained in 48-72h by exposition to TGFβ, ionizing radiation, or H_2O_2, with the need of NOX4-dependant ROS production. In co-culture with CRC cell lines, dermal fibroblasts isolated from the neonatal foreskin presented similar features than primary colon NIFs or CAFs, including their effect on cancer cell elongation and motility or their CAF markers[153].

As dermal fibroblasts have enhanced proliferative capacity *in vitro* compared with primary CAFs, they can conveniently replace them. Adult dermal fibroblasts used in co-culture with tumor cells induced significantly less invasion from the tumor than primary colon CAF, and much lower gene expression of HGF or TIMP1 was found in the tumoroid[154]. Therefore, the fetal and neonatal dermal fibroblasts may be better sources of activable fibroblasts than adult skin fibroblasts.

Another convenient source of CAFs is the use of commercially available MSCs, extracted from bone marrow or other localization, as they are natural precursors of CAFs. Once cultivated with cancer cells, they show a similar or enhanced effect than primary CAF, in term of increased proliferation and drug resistance, even if their secretion level of HGF differs[155,156].

Primary cancer-isolated CAFs represent more complex and reliable CAF models compared to CAF-like obtained from artificially activated NIFs. However, their properties are not stable over time and passages, and each CAF isolation gives another cell line with unique characteristics, making it difficult to reproduce the results obtained from a single study. Several techniques have been developed to obtain primary CAF from human tumor samples.

The main isolation technique of primary CAFs is based on enzyme digestion of the tumor. After mechanical cutting into mm pieces, tissue should be incubated at 37°C under agitation with a culture medium supplemented with dissociating enzymes[69,141,154]. The resulting single-cell suspension is a mix of all TME cells and should be processed for CAF purification. The stronger adherence and survival through cell passages of fibroblasts selects them spontaneously by a few passages on adherent flasks[145]. Another commercial tool is the use of anti-fibroblast microbeads, designed for further magnetic cell sorting[157], or a PDGFRα-based selection by fluorescence cell sorting (FACS)[158]. A smart and highly cited technique, developed for breast cancer CAFs and adapted to CRC is based on the differential sedimentation between fibroblasts and other cell types. After digestion and agitation, the cell-containing medium is left to stand for 5 min, the collected supernatant becoming stromal-cell enriched[141]. Moreover, the repetitive shaking with EDTA at 37°C before digestion has been considered to remove epithelial cells[69]. Finally, a simple and fast technique has been recently developed for numerous tissues, and could be expanded to tumor: The first digestion with trypsin is followed by second digestion with collagenase in an ultrasonic bath. The resultant tissue is filtered, centrifuged, and cultured as fibroblasts[159].

The other way to get fibroblasts from a tumor piece is the spontaneous outgrowth of fibroblasts under certain conditions. After seeding of the tumor pieces without digestion in 20% or pure serum with antibiotics during several weeks, CAF and NIFs have been obtained in an adherent plate[152,160]. The authors did not quantify if tumor cells could also migrate to the culture plate, but

CAF markers were well expressed from the obtained cells. The advantage of outgrowth is a gentle isolation process, making not necessary to further purify CAF but it requires a more prolonged time than digestion[159].

Primary CAF culture conditions are associated to different culture media. On one side, general culture media are used in most cases, such as Dulbecco/Vogt modified Eagle's minimal essential medium (DMEM) normal or low glucose, DMEM/F12 (Mix 1:1 of DMEM and Ham's F-12 medium), improved minimum essential medium (IMEM), or Iscove's modified Dulbecco's medium (IMDM), most often with 10% serum. On the other side, fibroblast tailored culture media can be used to improve the CAF culture or its selectivity over other cell types. Commercially available, those fibroblast growth media should contain a lower percentage of serum, basic human FGF, and insulin. A comparison between DMEM+10% FBS and EMEM + 5% FBS + insulin / human FGF / ascorbic acid, showed that the fibroblast tailored medium made possible the isolation of fibroblast by the outgrowth of trabeculectomy biopsy, whereas the DMEM kept an important proportion of epithelial cells and slowed down fibroblast growth[161]. As CAF metabolism of glucose and glutamine depends on cancer cell signals, their concentration is a crucial parameter and should be chosen with a rationale. The plastic surface has non-physiological physical properties that influence the CAF phenotype. There is currently no consensus about the type of matrix on which to culture CAF; substrate matrices, with representative properties of the tumor ECM would be preferable[106].

Primary CAF disadvantage is their senescence after a few passages. Several studies allowed the immortalization of their primary CAF by telomerase (HTERT) transfection. Immortalized dermal fibroblasts are available commercially (BJhTERT), whereas immortalized CAF cell lines have been obtained for PDAC by lentiviral vectors[162] and for CRC with CT5.3hTERT by a retroviral vector[163]. It has been warned that immortalized CAFs would not maintain some traits over passages[106]. However, CT5.3hTERTs have demonstrated to stably express CAF markers, to create tumor niches attracting cancer cells, and to model closely CAF reaction to radiotherapy or glucocorticoids[147,163–165].

Murine CAFs have a lower survival time and are not compatible with hTERT immortalization, which further reduces their availability. Primary murine lung or embryonal NIFs have been obtained, transfected, activated with TGFβ, and injected in vivo[152,166]. Murine tumor cell lines being often adherent, their isolation was obtained by FACS using PDGFRα[137,158,167] or PDGFRβ[109] as positive markers and Epcam, CD45, and CD31 as exclusion markers. Murine CAFs were isolated mainly from spontaneous or mutation-induced tumor models, with a more relevant TME. Only

one study isolated CAF from a CT26 xenograft, and surprisingly, the 6 obtained CAF cell lines expressed at different levels FAP, showing that even with a homogeneous tumor cell line in an inbred murine model, CAF can have distinct subtypes[137].

There are two main causes of CAF cell lines heterogeneity. First is the method of isolation and culture. The whole process may lead to subpopulation selection, activation, or transdifferentiation. Then is the patient source of tumors. Numerous studies have included several patients and compare their isolated CAF[69,154,168]. Even if the information is often missing, it is probably not possible to obtain a CAF cell line with all tumor samples. And it was reported that the resulting cells from the same protocol could have, depending on the initial tumor, a CAF phenotype or a cancer phenotype[169]. Focusing on the two main CAF markers, the FAP gene was expressed at a moderate to high level in only 3 of 6 CAF cell lines[154], and SMA was expressed at a higher level than NIF level in 3 out of 5 CAF cell lines in another study[170].

Solutions to take this heterogeneity into account have been recommended[106]. If the proteomics and transcriptomics data for each cell line are still too expensive, at least their expression level of some key functional proteins would be helpful to relate fibroblast markers to function. But such an identity card has not yet been defined. Moreover, the metadata of CAF obtention and culture should be better reported, including clinical features and CAF markers of the original tumor, short tandem repeat profile to secure their authenticity, culture conditions, and passage number.

To address the current challenge of a trustworthy source of primary CAF, the American National cancer institute has set up the patient-derived models repository. They collect primary tumor samples with a standard operative procedure and provide primary cells to laboratories that request it (only in the US). To obtain CAFs, they culture the cells on a Matrigel-coated plate with DMEM/F12 in most of the cases. In April 2020, 180 primary CAFs from different patients and cancer types were available[171].

II.3.3.2. CAF cocultured models in vitro

Keeping a stable CAF isolate cell line appears to be tricky. The restoration of the tumor-CAF dialog *in vitro* makes it possible to drive a truer and a more stable phenotype.

CAFs use in research is focused on its cross-talk with cancer cells, and the dialog modelization can have several levels of complexity. First of all, unidirectional signaling can use a conditioned medium (CM) of one population and its incubation with the other actor. CM is obtained by incubation of proliferative cell culture with ideally a serum-free (or low) medium, from 2 to 72h. This medium is then diluted or not and used to incubate with the target cells.

Tumor cells CM has a transformative effect on fibroblasts. Indeed it has been shown that lung cancer cells CM can repress p53 activation during camptothecin treatment, on NIFs and even more on primary CAFs [126]. Cancer cells CM promotes the CAF phenotype by increasing podoplanin or FAP expression of human dermal fibroblasts, inducing motility and migration of CAF towards cancer cells into a matrigel scaffold, leading to heterotypic 3D aggregates[172]. Therefore, an adapted cancer CM should be an ideal culture medium to activate and keep a true CAF phenotype.

CAFs CM has been used to evaluate the other direction of signaling, from CAFs to tumor cells. The comparison between NIFs and CAFs was relevant in this case because there was less possibility of feedback activation by cancer cells. CAFs CM induced more migration, invasion, metastasis, and tumor resistance to FOLFOX therapy by several CRC cell lines. The exosomes present in the CM were the main responsible factor[144]. CAFs CM showed also an effect on monocytes, increasing their tumor recruitment and M2 differentiation, also by Vcam-1 expression in cancer cells[136].

The reconstitution of the tumor-CAF crosstalk is obtained by co-culture. Cell culture inserts are a common tool for co-culture, with each cell line cultured in its own compartment into a shared culture medium. It allows preventing direct cell contact interactions and making easy the separation of populations for further analyses. PDGFβ-activated fibroblasts on the lower compartment or directly co-cultured in the upper chamber have been shown to increase CRC cell migration through an 8 μm transwell insert or their invasion into a Matrigel matrix[124]. Primary CAFs have also been co-cultured via inserts with monocytes, and further gene expression has demonstrated an M2 polarization. The same CAFs have shown a different impact on CRC cell proliferation depending on direct or indirect co-culture, demonstrating the importance of the heterotypic cell contact[136]. Direct seeding of both cell lines is possible, the analysis needing pre- or post-staining of the populations to distinguish them. For instance, GFP-transfected CRC cells co-cultured with dermal fibroblasts have shown increased cell elongation and motility by cell tracking, but not when they were incubated only with fibroblast CM[153].

The 2D cultures have shown to have a limited translational capacity with real tumors. To increase their relevant features, tumor cells have been cultured in 3D, such as spheroids. 3D cancer models model successfully the concentric architecture of tumors, with a hypoxic then necrotic core and an outer proliferative zone rich in glucose and O_2. Several methods have been developed to obtain 3D spheroids (Figure 9). They have been described in reviews[173,174]. Here the focus will be on CAF integration in 3D models, with homotypic (pure) or heterotypic (co-culture) spheroids.

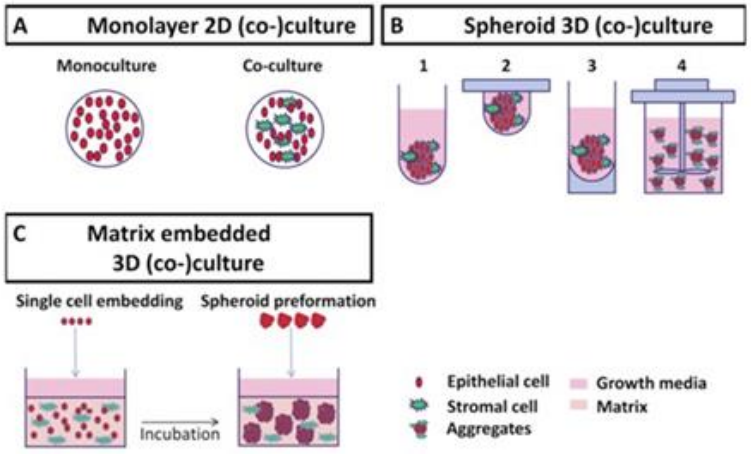

Figure 9. 2D and 3D cell culture systems. A) Conventional 2D monolayer (co-)culture. B) Forced floating spheroid (co-)cultures, 1 = non adhesive coating; poly hema, ultra-low attachment or agarose, 2 = hanging drop method, 3&4 = agitation based biotank. C) Matrix embedded 3D (co-) cultures either derived from single cells or preformed spheroids. Reproduced[174].

The study of CAFs interaction with tumor cells in three dimensions can take several forms. A first possibility is the deposit of a homotypic tumor spheroid on a monolayer of CAFs. At its contact, cancer cells can detach from the sphere and join fibroblasts in an invasion model[175]. In another study, CAFs but not NIFs have shown a spheroid growth support, and the further transcriptomic analysis of the spheroid after FACS helped to define a TGFβ activation signature[69]. The same model was put in hypoxia and it became highly resistant to FOLFOX therapy only in presence of CAFs. Another 3D method is the nesting of a spheroid into a hydrogel. A Matrigel matrix, with breast cancer cells, put on a fibroblast monolayer allowed visualizing the detachment of fibroblasts and their migration towards cancer cells, then their scaffold function to establish tumor cell aggregation and further coalescence into spheres[172]. CAFs or endothelial cells can be mixed with the surrounding matrix. For instance, CAFs have shown in two studies to promote tumor cells detachment from the spheroid and their invasion of a matrix, by direct interaction visualized by microscopy[154,175]. In these conditions, the presence of immune or endothelial cells is useful to understand their role in vivo. Endothelial cells, such as HUVEC or EA.hy296, added into the matrix reduce spheroid growth, and CAFs inhibit vascular network formation[154,175]. Finally, fibroblasts can be directly mixed with tumor cells during spheroid formation. The crosstalk between both populations is complete and CAFs markers are quickly expressed. CAFs migrate in the center of such a cocultured spheroid, increasing the IFP. In one study, peripheral blood mononuclear cells have been added in the culture medium around a heterotypic spheroid, and they differentiated into immune infiltrated cells, with markers such as CD3, CD56, or CD45. It allowed the evaluation of immunotherapy *in vitro*, which was not possible normally[149].

II.3.3.3. CAF-enriched models in vivo

Finally, CAF action and inhibition must be evaluated *in vivo*. It has been shown that most tumor models induced by the injection of cancer cells present much less stroma than their clinical representative samples[176]. To obtain a tumor with more CAFs, several studies have co-injected fibroblasts with cancer cells to establish a stroma-rich xenograft. Indeed, murine isograft with several cell lines including CT26 or MC38 showed only a minimal FAP expression, showing the need for these models to be stromal-enriched[177]. Most studies used a tumor:fibroblast ratio from 1:1 to 1:4, to take into account the lower survival and proliferation of CAFs. Co-injection of primary CAFs with breast MCF-7, or fetal foreskin fibroblasts with head and neck squamous cell carcinoma PT5 cells, increased the CAFs presence identified by SMA immunostaining[152,168]. NIFs should be activated before co-injection because co-injected murine lung fibroblasts have demonstrated an increase SMA staining only after 7 days of incubation with TGFβ[152]. Therefore, primary CAFs should be preferred to NIFs. The results in CRC are controversial. Several authors observed an increase in xenograft tumor growth after co-culture then co-injection with primary CAFs but not paired NIFs, or after co-injection with CT26 primary FAP^+ but not FAP^- CAFs[69,137]. In other cases, dermal fibroblasts orthotopically co-injected in the caecum did not change the tumor burden[175], and co-injection of LoVo cells with primary CAFs or paired NIFs have reduced tumor growth[120]. Surprisingly, most of the injected fibroblasts in animal experiments are replaced by host murine fibroblasts, which creates a heterogeneity along with the growth experiment[106].

CAFs have been associated to the metastasis process *in vivo*. Co-injection of primary colon CAFs with SW48 in the tail vein and under the splenic capsule has increased liver and lung nodules[156], whereas intrasplenic co-injection of CCD-18co has increased liver metastasis only in SMAD4 deficient HT29, in a BMP2-dependent manner[127]. CAF can be replaced by primary murine bone marrow-derived MSC, particularly in murine isografts, and they show similar pro-tumoral activity[136]. The advantage of murine isografts is that they keep their whole immune system, giving the opportunity of studying stroma-immune interaction.

The caveats of co-injection models promote other *in vivo* methods. Patient-derived xenografts, directly implanted from a patient tumor piece or after several murine passages, have shown to keep a representative TME, and SMA or FAP staining allows quantifying their presence in different conditions[178,179]. However, the progressive switch from the original human stromal cells to murine infiltrative cells still occurs. Transgenic manipulation on mice are better models, but there are rather uncommon in the microenvironment field. $KRAS^{G12D/+}$ $p53^{R172H/+}$ Pdx^{Cre} (KPC) mice are a standard model of spontaneous PDAC, which recapitulates the whole TME, including a desmoplastic stroma[180,181]. Genetically modified mouse models of CRC exist, but their complexity

has limited their use in CAF-oriented studies[182]. An $APC^{fl/fl}$, $KRAS^{LSL-G12D}$, $TGF\beta R2^{fl/fl}$, $Trp53^{fl/fl}$, and $LGR5^{eGFP-creERT2}$ (LAKTP) murine model has shown robust CRC tumors and metastasis development driven by TGFβ, with numerous CAFs, close to CMS4 tumors. Genetically engineered mouse models have been used to selectively deplete SMA^+ or $FSP1^+$ CAF, SHH-induced CAFs, or to delete VEGF produced by breast CAFs, enabling major advances in the knowledge of CAF markers-to-functions[142]. New transgenic models with CAFs functions modulated by a Cre-lox system are still hoped for further comprehension studies.

II.3.4. Targeting the stromal compartment as an anti-cancer strategy

CAFs are an important actor, responsible for tumor aggressiveness and chemotherapy resistance. Therefore, targeting CAFs has appeared as a new TME modulating therapeutic strategy. The attraction of such CAF-targeted strategies relies on CAF relative genotype and phenotype stability over time and across patients and tumor localization. Indeed, despite different subtypes and functions still not fully understood, CAFs remain more genetically stable compare to cancer cells. In addition, in desmoplastic tumors such as MS4 CRC, CAFs are dense and localized close to the tumor periphery or surrounding blood vessels, making it easier to reach them[183]. CAF therapy can be divided between the targeting of CAF activation and promotion to reduce CAFs content, and the inhibition of CAF specific functions. Besides, FAP protein targeting constitutes a full part as it has first allowed understanding the impact and challenges associated to anti-CAF therapy (Figure 10).

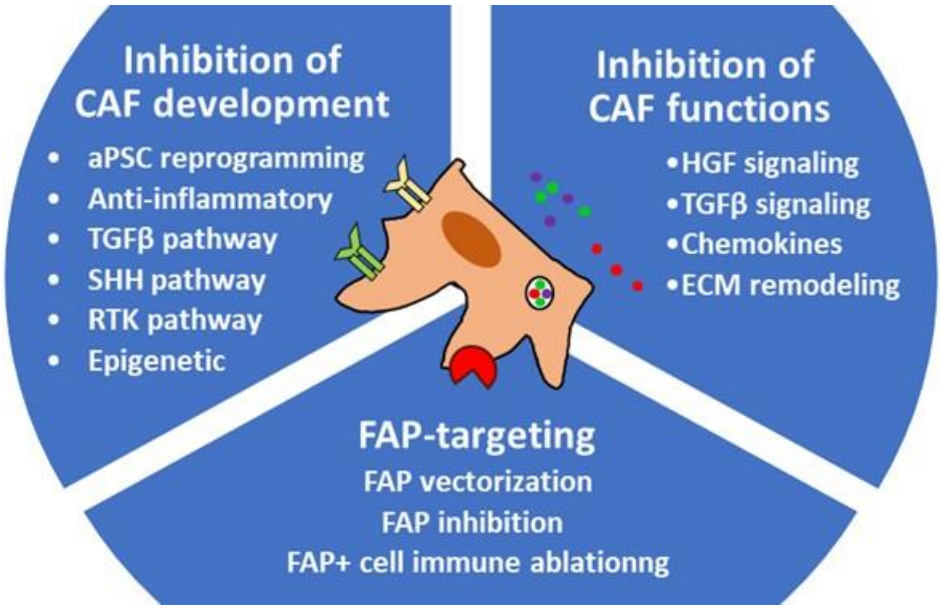

Figure 10. Different stromal targeting strategies

II.3.4.1. FAP targeting strategies

FAP has been described as a specific CAF marker, shared by over 90% of epithelial cancers, two features promoting FAP targeting therapies[184]. Multiples strategies have used FAP to inhibit CAF and their surrounding cancer cells, demonstrating numerous impacts on the whole TME (Figure 11). In 1994, FAP was targeted with a monoclonal antibody in a clinical phase I, by using the murine F19 antibody in mCRC, followed by a clinical phase II with the humanized sibrotuzumab[185,186]. Even if no tumor response was obtained with this unconjugated and not inhibiting antibody, the biodistribution showed an excellent uptake into the metastatic lesions of the liver or lung, and minimal uptake in normal tissues, demonstrating the capacity of tumor targeting by this antigen[187]. It has driven further development of FAP-targeted therapies. Enhanced FAP antibodies or single-chain variable fragments (scFv) have been conjugated to maytansinoid DM1, β-emitting radionuclide ^{177}Lu, or pseudomonas exotoxin-A to kill targeted cells and their surrounding cancer cells[176,188,189]. They have shown preclinical antitumor efficacy but have not been translated into clinical trials. A peptide-targeted radionuclide therapy, FAP-2286, has been recently licensed to Clovis Oncology, which could launch in 2020 a clinical trial[190,191]. FAP being a peptidase with putative action on the ECM, its activity has been targeted with PT630 and Talabostat, the latter having failed in phase II clinical trial for minimal activity[192,193]. There is still a confusion between the unknown and apparently minor function of FAP, and the significant consequences of the presence of FAP$^+$ cells in the tumor. Another strategy used a prodrug cleaved by FAP activity to release thapsigargin and obtained tumor stabilization in preclinical models[194].

In parallel, several studies brought additional evidence that FAP$^+$ cell inhibition or depletion has an impact on cancer outcomes. Two transgenic models associating FAP expression with diphtheria toxin have allowed their experimental ablation[195,196]. While cancer vaccines were ineffective in normal conditions, the ablation of FAP$^+$ cells activated the immune system, causing ischemic necrosis of the tumor during vaccination. However, a study of the same team 3 years after showed that FAP$^+$ cells reside in most tissues of the adult mouse and that their ablation caused cachexia and anemia.

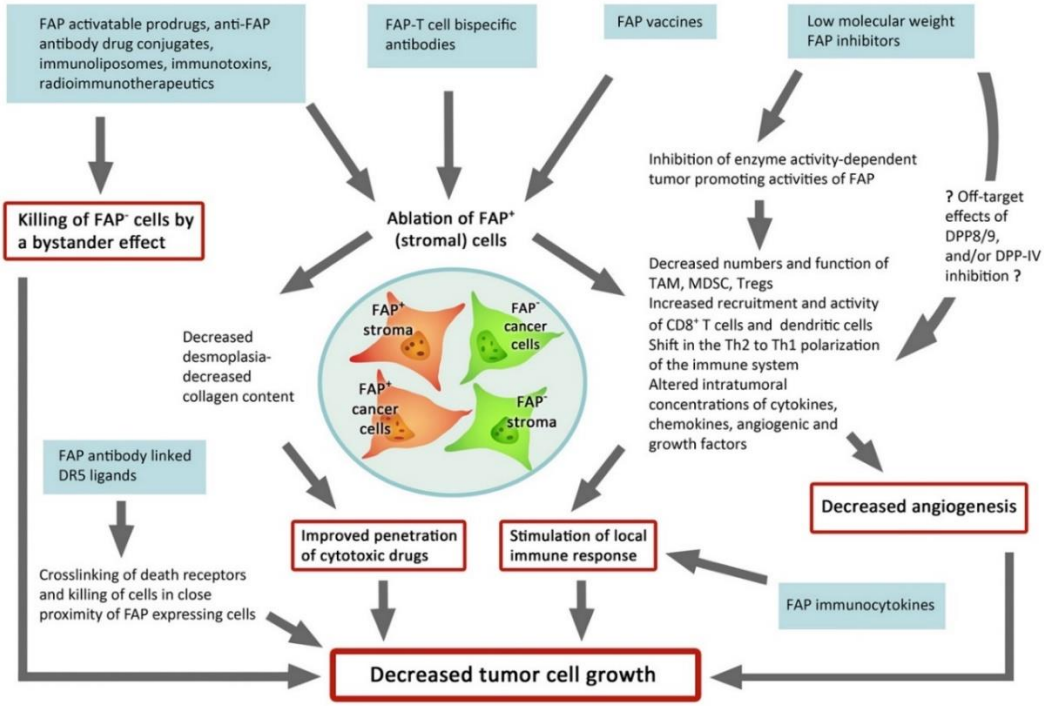

Figure 11. FAP targeting strategies general overview. Reproduced[123]

Preclinical and clinical immunotherapy against FAP$^+$ cells has been widely investigated. For instance, DNA vaccines against FAP have induced alteration of the ECM, increased further chemotherapy uptake and efficacy[197]. More recently, a synthetic consensus FAP DNA vaccine used in multiple murine tumor models showed expected FAP$^+$ cells and hyaluronan decrease, an immune shift with a reduction of TAM, and an infiltration of CTLs. This correlates with clinical tumor samples showing the FAP expression associated to TAM and poor CD8 infiltrates[198]. The targeting of stromal cells by immune cells can also be obtained with genetically engineered chimeric antigen receptor T cells (CAR-T). In monotherapy, anti-FAP CAR-T cells showed a reduction of the ECM, and a slow down of pancreatic tumor, while combined with another CAR-T cell therapy against a cancer cell antigen, they led to a nearly complete remission of the tumors[183,199,200]. Some oncolytic viruses have been designed to promote T cell cytotoxicity against FAP$^+$ cells, by the production of FAP targeting bispecific T-cell engager. After two preclinical studies with such combination[201,202], a first-in-human study has been launched with the NG-641 in 2019.

Upfront FAP therapies are currently developed by Roche with three FAP-targeted products. RG7386 is a bispecific antibody against FAP and DR5, a death receptor that induces apoptosis following its hyperclustering. It has shown direct antitumor efficacy dependent on close FAP$^+$ cells and complete tumor regression in association to doxorubicin (DOX)[178]. A clinical trial was launched in 2015, with no published results[203]. RG7461 is a bispecific immuno-cytokine combining

an engineered variant of IL-2 binding only to antitumor immune cells and an anti-FAP immunoglobulin. An *in vitro* heterotypic spheroid demonstrated RG7461 capacity to attract immune cells[149]. Five clinical trials are including FAP-ILv2 alone or in combination against various solid tumors, with positive preliminary safety, pharmacokinetic (PK), and tumor response[204]. RG7827 is another fusion protein with an antibody-like structure, with one arm directed against FAP and the other associated with 4-1BBL, an agonistic immune modulator and targeted T-cell co-stimulator, which inhibits tumor growth by activating tumor-specific T-cells[205]. A phase I clinical trial has evaluated RG7827. The three Roche products share the use of FAP as a targeted antigen to bring specific ligands to the tumor, without direct interaction with CAFs.

In summary, FAP-directed treatments are advancing after several clinical failures and experimental warnings about potential off-target toxicity. Its preferential expression in cancer stroma has made FAP a better target to vectorize molecules to the tumor instead of interfering with its activity or killing its expressing cells[123,206].

In PDAC, CAFs have shown pro and anti-tumor effects, and the complete depletion of SMA^+ cells has demonstrated an increased aggressiveness of the tumor, a change in the ECM associated with collagen 1 decrease but no hyaluronic acid (HA) change, and an increased proportion of Tregs. Anti-CTLA4 treatment improved the tumor outcome in this SMA-depleted PDAC model[133]. Following these results, in PDAC and also in other desmoplastic tumors, strategies have shifted from CAF depletion towards the inhibition of either CAF activation or CAF functions.

II.3.4.2. Inhibition of CAF development

The CAF phenotype is acquired by specific molecular pathways. Inhibiting fibroblast activation or reverting CAF to quiescent fibroblast may be an ideal therapy, reducing protumorigenic function and keeping protective effects from NIFs. It would be less risky than CAF depletion and more lasting.

The inhibition of TGFβ-induced CAF promotion has been obtained by targeting ITGA5 integrin with the AV3 peptide, inhibiting the TGFβ/ITGA5/FAK pathway. It maintained pancreatic stellate cells (PSCs) population in a quiescent state. AV3 reduced desmoplasia in three PDAC *in* vivo models and increased gemcitabine activity[179]. The same pathway can be targeted downstream, and FAK inhibition by clinically under-trial drug defactinib in combination with docetaxel showed high apoptosis in the presence of stroma on a pancreatic tumor explant[207].

In PDAC, PSCs constitute the main precursor origin of CAFs. The reversion of activated PSCs has been possible. The vitamin D receptor activation by calcipotriol has been shown to antagonize

TGFβ/SMAD signaling-induced activation of PSCs, mediated by the pro-stemness factors IL-6, CCL-2, and CXCL-1[181,183]. In combination with gemcitabine, KPC mice gained survival versus gemcitabine alone. This reprogramming of activated PSCs was also obtained with all-trans retinoic acid, inducing CAFs quiescence and surrounding cancer cells increased apoptosis. A phase I clinical trial adding retinoic acid to nab-paclitaxel (PTX) and gemcitabine in PDAC achieved its objectives in terms of safety and improved overall survival, with evidence of stromal modulation[208–210]. Other endogenous molecules inhibit the activation of PSCs, such as lipoxin A4, which has found to reduce fibrosis and tumor growth of a desmoplastic PDAC model[211]. And finally, p53 activation in PSCs obtained by nutlin-3A or RG7112 treatment reduced CAF presence in a KPC mouse model, by reprogramming PSCs to a quiescent state[212]. PSCs are distinct from fibroblasts, therefore these results might not be directly applicable in CRC but the mechanism of action could serve as an example of CAF reprogramming strategy.

SHH pathway has been widely investigated in the clinic, and smoothened inhibitors, such as vismodegib, sonidegib, or IPI-926 have been associated to stroma and fibrosis reduction, particularly in PDAC[110]. Vismodegib has demonstrated antitumor efficacy in preclinical PDAC and breast models in combination with chemotherapy or nanomedicines, due to a reduction of CAF proliferation and an increase of further drug delivery by remodeling ECM and decreasing IFP and elastic modulus[180,213]. However, in phase II clinical trials in association with gemcitabine, vismodegib did not demonstrate enhanced survival neither in PDAC nor in mCRC[214,215]. The suppression of SHH-induced CAF is effective, but these CAFs could have anti-tumor effects too, and their suppression could lead to more aggressive tumors, increasing patient mortality[208]. IPI-926 also failed in PDAC clinical trial, while sonidegib showed clinical benefit in phase I in breast cancer, probably due to cancer stemness inhibition more than CAF inhibition[132,216].

Tyrosine-kinase inhibitors targeting FGFR or PDGFR should also inhibit CAF activation. The pan-FGFR inhibitor JNJ-42756493 is currently in phase I and phase II trial in several solid tumors[217]. For PDGFR inhibitors, we can cite crenolanib, which has been part of several clinical trials[218], and the approved imatinib which has reduced FGF production by CAFs in a model of human cervical cancer[105]. Sunitinib and nintedanib are both PDGFR inhibitors, the latter with also FGFR inhibition being repurposed in idiopathic pulmonary fibrosis, another disease associated to fibroblast activation[106].

The repurposing of antifibrotic agents, such as pirfenidone or tranilast, has demonstrated preclinical proof of anti-CAF effect[219,220]. More interestingly, anti-angiotensin drugs have shown to block fibroblast activation, reduce CAFs density and ECM, allowing tumor blood vessels

decompression and increasing drug delivery [221]. Losartan was tested in two clinical trials for the localized PDAC in combination with neo-adjuvant FOLFIRINOX or also anti-PD1 nivolumab[222,223].

Inflammatory cytokine leukemia inhibitory factor initiates the epigenetic switch that activates JAK1/STAT3 signaling and DNA methyltransferase 3B, which strengthen each other and promote CAF aggressiveness. The combination of demethylating agent 5'-azacytidine and JAK inhibitor ruxolitinib has been able to prevent CAF activation during prolonged incubation with leukemia inhibitory factor[113]. Other proinflammatory cytokines may be antagonized such as IL-6 and its signaling molecules, like ROCKs and STAT3. AT13148 inhibits ROCK1/2, reduced contractility of PDAC tumors, and is in phase 1 clinical trial[105,106]. Anti-inflammatory glucocorticoids reduce the CAF paracrine secretion of HGF, tenascin C, MMP2, and MMP9. It reduces cancer cell proliferation, invasion, and the ability to form tumors induced by CAFs CM[165]. Co-administration of nonsteroidal anti-inflammatory drugs with vincristine prevented chemotherapy-induced CAF activation, reducing TGFβ and IL-6 secretion in a CM of an *in vitro* model[224]. Another approach has adapted chemotherapy schedule to administer low-dose metronomic chemotherapy regimen, preventing CAF activation and their ELR motif amino-acid positive chemokines, extending mice survival versus traditional maximum tolerated dose chemotherapy[225].

Epigenetic modulators have also demonstrated the capacity to alter cell activation. BETi JQ1 has been associated to CAF inhibition in two studies. In primary dermal CAFs, JQ1 rescued androgen receptor expression, causing a blockage in their protumorigenic activity *in vivo*[226]. In PSCs, JQ1 reduces collagen I production, their presence in PDAC stroma, and pushes them to a quiescent state[227]. A small-molecule screen has identified histone deacetylase inhibitor scriptaid as a repressor of TGFβ-mediated CAF differentiation. In melanoma, scriptaid inhibited ECM secretion, cellular contraction, and stiffness, and reduced CAF abundance[228]. In CRC, cancer cells have been shown to induce adenosine deaminase family acting on RNA 1 expression and activation of Antizyme inhibitor 1 RNA editing in surrounding fibroblasts, increasing their invasiveness promotion. It could be a new epigenetic target[229]. Another epigenetic strategy to target CAF activation and reprogramming is the miRNAs alteration. Several oncogenic miRNA manipulations have been sufficient to activate NIFs in CAFs or to reverse CAFs in NIFs. It was the case for miR-222 inhibition or Lamin B receptor activation in breast cancer, miR-214 and miR-31 in ovarian cancer, miR-1, miR-31, and miR-206 in lung cancer, and potentially miR-10b in CRC[230–232]. Preclinical proofs-of-concept were obtained only in PDAC with miR-21 and miR-29[208].

II.3.4.3. Inhibition of CAF specific functions

All the above-mentioned therapy strategies are very promising by blocking CAF recruitment and activation, but they may be not effective to reduce established CAF effects in advanced stages. The inhibition of CAF action by specific targeting of some of their functions could allow a faster impact on the TME.

TGFβ signaling is not only a CAF promotor but CAFs are also the main contributors to TGFβ production. TGFβR1-inhibitor galunisertib had a strong tumor and metastases inhibition in a genetically reconstituted colon cancer, as it reverted the immune evasion driven by CAF TGFβ signaling. Associated to the anti-PD-L1 antibody, it treated mice with established liver metastasis[109]. Another TGFβR-inhibitor, SD208, has been used in CRC in association to GLI2 inhibitor to prevent hypoxic CAF-induced stemness, dedifferentiation, and chemoresistance in tumor cells[69]. Matricellular protein CCN2 is a transcriptional target of TGFβ in CAFs, expressed during stromal infiltration in PDAC, with a potential role in CMS4 CRC[233]. It has been blocked with the antibody pamrevlumab (FG-3019) in a preclinical PDAC model, sensitizing resistant tumor cells to the cytotoxic gemcitabine[208,234]. After two early phase clinical trials, a phase III trial began in 2019, associating pamrevlumab with gemcitabine and nab-PTX[235].

Several signaling pathways should be envisioned for CAF function inhibitions, and most inhibitors already exist, without being developed for an anti-CAF purpose. HGF secretion by CAFs is associated to resistance to EGFR inhibitors. Several HGF or its receptor MET have been developed and approved in NSCLC, such as Cabozantinib and crizotinib. CAF HGF has been inhibited only *in vitro* with HGF/c-MET inhibitors[156].

CAFs are at the center of the chemokines network. IL-6 produced by CAFs and MSCs causes stemness and immunosuppression, via a systemic effect on metabolism. Inhibition is achieved by IL-6 blocking antibodies or STAT3 small inhibitors[183]. In cholangiocarcinoma, resveratrol inhibited IL-6 production, consequently reducing cancer invasion and autophagy[132,236]. CAFs express numerous CXCR-2 ligands, attracting MDSCs and fostering the growth and survival of stem cells. CXCR-2 inhibitors include SB225002, repertaxin, and AZD5069[183,237,238]. CXCR-4 inhibitor plerixafor has demonstrated antitumor immune activity and potentiated anti-PD-1 antibodies[139]. It reached clinical trial recently[239].

Apart from its immune implication, ECM remodeling by CAFs is part of their main protumor roles. One of the widely explored ECM normalization strategies is MMPs inhibition. Over fifty MMP inhibitors have been tested in clinical trials, with a complete failure to demonstrate clinical impacts and safety. For instance, Bay 12-9566 showed less efficacy than gemcitabine in PDAC, whereas

marimastat did not demonstrate additional benefits to gemcitabine[208]. It could be due to the lack of selectivity towards precise protumor MMPs, and new selective molecules development is ongoing. On the contrary, the poly(ethylene glycol) (PEG)-hyaluronidase PEGPH20 demonstrated a good selectivity for antitumor effects of ECM *in vivo* by targeting HA only. Therefore, it improved gemcitabine treatment by normalizing IFP and increasing microvasculature[240]. Six phase-II clinical trials are ongoing using PEGPH20, but the only one with published results showed a detrimental effect of the drug when added to FOLFIRINOX[241]. The ECM network regulation appears to be even more tricky to play with than the immune network to obtain positive outcomes.

To conclude this CAFs inhibition perspective, table 7 presents an overview of the clinically tested strategies against CAFs. It would be worth noting that desmoplastic tumors may react differently depending on their localization. PDAC has been the most targeted cancer with anti-stromal therapy and we can already take a look back. Several strategies have succeeded to reduce fibrosis and stromal cells, such as retinoic acid delivery or smoothened inhibitors. While preclinical trials have shown an enhanced delivery of concomitant gemcitabine, smoothened inhibition has shown a detrimental effect of this inhibition in patients. The fibrosis in PDAC has been described as a protective reaction from the host to contain tumor growth and invasion, with a good prognostic associated to an important stroma[242]. However, SMA expression has been considered as a bad prognostic factor in the same study. Therefore, the lack of specific markers and knowledge to distinguish protumorigenic and antitumor CAF subtypes prevented the development of more selective drugs[208]. In breast cancer, the $GPR77^+/CD10^+$ CAF subtype has been identified as this potential malignant CAF. Investigations should continue in this way. In CRC, there are much fewer clues of an antitumor CAF subpopulation that should be preserved to enhance patient outcomes. And at the same time, only CMS4 CRC appeared to be interesting for stroma modulation. Basket trials are clinical trials gathering patients who have different types and localizations of cancer that all share a targetable feature. Basket trials should be designed to test the most promising anti-CAF therapies on desmoplastic tumors, allowing a better understanding of their therapeutic capacity in each tumor type.

The use of stroma targeting therapies raises also the question of their combination. There is no reason to think that they could reach a sustained tumor regression in monotherapy. The best timing and choice of such combinations are not yet established. Recent clinical trials have highlighted their importance, with successful translation always dependent on the right combination schedule. Anti-stromal therapies can offer an enhanced bioavailability to a second-wave of therapeutics, by increasing perfusion and reducing IFP through ECM modifications. They have a clear impact on the vascular and immune compartment, hence their inhibition has shown synergy with

immunotherapy or antiangiogenic. Finally, an emergence of nanomedicines for anti-stromal therapy offers an opportunity for this field which is still in need of demonstrated efficacy.

Table 7. Current cancer-associated fibroblast clinical trial activity. Adapted[106]

Target	Name	Drug or biologic	Mechanism	Current status
Interference with CAF activation				
FGFR	JNJ-42756493	Small-molecule inhibitor	Prevents CAF activation	Phase I and phase II trials under way[217]
Hedgehog	IPI-926 (saridegib) and vismodegib	Small-molecule inhibitor	Reduces CAF activation	Clinical trials ongoing; some reported lack of efficacy[243,244]
Interference with CAF activation and CAF action				
TGFβ	Various, including galunisertib	Both blocking Abs and small-molecule receptor inhibitors	Prevents CAF activation and immunosuppression	Phase I, phase II and phase III trials under way[245,246]
Angiotensin receptor	Losartan	Small-molecule inhibitor	Reduces collagen and hyaluronan levels	Phase II trial completed; randomized trial ongoing[222,223]
Interference with CAF action				
CXCR4	Plerixafor (AMD3100)	Small-molecule inhibitor	Prevents signalling from CAFs to immune cells	Clinical trials ongoing[239]
ROCK	AT13148	Small-molecule inhibitor	Reduces contractility	Phase I trial completed[247]
FAK	Defactinib (VS-6063, PF-04554878)	Small-molecule inhibitor	Reduces signalling downstream of integrins	Clinical trials ongoing[248]
LOXL2	Simtuzumab (GS 6624)	Blocking Ab	Anticrosslinking	Preclinical and fibrosis trials[249]
CCN2	Pamrevlumab (FG-3019)	Blocking Ab	Blocks binding to receptors, including integrins	phase III ongoing for non-resesctable PDAC[235]
Hyaluronic acid	PEGPH20 (PVHA)	Pegylated enzyme	ECM degradation to increase the access and efficacy of cytotoxic therapies and immunotherapies	Phase III trial complete, awaiting final analysis[250,251]
FAP-expressing cells	Sibrotuzumab	Blocking Abs	FAP binding	Failed in phase II[186]
	Talabostat	FAP inhibitor	FAP enzymatic inhibition	Failed in phase II in metastatic CRC[252]
	RG7461 (RO6874281)	Ab–IL-2 fusion	Blocks FAP$^+$ CAF function, promotes T cell function	Phase I and phase II trials under way[253]
	NG-641	Oncolytic virus	Cell lysis	First-in-human[254]
CAF normalization				
Vitamin A metabolism	all-trans retinoic acid	Vitamin A metabolite	'Normalizes' stellate cells	Clinical trials ongoing[255,256]
Vitamin D receptor	Paricalcitol	Small-molecule agonist '	'Normalizes' stellate cells	Clinical trial started[257]

III. NANOMEDICINES THERAPY FOR STROMA AND COLORECTAL CANCER

III.1. NANOMEDICINES: A DEFINITION BEHIND DIVERSITY

To understand what nanomedicine is, it is possible to share some numbers: 25,000 research papers indexed on Embase, billions of $ invested by academic and industrial R&D, 4,000 clinical trials with a "nano" keyword in clinicaltrials.gov and over 100 nanomedicine applications to the FDA[258]. As Pr K. Park was mentioning during its debate with Pr. P. Couvreur in the Controlled Release society annual meeting 2019, "we are now living in a nano-world".

Nanomedicine field is the application of nanotechnology to medicine, it means to prevent, diagnose, or treat any diseases. And nanomedicines are nanoscale functional systems engineered with distinct materials and shapes, developed within a controlled size range, from one to hundreds of nanometers, similar in scale to bioactive molecules and functional constituents of living cells[259]. Among the diversity of nanomedicines, this chapter will focus on the nanocarriers, nanoparticles (NPs) dedicated to drug delivery.

A minimal overview of NPs could be a particle constituted of a core and containing a cargo (Figure 12). The NP core can be liquid (e.g. oil, water) or solid (e.g. polymer, solid lipid), stable or in dynamic equilibrium (i.e. micelles), homogeneous (e.g. nanospheres, inorganic NPs) or heterogeneous (e.g. nanocapsules, mesoporous silica NPs). NP carries some cargo, that can be into the core, at the membrane, or being part of the structure (i.e. squalene-based NP[260], gem-C12 lipid nanocapsules hydrogel[261]). This cargo can be, for instance, a drug with therapeutic activity, a nucleic acid, or a contrast agent for imaging diagnostic.

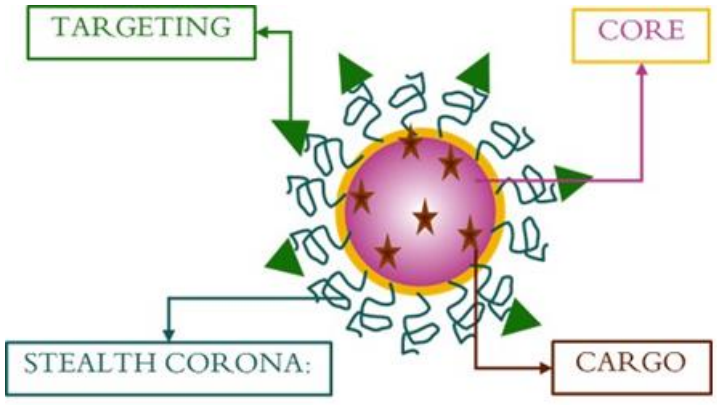

Figure 12. A basic representation of a general drug delivery nanoparticle

Multiple NPs have been developed with a huge diversity in terms of size, shape, materials, and production technologies. An overview of their diversity is presented in Figure 13. Polymeric nanocarriers rely on multi-block polymers playing with their polarity, charge, and length to adapt to their cargo and their target[262]. Lipid nanocarriers have good biocompatibility due to the wide choice of natural lipids easily metabolized by the body. Among them, liposomes are the most important family, with most of the currently approved NPs, such as Doxyl® or Ambisome®. Finally, inorganic nanocarriers are less biodegradable but their chemistry allows facile preparation with a more controlled nanostructure, and new functionalities are offered by some metals such as a contrast agent function in imagery, or photoresponse[263].

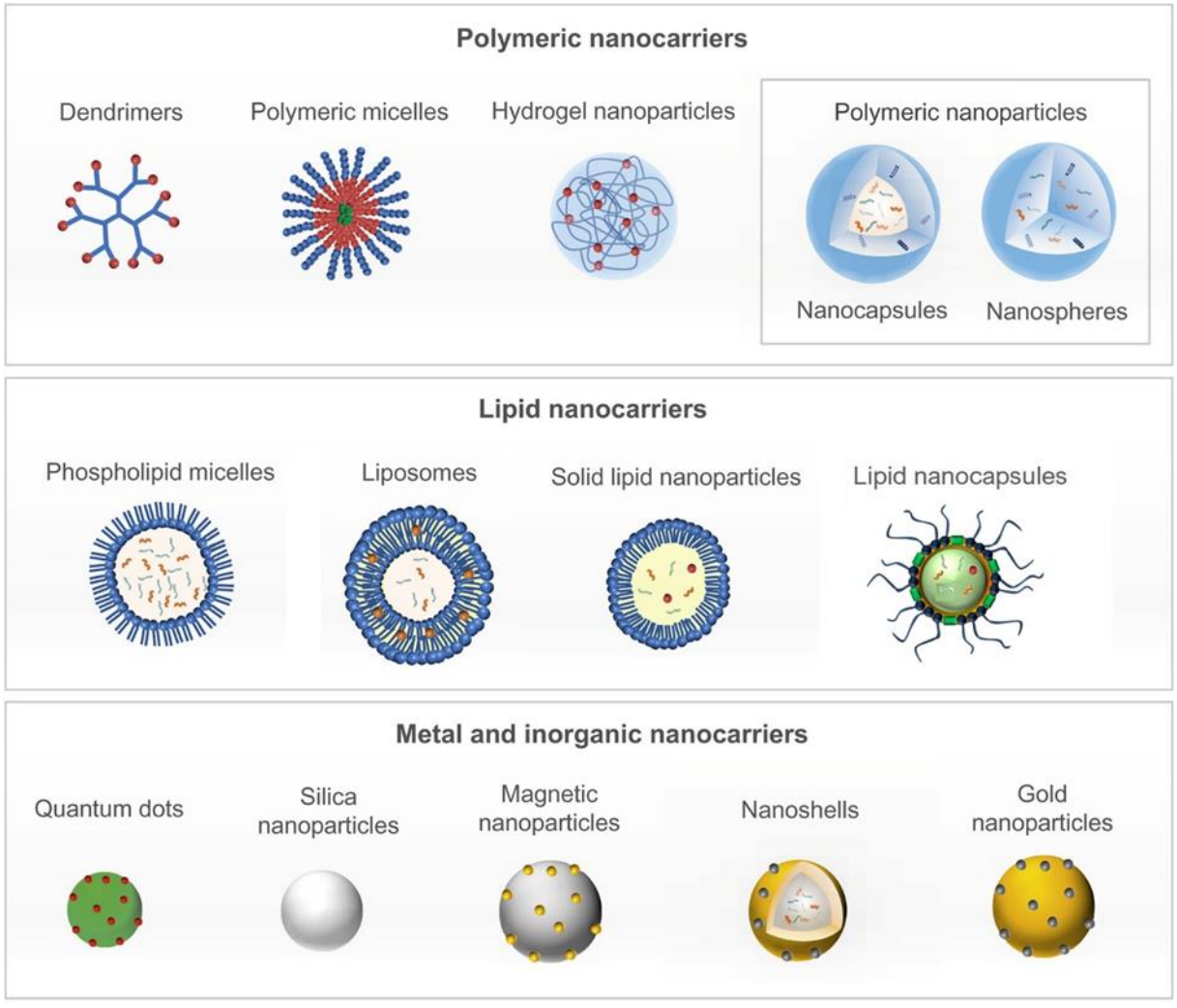

Figure 13. Diversity and classification of NPs. Adapted[264]

III.2. NANOCARRIER PROPERTIES FOR DRUG DELIVERY IN CANCER

A general sentence sums up the nanocarrier's goal: the right drug should be delivered to the right location of the right patient at the right time in the right concentration with limited systemic toxicity[265]. Cancer has concentrated the majority of effort from the academic and industrial NP development. Anticancer drugs being mostly highly toxic, the nanocarriers have been developed to combine site-specific and side-avoidance drug delivery, to optimize the benefit/risk ratio[266]. Indeed, the first property of NPs is to substitute their PK properties with those of the cargo. Nanoencapsulation might be useful for any drugs because they have the potential to carry active molecules until "the right location". To increase the tumor selectivity, NPs use various mechanisms including passive targeting, active targeting, and triggered release (Figure 14)[266].

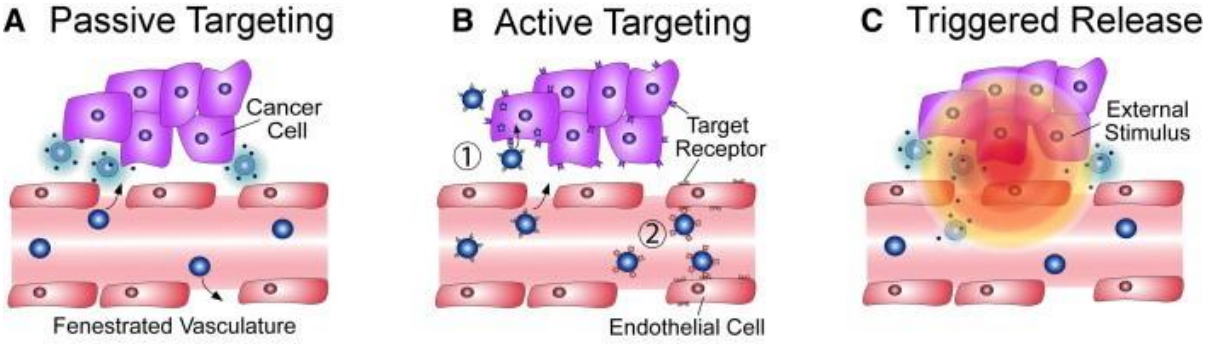

Figure 14. The three main strategies of tumor targeting with nanoparticles. **A)** Passive targeting thanks to the EPR effect. **B)** Active targeting via ligand-receptor binding. **C)** Triggered release caused by endogenous or exogenous stimulus. Reproduced[267]

Passive targeting relies on two main features, a long circulation time of NPs and a selective accumulation in tumor tissue. Hydrophobic NPs in the blood are quickly taken up by the reticuloendothelial system, preventing their delivery to the site of action. To slow down this elimination process, NPs have been improved by the addition of a stealth corona around the outer core[268]. PEG is the most frequently used polymer for stealthiness. Clinically approved Doxil® or Onivyde® are both PEGylated liposomes[269]. The selective accumulation in the tumor is related to the enhanced permeation and retention (EPR) effect[270]. EPR is the result of some hyperpermeability of tumor neovessels associated to impaired lymphatic drainage that enhances the accumulation of NP between 20 and 200 nm diameter. This effect has been questioned and is heterogeneous over time and between patients[271].

There is the possibility of adding a ligand to make actively targeted NPs, with selectivity for their site of action. The active targeting will be reviewed in detail in the fifth chapter. At last, a stimulus-responsive functionality can be added to the NP, to attract, retain, or trigger the drug release into tumor tissue. Endogenous stimuli from the tumor site include low pH, presence of redox gradients,

and particular enzymes. The use of external stimuli from medical devices has also demonstrated a good synergy with stimuli-responsive NP, such as ultrasound, magnetic field, light, or temperature[266].

Many active drugs in target binding assays have not been considered as druggable due to some of their properties. Almost half of the new molecular entities identified by the pharmaceutical industry have faced solubility issues[272]. Among other solutions, nanocarriers allow the solubilization and i.v. administration of "the right drug", even highly lipophilic. Many potential active pharmaceuticals also encounter fast degradation in the body. Once encapsulated, the cargo is protected from degradation by host enzymes.

A major finality of nanoencapsulation is also to reduce the systemic toxicity induced by a free drug, often due to their off-target effects. So far, the main clinical benefit from approved nanoformulation has been this reduction in toxicity, particularly for cardiac toxicity of DOX or PTX toxicity associated to its excipient polyethoxylated castor oil[266].

Another feature of nanocarriers is their ability to enhance combination therapies. When the two drugs are administered in two similar NPs, their PK profile will be similar too and their potential synergy is maximized. The drugs can also be co-encapsulated, ensuring that the majority of cells will be exposed to both molecules at the same time. siRNAs, for instance, are particularly in need of combination to reach the antitumor effect, and their nanoencapsulation may increase tumor sensitivity[269].

However, in the clinic, there is not yet any "nanorevolution". Drug delivery nanocarriers have faced technical barriers that prevented their successful translation. The EPR effect, used as the main hypothesis for cancer nanocarrier development, is controversial and considered scant for improving tumor delivery[271]. The several approved antitumor nanocarriers have not demonstrated significantly better efficacy compared to the free drug, and their higher cost has been hard to be accepted for only safety improvements[273]. Concerning the wide majority of nanomedicines that failed into clinical trials, the main issue is the lack of understanding of the underlying reasons for such discrepancy between preclinical and clinical outcomes. In nanocarrier more than classical drugs, the translation of PK/PD preclinical results to patient outcome is not yet mastered. Therefore, academic and industry have now to focus on the characterization of tumor heterogeneity in their response to NPs, the development of patient-focused nanomedicines, the use of more clinically relevant animal models, and the selection of patient subpopulations adapted to nanocarriers, thanks to biomarkers[273].

Finally, one important challenge associated with NP that prevented easier development in the clinic has been the scale-up of their production and the related costs. The production end of approved liposome Depocyt® by Pacira Pharmaceutical due to undisclosed manufacturing problems has highlighted this critical issue.

III.3. NANOCARRIERS FOR INNOVATIVE STROMAL THERAPY

Among the emergence and consolidation of the anti-stromal therapy field, NPs have taken an increasing role. To illustrate the previously described NPs advantages and properties, examples of anti-stroma and anti-CAF nanocarriers are hereafter detailed[274].

Many active molecules have a reduced blood circulation half-life, such as relaxin, an endogenous hormone that induces various MMPs expression. Relaxin was conjugated with superparamagnetic iron oxide NP and administered to a stroma-rich PDAC model, increasing its circulation time and demonstrating an MMP-associated reduced density of collagen I, desmin, and CD31, and to potentiate gemcitabine[275]. Anti-lysyl oxidase antibodies (LOX_{Ab}) can block this enzyme overexpressed in the TME, responsible for the increased stiffness by collagen cross-linking. By coating the surface of a poly(lactic-co-glycolic acid) (PLGA)-b-PEG NP with LOX_{Ab}, this particle benefited from the EPR effect, improving antibody PK[270]. The PLGA-PEG-LOX_{Ab} increased the residence time of LOX_{Ab} in the TME and demonstrated improved efficacy over soluble LOX_{Ab}[270].

Some NP-added functionalities further increase their controlled release into the targeted tumor tissue. To enhance the tumor availability of the anti-fibrotic drug pirfenidone, it was encapsulated into an MMP2-responsive peptide-hybrid liposome, benefiting from the MMP2 expression in tumor tissue to release the drug "at the right place", increasing the efficacy of the later administered gemcitabine in a PDAC model[276]. The desmoplastic tumors being difficult for NPs to diffuse, the same authors loaded DOX in a cell-penetrating peptide (CPP) NP, which increased the tumor tissue penetration, breaking the stromal barrier[277].

The NP can use original mechanisms to selectively target CAFs. Cellax is a carboxymethylcellulose-docetaxel NP that induced a preferential depletion of the tumor stroma in breast and PDAC models. In both cases, it altered the TME, increasing tumor perfusion and reducing IFP and metastasis. The authors demonstrated that Cellax adsorbed to blood serum albumin, and together they were able to interact with SPARC, predominantly produced and present in CAFs. This effect trapped the NP in the stroma, leading to the selective elimination of CAFs[278,279]. This mechanism has also been hypothesized for albumin-bound PTX particles (nab-PTX), that demonstrated clinical evidence of CAF depletion and collagen reduction in PDAC, but without overall survival

improvements[280,281]. CAFs have also been targeted by liposomes coated with a scFv against FAP, or an FH peptide targeting tenascin C, which allowed delivering the iron chelator deferoxamine to inhibit collagen synthesis or the anti-CAF drug navitoclax, respectively[282–284].

Quercetin has been identified as a natural inhibitor of Wnt16, a CAF paracrine secreted protein responsible for chemotherapy resistance in the neighboring cells. However, its poor solubility and bioavailability have prevented its use, particularly i.v.. A prodrug of quercetin has been precipitated into a lipid/calcium/phosphate NP, improving its bioavailability and metabolic stability. This NP has been tested on a bladder carcinoma model, increasing the second-wave of cisplatin-NP penetration and efficacy[285].

The activity of the collagenase enzyme is reduced by exposition to plasma. For this reason, collagenase has been encapsulated into a liposome before injection to reduce fibrosis in a PDAC model[286]. Other unstable molecules are the nitric oxide donors. Among multiple functions, nitric oxide can activate MMP production in the tumors. This strategy has been possible by the use of mesoporous silica NP coated with the nitric oxide donor S-nitrosothiol[287]. Finally, gene delivery with plasmid is not possible without a drug delivery system. As NPs preferentially accumulate into the CAFs, plasmids coding for IL-10 trap and CXCL-12 trap have been delivered by lipid-protamine-DNA NPs to offer the best gene expression in tumor stroma cells, responsible for changing the local immune TME[288].

Losartan has shown to effectively block the CAF conversion from fibroblasts. But losartan is an angiotensin II receptor inhibitor, causing hypotension and limiting administered doses. Nanoconjugates of losartan with pH-sensitive polymers have been designed to release their content at the slightly acidic pH specific of the TME. It has alleviated the TME immunosuppression and increased the proportion of complete regressions in combination with immune checkpoint inhibitors[289]. PEGPH20, the PEGylated hyaluronidase, has shown musculoskeletal pain and thromboembolism in clinical trials. To circumvent these severe side-effects, PLGA-PEG NPs have been coated with PEGPH20 then with another PEG layer. The tumor NP accumulation was 4-fold increased, minimizing off-target HA degradation[290].

When two drugs are administered in two similar NPs, their PK profile will be similar too. Thanks to this synergy, 4-methylumbelliferone, which directly suppresses HA synthesis, has been administered into liposomes as a pre-treatment of Doxil®, the commercial DOX-encapsulated liposome. Its HA inhibitory effect was directly translated into an improved distribution and efficacy of Doxil®[291]. Cisplatin and gemcitabine were also independently encapsulated into core-shell

lipid/calcium/phosphate-NPs, and their co-administration on a stroma-rich bladder carcinoma model demonstrated synergy only with the encapsulated forms of the drugs[292].

The drug can also be co-encapsulated, ensuring that the majority of cells will be exposed to both molecules at the same time. Thereby, retinoic acid and a siRNA against HSP47 have been co-encapsulated on a PEGylated poly(ethylenimine)-coated gold NP, with a pH-responsive PEG corona. Compared to free retinoic acid, co-delivery reduced collagen secretion thanks to HSP47 siRNA and was more efficient to reprogram CAFs into quiescent PSCs[293]. Another synergic co-delivery was reached by using DOX-loaded graphene oxide nanosheets anchoring promelittin-PEG-phospholipids, a FAP-sensitive prodrug of the cell pore-forming drug melittin. The administration of this formulation to a CRC model led to CAFs and their surrounding cancer cell death [294].

The use of NPs has led to several innovative CAF-targeting strategies. As FAP would be expressed at some level out of the tumor, it was proposed to eliminate CAFs by photoimmunotherapy, a combination of photoresponsive ferritin conjugated to a FAP-targeted scFv, with light irradiation of the tumor, preventing other FAP localizations that could retain some ferritin to be hurt. This strategy was used on a 4T1 tumor model with success[295]. NPs can also bring new functionalities by its intrinsic properties. Indeed, 20nm naked gold NPs have demonstrated strong inhibition of PDAC cells and CAFs proliferation and migration, by disrupting their bidirectional crosstalk. It was further demonstrated that they were inducing endogenous lipid synthesis by the fibroblasts, maintaining them on a quiescent phenotype. In this case, there were no active molecules in the gold NP[296,297].

Finally, NP can be a tool to play with CAF for antitumor therapy. Instead of reprogramming CAFs to a quiescent state, a study succeeded to turn them against their neighboring tumor cells. To do so, they benefited from the preferential CAF uptake of the majority of tumor-delivered NPs, and from CAF natural death-ligand TRAIL resistance. A plasmid coding for sTRAIL, a secreted form of TRAIL, encapsulated in a lipid-coated protamine DNA complex, was administered to allow CAFs to express sTRAIL. It triggered apoptosis of neighboring cancer cells. Besides, CAFs were also reprogrammed into a quiescent state by this transfection. This strategy demonstrated a strong response in a PDAC model, leaving an impaired tumor stroma, accessible for 2nd wave therapy[298]. Another original and elegant strategy, in CRC associated peritoneal invasion, used 500-750 μm microparticles loaded with CAF cells and superparamagnetic iron oxides. The microparticles were injected in the peritoneum at the same time than cancer cells and they trapped the cancer cells into the microparticles by CAF attraction. The particles were removed by using magnetic attraction[163].

There are not NPs, but a good illustration of the possibilities offered by biomaterials particles of multiple scales.

III.4. CRC COMBINED THERAPIES BASED ON NANOTECHNOLOGY-BASED APPROACHES

In the treatment of CRC, NP use is not reserved for stroma-targeted therapy[41]. Combinatorial and complementary approaches concerning chemotherapy, radiotherapy, immunotherapy, and immune TME modulation may be the key to modulate multiple pathways involved in tumorigenesis and dissemination. Therefore, the potential of CRC therapies may be based on rationally designed combinatorial nanomedicines that target multiple signaling pathways promoting a better and durable therapeutic efficacy and thereby attaining the cure, overwhelming disease resistance and severe toxicity.

Chemotherapy containing NPs have also their place in the immune TME modulation. NPs could also be used to inhibit tumor infiltrated cells, as it has been shown in other cancer types against immunosuppressive cells[299]. For example, the anti-PD1 antibodies with DOX, loaded in synthetic high-density lipoprotein–like nanodiscs induced an 80% cure on MC38 tumor growing in the cecum and a CTLs 3-fold increase compared to free DOX treatment[300].

Combinatorial nanomedicine regimens are emerging as promising solutions due to their ability to improve the therapeutic efficacy and prevent recurrence through a synergistic activity, allowing a decrease in dosages of individual active compounds and toxicity[301]. The ratio of administered agents also determines the clinical outcome of a combinatorial therapy once it regulates the degree of synergy or antagonism[302]. Because different therapeutic agents present dissimilar cellular uptake and PK profiles, their entrapment within nanoscale delivery systems able to keep synergistic cargo ratios through PK control is essential to overcome the exposure of sub-optimal or antagonistic cargo ratios at the tumor and improve the therapeutic index of combined active agents[302,303]. Ideally, the correct ratio of multiple therapeutic agents should also be simultaneously delivered using a single nanoconstruct to decrease manufacturing variability and costs[302,304–317]. Alternatively, the delivery of therapeutic agents with different PKs, biodistribution, and clearance profiles using different vehicles have also been explored against CRC[301,318–320]. However, it can induce more variability[321].

According to the different studies on combinatorial nanomedicines against CRC available in the literature and presented on tables 8 and 9, different nanomaterials, such as liposomes, solid lipid nanoparticles (SLN), polymeric NP, polymeric micelles (PM), NP-drug conjugates, and dendrimers have been explored. Different active agents (drugs, genes, anti-angiogenic agents, kinase signaling

pathway inhibitors, antibodies) against CRC were entrapped inside a single nanoconstruct among different combinations[302,304,306,311–315,317]. On the other hand, the combinatorial administration of individual nanosystems entrapping each one a single drug was also described in the literature for CRC[301,318–320]. NPs entrapping a single agent were also combined with other free active agents against CRC[321–325]. Finally, the combination of chemotherapy using nanosystems and radiotherapeutic treatment was also explored[326,327], with clinical translation[328]. A few drug delivery NPs combinations have entered into the clinic. We can highlight liposomal IRI approved and marketed under the name of Onivyde® in association with free 5-FU/LV for locally advanced or metastatic PDAC. It has been tested in phase II clinical trial for metastatic CRC, with comparable results to optimized FOLFIRI-3 treatment[311].

In general, all these combinatorial therapies based on nanotechnology against CRC attained a better response and improved overall survival compared to single-agent therapies, in both preclinical and clinical studies, and allow multiple combinatorial strategies to tackle TME-related resistance.

Table 8. Examples of clinical combinatorial nanotechnology-based therapeutic strategies against CRC. Reproduced[41]

Composition of nanomedicine	Association	Patients	Results	Ref.
Liposome PEP02 (MM-398) with IRI	Free bevacizumab and 5-FU/LV	Oxaliplatin- pretreated mCRC (Phase II)	Regimen active as the optimized FOLFIRI3 and more active than the standard FOLFIRI regimen. Acceptable safety profile and best RR.	322
Liposome (CPX-1) with IRI & floxuridine	Co-encapsulation in 1:1 ratio	33 advanced solid tumors, including 15 CRC (Phase I)	1 patient died of persistent diarrhea; partial response occurred in 12%, PFS> 6 months occurred in 36% of patients. Among CRC patients, median PFS was 5.4 months; 73.3% achieved disease control and 13.3% had partial response.	311
		59 CRC (Phase II)	In 26 IRI-naïve patients: RR 8%; RR + stable disease 65%. Median PFS 3.2 months with 35% > 4 months. In 33 IRI-refractory patients: 0% responses; RR + stable disease 38%. Median PFS 1.8 months, with 18% > 4 months. Safety data: 67% grade 3/4 toxicities. 1 treatment-related death. CPX-1 appears to be more active than FOLFIRI used after FOLFOX	329
NP– CPT conjugate CRLX101	Surgery, Capecitabin & radiotherapy	32 Rectal Cancer (Phase I/II)	19% of pathological complete response; 56% of moderate response; 22% of minimal response.	330

CPT: camptothecin; RR: Response rate; PFS: Progression-free survival

Table 9. Examples of preclinical combinatorial nanotechnology-based therapeutic strategies against CRC. Reproduced[41]

Composition	Association	Disease model	In vitro outcomes	In vivo outcomes	Ref
Associated chemotherapies					
Liposome with CUR	Free oxaliplatin	Colo205 & LoVo; SC xenografts on female nude mice.	Similar antiproliferative effect of equimolar combination compared to single CUR. Synergy of liposomal CUR and oxaliplatin at a 4:1 ratio.	No synergy for the combination. Highest tumor growth inhibition for liposomal CUR with or without oxaliplatin, but higher growth inhibition than oxaliplatin alone in Colo205 xenografts. Antiangiogenic effect including the attenuation of CD31, VEGF, and IL-8 expression.	331
SLN with cholesteryl butyrate, DOX or PTX	Co-administration	HT29	Synergistic antiproliferative effect of cholesteryl butyrate SLN with free DOX or PTX.		312
Mannosylated Albumin NP with disulfiram/copper complex and regorafenib	Co-encapsulation	HCT8/ADR drug-resistant colon tumor & Mouse macrophage Raw 264.7; HCT8/ADR s.c. xenograft	Better efficacy of encapsulation and dual targeting, and simultaneous action on cancer cells and M2-TAMs vs. free drug.	Tumor growth inhibition; improved apoptosis, upregulation of intracellular ROS, anti-angiogenesis, and TAM "re-education" vs. free drug.	303
CS-based NP with CUR or 5-FU	Co-administration	HT29	Enhanced anticancer effects vs. bare drugs.	Improved drug bioavailability vs. bare drugs.	318
N-succinyl CS NP with PTX and Gemcitabine	Co-encapsulation	HT29 s.c. xenograft	Swelling at colonic pH and sequential release pattern of drugs. Increased antiproliferative effect with the combination.	Prolonged survival time up to 45 days wherein 50% of mice treated with the combination was still alive.	301
Pullulan acetate NP with PTX; CS-based NP with all-trans retinoic acid	Co-administration	CT26	Synergistic antiproliferative effect, increased by NP encapsulation. Significant decrease of MMP-2 activity.		319
PCL-CS PM with doxifluridine (5-FU prodrug) and SN38	Co-encapsu-lation	HT29	Synergistic antiproliferative activity enhanced by addition of SN38.		313

Non-targeted or HA-functionalized, PLGA/CS-NP with CPT and CUR	Co-encapsulation at different weight ratios of CPT:CUR	Colon-26	Strong synergistic antiproliferative effects by CPT:CUR in a single HA-functionalized NP at ratios 1:1 or 4:1.		290 302
Micelles of PEG-poly (benzyl l-glutamate) with DOX or etoposide; micelles of PLA-PEG with PTX	Co-administration	CT26 s.c. syngeneic tumor	Synergy for free drugs.	Improved synergistic anti-tumor effects of DOX-micelles + PTX-PLA-PEG micelles or DOX-micelles + etoposide-GEG micelles compared with single therapy.	320
PEG-PLA micelles with PTX, 17-allylamino-17-demethoxygeldanamycin, and rapamycin	3-in-1 Co-encapsulation	LS180 human colon xenograft model	Synergy for blocking tumor growth vs. single encapsulation of PTX. Improved further uptake of dye-containing micelles.		315
Chemotherapy & antivascular / anti-angiogenic agents					
Squalene-based nanocomposites with gemcitabine and isocombretastatin A-4	Co-encapsulation	LS174-T human colon carcinoma xenograft nude mice model	Better cell uptake of squalene-based nanocomposites with isocombretastatin A-4 than without; comparable cytotoxic and antiproliferative effects than free drug.	Complete tumor regression (by 93%) with the co-delivery. Overall tolerance better than free drugs.	316
PEG-PLGA NP with PTX and pigment epithelium-derived factor plasmid gene	Co-encapsulation	Colon-26 & HUVEC; Colon-26 s.c. tumor	Higher antiangiogenic and antitumoral effects of pigment epithelium-derived factor and PTX simultaneously encapsulated in the same NP than either of single drug-loaded NP.	Improved anti-cancer effect, micro-vessel density reduction and tumor cell apoptosis vs. controls including co-administration	317
Chemotherapy & small inhibitors					
Layered double hydroxide with 5-FU	Free BEZ-235 (PI3K/Akt inhibitor)	HCT116	Synergy with improved antiproliferative effect vs. free BEZ-235 and layered double hydroxide-loaded 5-FU		323
HA-cloaked oleic acid NP with AZD6244 (ERK inhibitor) and cisplatin	Co-encapsulation	HCT116 & DLD-1	Synergy with inhibition of ERK1 and ERK2, DNA damage inducing cell death, in contrast to free drug cocktail		305

Chemotherapy & gene therapy					
Nanoscale coordinator polymers with miR-655-3p and oxaliplatin	Co-encapsulation with miRNA at the surface and oxaliplatin prodrug in the core	HCT116 xenogeneic hepatic metastasis model		Tumor growth suppression by co-delivery of miR-655-3p with oxaliplatin, suggesting additive or synergistic interactions	306
Polymeric NP based on cysteine trimethyl CS and carboxymethyl dextran, with SN38 and hSET1 antisense oligo-DNA	Co-encapsu-lation	HT29	Significantly higher cytotoxicity of hSET1/SN38 NP compared with NP containing SN38, free SN38 or hSET1.		308
PLGA-based multi-layered polymer NP with CPT and TRAIL plasmide	Co-encapsulation with pDNA at the first external layer, and penetrating peptide at the surface	HCT116 xenografts	Synergistic antiproliferative effect of co-delivered CPT and TRAIL plasmide.	Significant tumor growth inhibition using the combination therapy vs. monotherapy	309
PCL NP with 5-FU	Free doxycycline to activate suicide gene E (phage φX174)	SW480	Synergistic antiproliferative effect. E gene expression sensitizes cancer cells to the cytotoxic action of 5-FU.		324
CS/Carboxymethyl dextran NP with Snail siRNA and DOX	Co-encapsulation	HCT116	Significant changes of EMT genes, apoptosis cell death and migration inhibition.		307
PLGA NP with PVA and CS, encapsulating CPT and siRNA anti-CD98, embedded into a hydrogel for oral administration	Co-encapsulation	Orthotopic, induced by azoxymethane and dextran sulfate sodium	Improved cytotoxicity and migration/invasion inhibition vs. single drug NP	Reduction in tumor numbers and of inflammation, slight improvement vs. untargeted NP	332

Chemotherapy & antibodies					
PLGA NP with CPT	NP grafted with Conatumumab death receptor 5 antibody	HCT116	Enhanced cytotoxic effects through simultaneous drug delivery and apoptosis induction with targeted NP.		[310]
Self-assembled Panitumumab linked to dichloro(1,2-diamino-cyclohexane) Pt(II)	Co-encapsulation	HT29 & Caco-2 s.c. xenografts	Improved cytotoxicity vs. combination of free drug.	Complete inhibition of Caco-2 and 5-time reduction of HT29 tumor growth at day 35 with good tolerance.	[333]
sHDL-nanodiscs with DOX (sHDL-DOX)	Anti-PD-1 immuno-therapy	CT26 & MC38 s.c. CT26 orthotopic		Induced potent antitumor CD8+ T cell responses against established tumors. Complete regression of established tumors in 80 to 88% of mice, CT26 liver metastasis inhibition, and long-term survival against tumor recurrence compared with free DOX or sHDL-DOX treatment.	[300]
Vaccine & immune checkpoint inhibitor					
sHDL-nanodiscs with Adpgk neoantigen and cholesterol-CpG oligo-DNA	Anti-PD-1 immuno-therapy	MC38 syngeneic tumor		Combinative treatment shows 7/8 mice with complete remission in curative pattern vs. 2/8 for the combined therapy with a classical vaccine (soluble Adpgk, CpG, and anti-PD-1) and 0/8 for monotherapy. Immunological memory against recurrence.	[321]
Immune checkpoint inhibitors					
Immunoswitch iron-dextran NP	NP coated with agonistic antibodies against 4-1BB (co-stimulation of effector T cells) and antagonistic antibodies against PD-L1	MC38-ovalbumin s.c. xenograft		Significant delay of tumor growth and survival extend vs. no treatment and isotype NP. Complete remission of palpable tumors in 5/10 mice.	[334]
Gene Therapy Synergism					
PAMAM dendrimer with anti-EGFR and c-Src specific antisense oligo-DNA	Co-encapsulation	HT29	Reduction of EGFR and c-Src protein expression and enhanced antiproliferative effect.		[304]
PLGA-based NP with siRNA anti-DCAMKL-1	Free DAPT (γ-secretase inhibitor)	HCT116 xenograft nude mice model		Inhibition of tumor growth and Notch-1 pathway via a miR-144 dependent mechanism. No synergy.	[325]

Chemo & Radiotherapy					
PEGylated liposome (Promitil) with mitomycin C	5-FU-based chemoradio-therapy	HT29 & SW480; HT29 mouse xenograft	Increased mitomycin C release from Promitil, which potently radiosensitized irradiated HT29 (but no SW480).	Increased efficacy of radiotherapy and 5-FU combination. Improved antitumor efficacy compared to equitoxic doses of mitomycin C.	[314] [315]
NP-drug conjugate CRLX101 with CPT	5-FU-based chemora-diotherapy	HT29 & SW480; Mouse xenografts	Equivalent to free CPT in radiosensitizing cells.	CRLX101 combined with 5-FU-based chemoradiotherapy showed better therapeutic efficacy than combinations with oxaliplatin replacing CRLX101.	[330]
Chemo & Gene & Phototherapy					
Gold nanospheres with thiol-siRNA−DY647, HA1 peptide, and TCP-1 peptide (GNS); Gold nanorods with Avastin Thiol-PEG-COOH and TCP-1 peptide (GNR)	In a single hydrogel, co-delivery of both GNR (phototherapy + anti-VEGF) & GNS (phototherapy + anti-Kras gene therapy)	LoVo-6-Luc-1 SCID mice		Complete regression of tumor in 5 mice by the combination.	[335]

CPT: camptothecin; CS: chitosan; CUR: curcumin; PCL: Poly-ε-caprolactone; PLA: poly(lactic acid); sHDL: synthetic high-density lipoprotein-like
Human CRC cell lines: HT29, Caco-2, HCT116, SW480, Colo205, LoVo, Colon-28, LS180, LS174, DLD-1.
Murine CRC cell lines: CT26, MC38.

IV. LIPID NANOCAPSULES, CURRENT STATE-OF-THE-ART

IV.1. LIPID NANOCAPSULES PREPARATION AND PROPERTIES

Lipid nanocapsules (LNCs) are bioinspired from lipoproteins, constituted from an oily core stabilized by a pair of surfactants (Figure 15). The original oily core was constituted from Labrafac® WL1349, a mix made from triglycerides of capric and caprylic acids. Their shell is a mix made of a minor part of lecithin-based surfactants oriented towards the oily core, and a major part of water-oriented hydrophilic surfactant Solutol® HS15, a mixture of free PEG_{660} and PEG_{660} hydroxystearate. The originally selected lecithin Lipoid® S75-3, composed of hydrogenated soybean phosphatidylcholine (69%) and phosphatidylethanolamine (9%), has been replaced due to its commercial discontinuation by Lipoid® S100, composed of non-hydrogenated soybean phosphatidylcholine (>94%) but esterified with the same fatty acid chains, mainly C18 polyunsaturated omega-6 linoleic (>59%) and C16 saturated palmitic (>12%) acids.

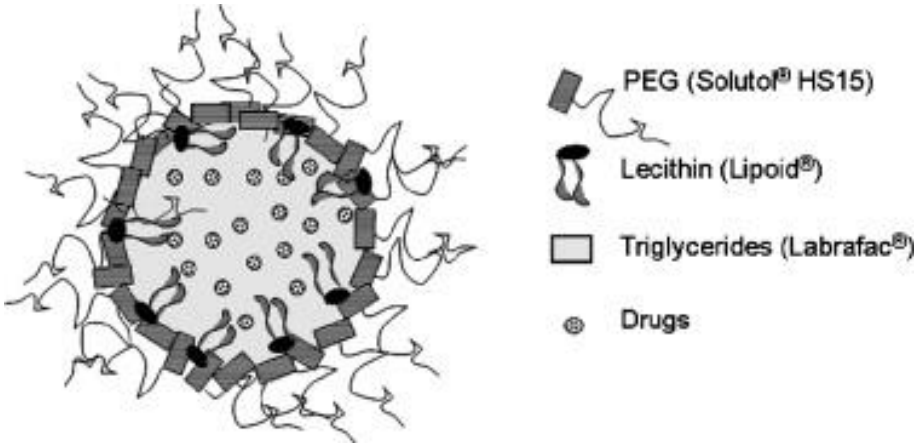

Figure 15. Schematic representation of drug-loaded LNCs. Reproduced[336]

LNCs are prepared by the phase-inversion temperature process, according to the initial publication (Figure 16)[337]. The phase-inversion principle is based on the differential solubility of the PEGylated surfactant according to temperature change. At low temperatures, the PEG chains are hydrated and stabilize oil in water (o/w) emulsion whereas, at high temperatures, the dehydration of the PEG chains caused a phase inversion into water in oil (w/o) emulsion. At the phase-inversion temperature, there is a balance between hydrophilic and lipophilic properties of the PEGylated surfactants in the mix, and a bicontinuous microemulsion structure appears[336]. To prepare LNCs, all the ingredients are mixed by magnetic stirring, then heated above the phase-inversion temperature. The mix is submitted to a defined number of heating and cooling cycles around the

phase-inversion temperature. Finally, an addition of cold water at the phase-inversion temperature induces an irreversible shock, breaking the microemulsion and forming stable LNCs. The number of temperature cycles has importance, each new cycle adding stability and monodispersity and reducing LNC size until a plateau[338].

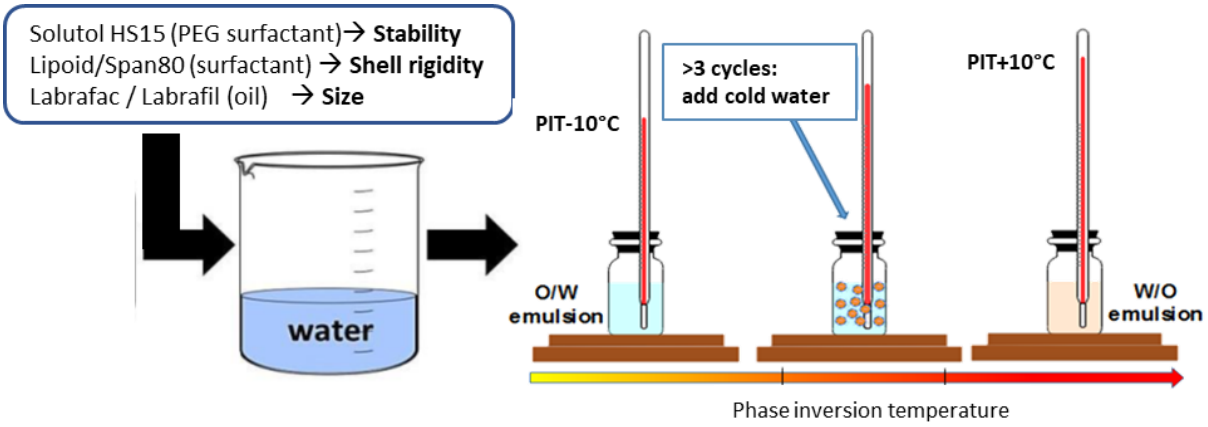

Figure 16. The phase-inversion method to produce LNCs. Depending on the formulation, the phase-inversion temperature varies between 60 and 80°C.

The ingredients relative mass is adjustable into a design space defined by the ternary diagram between oil, water, and the PEGylated surfactant. The relative quantities of oil and Solutol® define the size of LNCs. The size was initially maintained between 20 and 100 nm, ideal for i.v. administration and EPR effect[339]. By increasing the number of cycles, LNCs formulations up to 200 nm have been formulated recently for oral administration[340].

In order to prepare LNCs to its industrialization, the stability and the scale-up of LNCs have been investigated. Initially, empty LNCs samples have been described with a stability of 18 months at 4°C and 1.5 months at 37°C[337]. To further enhance LNC stability, a freeze-drying process was applied. Trehalose was the best cryoprotectant, while Lipoid® percentage was considered as a key parameter of the stability of LNCs through freeze-drying[337,341]. However, freeze-drying caused in all cases a significant size increase over 30-50 nm and a higher polydispersity. Another long-term storage method was developed by liquid nitrogen snap-freezing, followed by storage at different temperatures[342]. In this case, the formulations were loaded with PTX. The best result was obtained by the 6-months storage in liquid nitrogen, with no drug loss and only a 10 nm increase of the diameter. However, this process appears difficult to set in industrial practice. With its simple formulation process, LNCs were produced at a pilot-scale of 1 L with a constant size, ζ-potential, and ibuprofen payload[343].

IV.2. DRUG-LOADED LNCS ADVANTAGES AND LIMITS

In addition to their simple production, one of the main advantages of LNCs is their encapsulation ability. First of all, LNCs formulations can entrap a wide variety of molecules with high encapsulation into its oily core. Hydrophobic (PTX, docetaxel, regorafenib, etoposide,…) and amphiphilic (amiodarone, ibuprofen,…) molecules have been encapsulated with 90 to 100% of encapsulation efficacy, by using the standard formulation or by replacing Labrafac® (eg transcutol®, labrafil®, captex®) or Lipoid® (eg span 80)[336,338,343–346]. Hydrophilic molecules have also been incorporated into LNCs through reverse micelles. For instance, acriflavine (ACF) has been solubilized in w/o emulsion, then added at the end of the formulation to incorporate the aqueous droplets into the oily core[347]. Another strategy has been to combine hydrophilic drugs with a hydrophobic tail to allow their encapsulation. Lauroyl (C12)-gemcitabine, 5-FU-C12, Di-lauroyl-decitabine have been encapsulated by this way into LNC, with emergent properties such as the gelation ability of gem-C12-LNC[261,348,349]. Co-encapsulation of drugs has only been reported for PTX and gem-C12[350]. In addition to their high encapsulation efficiency, hydrophobic cargos has ve demonstrated a stable entrapment in LNCs. A low and sustained release has been described, with only 3% of PTX, 15% of amiodarone, or 5-25% of chlorpromazine released in 24h[336,344,351]. This LNC property was recently accused to reduce drug activity, with the hypothesis that LNC would keep entrapped its cargo after cell uptake. But no demonstration was brought[352]. With reverse micelles, the stability is lower with 50% of ACF released in 3h and 80% in 24h. Therefore, LNCs have attractive encapsulation capacity, particularly with hydrophobic and amphiphilic drugs.

LNCs behavior after administration *in vivo* has also demonstrated their advantageous properties. LNC-PTX has been the most investigated. Orally, LNC-PTX demonstrated enhanced absorption compared to Taxol®, by using vesicle-mediated transcytosis and Solutol® P-glycoprotein (P-gp) inhibition[353,354]. I.v., LNC-PTX did not show longer residence time, and only a slightly enhanced antitumor efficacy[355,356]. Its mean residence time in rats was estimated between 50 and 200 min. With hydrophilic molecules, such as decitabine, LNC-(C12-decitabine) neither increased the AUC after i.v. administration compared to free drug.

On the contrary, the toxicity profiles are enhanced by LNC nanoencapsulation. Indeed, the PTX i.v. maximum tolerated dose was eleven-fold higher with LNCs, whereas no acute toxicity was demonstrated with a maximal volume of blank LNCs[342]. ACF daily injections were advantageously replaced by weekly LNC-ACF injections, reducing murine weight loss[347]. Blood gas analysis showed after a single blank LNC i.v. injection a decrease of the base excess, but not of the pH[342]. *In vitro*, deep toxicity studies demonstrated a low complement activation and macrophage uptake by LNCs.

The single toxic component of LNCs is Solutol®, 25% of which was released by LNC formulation after 24h[344]. For this reason, the *in vitro* toxicity of LNCs decreased when the particle diameter increased[340,357].

Finally, several improvements have been developed for LNCs. Post-insertion of additional PEG chains has demonstrated the prolonged size and loading stability in plasma, while the blood circulation lifetime was also extended[358]. The addition of an amine moiety at the end of the post-inserted PEG increased two-fold the AUC of administered PTX i.v. and four-fold per os. However, the specific PK/PD relationship of the LNCs did not associate improved efficacy to this increased drug exposure[355]. Finally, to give the availability to load siRNA into LNCs, chitosan coating was obtained by the transacylation of the Solutol®[359].

In summary, a review of LNC development demonstrated that they were able to encapsulate and keep a wide number of active molecules, reducing their toxicity in vivo. However, the current use of parenteral LNC has not reached *in vivo* sufficient activity to enter clinical development.

V. CELL TARGETING BY LIPIDIC NANOPARTICLES

V.1. INTRODUCTION TO CELL TARGETING CONCEPT

V.1.1. Principles

Targeted nanomedicine has been the "magic bullet" dream of nanoscale drug delivery systems[360,361]. The objective of NPs is not anymore to increase drug circulation time and attain passively diseased tissue, but to actively recognize, bind, and be taken up by the targeted cell population. Specific cell targeting is achieved by the attachment of a ligand at the surface of a nanoparticle. This ligand molecule should recognize in a selective or specific manner another molecule, like a receptor, present in the targeted cells. Lipidic nanoparticles (LNPs) appear as an advantageous choice compared to polymeric or organic NPs due to the lipid membrane fluidity allowing ligand diffusion and the capacity to fuse with the cell membrane[362].

V.1.2. The clinical needs of targeted nanomedicines

The nanomedicine field has taken cancer as its main target for actively targeted NPs. However, targeting would have the ambition to potentially address most of the off-target associated toxicity and lack of efficacy associated to low drug concentration at the cell target place. The challenges and specificities of most organs are described in this recent review[363].

In oncology, a long circulation time together with the EPR effect allow the penetration of NPs into tumors, but it does not cause an increase in tumor intracellular drug bioavailability. This gap may be solved by active uptake, as demonstrated by the immunoliposomes field[364]. Tumor cells over-express a wide range of receptors and may also have specific mutated protein at their surface, constituting as many potential targets. EGFR, folate receptor, transferrin receptors, and $\alpha_v\beta_3$-integrin, among others, are commonly used targets of cancer cells[364]. TME immune, endothelial, or stromal cells are also therapeutic targets, as they express distinct membrane proteins. Their modulation appears essential in the development of immunotherapies, for instance[365]. Finally, targeted NPs have the potential to chase distance sites like metastasis following systemic administration.

Infectious diseases research is also looking after targeted NPs[366]. Viruses particles, as well as infected cells, express specific viral markers. Targeted NPs are developed for human immunodeficiency viruses or other viral diseases. Bacterias and protozoa are also targets in the digestive tract or in blood. Pathogen cells express distinct proteins, making them easier to target.

At the same time, it is also possible to use antibiotic molecules that do not interfere with human biology, making sometimes targeting useless.

Immune modulation is another important area of targeted NPs[367–369]. It may be desirable to activate the immune system with specific antigens, as in vaccination. Antigen presenting cells like dendritic cells are a good target by antigen-bearing NPs. Nanovaccines will benefit from the capacity to group in the same particle several antigens for CD4 and CD8 receptors together with immune adjuvants like danger signals. It will prompt adaptative immune activation. Innate immunity can also be activated by targeting pattern recognition receptors. Finally, tolerogenic NP can inhibit CTLs to reduce autoimmunity.

Other challenges potentially tackled by targeted NPs include brain neurodegenerative diseases, cardiovascular therapies[370], or other organ-specific diseases[363].

V.2. LIGANDS

In the design of targeting LNPs, the choice of the ligand nature is crucial. Antibodies are obvious ligands, as their function is to target a specific antigen. But alternatives also include antibody fragments, nanobodies, other proteins, peptides, aptamers, oligonucleotides, and small molecules like folic acid or carbohydrates[371,372]. Each ligand has its pros and cons (Table 10) and a particular ligand should be selected according to the targeted cells and the LNP, of course, but also to the range of molecules available.

Plenty of antibodies have been developed against the main pathogenic antigens, but their size is inconvenient. Smaller fragments and derived protein have been developed, to replace full-size antibodies. Peptides can recognize specific receptors such as integrins with arginine-glycine-aspartate peptide (RGD), or improving selective or unselective cell penetration when they are positively charged (CPP). Aptamers are short single-strand nucleic acid sequences, more sensitive and specific to their selected antigen than antibody, heat-stable and non-immunogenic. Polymer ligands are mainly represented by HA, targeting CD44 receptor overexpressed by many cancer cells. Finally, small molecules include sugars, like mannose against dendritic cells, or folate used for cancer targeting.

Table 10. Targeting ligands for LNPs (non exhaustive list)

Ligand (example)	Size	Advantages	Disadvantages
Proteins			
Antibody (Trastuzumab, Rituximab)	150 kDa	Available for a large range of antigens, selectivity improvement by protein evolution[373,374], good specificity	Large, unstable, immunogenic, need of proper orientation
Fab[375]	50 kDa	Vs antibodies, smaller, more stable, less immunogenic, same targeting capacity	
scFv[376]	25 kDa		
Nanobody[377]	12-15 kDa		
Affitin/affibody[378]	<10 kDa		
Transferrin	80 kDa	-	
Peptides[372]			
RGD[379], CPP (R6H4[380] TAT[381])	350 Da 1.5 kDa 1.6 kDa	Vs proteins, smaller, more stable, modulable immunogenicity (endogenous vs non-endogenous), easier production	Limited colloidal stability
Aptamers[372]			
AS1411[382], Transferrin receptor targeting	10 kDa	Very high affinity and specificity heat-stable, non-immunogenic, nucleic acid chemistry	Faster biodegradability
Polymers			
HA[383]	5-1500 kDa	Adjustable size and density	Limited targets
Small molecules[372,384]			
Mannose Folate	180 Da 441 Da	Vs macromolecules, more stable	Low choice, limited targets

CPP: Cell-penetrating peptide; Fab: Fragment antigen-binding; HA: Hyaluronic acid; scFv: Single-chain variable fragment

V.3. LIGAND GRAFTING TECHNIQUES

V.3.1. Non-covalent grafting

Targeting ligands must be associated with effective techniques to the surface of LNPs. Grafting must: i) keep the integrity and functionality of the ligand as well as of the LNP, ii) expose the ligand at the surface of the particle, and iii) preserve the ligand affinity for its target. Ideally, the conjugation should also i) be stereospecific to control the localization of the conjugation on the ligand; ii) be stable over the blood circulation time; iii) be well reproduced and scalable, iv) be efficient, to provide a high yield and thus limit costs[375]. The methods used to graft targeting ligands on liposomes have been reviewed in 2004[385]. In this section, we will focus on the progress of the last 10 years.

Table 11. Non-covalent grafting techniques

Technique	Ligands	Advantages	Disadvantages
Lipid anchor integration			
During nanoparticle formation	Folate[386], aptamer[382], peptide[387], mannose[388]	No additional step, stable	Not compatible with large ligands (proteins)
Post-insertion of the ligand with the anchor	Antibody[389], scFv[390,391], protein[392]	Stable	Additional step, heating
Ionic interaction			
Electrostatic interaction	HA+CPP[380], HA[393], CPP[394], antibody[395]	Simplest	Weak interaction, risk of dissociation, toxicity & clearance associated to positive charge
NTA chelation	Peptide[396], protein[397]	Spontaneous	Unstable, His-tag ligand
Co^{II}-porphyrin chelation	Protein[398]	More stable than NTA	His-tag ligand
Biological interaction			
Folate binding Biotin-strepatvidin	Antibody[399] Antibody[400]	Specific and stable interaction, mild conditions	Modified ligand

His-tag: Polyhistidine-tagged; NTA: Nitrilotriacetic acid

LNPs do not usually present reactive groups at their surface and do not support organic solvents after being formulated. Also, chemical reactions add some complexity and a risk of destabilization of the NPs. Therefore, non-covalent techniques have been developed to decorate LNP with targeting ligands, using mostly physical or biological forces (Figure 17, Table 11).

A common non-covalent attachment is the integration of a lipid anchor into the LNP during the formulation. This lipid anchor is often previously coupled with a polymer like PEG as a spacer with a terminal reactive group to react with the ligand[401]. Such lipid anchors include i) phospholipids, with the most popular 1,2-distearoyl-sn-glycero-3-phosphatidylethanolamine (DSPE)[389,402]; ii) cholesterol[382,402]; or iii) single fat chain, like stearate[403,404] (Figure 17a). Cholesterol-anchored conjugates have been described as less stable in the blood, due to their high hydrophobicity[364,405]; therefore, PE appears as the best lipid anchor choice.

Alternatively, miscellaneous lipid anchors can be post-inserted once the LNP has been formed. The post-insertion of micelles into LNP is time, temperature, and lipid concentration dependent[365,406]. Optimized conditions can be selected based on the temperature stability of the ligand, and comparison of different ligand/lipid ratios[365]. Post-insertion is mainly used for liposomes[389,392,407], but it has been adapted with success to phospholipids nanomicelles[408], lipid-

coated polystyrene NPs[409], LNCs[410], or exosomes using sonication to increase the efficacy of the post-insertion[411].

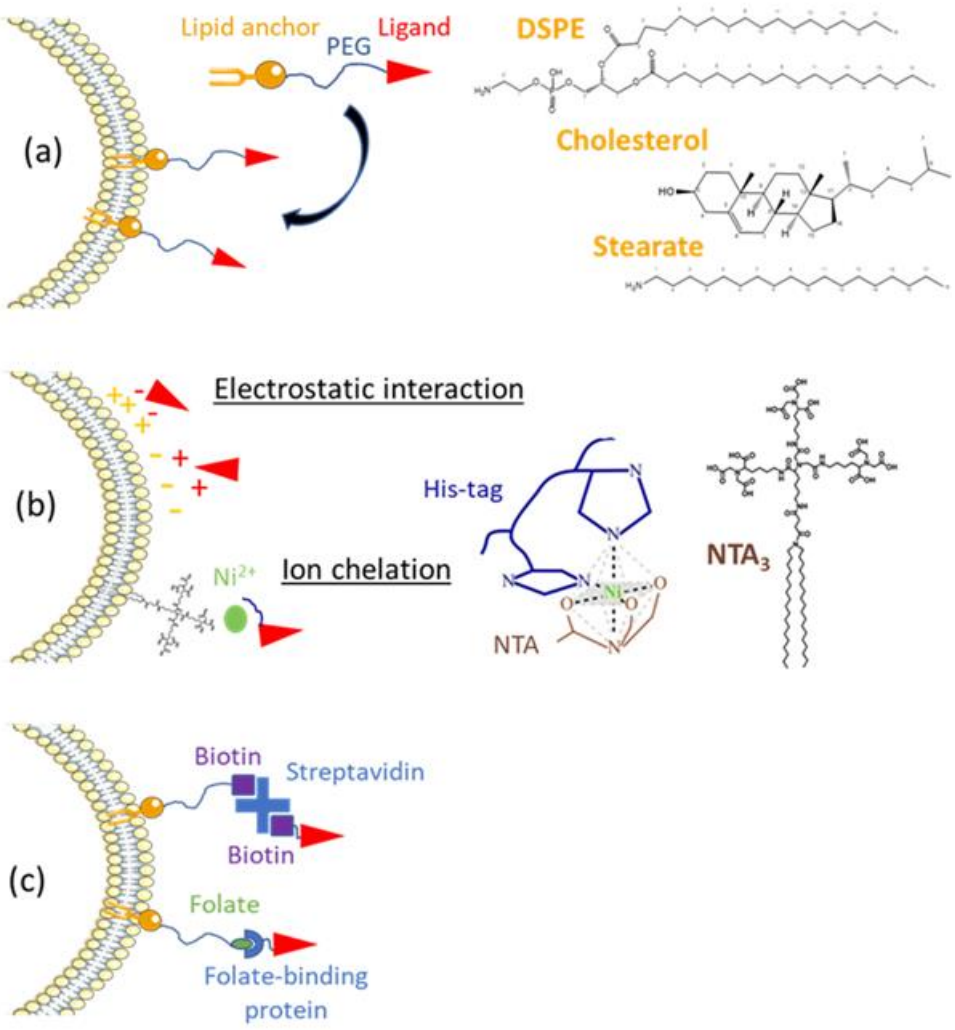

Figure 17. Non-covalent coupling methods. (a) Lipid anchor inserted in the membrane during formulation or by post-insertion and examples of lipid anchors. (b) Ionic interaction by electrostatic or NTA-Nickel-polyhistidine-tag (His-tag) chelation. (c) Biological interaction by streptavidin-biotin or folate-folate binding protein.

Ionic interactions have been used to adsorb targeting ligands at LNP surface. It includes electrostatic adsorption and chelation. Ionic interactions are quite weak and biological media can promote the ionic assembly dissociation or ion exchange[395]. Therefore, multiple ionic interactions are needed. The objective is to complex a charged NP with an oppositely charged ligand. It is the simplest method when it is feasible, as it does not need any chemical reaction. The ζ-potential measures the surface electric charges on a nanoparticle. By default, LNPs have a slightly to highly negative surface charge[380,394]. It is possible therefore to adsorb a positively charged ligand like a CPP. Another strategy is to add a cationic lipid surfactant in the formulation to produce positively

charged nanosystems that can then interact with a negatively charged ligand[393,412]. As a drawback, cationic nanoparticles can be toxic and quickly cleared from the blood compartment[380,413]. Therefore, it is important to neutralize the surface charge of cationic LNPs before using it for i.v. administration.

Ionic interactions can also be used for chelating strategies. It is indeed possible to create a stable noncovalent binding between nitrilotriacetic acid (NTA), nickel$^{(II)}$, and a His-tag coupled to the targeting ligand, by aqueous incubation at room temperature[414]. However, it has been shown that after i.v. administration Ni-based chelation was unstable and that associated ligand was lost by competition with endogenous proteins or nickel was removed by endogenous chelators[398,414]. Ni-NTA has been thus replaced by porphyrin-phospholipid which created a metallo-porphyrin-phospholipid bilayer in the presence of Cobalt$^{(II)}$ ions, resulting in a more stable binding with His-tag proteins[398]. Alternatively, His-tag chelation can be used as an intermediate for a subsequent covalent coupling, improving the final coupling yield by spatial interaction[415].

Biological interactions can also be used for non-covalent coupling of ligands. The advantages are that the conjugation happens in physiological medium, with good specificity. The biological interaction with the most affinity is between biotin and streptavidin.

The last technique which not requires chemical reaction is gene engineering: natural membrane vesicle exosomes can be produced with a previous transfection of the exosome producing cells by a vector associating lamp2b, an exosomal membrane protein, with the desired targeting peptide[416,417]. The produced exosomes have then targeting ligand at their surface without the need for further modifications.

V.3.2. Covalent grafting

Non-covalent grafting offers several advantages as described, but the link it creates can be less stable and versatile than covalent coupling[371,401]. A covalent link is most often the result of a reaction between the ligand and a head reactive group at the end of a PEGylated lipid[371]. To be compatible with fragile ligands, the reaction should be in an aqueous solvent and prevent side-products formation like ligand-ligand or particle-particle association. This significantly reduces the number of chemical reactions that can be used. We consider here the direct covalent coupling between a preformed lipid particle and the targeting ligand, but the same reactions can be used to link the ligand with a lipid polymer before formulation or post-insertion[371] (Table 12).

Amide-bond coupling between an amine and a carboxylic group is one of the most popular techniques used to form a covalent link between a ligand and an LNP. It is used for NPs showing

either carboxylate or amine moieties[418]. P*ara*-nitrophenylcarbonyl group can also be added in the formulation to react with primary amines in an aqueous buffer between pH 8 and 9.5. It does not need any adjuvant molecule or condition except the pH change[419].

Forming a thioether bond is also a popular way to attach a targeting ligand. Usually, a linker bearing a maleimide group reacts specifically with thiols in the pH range of 6.5-7.5 by a Michel addition[418]. The ligand must have a thiol group, that can be a cysteine or obtained by thiolation using Traut's reagent, also called 2-iminothiolane. It is is a cyclic imidothioester that can react with primary amines at pH 7-10 in a ring-opening reaction to exhibit a free sulfhydryl group[375]. N-succinimidyl 3-(2-pyridyldithio)propionate can also be used for adding the thiol group. Its N-succinimidyl part reacts with amine groups, whereas its pyridyldithiopropionate moiety can be reduced in thiol by tris(2-carboxyethyl) phosphine hydrochloride or dithiothreitol. Once the ligand has reacted with the maleimide moiety, it is advised to block remaining maleimide groups by the addition of cysteine[420].

Table 12. Covalent grafting techniques

Bond type	Technique	Examples	Advantages	Disadvantages
Cyanuric	Cyanuric chloride	Protein[421]	Selectivity, no derivatization	Potential toxicity, need basic pH≥9
Amide	EDC/sNHS	Small molecule[422], peptide[423], antibody[424], HA[425]	Common reactive groups: amine and carboxylate	Two steps, no stereoselectivity, low yield, adjuvants
Amide	pNP	Antibody[426]	Basic pH-specific, good yield, no adjuvant, hydrolysis of unreacted pNP	
Cross-linker	DSC	Antibody[427]		Homobifunctional
Isothiourea	Isothiocyanate-amine	Mannose[388]		
Secondary amine	Schiff's base	Mannose[428], antibody[429]	Common reactive groups: amide and amine (2 amines with glutaraldehyde[401])	No stereoselectivity
Cross-linker	SM(PEG)	Peptides or antibody[430]	Heterobifunctional	
Thioether	Thiol-maleimide	Peptide[431], Fab'[432], antibody[420]	Orthogonal, neutral pH-specific	Need of a thiol group (can be added)
Triazole	SPAAC	Protein[433], peptide[415]	Orthogonal, yield	Specific moieties (cyclooctyne and azide)

DSC: N,N'-Disuccinimidyl Carbonate; EDC: 1-ethyl-3-(3-dimethylaminopropyl)carbodiimide; sNHS: sulfo-N-hydroxysuccinimide; pNP: Para-nitrophenycarbonyl; SM(PEG): succinimidyl-[(N-maleimidopropionamido)-tetracosaethyleneglycol] ester; SPAAC: copper-free strain-promoted cycloalkyne−azide cycloaddition.

Another strategy is to use a crosslinker agent, that will successively bind to both LNP and ligand thanks to 2 adapted reactive groups. The crosslinker agent can be homobifunctional or heterobifunctional. The latter option has the advantage to prevent homologous ligations between two lipid nanoparticles or ligands. A very wide choice of commercial crosslinker agent is available[375].

The formation of a Schiff's base between an amine and an aldehyde group can also be used to produce a secondary amine bond[428]. The same reaction can be performed using glutaraldehyde to create 2 Schiff's bases bonding between amine moieties of the LNP and the ligand[401].

Stable triazole bonding is obtained by click chemistry with copper-free strain-promoted cycloalkyne−azide cycloaddition based on Cu(I)-catalyzed Huisgen 1,3-dipolar cycloaddition of azides to terminal alkynes. In aqueous medium, this reaction is orthogonal against other biological functional groups and shows a good yield.

Finally, cyanuric chloride is a reagent with 3 aromatic chlorides that can react by nucleophilic substitution at basic pH. Each substitution requires specific temperature and time conditions, allowing selectivity. No derivatization is necessary and unmodified protein will be coupled by its nucleophilic amino-acids[375].

Other techniques like disulfide bond or hydrazone bond formation have been used in the past, but not in our literature review of the last 10 years. The disulfide bond is unstable in reducing and acidic environments[434], and hydrazone is also sensitive to hydrolysis[375].

V.4. PURIFICATION AND CHARACTERIZATION OF TARGETED LNP

Different techniques have been used to separate the final targeted LNP from unbound ligands (Table 13), and to validate and quantify bound ligands (Table 14).

V.4.1. Purification

Most of the coupling reactions leave some unbound ligands, potentially responsible for competition with grafted ligands for the targeted sites or increased immune reactions. This is likely a crucial step in the preparation of targeted NPs, that can be challenging and have a considerable impact on the final product, but surprisingly, most articles reviewed for this work do not mention if and how they purify free ligands.

Size exclusion chromatography (SEC) and gel filtration are common purification techniques. They allow a quick and efficient separation and recovery of NPs. Sephadex G-50 has been used to

remove small ligands from liposome or exosome while Sepharose CL-4B has been used to remove bigger ligands like antibodies from LNC or liposomes.

Table 13. Purification techniques of targeted lipidic nanoparticles

Technique	Advantages	Disadvantages	Ligands
SEC	Fast, effective, robust	Complexity, sample dilution (≥x2), cost	Post-insertion micelle[365,389], protein[410,435], peptide[396,431], small molecule[436], polymer[412]
Dialysis	No dilution	Slow (days), risk of drug release	Post-insertion micelle[437,438], protein[424,426], peptide[439], small molecule[428], polymer[425]
Ultracentri-fugation	Simple, LNP concentration	Not applicable to all LNPs	Post-insertion micelle[409], protein[395,422], peptide[430,440], small molecule[422]
Ultrafiltration	LNP concentration, unbound ligands dosage allowed	Risk of LNP partial loss	protein[420,441], peptide[394,440], aptamer[382]

Dialysis is also commonly used to remove unbound ligands. The molecular weight cut-off can be adapted to the size of the ligand. A small cut-off was used to remove free HA[425] or peptides[401,439] from liposomes and SLN, while for antibodies, higher cut-offs of 100, 300, or 1,000 kDa were used[265,424].

Ultra-centrifugation is a very simple technique for purification and concentration of NPs. Unfortunately, not all LNPs tolerate ultracentrifugation. LNCs, for instance, are less dense than water due to their oily core and destroyed by centrifugation. Most liposomes tolerate ultracentrifugation, with described cycles of 5,900 g 5 min to 100,000 g 45 min[395,422]. Hybrid nanoparticles with a lipidic membrane handle centrifugation well[409,430].

Ultrafiltration uses centrifugation forces often much lower than ultracentrifugation (below 5,000 g). With an adapted cut-off, ultrafiltration is efficient and compatible with all NPs, with the limit of LNP recovery that may be impaired by particle adhesion to the ultrafiltration membranes.

V.4.2. Characterization of targeted LNPs

The final step of targeted LNP formulation is the characterization of their physicochemical properties, the validation of the ligand presence at the nanoparticle surface and if possible, its quantification. This last step is not always described in the papers we reviewed for this work. Several complementary methods are often used to characterize targeted LNPs (Table 14).

V.4.2.1. NP physicochemical properties

Size measurement is the first analysis performed on NPs. Dynamic light scattering is the most common method for NP size determination, but it is also available from electron microscopy or nanoparticle tracking analysis. The effect of ligand grafting on nanoparticle size is highly variable. LNP hydrodynamic diameter, taking into account the coated solvent layer, can slightly increase after the post-insertion of PEGylated ligands, depending on the number of inserted ligands, the presence of a polymer corona, and this polymer molecular weight[383,411,425]. However, grafting of small molecules[403,422], aptamer[382], peptides[431,442], or antibodies[420,422] generally does not increase the size of the LNPs, even if occasionally a slight increase of 5-15nm with mannose coating[428], anchor peptides[440], or CPPs[394], and of 15-30 nm with antibodies[389,395] has been reported.

Impact of surface charge (ζ potential) depends on the ligand charge and grafting reaction. For most cases, a significant change can be observed[382,433].

Transmission Electronic microscopy (TEM) allows direct visualization of the LNPs, giving information on their size, shape, and surface morphology. Coating with HA has the shape of fluffy dark structures under TEM[383]. Ligands can also present a different contrast due to a changed bilayer structure[412,443]. However, TEM is useless to visualize antibodies[420,424]. Scanning Electron microscopy can also unveil the HA coating, with a flower-like shape on the particle[425]. Atomic Force Microscopy is also used for the characterization of liposome and nanostructured lipid carrier[422,442].

V.4.2.2. Detection and quantification of ligands on NP surface

Absorbance and fluorescence spectroscopies are commonly used to quantify ligands as many biological molecules absorb in ultraviolet (i.e. peptides via tryptophan[431] or aptamers[382]). Unfortunately, antibody concentration is often too low to allow absorbance detection. Spectroscopy based on X-ray photon allows the detection of specific atoms like nitrogen, in the case of this atom is present specifically in the ligand and not on the LNP surface[403]. Infrared spectroscopy can also be used to detect new chemical groups[428]. If the ligand is labelled with a fluorescent dye, FACS can be used with the advantage to quantify the proportion of ligand-grafted LNPs[440]. However, FACS does not work properly with particles with a size below 300 nm.

Table 14. Characterization techniques of targeted LBN

Technique	Advantages	Disadvantages	Ligands
Physico-chemical characterization			
Dynamic light scattering	Checking NP integrity	No or low impact of grafting	Protein[389,395], peptide[394,440], small molecule[428], polymer[383,411]
NP tracking analysis			Peptide[416]
Surface charge (ζ)	Visible changes after grafting	Salinity and pH artefacts	Protein[395,444], peptide[387,394], aptamer[382], small molecule[388,428], polymer[383,411]
Electronic microscopy	Direct visualization,	Cost, no or low impact of grafting	Protein[420,424], small molecule[428], polymer[383,425]
Atomic force microscopy		No impact of grafting except for polymers	Protein[422], peptide[442], small molecule[422]
Ligand detection & quantification			
Absorbance / fluorescence spectroscopy	Sensitivity (fluorescence), fluorescent dye	Sensitivity (absorbance), limited applicability	Peptide[431,436], aptamer[382]
X-ray photon spectroscopy	High sensitivity	Not quantitative, limited applicability	Small molecule[403] polymers[383]
Infrared spectroscopy		Not quantitative, limited applicability	Small molecule[428]
FACS	Quantitative, signal for each particle	not for particles <300 nm	Peptide[440]
(micro)BCA		Interferences with lipids	Protein[426,441], peptide[394]
Bradford		Interferences with lipids	Protein[422]
CBQCA	High sensitivity, no interference with lipids		Protein[395]
Fluorescamine	No interference with lipids	Low sensitivity	Peptide[368]
SDS electrophoresis gel	Purification & characterization	Semi-quantitative, destructive	Protein[389,432], peptide[430]
Western blot	Purification & characterization	Semi-quantitative, limited applicability	Protein[433], peptide[417]
FRET-electrophoretic mobility shift assay	Purification & characterization	Low applicability	peptide[398]
(U/H)PLC		Applicable only to small ligands, indirect measure (unbound ligand)	Peptide[415,431], small molecule[422,433]
Microbead assay	Direct information on ligand density	complex	Protein[424]
^{3}H-assay	quantitative	radioactivity	Polymer[425]

CBQCA: 3-(4-carboxybenzoyl)quinoline-2-carboxaldehyde; FRET : Förster resonance energy transfer

Amine quantification by colorimetric assays is used to quantify the percentage of bound or unbound ligand to the NPs providing that the NP itself does not react with the test reagent. Indeed, bicinchoninic acid (BCA) assay[426,432,445] and Bradford assay[395] have been used to quantify proteins grafted at LNP surface, but can't be used with LNC, for instance, due to a strong interaction with the assay reagents. Alternatively, (3-(4-carboxybenzoyl)quinoline-2-carboxaldehyde) (CBQCA) assay and amine quantification via fluorescamine can be used. BCA assay is very sensitive to lipids and surfactants, CBQCA is very sensitive, down to 10 ng/ml[446], whereas micro-BCA is limited at 500 ng/mL[422]. The fluorescamine fluorometric assay does not interfere with other components like lipids, but it lacks precision[368].

Peptides and protein ligands can also be detected, and even quantified, by electrophoresis techniques. LNP electrophoresis allows the separation and detection of any remaining unbound ligand[432]. Associated with a curve of calibration and image analysis, quantification is also possible[389,430]. Western blot can also be used to detect specific proteins at NP surface[433]. Alvarez-Erviti et al. separated targeted exosomes from their unbound ligand using beads grafted antibodies against the ligand, then performed a western blot for semi-quantification[417]. Finally, the association of electrophoretic mobility shift assay with Förster resonance energy transfer has been used for a fusion peptide inserted on a liposome, by metal complexation with its His-tag tail[398]. Liposomes were separated from the free peptide by electrophoretic mobility shift assay, then two excitation wavelengths allowed distinguishing the free peptide by its FRET emission, and the coupled peptide to whom FRET emission was inhibited by the lipid membrane.

For smaller ligands, like peptides and small molecules, ultra or high-performance liquid chromatography (HPLC) are used to quantify unbound ligands[422,431]. Large proteins like antibodies are not suitable for ultraviolet-associated chromatography due to a lack of sensitivity.

A microbead assay was used to inform on the surface density of antibody-grafted liposomes[424]. It was obtained by comparison between reference microbeads containing a defined antibody density and the liposomes encapsulated by microbeads that reacted with the ligand. Giving the importance of ligand density on targeting ability[447], more techniques should follow this example. The impact of post-insertion on LNP membrane fluidity can be studied using BODIPY-PC compound, followed by fluorescence polarization measurements[411]. Finally, tritium (^{3}H)-labelled molecules can also be used to quantify the number of ligands in a formulation[425].

V.4.2.3. Evaluation of LNP targeting ability

Once the presence of the ligand at the NP surface has been confirmed, its targeting activity has to be validated in a biological model (mainly *in vitro* but also *in vivo*). Most techniques need fluorescent-labeled LNPs incorporating a lipophilic tracer or a fluorescent cargo in the formulation. The first step is mostly always an incubation of the LNP with the targeted cell or receptor, in general for a duration of 1 h to 24 h. The techniques used to quantify the percentage of NPs associated with the cells vary and are summarized below.

FACS provides relatively accurate cell numbers but requires that adherent cells are detached[388,426]. Confocal microscopy allows localizing NPs in the cells and can be associated with endosome and Golgi markers to study LNP trafficking[411,444]. The quantification is harder than by FACS but the two techniques can provide complementary information. It is also possible to quantify cell uptake in a 3D spheroid model by FACS and confocal microscopy[386]. Direct plate absorbance or fluorescence reading is also possible either with cell-cultured[390,411] or with immobilized targeted receptors in the wells[416].

Alternatively, targeting activity of LNPs can be measured without using fluorescence dye. Surface plasmon resonance analysis measures the binding kinetic of targeted LNPs to receptors coated on a Biacore sensor chip[390,426]. Finally, the cell uptake can be investigated by HPLC, by quantifying the drug from the cell lysate[441].

In vivo targeting analysis brings high-value information about the real comportment of targeted LNPs in a living organism. It is possible to follow targeted LNPs fate using an in vivo fluorescent imaging system (i.e. IVIS). Longitudinal quantification can be done on the whole animal or separated organs[395,427]. Blood samples can also be analyzed for PK modelization[426]. Targeted LNP localization and association with the targeted cell type can also be assessed by immunofluorescence[411].

V.5. CURRENT LIMITS AND CHALLENGES OF CELL ACTIVE TARGETING

Despite the almost 40 years of research on the targeting of NPs, none of them has been approved for clinical application yet. And the recent improvements would not be able to translate as such in the clinics. It appears that the ligand targeting strategy faces many challenges. The whole paradigm of ligand targeting might be challenged, as comparative works have shown that most targeted liposomes have limited penetration efficiency in reaching the target site, with the liver being still the first organ where materials accumulate[372]. Meta-analysis comparing active versus passive targeting shows a non-significant delivery efficiency improvement in the tumor, growing from 0.6% to 0.9% of the injected dose[448,449].

Ligand targeting has been based on a simplified vision of targeted NPs acting as targeted missiles. In the reality of living organisms, targeted nanocarriers, from the point-of-injection to the point-of-action, have to cross several barriers of distinct scale: i) systemic distribution through blood vessels, ii) vascular extravasation to the targeted organs, iii) tissue diffusion to the targeted cells[450], and iv) cell uptake and cellular trafficking machinery processing. The rate-limiting steps seem to be vascular extravasation and the tissue microenvironment for tumors[450,451]. It has been shown that cell targeting mainly helps the NP fate once the targeted tissue is attained. However, this targeting capacity can be lost during circulation in the blood due to the protein corona adhesion[450,452]. Besides, once into the tumor tissue, high-affinity ligand drives a fast cell-binding that prevents NP diffusion within the tissue[453].

The future of nanomedicine targeting has to deal with simple and robust solutions into complex biological modeling. Fundamental research has to be performed concerning the biological fate of targeted LNPs. Physicochemical analysis of the targeted NPs interactions with its biological environment should be studied more thoroughly. Innovative approaches like computational modeling should help. The use of mathematical or computational multiscale modeling, taking into account the whole body, organ, tissue, and cell interactions, could facilitate the focus on the entire process of targeted drug delivery[453].

Nanomedicine design should be improved towards smart particles, taking into account the different steps of targeted NP travel through optimizing ligand localization and availability to interactions for instance[451]. Its design should improve *in vivo* stability and PK, reduce circulation loss and off-target effects, play with cellular trafficking to direct efficient endosome release or escape depending on the cargo sensitivity. Quantifying the nanotoxicity of target tissues must routinely be implemented within an investigational workflow. This will improve the translational potential of nanotechnology more than adding new proofs-of-concept with fancy nanomaterials

or disease models with little to no therapeutic benefit [372]. Finally, the scale-up of such smart particles should be envisioned from the beginning of the material design.

To end this chapter on cell-specific targeting, it is worth noting that alternatives to ligand-associated targeting exist. It could be a short-term solution for the challenges associated with ligand coating. The main constituents of an LNP can help to selectively deliver its cargo to a targeted population. For instance, cholesterol-based nanostructured lipid carriers have selectivity towards over-expressing LDL-receptors cells, such as some tumor cells [454]. In this case, cholesterol is not exposed at the surface but constitutes 60% of the nanostructured lipid carrier excipients. The same LDL-receptor has been used recently in an elegant study where squalene-based nanoparticles were designed to interact with lipoprotein and to be carried by LDL towards tumors[455]. Therefore, there is for sure a place for innovative strategies for tissue and cell targeting.

VI. REFERENCES

1. Bray, F. *et al.* Global cancer statistics 2018: GLOBOCAN estimates of incidence and mortality worldwide for 36 cancers in 185 countries. *CA. Cancer J. Clin.* **68**, 394–424 (2018).

2. American Cancer Society. Colorectal Cancer Stages. (2018). Available at: https://www.cancer.org/cancer/colon-rectal-cancer/detection-diagnosis-staging/staged.html.

3. Davis, L. E., Sun, W. & Medina, P. J. Pharmacotherapy: a Pathophysiologic Approach, Ninth Edition: Chapter 107. Colorectal Cancer. *Access Pharm.* (2014).

4. Los Angeles Colon and Rectal surgical Associates (institution). colon cancer survival rates by stages. (2013). Available at: https://colon90210.com/blog/colon-cancer-survival-rates-stages.

5. Benson, A. B. *et al.* NCCN Guidelines ® Insights Colon Cancer, Version 2.2018 Featured Updates to the NCCN Guidelines. *JNCCN J. Natl. Compr. Cancer Netw.* **16**, 359–369 (2018).

6. American Cancer Society. Survival Rates for Colorectal Cancer. (2018). Available at: https://www.cancer.org/cancer/colon-rectal-cancer/detection-diagnosis-staging/survival-rates.html.

7. Guinney, J. *et al.* The consensus molecular subtypes of colorectal cancer. *Nat. Med.* **21**, 1350–1356 (2015).

8. Colangelo, T. *et al.* Friend or foe?: The tumour microenvironment dilemma in colorectal cancer. *Biochim. Biophys. Acta - Rev. Cancer* **1867**, 1–18 (2017).

9. Becht, E. *et al.* Immune and stromal classification of Colorectal cancer is associated with molecular subtypes and relevant for precision immunotherapy. *Clin. Cancer Res.* **22**, 4057–4066 (2016).

10. Mojarad, E. N., Kuppen, P. J. K., Aghdaei, H. A. & Zali, M. R. The CpG island methylator phenotype (CIMP) in colorectal cancer. *Gastroenterol. Hepatol. from Bed to Bench* **6**, 120–128 (2013).

11. Battaglin, F., Naseem, M., Lenz, H.-J. & Salem, M. E. Microsatellite instability in colorectal cancer: overview of its clinical significance and novel perspectives. *Clin. Adv. Hematol. Oncol.* **16**, 735–745 (2018).

12. Pino, M. S. & Chung, D. C. The Chromosomal Instability Pathway in Colon Cancer. *Gastroenterology* **138**, 2059–2072 (2010).

13. Schatoff, E. M., Leach, B. I. & Dow, L. E. WNT Signaling and Colorectal Cancer. *Curr. Colorectal Cancer Rep.* **13**, 101–110 (2017).

14. Hong, S. N. Genetic and epigenetic alterations of colorectal cancer. *Intest. Res.* **16**, 327 (2018).

15. Villalba, M., Evans, S. R., Vidal-Vanaclocha, F. & Calvo, A. Role of TGF-β in metastatic colon cancer: it is finally time for targeted therapy. *Cell Tissue Res.* **370**, 29–39 (2017).

16. Smeby, J. *et al.* CMS-dependent prognostic impact of KRAS and BRAFV600E mutations in primary colorectal cancer. *Ann. Oncol.* **29**, 1227–1234 (2018).

17. Muzny, D. M. *et al.* Comprehensive molecular characterization of human colon and rectal cancer. *Nature* **487**, 330–337 (2012).

18. Fearon, E. R. & Vogelstein, B. A genetic model for colorectal tumorigenesis. *Cell* **61**, 759–767 (1990).

19. Elbadawy, M., Usui, T., Yamawaki, H. & Sasaki, K. Emerging Roles of C-Myc in Cancer Stem Cell-Related Signaling and Resistance to Cancer Chemotherapy: A Potential Therapeutic Target Against Colorectal Cancer. *Int. J. Mol. Sci.* **20**, 2340 (2019).

20. Miller, D. M., Thomas, S. D., Islam, A., Muench, D. & Sedoris, K. c-Myc and cancer metabolism. *Clin. Cancer Res.* **18**, 5546–5553 (2012).

21. Patel, J. H., Loboda, A. P., Showe, M. K., Showe, L. C. & McMahon, S. B. Analysis of genomic targets reveals complex functions of MYC. *Nat. Rev. Cancer* **4**, 562–568 (2004).

22. Qiao, L. & Wong, B. C. Y. Role of notch signaling in colorectal cancer. *Carcinogenesis* **30**, 1979–1986 (2009).

23. Zhang, X., Ge, Y. L. & Tian, R. H. The knockdown of c-myc expression by RNAi inhibits cell proliferation in human colon cancer HT-29 cells in vitro and in vivo. *Cell. Mol. Biol. Lett.* **14**, 305–318 (2009).

24. Zhang, H. Le, Wang, P., Lu, M. Z., Zhang, S. D. & Zheng, L. c-Myc maintains the self-renewal and chemoresistance properties of colon cancer stem cells. *Oncol. Lett.* **17**, 4487–4493 (2019).

25. Gabay, M., Li, Y. & Felsher, D. W. MYC activation is a hallmark of cancer initiation and maintenance. *Cold Spring Harb. Perspect. Med.* **4**, 1–14 (2014).

26. Chen, C. *et al.* C-Myc enhances colon cancer cell-mediated angiogenesis through the regulation of HIF-1α. *Biochem. Biophys. Res. Commun.* **430**, 505–511 (2013).

27. Kortlever, R. M. *et al.* Myc Cooperates with Ras by Programming Inflammation and Immune Suppression. *Cell* **171**, 1301-1315.e14 (2017).

28. Delmore, J. E. *et al.* BET bromodomain inhibition as a therapeutic strategy to target c-Myc. *Cell* **146**, 904–917 (2011).

29. Lovén, J. *et al.* Selective inhibition of tumor oncogenes by disruption of super-enhancers. *Cell* **153**, 320–334 (2013).

30. Tögel, L. *et al.* Dual Targeting of Bromodomain and Extraterminal Domain Proteins, and WNT or MAPK Signaling, Inhibits c-MYC Expression and Proliferation of Colorectal Cancer Cells. *Mol. Cancer Ther.* **15**, 1217–1226 (2016).

31. Filippakopoulos, P. *et al.* Selective inhibition of BET bromodomains. *Nature* **468**, 1067–1073 (2010).

32. Vogel, J. D., Eskicioglu, C., Weiser, M. R., Feingold, D. L. & Steele, S. R. The American society of colon and rectal surgeons clinical practice guidelines for the treatment of colon cancer. *Dis. Colon Rectum* **60**, 999–1017 (2017).

33. Riihimäki, M., Hemminki, A., Sundquist, J. & Hemminki, K. Patterns of metastasis in colon and rectal cancer. *Sci. Rep.* **6**, 29765 (2016).

34. Royce, M. E. *et al.* Colorectal cancer: Chemotherapy treatment overview. *Oncology* **14**, 40–46 (2000).

35. Machover, D. *et al.* Treatment of advanced colorectal and gastric adenocarcinomas with 5-fluorouracil and high-dose folinic acid. *NCI Monogr.* 193–8 (1987).

36. Cutsem, E. Van *et al.* Oral capecitabine vs intravenous 5-fluorouracil and leucovorin: integrated efficacy data and novel analyses from two large, randomised, phase III trials. *Br. J. Cancer* **90**, 1190–1197 (2004).

37. Des Guetz, G. *et al.* Microsatellite instability and sensitivitiy to FOLFOX treatment in metastatic colorectal cancer. *Anticancer Res.* (2007).

38. Fuchs, C. S. *et al.* Randomized, Controlled Trial of Irinotecan Plus Infusional, Bolus, or Oral Fluoropyrimidines in First-Line Treatment of Metastatic Colorectal Cancer: Results From the BICC-C Study. *J. Clin. Oncol.* **25**, 4779–4786 (2007).

39. Colon Cancer Treatment Regimens. *CancerTherapyAdvisor.com* Available at: https://www.cancertherapyadvisor.com/home/cancer-topics/gastrointestinal-cancers/gastrointestinal-cancers-treatment-regimens/colon-cancer-treatment-regimens/. (Accessed: 30th June 2020)

40. Martinelli, E. *et al.* Implementing anti-epidermal growth factor receptor (EGFR) therapy in metastatic colorectal cancer: challenges and future perspectives. *Ann. Oncol.* **31**, 30–40 (2020).

41. Matos, A. I. *et al.* Nanotechnology is an important strategy for combinational innovative chemo-immunotherapies against colorectal cancer. *Journal of Controlled Release* **307**, 108–138 (2019).

42. Sargent, D. *et al.* Evidence for cure by adjuvant therapy in colon cancer: Observations based on individual patient data from 20,898 patients on 18 randomized trials. *J. Clin. Oncol.* **27**, 872–877 (2009).

43. The Meta-Analysis Group in Cancer. Modulation of fluorouracil by leucovorin in patients with advanced colorectal cancer: An updated meta-analysis. *J. Clin. Oncol.* **22**, 3766–3775 (2004).

44. Petrelli, N. *et al.* A prospective randomized trial of 5-fluorouracil versus 5-fluorouracil and high-dose leucovorin versus 5-fluorouracil and methotrexate in previously untreated patients with advanced colorectal carcinoma. *J. Clin. Oncol.* **5**, 1559–1565 (1987).

45. Petrelli, N. *et al.* The Modulation of Fluorouracil With Leucovorin in Metastatic Colorectal Carcinoma: A Prospective Randomized Phase III Trial. *J. Clin. Oncol.* **8**, 185–185 (1990).

46. O'Connell, M. J. A phase III trial of 5-fluorouracil and leucovorin in the treatment of advanced colorectal cancer. A Mayo Clinic/North Central Cancer Treatment Group study. *Cancer* **63**, 1026–30 (1989).

47. Cassidy, J. *et al.* Randomized phase III study of capecitabine plus oxaliplatin compared with fluorouracil/folinic acid plus oxaliplatin as first-line therapy for metastatic colorectal cancer. *J. Clin. Oncol.* **26**, 2006–2012 (2008).

48. Saltz, L. B. *et al.* Irinotecan plus Fluorouracil and Leucovorin for Metastatic Colorectal Cancer. *N. Engl. J. Med.* **343**, 905–914 (2000).

49. Douillard, J. Y. *et al.* Irinotecan combined with fluorouracil compared with fluorouracil alone. as first-line treatment for metastatic colorectal cancer: a multicentre randomised trial. *Lancet* **355**, 1041–1047 (2000).

50. Köhne, C. H. *et al.* Phase III study of weekly high-dose infusional fluorouracil plus folinic acid with or without irinotecan in patients with metastatic colorectal cancer: European Organisation for Research and Treatment of Cancer Gastrointestinal Group Study 40986. *J. Clin. Oncol.* **23**, 4856–4865 (2005).

51. Seymour, M. T. *et al.* Different strategies of sequential and combination chemotherapy for patients with poor prognosis advanced colorectal cancer (MRC FOCUS): a randomised controlled trial. *Lancet* **370**, 143–152 (2007).

52. Grothey, A. *et al.* Phase III study of bolus 5-fluorouracil (5-FU)/ folinic acid (FA) (Mayo) vs weekly high-dose 24h 5-FU infusion/ FA + oxaliplatin (OXA) (FUFOX) in advanced colorectal cancer (ACRC). *Proc Am Soc Clin Oncol* **21**, (A512) (2002).

53. Goldberg, R. M. *et al.* Randomized controlled trial of reduced-dose bolus fluorouracil plus leucovorin and irinotecan or infused fluorouracil plus leucovorin and oxaliplatin in patients with previously untreated metastatic colorectal cancer: A North American intergroup trial. *J. Clin. Oncol.* **24**, 3347–3353 (2006).

54. Tournigand, C. *et al.* FOLFIRI followed by FOLFOX6 or the reverse sequence in advanced colorectal cancer: A randomized GERCOR study. *J. Clin. Oncol.* **22**, 229–237 (2004).

55. Colucci, G. *et al.* Phase III randomized trial of FOLFIRI versus FOLFOX4 in the treatment of advanced colorectal cancer: A Multicenter Study of the Gruppo Oncologico Dell'Italia Meridionale. *J. Clin. Oncol.* **23**, 4866–4875 (2005).

56. Souglakos, J. *et al.* FOLFOXIRI (folinic acid, 5-fluorouracil, oxaliplatin and irinotecan) vs FOLFIRI (folinic acid, 5-fluorouracil and irinotecan) as first-line treatment in metastatic colorectal cancer (MCC): A multicentre randomised phase III trial from the Hellenic Oncolog. *Br. J. Cancer* **94**, 798–805 (2006).

57. Falcone, A. *et al.* Phase III trial of infusional fluorouracil, leucovorin, oxaliplatin, and irinotecan (FOLFOXIRI) compared with infusional fluorouracil, leucovorin, and irinotecan (FOLFIRI) as first-line treatment for metastatic colorectal cancer: The gruppo oncologico nor. *J. Clin. Oncol.* **25**, 1670–1676 (2007).

58. Kalinski, P. *Tumor immune microenvironment in cancer progression and cancer therapy*. **1036**, (Springer International Publishing, 2017).

59. Paget, S. The Distribution of Secondary Growths in Cancer of the Breast. *Lancet* **133**, 571–573 (1889).

60. Bergers, G. & Benjamin, L. E. Tumorigenesis and the angiogenic switch. *Nat. Rev. Cancer* **3**, 401–410 (2003).

61. Fridman, W. H., Miller, I., Sautès-Fridman, C. & Byrne, A. T. Therapeutic Targeting of the Colorectal Tumor Stroma. *Gastroenterology* **158**, 303–321 (2020).

62. Katayama, Y. *et al.* Tumor Neovascularization and Developments in Therapeutics. *Cancers (Basel).* **11**, 316 (2019).

63. Semenza, G. L. Cancer-stromal cell interactions mediated by hypoxia-inducible factors promote angiogenesis, lymphangiogenesis, and metastasis. *Oncogene* **32**, 4057–4063 (2013).

64. Wang, G. *et al.* Quantitative proteomic profiling of tumor-associated vascular endothelial cells in colorectal cancer. *Biol. Open* **8**, bio042838 (2019).

65. Ribeiro, A. L. & Okamoto, O. K. Combined effects of pericytes in the tumor microenvironment. *Stem Cells Int.* **2015**, 1–8 (2015).

66. Meng, M. Bin *et al.* Pericytes: A double-edged sword in cancer therapy. *Futur. Oncol.* **11**, 169–179 (2015).

67. Siegler, E. L., Kim, Y. J. & Wang, P. Nanomedicine targeting the tumor microenvironment: Therapeutic strategies to inhibit angiogenesis, remodel matrix, and modulate immune responses. *J. Cell. Immunother.* **2**, 69–78 (2016).

68. Xu, K. *et al.* Hypoxia Induces Drug Resistance in Colorectal Cancer through the HIF-1α/miR-338-5p/IL-6 Feedback Loop. *Mol. Ther.* **27**, 1810–1824 (2019).

69. Tang, Y.-A. *et al.* Hypoxic tumor microenvironment activates GLI2 via HIF-1α and TGF-β2 to promote chemoresistance in colorectal cancer. *Proc. Natl. Acad. Sci.* **115**, E5990–E5999 (2018).

70. Folkman, J. Tumor Angiogenesis: Therapeutic Implications. *N. Engl. J. Med.* **285**, 1182–1186 (1971).

71. Hurwitz, H. *et al.* Bevacizumab plus irinotecan, fluorouracil, and leucovorin for metastatic colorectal cancer. *N. Engl. J. Med.* **350**, 2335–2342 (2004).

72. Lugano, R., Ramachandran, M. & Dimberg, A. Tumor angiogenesis: causes, consequences, challenges and opportunities. *Cell. Mol. Life Sci.* **77**, 1745–1770 (2020).

73. Rivera, L. B. & Bergers, G. Tumor angiogenesis, from foe to friend. *Science (80-.).* **349**, 694–695 (2015).

74. Calì, B., Molon, B. & Viola, A. Tuning cancer fate: the unremitting role of host immunity. *Open Biol.* **7**, 170006 (2017).

75. Church, S. E. & Galon, J. Regulation of CTL Infiltration Within the Tumor Microenvironment. in *Advances in Experimental Medicine and Biology* 33–49 (2017). doi:10.1007/978-3-319-67577-0_3

76. Weigelin, B., Krause, M. & Friedl, P. Cytotoxic T lymphocyte migration and effector function in the tumor microenvironment. *Immunol. Lett.* **138**, 19–21 (2011).

77. Dobrzanski, M. J. Expanding roles for CD4 T cells and their subpopulations in tumor immunity and therapy. *Front. Oncol.* **3 MAR**, (2013).

78. Kiraz, Y., Baran, Y. & Nalbant, A. T cells in tumor microenvironment. *Tumor Biol.* **37**, 39–45 (2016).

79. Silva-Santos, B., Mensurado, S. & Coffelt, S. B. γδ T cells: pleiotropic immune effectors with therapeutic potential in cancer. *Nat. Rev. Cancer* **19**, 392–404 (2019).

80. Wu, P. *et al.* γδT17 cells promote the accumulation and expansion of myeloid-derived suppressor cells in human colorectal cancer. *Immunity* **40**, 785–800 (2014).

81. Meraviglia, S. *et al.* Distinctive features of tumor-infiltrating γδ T lymphocytes in human colorectal cancer. *Oncoimmunology* **6**, e1347742 (2017).

82. Sarvaria, A., Madrigal, J. A. & Saudemont, A. B cell regulation in cancer and anti-tumor immunity. *Cell. Mol. Immunol.* **14**, 662–674 (2017).

83. Tsou, P., Katayama, H., Ostrin, E. J. & Hanash, S. M. The Emerging Role of B Cells in Tumor Immunity. *Cancer Res.* **76**, 5597–5601 (2016).

84. Berntsson, J., Nodin, B., Eberhard, J., Micke, P. & Jirström, K. Prognostic impact of tumour-infiltrating B cells and plasma cells in colorectal cancer. *Int. J. Cancer* **139**, 1129–1139 (2016).

85. Böttcher, J. P. *et al.* NK Cells Stimulate Recruitment of cDC1 into the Tumor Microenvironment Promoting Cancer Immune Control. *Cell* **172**, 1022-1037.e14 (2018).

86. Dyck, L. & Lynch, L. New Job for NK Cells: Architects of the Tumor Microenvironment. *Immunity* **48**, 9–11 (2018).

87. Bendelac, A., Savage, P. B. & Teyton, L. The Biology of NKT Cells. *Annu. Rev. Immunol.* **25**, 297–336 (2007).

88. Tachibana, T. Increased Intratumor V 24-Positive Natural Killer T Cells: A Prognostic Factor for Primary Colorectal Carcinomas. *Clin. Cancer Res.* **11**, 7322–7327 (2005).

89. Kim, J. & Bae, J. S. Tumor-associated macrophages and neutrophils in tumor microenvironment. *Mediators Inflamm.* **2016**, 1–11 (2016).

90. Xiang, W. *et al.* Monoacylglycerol lipase regulates cannabinoid receptor 2-dependent macrophage activation and cancer progression. *Nat. Commun.* **9**, 2574 (2018).

91. Kumar, V., Patel, S., Tcyganov, E. & Gabrilovich, D. I. The Nature of Myeloid-Derived Suppressor Cells in the Tumor Microenvironment. *Trends Immunol.* **37**, 208–220 (2016).

92. Malfettone, A. *et al.* High density of tryptase-positive mast cells in human colorectal cancer: a poor prognostic factor related to protease-activated receptor 2 expression. *J. Cell. Mol. Med.* **17**, 1025–1037 (2013).

93. Fridlender, Z. G. & Albelda, S. M. Tumor-associated neutrophils: friend or foe? *Carcinogenesis* **33**, 949–955 (2012).

94. Hsu, Y.-L. *et al.* Interaction between Tumor-Associated Dendritic Cells and Colon Cancer Cells Contributes to Tumor Progression via CXCL1. *Int. J. Mol. Sci.* **19**, 2427 (2018).

95. Palucka, K. & Banchereau, J. Cancer immunotherapy via dendritic cells. *Nat. Rev. Cancer* **12**, 265–277 (2012).

96. Zeitoun, G. *et al.* The immunoscore in the clinical practice of patients with colon and rectal cancers. *Chir.* **114**, 152–161 (2019).

97. Galon, J. Type, Density, and Location of Immune Cells Within Human Colorectal Tumors Predict Clinical Outcome. *Science (80-.).* **313**, 1960–1964 (2006).

98. Pagès, F. *et al.* International validation of the consensus Immunoscore for the classification of colon cancer: a prognostic and accuracy study. *Lancet* **391**, 2128–2139 (2018).

99. Mlecnik, B. *et al.* Comprehensive intrametastatic immune quantification and major impact of immunoscore on survival. *J. Natl. Cancer Inst.* **110**, 97–108 (2018).

100. Andre, T. *et al.* Pembrolizumab versus chemotherapy for microsatellite instability-high/mismatch repair deficient metastatic colorectal cancer: The phase 3 KEYNOTE-177 Study. *J. Clin. Oncol.* **38**, LBA4–LBA4 (2020).

101. Kanterman, J. *et al.* Adverse immunoregulatory effects of 5FU and CPT11 chemotherapy on myeloid-derived suppressor cells and colorectal cancer outcomes. *Cancer Res.* **74**, 6022–6035 (2014).

102. Wang, Y.-J., Fletcher, R., Yu, J. & Zhang, L. Immunogenic effects of chemotherapy-induced tumor cell death. *Genes Dis.* **5**, 194–203 (2018).

103. Mukaida, N. & Sasaki, S. Fibroblasts, an inconspicuous but essential player in colon cancer development and progression. *World J. Gastroenterol.* **22**, 5301–5316 (2016).

104. Shi, Y., Du, L., Lin, L. & Wang, Y. Tumour-associated mesenchymal stem/stromal cells: emerging therapeutic targets. *Nat Rev Drug Discov* **16**, 35–52 (2017).

105. Chen, X. & Song, E. Turning foes to friends: targeting cancer-associated fibroblasts. *Nat. Rev. Drug Discov.* **18**, 99–115 (2019).

106. Sahai, E. *et al.* A framework for advancing our understanding of cancer-associated fibroblasts. *Nat. Rev. Cancer* **20**, 174–186 (2020).

107. Liu, T. *et al.* Cancer-associated fibroblasts: An emerging target of anti-cancer immunotherapy. *Journal of Hematology and Oncology* **12**, 1–15 (2019).

108. Santi, A., Kugeratski, F. G. & Zanivan, S. Cancer Associated Fibroblasts: The Architects of Stroma Remodeling. *Proteomics* **18**, 1700167 (2018).

109. Tauriello, D. V. F. *et al.* TGFβ drives immune evasion in genetically reconstituted colon cancer metastasis. *Nature* **554**, 538–543 (2018).

110. Amakye, D., Jagani, Z. & Dorsch, M. Unraveling the therapeutic potential of the Hedgehog pathway in cancer. *Nat. Med.* **19**, 1410–1422 (2013).

111. Gerling, M. *et al.* Stromal Hedgehog signalling is downregulated in colon cancer and its restoration restrains tumour growth. *Nat. Commun.* **7**, 12321 (2016).

112. Sanz-Moreno, V. *et al.* ROCK and JAK1 Signaling Cooperate to Control Actomyosin Contractility in Tumor Cells and Stroma. *Cancer Cell* **20**, 229–245 (2011).

113. Albrengues, J. *et al.* Epigenetic switch drives the conversion of fibroblasts into proinvasive cancer-associated fibroblasts. *Nat. Commun.* **6**, 10204 (2015).

114. Fiori, M. E. *et al.* Cancer-associated fibroblasts as abettors of tumor progression at the crossroads of EMT and therapy resistance. *Mol. Cancer* **18**, 1–16 (2019).

115. Lotti, F. *et al.* Chemotherapy activates cancer-associated fibroblasts to maintain colorectal cancer-initiating cells by IL-17A. *J. Exp. Med.* **210**, 2851–2872 (2013).

116. Li, H. *et al.* Reference component analysis of single-cell transcriptomes elucidates cellular heterogeneity in human colorectal tumors. *Nat. Genet.* **49**, 708–718 (2017).

117. Liu, F. *et al.* Fibroblast activation protein overexpression and clinical implications in solid tumors: A meta-analysis. *PLoS One* **10**, 1–18 (2015).

118. Tsujino, T. *et al.* Stromal myofibroblasts predict disease recurrence for colorectal cancer. *Clin. Cancer Res.* **13**, 2082–2090 (2007).

119. Son, G. M. *et al.* Comparisons of cancer-associated fibroblasts in the intratumoral stroma and invasive front in colorectal cancer. *Med. (United States)* **98**, e15164 (2019).

120. Chen, S.-X. *et al.* Identification of colonic fibroblast secretomes reveals secretory factors regulating colon cancer cell proliferation. *J. Proteomics* **110**, 155–171 (2014).

121. Sandberg, T. P. *et al.* Increased expression of cancer-associated fibroblast markers at the invasive front and its association with tumor-stroma ratio in colorectal cancer. *BMC Cancer* **19**, 1–9 (2019).

122. Nurmik, M., Ullmann, P., Rodriguez, F., Haan, S. & Letellier, E. In search of definitions: Cancer-associated fibroblasts and their markers. *Int. J. Cancer* **146**, 895–905 (2020).

123. Busek, P., Mateu, R., Zubal, M., Kotackova, L. & Sedo, A. Targeting Fibroblast activation protein in cancer - Prospects and caveats. *Front. Biosci. - Landmark* **23**, 1933–1968 (2018).

124. Pena, C. *et al.* STC1 expression by cancer-associated fibroblasts drives metastasis of colorectal cancer. *Cancer Res.* **73**, 1287–1297 (2013).

125. Tommelein, J. *et al.* Cancer-Associated Fibroblasts Connect Metastasis-Promoting Communication in Colorectal Cancer. *Front. Oncol.* **5**, 1–11 (2015).

126. Bar, J. *et al.* Cancer cells suppress p53 in adjacent fibroblasts. *Oncogene* **28**, 933–936 (2009).

127. Ouahoud, S. *et al.* Bidirectional tumor/stroma crosstalk promotes metastasis in mesenchymal colorectal cancer. *Oncogene* **39**, 2453–2466 (2020).

128. Avagliano, A. *et al.* Metabolic Reprogramming of Cancer Associated Fibroblasts: The Slavery of Stromal Fibroblasts. *Biomed Res. Int.* **2018**, 1–12 (2018).

129. Bu, L. *et al.* Biological heterogeneity and versatility of cancer-associated fibroblasts in the tumor microenvironment. *Oncogene* **38**, (2019).

130. Yan, W. *et al.* Cancer-cell-secreted exosomal miR-105 promotes tumour growth through the MYC-dependent metabolic reprogramming of stromal cells. *Nat. Cell Biol.* **20**, 597–609 (2018).

131. De Wever, O. *et al.* Tenascin-C and SF/HGF produced by myofibroblasts in vitro provide convergent proinvasive signals to human colon cancer cells through RhoA and Rac. *FASEB J.* **18**, 1016–1018 (2004).

132. Gieniec, K. A., Butler, L. M., Worthley, D. L. & Woods, S. L. Cancer-associated fibroblasts—heroes or villains? *Br. J. Cancer* **121**, 293–302 (2019).

133. Özdemir, B. C. *et al.* Depletion of carcinoma-associated fibroblasts and fibrosis induces immunosuppression and accelerates pancreas cancer with reduced survival. *Cancer Cell* **25**, 719–734 (2014).

134. Yamanashi, T. *et al.* Podoplanin Expression Identified in Stromal Fibroblasts as a Favorable Prognostic Marker in Patients with Colorectal Carcinoma. *Oncology* **77**, 53–62 (2009).

135. De Jaeghere, E. A., Denys, H. G. & De Wever, O. Fibroblasts Fuel Immune Escape in the Tumor Microenvironment. *Trends in Cancer* **5**, 704–723 (2019).

136. Zhang, R. *et al.* Cancer-associated fibroblasts enhance tumor-associated macrophages enrichment and suppress NK cells function in colorectal cancer. *Cell Death Dis.* **10**, 273 (2019).

137. Chen, L., Qiu, X., Wang, X. & He, J. FAP positive fibroblasts induce immune checkpoint blockade resistance in colorectal cancer via promoting immunosuppression. *Biochem. Biophys. Res. Commun.* **487**, 8–14 (2017).

138. Lakins, M. A., Ghorani, E., Munir, H., Martins, C. P. & Shields, J. D. Cancer-associated fibroblasts induce antigen-specific deletion of CD8 + T Cells to protect tumour cells. *Nat. Commun.* **9**, 948 (2018).

139. Feig, C. *et al.* Targeting CXCL12 from FAP-expressing carcinoma-associated fibroblasts synergizes with anti-PD-L1 immunotherapy in pancreatic cancer. *Proc. Natl. Acad. Sci. U. S. A.* **110**, 20212–20217 (2013).

140. Ma, J. *et al.* Fibroblast-derived CXCL12 regulates PTEN expression and is associated with the proliferation and invasion of colon cancer cells via PI3k/Akt signaling. *Cell Commun. Signal.* **17**, 119 (2019).

141. Orimo, A. *et al.* Stromal Fibroblasts Present in Invasive Human Breast Carcinomas Promote Tumor Growth and Angiogenesis through Elevated SDF-1/CXCL12 Secretion. *Cell* **121**, 335–348 (2005).

142. LeBleu, V. S. & Kalluri, R. A peek into cancer-associated fibroblasts: Origins, functions and translational impact. *DMM Dis. Model. Mech.* **11**, 1–9 (2018).

143. Ziani, L., Chouaib, S. & Thiery, J. Alteration of the antitumor immune response by cancer-associated fibroblasts. *Front. Immunol.* **9**, Article 414 (2018).

144. Hu, J. L. *et al.* CAFs secreted exosomes promote metastasis and chemotherapy resistance by enhancing cell stemness and epithelial-mesenchymal transition in colorectal cancer. *Mol. Cancer* **18**, 1–15 (2019).

145. Hu, Y. *et al.* Fibroblast-Derived Exosomes Contribute to Chemoresistance through Priming Cancer Stem Cells in Colorectal Cancer. *PLoS One* **10**, e0125625 (2015).

146. Gonçalves-Ribeiro, S. *et al.* Carcinoma-associated fibroblasts affect sensitivity to oxaliplatin and 5FU in colorectal cancer cells. *Oncotarget* **7**, 59766–59780 (2016).

147. Tommelein, J. *et al.* Radiotherapy-activated cancer-associated fibroblasts promote tumor progression through paracrine IGF1R activation. *Cancer Res.* **78**, 659–670 (2018).

148. Bauer, J. *et al.* Increased stiffness of the tumor microenvironment in colon cancer stimulates cancer associated fibroblast-mediated prometastatic activin A signaling. *Sci. Rep.* **10**, 1–11 (2020).

149. Herter, S. *et al.* A novel three-dimensional heterotypic spheroid model for the assessment of the activity of cancer immunotherapy agents. *Cancer Immunol. Immunother.* **66**, 129–140 (2017).

150. Jing, Y. *et al.* Molecular Effects of Stromal-Selective Targeting by uPAR-Retargeted Oncolytic Virus in Breast Cancer. *Mol. Cancer Res.* **15**, 1410–1420 (2017).

151. Steer, A., Cordes, N., Jendrossek, V. & Klein, D. Impact of Cancer-Associated Fibroblast on the Radiation-Response of Solid Xenograft Tumors. *Front. Mol. Biosci.* **6**, Article 70 (2019).

152. Hanley, C. J. *et al.* Targeting the Myofibroblastic Cancer-Associated Fibroblast Phenotype Through Inhibition of NOX4. *JNCI J. Natl. Cancer Inst.* **110**, 109–120 (2018).

153. Knuchel, S., Anderle, P., Werfelli, P., Diamantis, E. & Rüegg, C. Fibroblast surface-associated FGF-2 promotes contact-dependent colorectal cancer cell migration and invasion through FGFR-SRC signaling and integrin αvβ5-mediated adhesion. *Oncotarget* **6**, 1–18 (2015).

154. Pape, J. *et al.* Cancer Associated Fibroblasts Mediate Cancer Progression and Remodel the Tumouroid Stroma. *bioRxiv (preprint)* 859041 (2019). doi:10.1101/859041

155. Onion, D. *et al.* 3-Dimensional Patient-Derived Lung Cancer Assays Reveal Resistance To Standards-of-Care Promoted By Stromal Cells But Sensitivity To Histone Deacetylase Inhibitors. *Mol. Cancer Ther.* **15**, 753–763 (2016).

156. Zhang, R., Qi, F., Shao, S., Li, G. & Feng, Y. Human colorectal cancer-derived carcinoma associated fibroblasts promote CD44-mediated adhesion of colorectal cancer cells to endothelial cells by secretion of HGF. *Cancer Cell Int.* **19**, 1–12 (2019).

157. Sha, M. *et al.* Isolation of cancer-associated fibroblasts and its promotion to the progression of intrahepatic cholangiocarcinoma. *Cancer Med.* **7**, 4665–4677 (2018).

158. Sharon, Y., Alon, L., Glanz, S., Servais, C. & Erez, N. Isolation of normal and cancer-associated fibroblasts from fresh tissues by fluorescence activated cell sorting (FACS). *J. Vis. Exp.* 1–6 (2013). doi:10.3791/4425

159. Künzel, S. R. *et al.* Ultrasonic-augmented Primary Adult Fibroblast Isolation. *J. Vis. Exp.* 1–7 (2019). doi:10.3791/59858

160. Herrera, M. *et al.* Functional heterogeneity of cancer-associated fibroblasts from human colon tumors shows specific prognostic gene expression signature. *Clin. Cancer Res.* **19**, 5914–5926 (2013).

161. Przekora, A., Zarnowski, T. & Ginalska, G. A simple and effective protocol for fast isolation of human Tenon's fibroblasts from a single trabeculectomy biopsy - A comparison of cell behaviour in different culture media. *Cell. Mol. Biol. Lett.* **22**, 1–16 (2017).

162. Cavaco, A. C. M. *et al.* The Interaction between Laminin-332 and α3β1 Integrin Determines Differentiation and Maintenance of CAFs, and Supports Invasion of Pancreatic Duct Adenocarcinoma Cells. *Cancers (Basel).* **11**, 14 (2018).

163. De Vlieghere, E. *et al.* Tumor-environment biomimetics delay peritoneal metastasis formation by deceiving and redirecting disseminated cancer cells. *Biomaterials* **54**, 148–157 (2015).

164. Koczorowska, M. M. *et al.* Fibroblast activation protein-α, a stromal cell surface protease, shapes key features of cancer associated fibroblasts through proteome and degradome alterations. *Mol. Oncol.* **10**, 40–58 (2016).

165. Drebert, Z. *et al.* Glucocorticoids indirectly decrease colon cancer cell proliferation and invasion via effects on cancer-associated fibroblasts. *Exp. Cell Res.* **362**, 332–342 (2018).

166. Gullotti, L. *et al.* FHL2 expression in peritumoural fibroblasts correlates with lymphatic metastasis in sporadic but not in HNPCC-associated colon cancer. *Lab. Investig.* **91**, 1695–1705 (2011).

167. Erez, N., Truitt, M., Olson, P. & Hanahan, D. Cancer-Associated Fibroblasts Are Activated in Incipient Neoplasia to Orchestrate Tumor-Promoting Inflammation in an NF-κB-Dependent Manner. *Cancer Cell* **17**, 135–147 (2010).

168. Su, S. *et al.* CD10+GPR77+ Cancer-Associated Fibroblasts Promote Cancer Formation and Chemoresistance by Sustaining Cancer Stemness. *Cell* **172**, 841-856.e16 (2018).

169. Drews-Elger, K. *et al.* Primary breast tumor-derived cellular models: Characterization of tumorigenic, metastatic, and cancer-associated fibroblasts in dissociated tumor (DT) cultures. *Breast Cancer Res. Treat.* **144**, 503–517 (2014).

170. Herrera, A. *et al.* Protumorigenic effects of Snail-expression fibroblasts on colon cancer cells. *Int. J. Cancer* **134**, 2984–2990 (2014).

171. NCI-Frederick, Frederick National Laboratory for Cancer Research, Frederick, M. The NCI Patient-Derived Models Repository (PDMR). (2020). Available at: https://pdmr.cancer.gov/.

172. Wessels, D. J. *et al.* Reciprocal signaling and direct physical interactions between fibroblasts and breast cancer cells in a 3D environment. *PLoS One* **14**, 1–27 (2019).

173. Bartlett, R. *et al.* Personalized in vitro cancer modeling — Fantasy or reality? *Transl. Oncol.* **7**, 657–664 (2014).

174. Hickman, J. A. *et al.* Three-dimensional models of cancer for pharmacology and cancer cell biology: Capturing tumor complexity in vitro/ex vivo. *Biotechnol. J.* **9**, 1115–1128 (2014).

175. Cattin, S., Ramont, L. & Rüegg, C. Characterization and In Vivo Validation of a Three-Dimensional Multi-Cellular Culture Model to Study Heterotypic Interactions in Colorectal Cancer Cell Growth, Invasion and Metastasis. *Front. Bioeng. Biotechnol.* **6**, 1–14 (2018).

176. Ostermann, E. *et al.* Effective immunoconjugate therapy in cancer models targeting a serine protease of tumor fibroblasts. *Clin. Cancer Res.* **14**, 4584–4592 (2008).

177. Tran, E. *et al.* Immune targeting of fibroblast activation protein triggers recognition of multipotent bone marrow stromal cells and cachexia. *J Exp Med* **210**, 1125–1135 (2013).

178. Brunker, P. *et al.* RG7386, a Novel Tetravalent FAP-DR5 Antibody, Effectively Triggers FAP-Dependent, Avidity-Driven DR5 Hyperclustering and Tumor Cell Apoptosis. *Mol. Cancer Ther.* **15**, 946–957 (2016).

179. Kuninty, P. R. *et al.* ITGA5 inhibition in pancreatic stellate cells attenuates desmoplasia and potentiates efficacy of chemotherapy in pancreatic cancer. *Sci. Adv.* **5**, eaax2770 (2019).

180. Olive, K. P. *et al.* Inhibition of Hedgehog Signaling Enhances Delivery of Chemotherapy in a Mouse Model of Pancreatic Cancer. *Science (80-.).* **324**, 1457–1461 (2009).

181. Sherman, M. H. *et al.* Vitamin D receptor-mediated stromal reprogramming suppresses pancreatitis and enhances pancreatic cancer therapy. *Cell* **159**, 80–93 (2014).

182. Mcintyre, R. E., Buczacki, S. J. A., Arends, M. J. & Adams, D. J. Mouse models of colorectal cancer as preclinical models. *BioEssays* **37**, 909–920 (2015).

183. Chan, T.-S., Shaked, Y. & Tsai, K. K. Targeting the Interplay Between Cancer Fibroblasts, Mesenchymal Stem Cells, and Cancer Stem Cells in Desmoplastic Cancers. *Front. Oncol.* **9**, 1–15 (2019).

184. Garin-Chesa, P., Old, L. J. & Rettig, W. J. Cell surface glycoprotein of reactive stromal fibroblasts as a potential antibody target in human epithelial cancers. *Proc. Natl. Acad. Sci. U. S. A.* **87**, 7235–7239 (1990).

185. Welt, S. *et al.* Antibody targeting in metastatic colon cancer: a phase I study of monoclonal antibody F19 against a cell-surface protein of reactive tumor stromal fibroblasts. *J. Clin. Oncol.* **12**, 1193–1203 (1994).

186. Hofheinz, R. D. *et al.* Stromal antigen targeting by a humanised monoclonal antibody: An early phase II trial of sibrotuzumab in patients with metastatic colorectal cancer. *Onkologie* **26**, 44–48 (2003).

187. Scott, A. M. *et al.* A phase I dose-escalation study of sibrotuzumab in patients with advanced or metastatic fibroblast activation protein-positive cancer. *Clin. Cancer Res.* **9**, 1639–1647 (2003).

188. Fischer, E. *et al.* Radioimmunotherapy of fibroblast activation protein positive tumors by rapidly internalizing antibodies. *Clin. Cancer Res.* **18**, 6208–6218 (2012).

189. Fang, J. *et al.* A potent immunotoxin targeting fibroblast activation protein for treatment of breast cancer in mice. *Int. J. Cancer* **138**, 1013–1023 (2016).

190. Brown, A. As the heat rises, Clovis turns to radionuclides. *Vantage* (2019).

191. Oncology, C. FAP-2286 Targeted Radiopharmaceutical Program Development. (2020). Available at: https://clovisoncology.com/pipeline/fap-2286/.

192. Santos, A. M., Jung, J., Aziz, N., Kissil, J. L. & Puré, E. Targeting fibroblast activation protein inhibits tumor stromagenesis and growth in mice. *J. Clin. Invest.* **119**, 3613–3625 (2009).

193. Narra, K. *et al.* Phase II trial of single agent Val-boroPro (Talabostat) inhibiting fibroblast activation protein in patients with metastatic colorectal cancer. *Cancer Biol. Ther.* **6**, 1691–1699 (2007).

194. Brennen, W. N., Rosen, D. M., Wang, H., Isaacs, J. T. & Denmeade, S. R. Targeting carcinoma-associated fibroblasts within the tumor stroma with a fibroblast activation protein-activated prodrug. *J. Natl. Cancer Inst.* **104**, 1320–1334 (2012).

195. Kraman, M. *et al.* Suppression of antitumor immunity by stromal cells expressing fibroblast activation protein-α. *Science (80-.).* **330**, 827–830 (2010).

196. Roberts, E. W. *et al.* Depletion of stromal cells expressing fibroblast activation protein-α from skeletal muscle and bone marrow results in cachexia and anemia. *J. Exp. Med.* **210**, 1137–1151 (2013).

197. Loeffler, M., Krüger, J. A., Niethammer, A. G. & Reisfeld, R. A. Targeting tumor-associated fibroblasts improves cancer chemotherapy by increasing intratumoral drug uptake. *J. Clin. Invest.* **116**, 1955–1962 (2006).

198. Duperret, E. K. *et al.* Alteration of the tumor stroma using a consensus DNA vaccine targeting Fibroblast Activation Protein (FAP) synergizes with antitumor vaccine therapy in Mice. *Clin. Cancer Res.* **24**, 1190–1201 (2018).

199. Lo, A. *et al.* Tumor-promoting desmoplasia is disrupted by depleting FAP-expressing stromal cells. *Cancer Res.* **75**, 2800–2810 (2015).

200. Kakarla, S. *et al.* Antitumor Effects of Chimeric Receptor Engineered Human T Cells Directed to Tumor Stroma. *Mol. Ther.* **21**, 1611–1620 (2013).

201. de Sostoa, J. *et al.* Targeting the tumor stroma with an oncolytic adenovirus secreting a fibroblast activation protein-targeted bispecific T-cell engager. *J. Immunother. Cancer* **7**, 19 (2019).

202. Freedman, J. D. *et al.* An Oncolytic Virus Expressing a T-cell Engager Simultaneously Targets Cancer and Immunosuppressive Stromal Cells. *Cancer Res.* **78**, 6852–6865 (2018).

203. US National Library of Medicine. A Dose Escalation Study of RO6874813 in Participants With Locally Advanced or Metastatic Solid Tumors. (2017). Available at: https://clinicaltrials.gov/ct2/show/NCT02558140.

204. Soerensen, M. M. *et al.* Safety, PK/PD, and anti-tumor activity of RO6874281, an engineered variant of interleukin-2 (IL-2v) targeted to tumor-associated fibroblasts via binding to fibroblast activation protein (FAP). *J. Clin. Oncol.* **36**, e15155 (2018).

205. Hornig, N. *et al.* Combination of a bispecific antibody and costimulatory antibody-ligand fusion proteins for targeted cancer immunotherapy. *J. Immunother.* **35**, 418–429 (2012).

206. Puré, E. & Blomberg, R. Pro-tumorigenic roles of fibroblast activation protein in cancer: back to the basics. *Oncogene* **37**, 4343–4357 (2018).

207. Lin, H.-M. *et al.* Effect of FAK inhibitor VS-6063 (defactinib) on docetaxel efficacy in prostate cancer. *Prostate* **78**, 308–317 (2018).

208. Schnittert, J., Bansal, R. & Prakash, J. Targeting Pancreatic Stellate Cells in Cancer. *Trends in Cancer* **5**, 128–142 (2019).

209. Froeling, F. E. M. *et al.* Retinoic acid-induced pancreatic stellate cell quiescence reduces paracrine Wntβ-catenin signaling to slow tumor progression. *Gastroenterology* **141**, 1486-1497.e14 (2011).

210. Kocher, H. M. *et al.* STAR-PAC: Phase I clinical trial repurposing all trans retinoic acid (ATRA) as stromal targeting agent in a novel drug combination for pancreatic cancer. *Ann. Oncol.* **30**, v267 (2019).

211. Schnittert, J., Heinrich, M. A., Kuninty, P. R., Storm, G. & Prakash, J. Reprogramming tumor stroma using an endogenous lipid lipoxin A4 to treat pancreatic cancer. *Cancer Lett.* **420**, 247–258 (2018).

212. Saison-Ridinger, M. *et al.* Reprogramming pancreatic stellate cells via p53 activation: A putative target for pancreatic cancer therapy. *PLoS One* **12**, 1–22 (2017).

213. Mpekris, F. *et al.* Sonic-hedgehog pathway inhibition normalizes desmoplastic tumor microenvironment to improve chemo- and nanotherapy. *J. Control. Release* **261**, 105–112 (2017).

214. Catenacci, D. V. T. *et al.* Randomized Phase Ib/II Study of Gemcitabine Plus Placebo or Vismodegib, a Hedgehog Pathway Inhibitor, in Patients With Metastatic Pancreatic Cancer. *J. Clin. Oncol.* **33**, 4284–4292 (2015).

215. Berlin, J. *et al.* A randomized phase II trial of vismodegib versus placebo with FOLFOX or FOLFIRI and bevacizumab in patients with previously untreated metastatic colorectal cancer. *Clin. Cancer Res.* **19**, 258–267 (2013).

216. Ko, A. H. *et al.* A phase I study of FOLFIRINOX Plus IPI-926, a hedgehog pathway inhibitor, for advanced pancreatic adenocarcinoma. *Pancreas* **45**, 370–375 (2016).

217. US National Library of Medicine. A Study to Evaluate the Clinical Efficacy of JNJ-42756493 (Erdafitinib), A Pan-Fibroblast Growth Factor Receptor (FGFR) Tyrosine Kinase Inhibitor, In Asian Participants With Advanced Non-Small-Cell Lung Cancer, Urothelial Cancer, Esophageal Cancer Or Chol. (2020). Available at: https://clinicaltrials.gov/ct2/show/NCT02699606.

218. Gascard, P. & Tlsty, T. D. Carcinoma-associated fibroblasts: Orchestrating the composition of malignancy. *Genes Dev.* **30**, 1002–1019 (2016).

219. Ohshio, Y., Hanaoka, J., Kontani, K. & Teramoto, K. Tranilast Inhibits the Function of Cancer-Associated Fibroblasts Responsible for the Induction of Immune Suppressor Cell Types. *Scand. J. Immunol.* **80**, 408–416 (2014).

220. Takai, K., Le, A., Weaver, V. M. & Werb, Z. Targeting the cancer-associated fibroblasts as a treatment in triple-negative breast cancer. *Oncotarget* **7**, 82889–82901 (2016).

221. Chauhan, V. P. *et al.* Angiotensin inhibition enhances drug delivery and potentiates chemotherapy by decompressing tumour blood vessels. *Nat. Commun.* **4**, 2516 (2013).

222. Murphy, J. E. *et al.* Total Neoadjuvant Therapy With FOLFIRINOX in Combination With Losartan Followed by Chemoradiotherapy for Locally Advanced Pancreatic Cancer. *JAMA Oncol.* **5**, 1020 (2019).

223. US National Library of Medicine. Losartan and Nivolumab in Combination With FOLFIRINOX and SBRT in Localized Pancreatic Cancer. (2019). Available at: https://clinicaltrials.gov/ct2/show/NCT03563248.

224. Wawro, M. E., Sobierajska, K., Ciszewski, W. M. & Niewiarowska, J. Nonsteroidal anti-inflammatory drugs prevent vincristine-dependent cancer-associated fibroblasts formation. *Int. J. Mol. Sci.* **20**, 1941 (2019).

225. Chan, T. S. *et al.* Metronomic chemotherapy prevents therapy-induced stromal activation and induction of tumor-initiating cells. *J. Exp. Med.* **213**, 2967–2988 (2016).

226. Clocchiatti, A. *et al.* Androgen receptor functions as transcriptional repressor of cancer-associated fibroblast activation. *J. Clin. Invest.* **128**, 5531–5548 (2018).

227. Kumar, K. *et al.* BET inhibitors block pancreatic stellate cell collagen I production and attenuate fibrosis in vivo. *JCI Insight* **2**, e88032 (2017).

228. Kim, D. J. *et al.* Suppression of TGFβ-mediated conversion of endothelial cells and fibroblasts into cancer associated (myo)fibroblasts via HDAC inhibition. *Br. J. Cancer* **118**, 1359–1368 (2018).

229. Takeda, S. *et al.* Activation of AZIN1 RNA editing is a novel mechanism that promotes invasive potential of cancer-associated fibroblasts in colorectal cancer. *Cancer Lett.* **444**, 127–135 (2019).

230. Savardashtaki, A. *et al.* MiRNAs derived from cancer-associated fibroblasts in colorectal cancer. *Epigenomics* **11**, 1627–1645 (2019).

231. Dai, G. *et al.* Colorectal cancer cell–derived exosomes containing miR-10b regulate fibroblast cells via the PI3K/Akt pathway. *Bull. Cancer* **105**, 336–349 (2018).

232. Chatterjee, A. *et al.* MicroRNA-222 reprogrammed cancer-associated fibroblasts enhance growth and metastasis of breast cancer. *Br. J. Cancer* **121**, 679–689 (2019).

233. Ubink, I., Verhaar, E. R., Kranenburg, O. & Goldschmeding, R. A potential role for CCN2/CTGF in aggressive colorectal cancer. *J. Cell Commun. Signal.* **10**, 223–227 (2016).

234. Neesse, A. *et al.* CTGF antagonism with mAb FG-3019 enhances chemotherapy response without increasing drug delivery in murine ductal pancreas cancer. *Proc. Natl. Acad. Sci. U. S. A.* **110**, 12325–12330 (2013).

235. US National Library of Medicine. Evaluation of Efficacy and Safety of Neoadjuvant Treatment With Pamrevlumab in Combination With Chemotherapy (Gemcitabine and Nab-paclitaxel) in Locally Advanced Pancreatic Cancer. (2020). Available at: https://clinicaltrials.gov/ct2/show/NCT03941093.

236. Thongchot, S. *et al.* Resveratrol interrupts the pro-invasive communication between cancer associated fibroblasts and cholangiocarcinoma cells. *Cancer Lett.* **430**, 160–171 (2018).

237. Ijichi, H. *et al.* Inhibiting Cxcr2 disrupts tumor-stromal interactions and improves survival in a mouse model of pancreatic ductal adenocarcinoma. *J. Clin. Invest.* **121**, 4106–4117 (2011).

238. Kumar, V. *et al.* Cancer-Associated Fibroblasts Neutralize the Anti-tumor Effect of CSF1 Receptor Blockade by Inducing PMN-MDSC Infiltration of Tumors. *Cancer Cell* **32**, 654-668.e5 (2017).

239. US National Library of Medicine. To Assess the Safety of Continuous IV Administration of Plerixafor and Assess Impact on the Immune Microenvironment in Patients With Pancreatic, Ovarian and Colorectal Adenocarcinomas. (2019). Available at: https://clinicaltrials.gov/ct2/show/NCT03277209.

240. Provenzano, P. P. *et al.* Enzymatic Targeting of the Stroma Ablates Physical Barriers to Treatment of Pancreatic Ductal Adenocarcinoma. *Cancer Cell* **21**, 418–429 (2012).

241. Ramanathan, R. K. *et al.* Phase IB/II randomized study of FOLFIRINOX plus pegylated recombinant human hyaluronidase versus FOLFIRINOX alone in patients with metastatic pancreatic adenocarcinoma: SWOG S1313. *J. Clin. Oncol.* **37**, 1062–1069 (2019).

242. Wang, L. M. *et al.* The prognostic role of desmoplastic stroma in pancreatic ductal adenocarcinoma. *Oncotarget* **7**, 4183–4194 (2016).

243. US National Library of Medicine. A Study Evaluating IPI-926 in Combination With Gemcitabine in Patients With Metastatic Pancreatic Cancer. (2017). Available at: https://clinicaltrials.gov/ct2/show/NCT01130142.

244. US National Library of Medicine. Vismodegib and Gemcitabine Hydrochloride in Treating Patients With Advanced Pancreatic Cancer. (2017). Available at: https://clinicaltrials.gov/ct2/show/NCT01195415.

245. US National Library of Medicine. ExIST Study of LY2157299 (Galunisertib) in Rectal Cancer. (2019). Available at: https://clinicaltrials.gov/ct2/show/NCT02688712.

246. US National Library of Medicine. A Study in Metastatic Cancer and Advanced or Metastatic Unresectable Pancreatic Cancer. (2018). Available at: https://www.clinicaltrials.gov/ct2/show/NCT01373164.

247. US National Library of Medicine. Phase I Study of AT13148, a Novel AGC Kinase Inhibitor. (2018). Available at: https://clinicaltrials.gov/ct2/show/NCT01585701.

248. US National Library of Medicine. Phase II Study of VS-6063 in Patients With KRAS Mutant Non-Small Cell Lung Cancer. (2017). Available at: https://clinicaltrials.gov/ct2/show/NCT01951690.

249. US National Library of Medicine. A Study to Evaluate the Efficacy and Safety of Simtuzumab Combined With Gemcitabine for Metastatic Pancreatic Adenocarcinoma. (2015). Available at: https://clinicaltrials.gov/ct2/show/NCT01472198.

250. Hingorani, S. R. *et al.* HALO 202: Randomized phase II Study of PEGPH20 Plus Nab-Paclitaxel/Gemcitabine Versus Nab-Paclitaxel/Gemcitabine in Patients With Untreated, Metastatic Pancreatic Ductal Adenocarcinoma. in *Journal of Clinical Oncology* (2018). doi:10.1200/JCO.2017.74.9564

251. US National Library of Medicine. Second-line Study of PEGPH20 and Pembro for HA High Metastatic PDAC. (2019). Available at: https://clinicaltrials.gov/ct2/show/NCT03634332.

252. Narra, K. *et al.* Phase II trial of single agent Val-boroPro (Talabostat) inhibiting fibroblast activation protein in patients with metastatic colorectal cancer. *Cancer Biol. Ther.* (2007). doi:10.4161/cbt.6.11.4874

253. US National Library of Medicine. Basket Study to Evaluate the Therapeutic Activity of RO6874281 as a Combination Therapy in Participants With Advanced and/or Metastatic Solid Tumors. (2020). Available at: https://clinicaltrials.gov/ct2/show/NCT03386721.

254. US National Library of Medicine. First in Human Study With NG-641, an Oncolytic Transgene Expressing Adenoviral Vector. (2020). Available at: https://clinicaltrials.gov/ct2/show/NCT04053283.

255. North, B., Kocher, H. M. & Sasieni, P. A new pragmatic design for dose escalation in phase 1 clinical trials using an adaptive continual reassessment method. *BMC Cancer* **19**, 632 (2019).

256. US National Library of Medicine. Stromal TARgeting for PAncreatic Cancer (STAR_PAC) (STAR_PAC). (2019). Available at: https://clinicaltrials.gov/ct2/show/NCT03307148.

257. US National Library of Medicine. Paricalcitol Plus Gemcitabine and Nab-paclitaxel in Metastatic Pancreatic Cancer. (2019). Available at: https://clinicaltrials.gov/ct2/show/NCT03520790.

258. Farjadian, F. *et al.* Nanopharmaceuticals and nanomedicines currently on the market: challenges and opportunities. *Nanomedicine* **14**, 93–126 (2019).

259. Moran, N. Nanomedicine lacks recognition in Europe. *Nat. Biotechnol.* **24**, 121 (2006).

260. Bui, D. T., Nicolas, J., Maksimenko, A., Desmaële, D. & Couvreur, P. Multifunctional squalene-based prodrug nanoparticles for targeted cancer therapy. *Chem. Commun.* **50**, 5336–5338 (2014).

261. Bastiancich, C. *et al.* Lauroyl-gemcitabine-loaded lipid nanocapsule hydrogel for the treatment of glioblastoma. *J. Control. Release* **225**, 283–293 (2016).

262. Yang, Q., Li, L., Sun, W., Zhou, Z. & Huang, Y. Dual Stimuli-Responsive Hybrid Polymeric Nanoparticles Self-Assembled from POSS-Based Starlike Copolymer-Drug Conjugates for Efficient Intracellular Delivery of Hydrophobic Drugs. *ACS Appl. Mater. Interfaces* **8**, 13251–13261 (2016).

263. Chen, S. *et al.* Inorganic nanomaterials as carriers for drug delivery. *J. Biomed. Nanotechnol.* **12**, 1–27 (2016).

264. Conniot, J. *et al.* Cancer immunotherapy: Nanodelivery approaches for immune cell targeting and tracking. *Front. Chem.* **2**, (2014).

265. He, H., Liu, L., Morin, E. E., Liu, M. & Schwendeman, A. Survey of Clinical Translation of Cancer Nanomedicines - Lessons Learned from Successes and Failures. *Acc. Chem. Res.* **52**, 2673–2683 (2019).

266. Hua, S., de Matos, M. B. C., Metselaar, J. M. & Storm, G. Current trends and challenges in the clinical translation of nanoparticulate nanomedicines: Pathways for translational development and commercialization. *Front. Pharmacol.* **9**, 1–14 (2018).

267. Wicki, A., Witzigmann, D., Balasubramanian, V. & Huwyler, J. Nanomedicine in cancer therapy: Challenges, opportunities, and clinical applications. *J. Control. Release* **200**, 138–157 (2015).

268. Gref, R. *et al.* Biodegradable long-circulating polymeric nanospheres. *Science (80-.).* **263**, 1600–1603 (1994).

269. Tran, S., DeGiovanni, P.-J., Piel, B. & Rai, P. Cancer nanomedicine: a review of recent success in drug delivery. *Clin. Transl. Med.* **6**, 44 (2017).

270. Kanapathipillai, M. *et al.* Inhibition of mammary tumor growth using lysyl oxidase-targeting nanoparticles to modify extracellular matrix. *Nano Lett.* **12**, 3213–3217 (2012).

271. Danhier, F. To exploit the tumor microenvironment: Since the EPR effect fails in the clinic, what is the future of nanomedicine? *J. Control. Release* **244**, 108–121 (2016).

272. Saffie-Siebert, R., Ogden, J. & Parry-Billings, M. Nanotechnology approaches to solving the problems of poorly water-soluble drugs. *Drug Discov. World* **6**, 71–76 (2005).

273. Hare, J. I. *et al.* Challenges and strategies in anti-cancer nanomedicine development: An industry perspective. *Adv. Drug Deliv. Rev.* **108**, 25–38 (2017).

274. Han, X. *et al.* Emerging nanomedicines for anti-stromal therapy against desmoplastic tumors. *Biomaterials* **232**, 119745 (2020).

275. Mardhian, D. F., Storm, G., Bansal, R. & Prakash, J. Nano-targeted relaxin impairs fibrosis and tumor growth in pancreatic cancer and improves the efficacy of gemcitabine in vivo. *J. Control. Release* **290**, 1–10 (2018).

276. Ji, T. *et al.* Designing Liposomes to Suppress Extracellular Matrix Expression to Enhance Drug Penetration and Pancreatic Tumor Therapy. *ACS Nano* **11**, 8668–8678 (2017).

277. Ji, T. *et al.* Peptide Assembly Integration of Fibroblast-Targeting and Cell-Penetration Features for Enhanced Antitumor Drug Delivery. *Adv. Mater.* **27**, 1865–1873 (2015).

278. Murakami, M. *et al.* Docetaxel conjugate nanoparticles that target a-smooth muscle actin-expressing stromal cells suppress breast cancer metastasis. *Cancer Res.* **73**, 4862–4871 (2013).

279. Ernsting, M. J. *et al.* Targeting of metastasis-promoting tumor-associated fibroblasts and modulation of pancreatic tumor-associated stroma with a carboxymethylcellulose-docetaxel nanoparticle. *J. Control. Release* **206**, 122–130 (2015).

280. Alvarez, R. *et al.* Stromal disrupting effects of nab-paclitaxel in pancreatic cancer. *Br J Cancer* **109**, 926–933 (2013).

281. Miyashita, T. *et al.* Neoadjuvant Chemotherapy with Gemcitabine Plus Nab-paclitaxel Reduces the Number of Cancer-associated Fibroblasts Through Depletion of Pancreatic Stroma. *Anticancer Res* **38**, 337–343 (2018).

282. Schuster, L. *et al.* Immunoliposomes for Targeted Delivery of an Antifibrotic Drug. *Mol. Pharm.* **12**, 3146–3157 (2015).

283. Chen, B. *et al.* Comprehensively priming the tumor microenvironment by cancer-associated fibroblast-targeted liposomes for combined therapy with cancer cell-targeted chemotherapeutic drug delivery system. *J. Control. Release* **241**, 68–80 (2016).

284. Chen, B. *et al.* A tenascin C targeted nanoliposome with navitoclax for specifically eradicating of cancer-associated fibroblasts. *Nanomedicine Nanotechnology, Biol. Med.* **12**, 131–141 (2016).

285. Hu, K. *et al.* Quercetin Remodels the Tumor Microenvironment to Improve the Permeation, Retention, and Antitumor Effects of Nanoparticles. *ACS Nano* **11**, 4916–4925 (2017).

286. Zinger, A. *et al.* Collagenase Nanoparticles Enhance the Penetration of Drugs into Pancreatic Tumors. *ACS Nano* **13**, 11008–11021 (2019).

287. Dong, X. *et al.* Enhanced Drug Delivery by Nanoscale Integration of a Nitric Oxide Donor to Induce Tumor Collagen Depletion. *Nano Lett.* **19**, 997–1008 (2019).

288. Shen, L. *et al.* Local Blockade of Interleukin 10 and C-X-C Motif Chemokine Ligand 12 with Nano-Delivery Promotes Antitumor Response in Murine Cancers. *ACS Nano* **12**, 9830–9841 (2018).

289. Chauhan, V. P. *et al.* Reprogramming the microenvironment with tumor-selective angiotensin blockers enhances cancer immunotherapy. *Proc. Natl. Acad. Sci.* **116**, 10674–10680 (2019).

290. Zhou, H. *et al.* Hyaluronidase Embedded in Nanocarrier PEG Shell for Enhanced Tumor Penetration and Highly Efficient Antitumor Efficacy. *Nano Lett.* **16**, 3268–3277 (2016).

291. Kohli, A. G., Kivimäe, S., Tiffany, M. R. & Szoka, F. C. Improving the distribution of Doxil® in the tumormatrix by depletion of tumor hyaluronan. *J. Control. Release* **191**, 105–114 (2014).

292. Zhang, J. *et al.* Synergistic anti-tumor effects of combined gemcitabine and cisplatin nanoparticles in a stroma-rich bladder carcinoma model. *J. Control. Release* **182**, 90–96 (2014).

293. Han, X. *et al.* Reversal of pancreatic desmoplasia by re-educating stellate cells with a tumour microenvironment-activated nanosystem. *Nat. Commun.* **9**, 3390 (2018).

294. Kim, M. G., Shon, Y., Kim, J. & Oh, Y. K. Selective activation of anticancer chemotherapy by cancer-associated fibroblasts in the tumor microenvironment. *J. Natl. Cancer Inst.* **109**, 1–10 (2017).

295. Zhen, Z. *et al.* Protein Nanocage Mediated Fibroblast-Activation Protein Targeted Photoimmunotherapy to Enhance Cytotoxic T Cell Infiltration and Tumor Control. *Nano Lett.* **17**, 862–869 (2017).

296. Saha, S. *et al.* Gold Nanoparticle Reprograms Pancreatic Tumor Microenvironment and Inhibits Tumor Growth. *ACS Nano* **10**, 10636–10651 (2016).

297. Hossen, M. N. *et al.* Gold Nanoparticle Transforms Activated Cancer-Associated Fibroblasts to Quiescence. *ACS Appl. Mater. Interfaces* **11**, 26060–26068 (2019).

298. Miao, L. *et al.* Targeting Tumor-Associated Fibroblasts for Therapeutic Delivery in Desmoplastic Tumors. *Cancer Res.* **77**, 719–731 (2017).

299. Torres Andón, F. & Alonso, M. J. Nanomedicine and cancer immunotherapy - Targeting immunosuppressive cells. *J. Drug Target.* **23**, 656–671 (2015).

300. Kuai, R. *et al.* Elimination of established tumors with nanodisc-based combination chemoimmunotherapy. *Sci. Adv.* **4**, eaao1736 (2018).

301. Guo, X.-Y. *et al.* Paclitaxel and Gemcitabine Combinational Drug-loaded Mucoadhesive Delivery System in the Treatment of Colon Cancers. *Drug Res. (Stuttg).* **65**, 199–204 (2014).

302. Xiao, B. *et al.* Co-delivery of camptothecin and curcumin by cationic polymeric nanoparticles for synergistic colon cancer combination chemotherapy. *J. Mater. Chem. B* **3**, 7724–7733 (2015).

303. Zhao, P. *et al.* Dual-Targeting to Cancer Cells and M2 Macrophages via Biomimetic Delivery of Mannosylated Albumin Nanoparticles for Drug-Resistant Cancer Therapy. *Adv. Funct. Mater.* **27**, 1700403 (2017).

304. Nourazarian, A. R. *et al.* Combined EGFR and c-Src Antisense Oligodeoxynucleotides Encapsulated with PAMAM Denderimers Inhibit HT-29 Colon Cancer Cell Proliferation. *Asian Pacific J. Cancer Prev.* **13**, 4751–4756 (2012).

305. Palvai, S., Kuman, M. M. & Basu, S. Hyaluronic acid cloaked oleic acid nanoparticles inhibit MAPK signaling with sub-cellular DNA damage in colon cancer cells. *J. Mater. Chem. B* **5**, 3658–3666 (2017).

306. Oshima, G. *et al.* In Vivo Delivery and Therapeutic Effects of a MicroRNA on Colorectal Liver Metastases. *Mol. Ther.* **25**, 1588–1595 (2017).

307. Sadreddini, S. *et al.* Chitosan nanoparticles as a dual drug/siRNA delivery system for treatment of colorectal cancer. *Immunol. Lett.* **181**, 79–86 (2017).

308. Dinarvand, M. *et al.* Oral delivery of nanoparticles containing anticancer SN38 and hSET1 antisense for dual therapy of colon cancer. *Int. J. Biol. Macromol.* **78**, 112–121 (2015).

309. Ediriwickrema, A., Zhou, J., Deng, Y. & Saltzman, W. M. Multi-layered nanoparticles for combination gene and drug delivery to tumors. *Biomaterials* **35**, 9343–9354 (2014).

310. Fay, F. *et al.* Conatumumab (AMG 655) coated nanoparticles for targeted pro-apoptotic drug delivery. *Biomaterials* **32**, 8645–8653 (2011).

311. Batist, G. *et al.* Safety, pharmacokinetics, and efficacy of CPX-1 liposome injection in patients with advanced solid tumors. *Clin. Cancer Res.* **15**, 692–700 (2009).

312. Serpe, L. *et al.* Cytotoxicity of anticancer drugs incorporated in solid lipid nanoparticles on HT-29 colorectal cancer cell line. *Eur. J. Pharm. Biopharm.* **58**, 673–680 (2004).

313. Wang, J. & Peng, C. A. Anticancer effectiveness of polymeric drug nanocarriers on colorectal cancer cells. in *Proceedings of the Annual International Conference of the IEEE Engineering in Medicine and Biology Society, EMBS* 3249–3252 (IEEE, 2011). doi:10.1109/IEMBS.2011.6090883

314. Xiao, B. *et al.* Hyaluronic acid-functionalized polymeric nanoparticles for colon cancer-targeted combination chemotherapy. *Nanoscale* **7**, 17745–17755 (2015).

315. Cho, H. & Kwon, G. S. Polymeric Micelles for Neoadjuvant Cancer Therapy and Tumor-Primed Optical Imaging. *ACS Nano* **5**, 8721–8729 (2011).

316. Maksimenko, A. *et al.* Therapeutic Modalities of Squalenoyl Nanocomposites in Colon Cancer: An Ongoing Search for Improved Efficacy. *ACS Nano* **8**, 2018–2032 (2014).

317. Xu, B. *et al.* Polymeric Nanomedicine for Combined Gene/Chemotherapy Elicits Enhanced Tumor Suppression. *Mol. Pharm.* **13**, 663–676 (2016).

318. Anitha, A., Deepa, N., Chennazhi, K. P., Lakshmanan, V. K. & Jayakumar, R. Combinatorial anticancer effects of curcumin and 5-fluorouracil loaded thiolated chitosan nanoparticles towards colon cancer treatment. *Biochim. Biophys. Acta - Gen. Subj.* **1840**, 2730–2743 (2014).

319. Hong, G. Y. *et al.* Combination of paclitaxel- and retinoic acid-incorporated nanoparticles for the treatment of CT-26 colon carcinoma. *Arch. Pharm. Res.* **34**, 407–417 (2011).

320. Na, H. S. *et al.* Combination antitumor effects of micelle-loaded anticancer drugs in a CT-26 murine colorectal carcinoma model. *Int. J. Pharm.* **383**, 192–200 (2010).

321. Kuai, R., Ochyl, L. J., Bahjat, K. S., Schwendeman, A. & Moon, J. J. Designer vaccine nanodiscs for personalized cancer immunotherapy. *Nat. Mater.* **16**, 489–496 (2017).

322. Chibaudel, B. *et al.* PEPCOL: a GERCOR randomized phase II study of nanoliposomal irinotecan PEP02 (MM-398) or irinotecan with leucovorin/5-fluorouracil as second-line therapy in metastatic colorectal cancer. *Cancer Med.* **5**, 676–683 (2016).

323. Chen, J., Shao, R., Li, L., Xu, Z. P. & Gu, W. Effective inhibition of colon cancer cell growth with MgAl-layered double hydroxide (LDH) loaded 5-FU and PI3K/mTOR dual inhibitor BEZ-235 through apoptotic pathways. *Int. J. Nanomedicine* **9**, 3403–3411 (2014).

324. Ortiz, R. *et al.* 5-fluorouracil-loaded poly(ε-caprolactone) nanoparticles combined with phage E gene therapy as a new strategy against colon cancer. *Int. J. Nanomedicine* **7**, 95–107 (2012).

325. Sureban, S. M. *et al.* Nanoparticle-based delivery of siDCAMKL-1 increases microRNA-144 and inhibits colorectal cancer tumor growth via a Notch-1 dependent mechanism. *J. Nanobiotechnology* **9**, 40 (2011).

326. Tian, X. *et al.* Preclinical Evaluation of Promitil, a Radiation-Responsive Liposomal Formulation of Mitomycin C Prodrug, in Chemoradiotherapy. *Int. J. Radiat. Oncol.* **96**, 547–555 (2016).

327. Gabizon, A. *et al.* Therapeutic efficacy of a lipid-based prodrug of mitomycin C in pegylated liposomes: Studies with human gastro-entero-pancreatic ectopic tumor models. *J. Control. Release* **160**, 245–253 (2012).

328. Golan, T. *et al.* Pegylated liposomal mitomycin C prodrug enhances tolerance of mitomycin C: a phase 1 study in advanced solid tumor patients. *Cancer Med.* **4**, 1472–1483 (2015).

329. Batist, G. *et al.* A multicenter, phase II study of CPX-1 liposome injection in patients (pts) with advanced colorectal cancer (CRC). *J. Clin. Oncol.* **26**, 4108–4108 (2008).

330. Tian, X. *et al.* CRLX101, a Nanoparticle–Drug Conjugate Containing Camptothecin, Improves Rectal Cancer Chemoradiotherapy by Inhibiting DNA Repair and HIF1α. *Cancer Res.* **77**, 112–122 (2017).

331. Li, L., Ahmed, B., Mehta, K. & Kurzrock, R. Liposomal curcumin with and without oxaliplatin: effects on cell growth, apoptosis, and angiogenesis in colorectal cancer. *Mol. Cancer Ther.* **6**, 1276–1282 (2007).

332. Xiao, B. *et al.* Silencing of Intestinal Glycoprotein CD98 by Orally Targeted Nanoparticles Enhances Chemosensitization of Colon Cancer. *ACS Nano* **12**, 5253–5265 (2018).

333. Tsai, M.-H., Pan, C.-H., Peng, C.-L. & Shieh, M.-J. Panitumumab-Conjugated Pt-Drug Nanomedicine for Enhanced Efficacy of Combination Targeted Chemotherapy against Colorectal Cancer. *Adv. Healthc. Mater.* **6**, 1700111 (2017).

334. Kosmides, A. K., Sidhom, J.-W., Fraser, A., Bessell, C. A. & Schneck, J. P. Dual Targeting Nanoparticle Stimulates the Immune System To Inhibit Tumor Growth. *ACS Nano* **11**, 5417–5429 (2017).

335. Conde, J., Oliva, N., Zhang, Y. & Artzi, N. Local triple-combination therapy results in tumour regression and prevents recurrence in a colon cancer model. *Nat. Mater.* **15**, 1128–1138 (2016).

336. Huynh, N. T., Passirani, C., Saulnier, P. & Benoit, J. P. Lipid nanocapsules: A new platform for nanomedicine. *Int. J. Pharm.* **379**, 201–209 (2009).

337. Heurtault, B., Saulnier, P., Pech, B., Proust, J. E. & Benoit, J. P. A novel phase inversion-based process for the preparation of lipid nanocarriers. *Pharm. Res.* **19**, 875–880 (2002).

338. Anton, N., Gayet, P., Benoit, J. P. & Saulnier, P. Nano-emulsions and nanocapsules by the PIT method: An investigation on the role of the temperature cycling on the emulsion phase inversion. *Int. J. Pharm.* **344**, 44–52 (2007).

339. Heurtault, B. *et al.* The influence of lipid nanocapsule composition on their size distribution. *Eur. J. Pharm. Sci.* **18**, 55–61 (2003).

340. Xu, Y. *et al.* Size Effect on Lipid Nanocapsule-Mediated GLP-1 Secretion from Enteroendocrine L Cells. *Mol. Pharm.* **15**, 108–115 (2018).

341. Dulieu, C. & Bazile, D. Influence of lipid nanocapsules composition on their aptness to freeze-drying. *Pharm. Res.* **22**, 285–292 (2005).

342. Hureaux, J. *et al.* The adaptation of lipid nanocapsule formulations for blood administration in animals. *Int. J. Pharm.* **379**, 266–269 (2009).

343. Thomas, O. & Lagarce, F. Lipid Nanocapsules: A Nanocarrier Suitable for Scale-Up Process. *J. Drug Deliv. Sci. Technol.* **23**, 555–559 (2013).

344. Garcion, E. *et al.* A new generation of anticancer, drug-loaded, colloidal vectors reverses multidrug resistance in glioma and reduces tumor progression in rats. *Mol. Cancer Ther.* **5**, 1710–1722 (2006).

345. Tsakiris, N. *et al.* Combinational drug-loaded lipid nanocapsules for the treatment of cancer. *Int. J. Pharm.* **569**, 118588 (2019).

346. Lamprecht, A. & Benoit, J. P. Etoposide nanocarriers suppress glioma cell growth by intracellular drug delivery and simultaneous P-glycoprotein inhibition. *J. Control. Release* **112**, 208–213 (2006).

347. Montigaud, Y. *et al.* Optimized acriflavine-loaded lipid nanocapsules as a safe and effective delivery system to treat breast cancer. *Int. J. Pharm.* **551**, 322–328 (2018).

348. Lollo, G. *et al.* Drug delivery to tumours using a novel 5-FU derivative encapsulated into lipid nanocapsules. *J. Drug Target.* **27**, 634–645 (2019).

349. Briot, T. *et al.* Di-O-lauroyl-decitabine-lipid nanocapsules: Toward extending decitabine activity. *Int. J. Nanomedicine* **14**, 2091–2102 (2019).

350. Bastiancich, C. *et al.* Drug combination using an injectable nanomedicine hydrogel for glioblastoma treatment. *Int. J. Pharm.* **559**, 220–227 (2019).

351. Nehme, H. *et al.* Antibacterial activity of antipsychotic agents, their association with lipid nanocapsules and its impact on the properties of the nanocarriers and on antibacterial activity. *PLoS One* **13**, 1–18 (2018).

352. Bohley, M., Haunberger, A. & Goepferich, A. M. Intracellular availability of poorly soluble drugs from lipid nanocapsules. *Eur. J. Pharm. Biopharm.* **139**, 23–32 (2019).

353. Peltier, S., Oger, J. M., Lagarce, F., Couet, W. & Benoît, J. P. Enhanced oral paclitaxel bioavailability after administration of paclitaxel-loaded lipid nanocapsules. *Pharm. Res.* **23**, 1243–1250 (2006).

354. Roger, E., Lagarce, F., Garcion, E. & Benoit, J. P. Lipid nanocarriers improve paclitaxel transport throughout human intestinal epithelial cells by using vesicle-mediated transcytosis. *J. Control. Release* **140**, 174–181 (2009).

355. Groo, A. C. *et al.* In vivo evaluation of paclitaxel-loaded lipid nanocapsules after intravenous and oral administration on resistant tumor. *Nanomedicine* **10**, 589–601 (2015).

356. Lacoeuille, F. *et al.* In vivo evaluation of lipid nanocapsules as a promising colloidal carrier for paclitaxel. *Int. J. Pharm.* **344**, 143–149 (2007).

357. Le Roux, G. *et al.* Cytotoxicity and genotoxicity of lipid nanocapsules. *Toxicol. Vitr.* **41**, 189–199 (2017).

358. Lainé, A. L. *et al.* Conventional versus stealth lipid nanoparticles: Formulation and in vivo fate prediction through FRET monitoring. *J. Control. Release* **188**, 1–8 (2014).

359. Messaoudi, K., Saulnier, P., Boesen, K., Benoit, J. P. & Lagarce, F. Anti-epidermal growth factor receptor siRNA carried by chitosan-transacylated lipid nanocapsules increases sensitivity of glioblastoma cells to temozolomide. *Int. J. Nanomedicine* **9**, 1479–1490 (2014).

360. Lehner, R., Wang, X., Marsch, S. & Hunziker, P. Intelligent nanomaterials for medicine: Carrier platforms and targeting strategies in the context of clinical application. *Nanomedicine Nanotechnology, Biol. Med.* **9**, 742–757 (2013).

361. Strebhardt, K. & Ullrich, A. Paul Ehrlich's magic bullet concept: 100 Years of progress. *Nat. Rev. Cancer* **8**, 473–480 (2008).

362. Li, Z. & Gorfe, A. A. Receptor-mediated membrane adhesion of lipid-polymer hybrid (LPH) nanoparticles studied by dissipative particle dynamics simulations. *Nanoscale* **7**, 814–824 (2015).

363. Alsaggar, M. & Liu, D. Organ-based drug delivery. *J. Drug Target.* **26**, 385–397 (2018).

364. Merino, M., Zalba, S. & Garrido, M. J. Immunoliposomes in clinical oncology: State of the art and future perspectives. *J. Control. Release* **275**, 162–176 (2018).

365. Tansi, F. L. *et al.* Activatable bispecific liposomes bearing fibroblast activation protein directed single chain fragment/Trastuzumab deliver encapsulated cargo into the nuclei of tumor cells and the tumor microenvironment simultaneously. *Acta Biomater.* **54**, 281–293 (2017).

366. Eloy, J. O., Petrilli, R., Trevizan, L. N. F. & Chorilli, M. Immunoliposomes: A review on functionalization strategies and targets for drug delivery. *Colloids Surfaces B Biointerfaces* **159**, 454–467 (2017).

367. Mccarthy, D. P., Hunter, Z. N., Chackerian, B., Shea, L. D. & Miller, S. D. Targeted immunomodulation using antigen-conjugated nanoparticles. *Wiley Interdiscip. Rev. Nanomedicine Nanobiotechnology* **6**, 298–315 (2014).

368. Jacoberger-Foissac, C. *et al.* Optimization of peptide-based cancer vaccine compositions, by sequential screening, using versatile liposomal platform. *Int. J. Pharm.* **562**, 342–350 (2019).

369. Du, J., Zhang, Y. S., Hobson, D. & Hydbring, P. Nanoparticles for immune system targeting. *Drug Discov. Today* **22**, 1295–1301 (2017).

370. Tan, K. X., Pan, S., Jeevanandam, J. & Danquah, M. K. Cardiovascular therapies utilizing targeted delivery of nanomedicines and aptamers. *Int. J. Pharm.* **558**, 413–425 (2019).

371. Nogueira, E., Gomes, A. C., Preto, A. & Cavaco-Paulo, A. Design of liposomal formulations for cell targeting. *Colloids Surfaces B Biointerfaces* **136**, 514–526 (2015).

372. Zylberberg, C., Gaskill, K., Pasley, S. & Matosevic, S. Engineering liposomal nanoparticles for targeted gene therapy. *Gene Therapy* **24**, 441–452 (2017).

373. Könning, D. & Kolmar, H. Beyond antibody engineering: Directed evolution of alternative binding scaffolds and enzymes using yeast surface display. *Microb. Cell Fact.* **17**, 32 (2018).

374. Linse, S. S. Directed evolution of enzymes and binding proteins. *Scientific Background on the Nobel Prize in Chemistry* (2018).

375. Manjappa, A. S. *et al.* Antibody derivatization and conjugation strategies: Application in preparation of stealth immunoliposome to target chemotherapeutics to tumor. *J. Control. Release* **150**, 2–22 (2011).

376. Weisser, N. E. & Hall, J. C. Applications of single-chain variable fragment antibodies in therapeutics and diagnostics. *Biotechnol. Adv.* **27**, 502–520 (2009).

377. Wang, Y. *et al.* Nanobody-derived nanobiotechnology tool kits for diverse biomedical and biotechnology applications. *Int. J. Nanomedicine* **11**, 3287–3303 (2016).

378. Beuttler, J., Rothdiener, M., Müller, D., Frejd, F. Y. & Kontermann, R. E. Targeting of epidermal growth factor receptor (EGFR)-expressing tumor cells with sterically stabilized affibody liposomes (SAL). *Bioconjug. Chem.* **20**, 1201–1208 (2009).

379. Danhier, F. *et al.* Tumor Targeting by RGD-Grafted PLGA-Based Nanotheranostics Loaded with Paclitaxel and Superparamagnetic Iron Oxides. in *Methods in Pharmacology and Toxicology* (ed. Press, H.) 1–17 (2015). doi:10.1007/7653_2015_43

380. Jiang, T. *et al.* Dual-functional liposomes based on pH-responsive cell-penetrating peptide and hyaluronic acid for tumor-targeted anticancer drug delivery. *Biomaterials* **33**, 9246–9258 (2012).

381. Qin, Y. *et al.* Liposome formulated with TAT-modified cholesterol for improving brain delivery and therapeutic efficacy on brain glioma in animals. *Int. J. Pharm.* **420**, 304–312 (2011).

382. Hong, S. *et al.* Aptamer-integrated α-Gal liposomes as bispecific agents to trigger immune response for killing tumor cells. *J. Biomed. Mater. Res. Part A* **107**, 1176–1183 (2019).

383. Nascimento, T. L., Hillaireau, H., Vergnaud, J. & Fattal, E. Lipid-based nanosystems for CD44 targeting in cancer treatment: Recent significant advances, ongoing challenges and unmet needs. *Nanomedicine* **11**, 1865–1887 (2016).

384. Franzen, S. A comparison of peptide and folate receptor targeting of cancer cells: from single agent to nanoparticle. *Expert Opin. Drug Deliv.* **8**, 281–298 (2011).

385. Nobs, L., Buchegger, F., Gurny, R. & Allémann, E. Current methods for attaching targeting ligands to liposomes and nanoparticles. *J. Pharm. Sci.* **93**, 1980–1992 (2004).

386. Ran, R., Middelberg, A. P. J. & Zhao, C. X. Microfluidic synthesis of multifunctional liposomes for tumour targeting. *Colloids Surfaces B Biointerfaces* **148**, 402–410 (2016).

387. Song, S., Mao, G., Du, J. & Zhu, X. Novel RGD containing, temozolomide-loading nanostructured lipid carriers for glioblastoma multiforme chemotherapy. *Drug Deliv.* **23**, 1404–1408 (2016).

388. Zhang, L. *et al.* Targeted Codelivery of an Antigen and Dual Agonists by Hybrid Nanoparticles for Enhanced Cancer Immunotherapy. *Nano Lett.* **19**, 4237–4249 (2019).

389. Dumont, N. *et al.* Nanoliposome targeting in breast cancer is influenced by the tumor microenvironment. *Nanomedicine Nanotechnology, Biol. Med.* **17**, 71–81 (2019).

390. Nellis, D. F. *et al.* Preclinical manufacture of anti-HER2 liposome-inserting, scFv-PEG-lipid conjugate. 2. Conjugate micelle identity, purity, stability, and potency analysis. *Biotechnol. Prog.* **21**, 221–232 (2005).

391. Nellis, D. F. *et al.* Preclinical manufacture of an anti-HER2 scFv-PEG-DSPE, liposome-inserting conjugate. 1. Gram-scale production and purification. *Biotechnol. Prog.* **21**, 205–220 (2005).

392. Mitchell, M. J., Chen, C. S., Ponmudi, V., Hughes, A. D. & King, M. R. E-selectin liposomal and nanotube-targeted delivery of doxorubicin to circulating tumor cells. *J. Control. Release* **160**, 609–617 (2012).

393. Apaolaza, P. S., Delgado, D., Pozo-Rodríguez, A. Del, Gascón, A. R. & Solinís, M. Á. A novel gene therapy vector based on hyaluronic acid and solid lipid nanoparticles for ocular diseases. *Int. J. Pharm.* **465**, 413–426 (2014).

394. Carradori, D., Saulnier, P., Préat, V., des Rieux, A. & Eyer, J. NFL-lipid nanocapsules for brain neural stem cell targeting in vitro and in vivo. *J. Control. Release* **238**, 253–262 (2016).

395. Lin, Y. L. *et al.* Specific drug delivery efficiently induced human breast tumor regression using a lipoplex by non-covalent association with anti-tumor antibodies. *J. Nanobiotechnology* **17**, 1–11 (2019).

396. Herringson, T. P. & Altin, J. G. Increasing the antitumor efficacy of doxorubicin-loaded liposomes with peptides anchored via a chelator lipid. *J. Drug Target.* **19**, 681–689 (2011).

397. Mitchell, M. J., Wayne, E. C., Rana, K., Schaffer, C. B. & King, M. R. Unnatural killer cells: TRAIL-coated leukocytes that kill cancer cells in the circulation. *Proc. IEEE Annu. Northeast Bioeng. Conf. NEBEC* **2014-Decem**, 1–6 (2014).

398. Shao, S. *et al.* Functionalization of cobalt porphyrin-phospholipid bilayers with his-tagged ligands and antigens. *Nat. Chem.* **7**, 438–46 (2015).

399. Pan, X. & Lee, R. J. Construction of anti-EGFR immunoliposomes via folate–folate binding protein affinity. *Int. J. Pharm.* **336**, 276–283 (2007).

400. Kuijten, M. M. P. *et al.* Multimodal targeted high relaxivity thermosensitive liposome for in vivo imaging. *Sci. Rep.* **5**, 1–11 (2015).

401. Marqués-Gallego, P. & de Kroon, A. I. P. M. Ligation Strategies for Targeting Liposomal Nanocarriers. *Biomed Res. Int.* **2014**, 1–12 (2014).

402. Vabbilisetty, P., Boron, M., Nie, H., Ozhegov, E. & Sun, X. L. Chemical Reactive Anchoring Lipids with Different Performance for Cell Surface Re-engineering Application. *ACS Omega* **3**, 1589–1599 (2018).

403. Baek, J.-S. & Cho, C.-W. A multifunctional lipid nanoparticle for co-delivery of paclitaxel and curcumin for targeted delivery and enhanced cytotoxicity in multidrug resistant breast cancer cells. *Oncotarget* **8**, 30369–30382 (2017).

404. Toriyabe, N., Hayashi, Y., Hyodo, M. & Harashima, H. Synthesis and Evaluation of Stearylated Hyaluronic Acid for the Active Delivery of Liposomes to Liver Endothelial Cells. *Biol. Pharm. Bull.* **34**, 1084–1089 (2011).

405. Radwan, A. A. & Alanazi, F. K. Targeting cancer using cholesterol conjugates. *Saudi Pharm. J.* **22**, 3–16 (2014).

406. Allen, T. M., Sapra, P. & Moase, E. Use of the post-insertion method for the formation of ligand-coupled liposomes. *Cell. Mol. Biol. Lett.* **7**, 889–94 (2002).

407. He, Y., Zhang, L. & Song, C. Luteinizing hormone-releasing hormone receptor-mediated delivery of mitoxantrone using LHRH analogs modified with PEGylated liposomes. *Int. J. Nanomedicine* **5**, 697–705 (2010).

408. Önyüksel, H., Jeon, E. & Rubinstein, I. Nanomicellar paclitaxel increases cytotoxicity of multidrug resistant breast cancer cells. *Cancer Lett.* **274**, 327–330 (2009).

409. Messerschmidt, S. K. E. *et al.* Targeted lipid-coated nanoparticles: Delivery of tumor necrosis factor-functionalized particles to tumor cells. *J. Control. Release* **137**, 69–77 (2009).

410. Bourseau-Guilmain, E. *et al.* Development and characterization of immuno-nanocarriers targeting the cancer stem cell marker AC133. *Int. J. Pharm.* **423**, 93–101 (2012).

411. Kim, M. S. *et al.* Engineering macrophage-derived exosomes for targeted paclitaxel delivery to pulmonary metastases: in vitro and in vivo evaluations. *Nanomedicine Nanotechnology, Biol. Med.* **14**, 195–204 (2018).

412. Tiantian, Y. *et al.* Study on intralymphatic-targeted hyaluronic acid-modified nanoliposome: Influence of formulation factors on the lymphatic targeting. *Int. J. Pharm.* **471**, 245–257 (2014).

413. Fischer, D., Li, Y., Ahlemeyer, B., Krieglstein, J. & Kissel, T. In vitro cytotoxicity testing of polycations: influence of polymer structure on cell viability and hemolysis. *Biomaterials* **24**, 1121–31 (2003).

414. Platt, V. *et al.* Influence of Multivalent Nitrilotriacetic Acid Lipid−Ligand Affinity on the Circulation Half-Life in Mice of a Liposome-Attached His 6 -Protein. *Bioconjug. Chem.* **21**, 892–902 (2010).

415. Bak, M., Jølck, R. I., Eliasen, R. & Andresen, T. L. Affinity Induced Surface Functionalization of Liposomes Using Cu-Free Click Chemistry. *Bioconjug. Chem.* **27**, 1673–1680 (2016).

416. Tian, Y. *et al.* A doxorubicin delivery platform using engineered natural membrane vesicle exosomes for targeted tumor therapy. *Biomaterials* **35**, 2383–2390 (2014).

417. Alvarez-Erviti, L. *et al.* Delivery of siRNA to the mouse brain by systemic injection of targeted exosomes. *Nat. Biotechnol.* **29**, 341–345 (2011).

418. Hermanson, G. T. *Bioconjugate Techniques*. *Bioconjugate Techniques* (Elsevier, 2013). doi:10.1016/B978-0-12-382239-0.00001-7

419. Torchilin, V. P. *et al.* p-nitrophenylcarbonyl-PEG-PE-liposomes: Fast and simple attachment of specific ligands, including monoclonal antibodies, to distal ends of PEG chains via p-nitrophenylcarbonyl groups. *Biochim. Biophys. Acta - Biomembr.* **1511**, 397–411 (2001).

420. Khayrani, A. C. *et al.* Targeting Ovarian Cancer Cells Overexpressing CD44 with Immunoliposomes Encapsulating Glycosylated Paclitaxel. *Int. J. Mol. Sci.* **20**, 1042 (2019).

421. Krieger, M. L. *et al.* Overcoming cisplatin resistance of ovarian cancer cells by targeted liposomes in vitro. *Int. J. Pharm.* **389**, 10–17 (2010).

422. Hua, S. & Vaughan, B. In vitro comparison of liposomal drug delivery systems targeting the oxytocin receptor: A potential novel treatment for obstetric complications. *Int. J. Nanomedicine* **14**, 2191–2206 (2019).

423. Dvir, T. *et al.* Nanoparticles targeting the infarcted heart. *Nano Lett.* **11**, 4411–4414 (2011).

424. Guo, P., Moses-Gardner, A., Huang, J., Smith, E. R. & Moses, M. A. ITGA2 as a potential nanotherapeutic target for glioblastoma. *Sci. Rep.* **9**, 3–12 (2019).

425. Cohen, Z. R. *et al.* Localized RNAi therapeutics of chemoresistant grade IV glioma using hyaluronan-grafted lipid-based nanoparticles. *ACS Nano* **9**, 1581–1591 (2015).

426. Rafique, A. *et al.* Targeted lipid nanoparticle delivery of calcitriol to human monocyte-derived macrophages in vitro and in vivo: investigation of the anti-inflammatory effects of calcitriol. *Int. J. Nanomedicine* **Volume 14**, 2829–2846 (2019).

427. Lu, Y. mei *et al.* Targeted therapy of brain ischaemia using Fas ligand antibody conjugated PEG-lipid nanoparticles. *Biomaterials* **35**, 530–537 (2014).

428. Sinhmar, G. K. *et al.* Surface engineered lipid nanoparticle-mediated site-specific drug delivery system for the treatment of inflammatory bowel disease. *Artif. Cells, Nanomedicine Biotechnol.* **46**, 565–578 (2018).

429. Mei, L. P. *et al.* Enediol-Ligands-Encapsulated Liposomes Enables Sensitive Immunoassay: A Proof-of-Concept for General Liposomes-Based Photoelectrochemical Bioanalysis. *Anal. Chem.* **89**, 6300–6304 (2017).

430. Ashley, C. E. *et al.* The targeted delivery of multicomponent cargos to cancer cells by nanoporous particle-supported lipid bilayers. *Nat. Mater.* **10**, 389–397 (2011).

431. Accardo, A. *et al.* Easy formulation of liposomal doxorubicin modified with a bombesin peptide analogue for selective targeting of GRP receptors overexpressed by cancer cells. *Drug Deliv. Transl. Res.* **9**, 215–226 (2019).

432. Zalba, S. *et al.* Cetuximab-oxaliplatin-liposomes for epidermal growth factor receptor targeted chemotherapy of colorectal cancer. *J. Control. Release* **210**, 26–38 (2015).

433. Oude Blenke, E. *et al.* Liposome functionalization with copper-free 'click chemistry'. *J. Control. Release* **202**, 14–20 (2015).

434. Noble, G. T., Stefanick, J. F., Ashley, J. D., Kiziltepe, T. & Bilgicer, B. Ligand-targeted liposome design: Challenges and fundamental considerations. *Trends Biotechnol.* **32**, 32–45 (2014).

435. Kim, S., Subramanya, S., Peer, D., Shimaoka, M. & Shankar, P. Antibody-Mediated Delivery of siRNAs for Anti-HIV Therapy. *Methods Mol. Biol.* **721**, 339–353 (2011).

436. Lee, J. *et al.* Cellular Engineering with Membrane Fusogenic Liposomes to Produce Functionalized Extracellular Vesicles. *ACS Appl. Mater. Interfaces* **8**, 6790–6795 (2016).

437. Perrier, T., Saulnier, P., Fouchet, F., Lautram, N. & Benoît, J. P. Post-insertion into Lipid NanoCapsules (LNCs): From experimental aspects to mechanisms. *Int. J. Pharm.* **396**, 204–209 (2010).

438. Song, S. *et al.* Peptide ligand-mediated liposome distribution and targeting to EGFR expressing tumor in vivo. *Int. J. Pharm.* **363**, 155–161 (2008).

439. Palekar, R. U. *et al.* Thrombin-targeted liposomes establish a sustained localized anticlotting barrier against acute thrombosis. *Mol. Pharm.* **10**, 4168–4175 (2013).

440. Gao, X. *et al.* Anchor peptide captures, targets, and loads exosomes of diverse origins for diagnostics and therapy. *Sci. Transl. Med.* **10**, eaat0195 (2018).

441. Li, J. *et al.* Polymer-lipid hybrid anti-HER 2 nanoparticles for targeted salinomycin delivery to HER 2-positive breast cancer stem cells and cancer cells. *Int. J. Nanomedicine* **12**, 6909–6921 (2017).

442. Yang, Y., Yang, Y., Xie, X., Cai, X. & Mei, X. Preparation and characterization of photo-responsive cell-penetrating peptide-mediated nanostructured lipid carrier. *J. Drug Target.* **22**, 891–900 (2014).

443. Tran, T. H. *et al.* Hyaluronic acid-coated solid lipid nanoparticles for targeted delivery of vorinostat to CD44 overexpressing cancer cells. *Carbohydr. Polym.* **114**, 407–415 (2014).

444. Liu, K. C. *et al.* Development of a novel thermal-sensitive multifunctional liposome with antibody conjugation to target EGFR-expressing tumors. *Nanomedicine Nanotechnology, Biol. Med.* **15**, 285–294 (2019).

445. Jhaveri, A., Luther, E. & Torchilin, V. The effect of transferrin-targeted, resveratrol-loaded liposomes on neurosphere cultures of glioblastoma: implications for targeting tumour-initiating cells. *J. Drug Target.* **27**, 601–613 (2019).

446. You, W. W., Haugland, R. P., Ryan, D. K. & Haugland, R. P. 3-(4-Carboxybenzoyl)Quinoline-2-Carboxaldehyde, a Reagent With Broad Dynamic Range for the Assay of Proteins and Lipoproteins in Solution. *Anal. Biochem.* **244**, 277–282 (1997).

447. Alkilany, A. M. *et al.* Ligand density on nanoparticles: A parameter with critical impact on nanomedicine. *Adv. Drug Deliv. Rev.* **143**, 22–36 (2019).

448. Sykes, E. A., Chen, J., Zheng, G. & Chan, W. C. W. Investigating the Impact of Nanoparticle Size on Active and Passive Tumor Targeting Efficiency. *ACS Nano* **8**, 5696–5706 (2014).

449. Wilhelm, S. *et al.* Analysis of nanoparticle delivery to tumours. *Nat. Rev. Mater.* **1**, 16014 (2016).

450. Peng, J. *et al.* Intratumoral fate of functional nanoparticles in response to microenvironment factor: Implications on cancer diagnosis and therapy. *Adv. Drug Deliv. Rev.* **143**, 37–67 (2019).

451. Sawant, R. R. & Torchilin, V. P. Challenges in Development of Targeted Liposomal Therapeutics. *AAPS J.* **14**, 303–315 (2012).

452. Salvati, A. *et al.* Transferrin-functionalized nanoparticles lose their targeting capabilities when a biomolecule corona adsorbs on the surface. *Nat. Nanotechnol.* **8**, 137–143 (2013).

453. Hassanzadeh, P., Atyabi, F. & Dinarvand, R. Ignoring the modeling approaches: Towards the shadowy paths in nanomedicine. *J. Control. Release* **280**, 58–75 (2018).

454. Varshosaz, J., Hassanzadeh, F., Sadeghi, H. & Andalib, S. Synthesis of octadecylamine-retinoic acid conjugate for enhanced cytotoxic effects of 5-FU using LDL targeted nanostructured lipid carriers. *Eur. J. Med. Chem.* **54**, 429–438 (2012).

455. Sobot, D. *et al.* Conjugation of squalene to gemcitabine as unique approach exploiting endogenous lipoproteins for drug delivery. *Nat. Commun.* **8**, 1–9 (2017).

CHAPTER II
AIM OF THE THESIS

Nanocarriers have been developed to allow drug administration with improved tumor delivery and selective cell targeting. Lipid nanocapsules have been used to deliver antitumor drugs. Numerous studies have already demonstrated their ability to encapsulate drugs, their safety, and the translation potential of their manufacturing. However, the assessment of their real tumor uptake *in vivo* and their advantages over other established nanotechnologies are still lacking for a clinical translation of more effective antitumor LNCs i.v. CRC is currently the 2nd cancer localization in terms of mortality at the world level. Most of the mortality is associated with metastasis, with the need for systemic therapy. The CMS4 CRCs, associated to a desmoplastic stroma is the most challenging. Indeed, TME is a major cause of cancer resistance to classical therapy and metastasis. Antiangiogenic and immunotherapy have already improved significantly cancer treatment, but there is a gap in the development of a new therapy targeting the stromal compartment. The targeting of FAP, the inhibition of CAFs activation, or the blockade of CAF paracrine factors and ECM remodeling have demonstrated the positive impact they could have on cancer therapy. Despite the preclinical and clinical efforts, targeting CAFs faces challenges of CAF heterogeneity, limited relevant models, and their combination with other therapies.

MYC oncogene leads a canonical signaling pathway in CRC. It is a highly desirable therapeutic target that has not yet clinically approved therapies. BET inhibitors have demonstrated MYC inhibition and anti-CRC activity, but their current clinical trials are trapped with the under-estimated complexity of their mechanism of action. Besides, BETi JQ1 PK properties, mainly poor water solubility and short half-life, do not allow a translation to clinical trials.

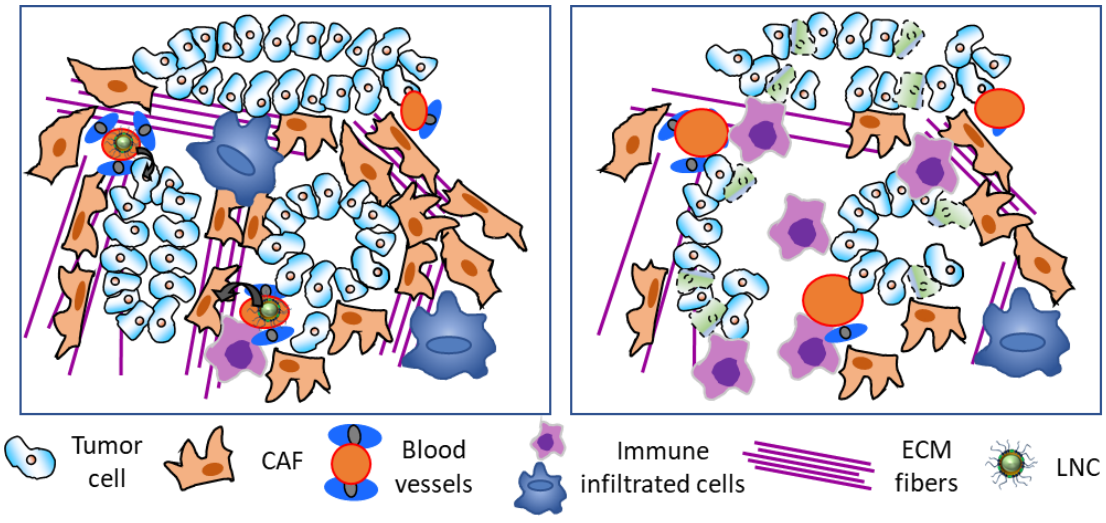

Figure 1. Graphical objectives of the anti-CAFs LNC therapy. At left, desmoplastic stroma with many CAFs, dense ECM, compressed blood vessels, and a majority of immunosuppressive myeloid cells. Treatment with LNCs against CAFs and tumor cells would lead to the right TME state, with reduced stromal cells and extracellular fibers, immune shift towards antitumor immune cells, blood vessels decompression, and tumor cells elimination.

This thesis project is based on the hypothesis that new LNC-based strategies would have better anti-CRC efficacy than classical administration or other nanotechnologies for rational drug delivery to tumor. To get a step forward in LNC development, we proposed two independent approaches to obtain translational formulations: i) use CAFs as a therapeutic target to develop LNCs encapsulating drugs having demonstrated anti-CAF properties (Figure 1); and ii) use the experimental anti-CRC and potentially TME-modulating drug JQ1 to assess the translation ability of JQ1-loaded LNC compared with free drug or another nanotechnology.

In this thesis, new LNCs were evaluated on relevant CRC models including CAFs, such as a 2D CAF monoculture, a new 3D co-culture with CRC cells, and syngeneic tumor-bearing mice (Figure 2).

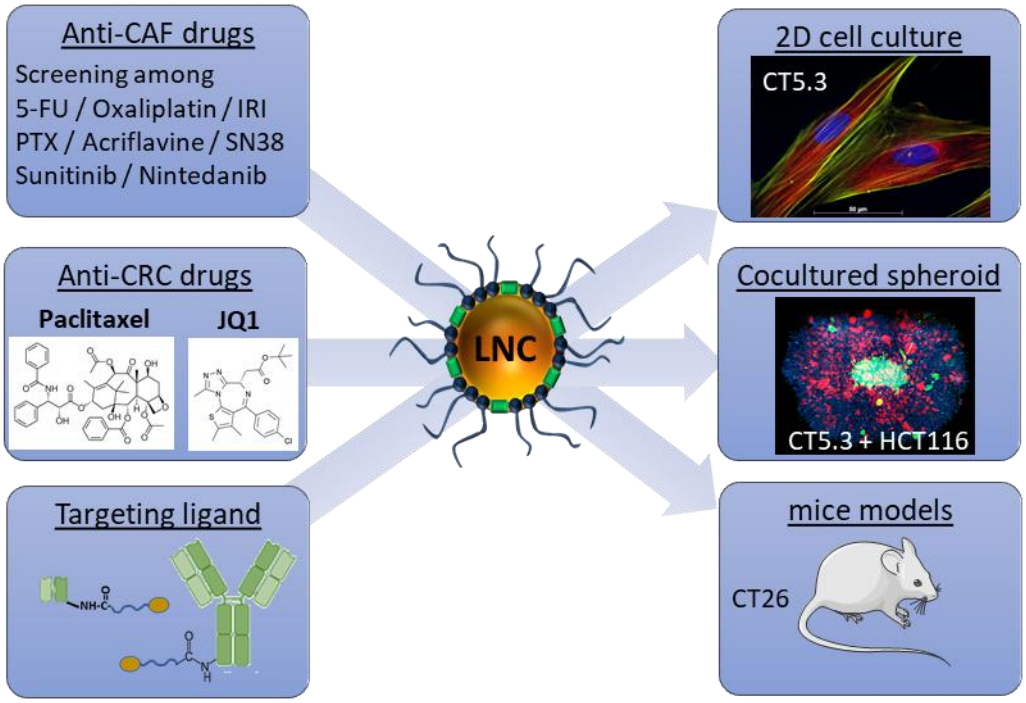

Figure 2. The general plan of the thesis work

The experimental results of the thesis will be organized with the two following chapters

- Chapter III: Inhibition of colorectal cancer-associated fibroblasts by lipid nanocapsules loaded with acriflavine or paclitaxel
- Chapter IV: Comparison of two nano-encapsulated JQ1 for treatment of colorectal cancer

The results of this thesis have the ambition to bring decisive information about the LNC potential for systemic CRC therapy.

CHAPTER III
INHIBITION OF COLORECTAL CANCER-ASSOCIATED FIBROBLASTS BY LIPID NANOCAPSULES LOADED WITH ACRIFLAVINE OR PACLITAXEL

Adapted from Inhibition of colorectal cancer-associated fibroblasts by lipid nanocapsules loaded with acriflavine or paclitaxel, Thibaut Fourniols**,** Estelle Bastien, Alizée Canevat, Olivier Feron, Véronique Préat, *International Journal of Pharmaceutics* 584, 119337 (2020).

ABSTRACT

Crosstalk between cancer-associated fibroblasts (CAFs) and colorectal cancer cells promotes tumor growth and contributes to chemoresistance. In this study, we assessed the sensitivity of a CAF cell line, CT5.3hTERT, to standard-of-care and alternative cytotoxic treatments. Paclitaxel (PTX) and acriflavine (ACF) were identified as the most promising molecules to inhibit CAF development. To allow the translational use of both drugs, we developed lipid nanocapsule (LNC) formulations for PTX and ACF. Finally, we mixed CAFs and tumor cell lines in a cocultured spheroid, and the effect of both drugs was investigated by histological analyses. We demonstrated CAF inhibition by LNC-ACF and whole tumor inhibition by LNC-PTX. Altogether, we proposed a new strategy to reduce CAF populations in the colorectal microenvironment that should be tested in vivo.

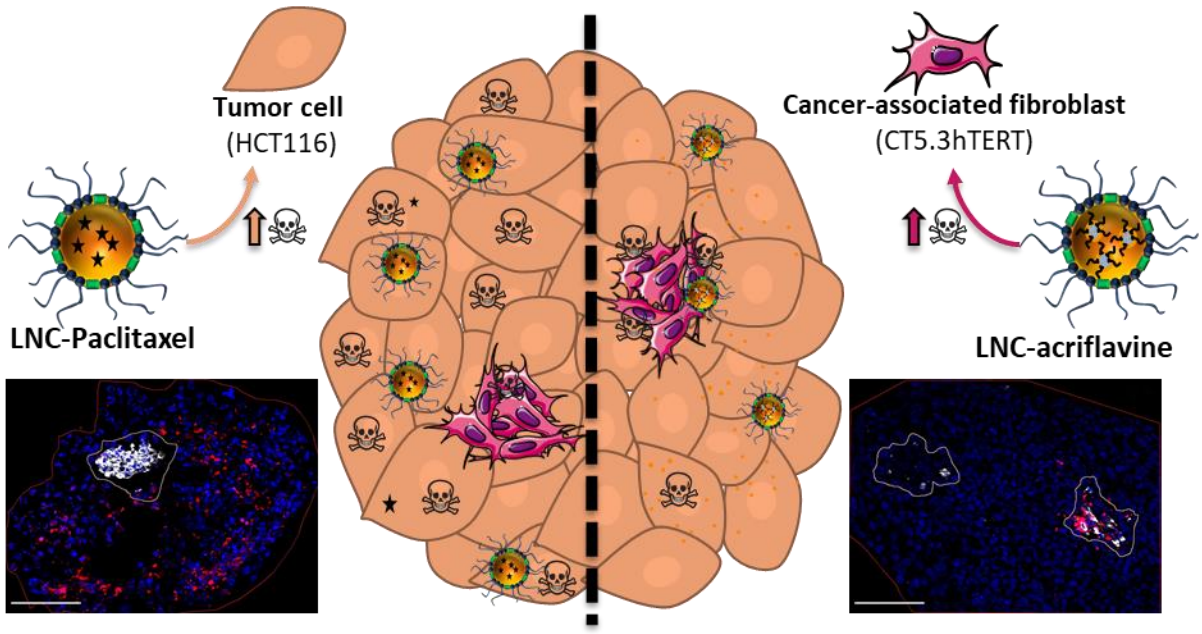

KEYWORDS

Cancer-associated fibroblast, tumor spheroid, paclitaxel, acriflavine, lipid nanocapsule

TABLE OF CONTENTS

I. INTRODUCTION

The tumor microenvironment (TME) significantly influences cancer evolution. In colorectal cancer (CRC), the consensus molecular subtypes (CMS) classification is partly dependent on the TME nature. mesenchymal CMS4, associated with an important population of cancer-associated fibroblasts (CAFs), shows the worst prognosis and a lower therapeutic response to classical chemotherapy associated with 5-fluorouracil (5-FU), irinotecan (IRI) and/or oxaliplatin[1–3]. Crosstalk between CAFs and CRC cancer cells promotes tumor growth and metastatic dissemination and confers chemoresistance. This represents a key TME population with several roles, including angiogenesis promotion, extracellular matrix remodeling, immune cell recruitment, and direct interaction with tumor cells, with a major impact from the TGF-β signaling pathway[4,5]. Their roles make them a potential therapeutic target to inhibit tumor development and resistance. Several preclinical strategies have been developed with promising results but without successful clinical translation, creating a gap into TME-related treatment[6].

Drug-loaded nanoparticles (NPs) are a major field of anticancer therapy development. They offer improved properties compared to free drug administration, such as increased tumor delivery, slower clearance from serum, or reduced toxicity[7]. They have shown promising results in TME modulation[7]. In the domain of CAF inhibition, nab-paclitaxel (PTX), docetaxel, or navitoclax have been associated with CAF depletion in pancreatic cancer[8–10]. However, targeting CAFs has never been applied to CRC models, and a rational choice of an anti-CAF drug or a specific nanomedicine has not been reported.

Spheroid models share some features with tumors that are not present in 2D cultures, such as a structural organization, a cellular layered assembling, hypoxia, and nutrient gradient[11]. Due to their properties, they have been considered as a relevant model to challenge in vitro antitumor drugs. Stromal-cancer cells cocultured spheroids have added a layer of complexity and have also been used to test experimental CAF-targeted liposomes or T cell bispecific antibody[8,12]. However, there was no study about heterotypic CRC spheroid sensitivity to NPs to our knowledge.

The aim of the study was to select rational assay molecule(s) with anti-CAF activity and to load these drugs into NPs to improve their effectiveness. We used a recognized model of immortalized CAFs from human CRC and developed a cocultured 3D spheroid model to take into account the interactions between CAFs and tumor cells. The repurposing or the selection and evaluation of molecules already approved for another indication has appeared as a strategy for quick translational access[13]. Several drugs, including chemotherapeutic drugs, kinase inhibitors, and acriflavine (ACF), were evaluated in a drug screening against the CAF cell line and tumor cell line. LNCs were used

to encapsulate the drugs because they demonstrated efficient drug delivery in cancer and can be tailored for each cargo[14,15]. LNC formulations were tested against the cocultured spheroid model to evaluate their inhibition potential on both CAFs and CRC cells. Altogether, we have designed a new NP-based combinatorial strategy to target CAFs in CRC.

II. MATERIALS AND METHODS

II.1. MATERIALS

Labrafac® lipophile WL 1349 (caprylic/capric triglycerides) and Labrafil® M2125 CS (linoleoyl polyoxyl-6 glycerides) were a gift from Gattefossé S.A. (Saint-Priest, France). Solutol® HS 15 (a mixture of free polyethylene glycol 660 and polyethylene glycol 660 hydroxystearate), polysorbate 80, sorbitane monooleate, and ACF were purchased from Sigma-Aldrich (USA). Lipoid S-100 (soybean phosphatidylcholine) was purchased from Lipoid Gmbh (Germany). Sunitinib malate and nintedanib esylate were purchased from Adooq Biosciences (USA). SN-38 and IRI were purchased from MCE-MedChemExpress (USA). 5-FU, oxaliplatin, and PTX were purchased from Chemieliva (China).

CT5.3hTERT cells were obtained from the Cancer Research Institute Ghent (Belgium). HCT116 and CT26 cells were obtained from the ATCC (American Type Culture Collection, USA). The cell lines were cultured in high glucose (25 mM) DMEM (ThermoFisher 41965) supplemented with 10% fetal bovine serum, 1% 200 mM L-glutamine solution (final concentration of 6 mM), 1% 10,000 U/mL penicillin, and 10,000 μg/mL streptomycin solution at 37°C in a 5% CO2 incubator. All cell culture reagents were purchased from Gibco (Thermo Fisher Scientific, USA).

II.2. CELL IMMUNOCYTOCHEMISTRY

CT5.3hTERT and HCT116 cells were seeded on a coverslip coated with poly-L-lysine for HCT116 cells and uncoated for CT5.3hTERT cells, and then cultured as described in the general methods. When cells reached 50% confluence, they were rinsed with PBS, fixed with 4% (w/v) paraformaldehyde (PFA) for 10 min at RT, and rinsed 3 times with PBS. The cells were blocked and permeabilized in PBS supplemented with 0.3% Triton X-100, 10% goat serum, and 2% bovine serum albumin (BSA) for less than 60 min at RT. The cells were then incubated overnight at 4°C with the primary antibody, anti-alpha smooth muscle actin (SMA) 1/100 (clone RM253, Bio-Techne, USA), and anti-alpha fibroblast activation protein (FAP) 1/250 (ESC11, provided by the Olivia Newton-John Research Institute, Australia)[16], in the blocking solution diluted 1:1 in PBS. The cells were rinsed 3 times with PBS and then incubated with the secondary antibody goat anti-human IgG, Alexa Fluor 647 (Thermo Fisher Scientific) for FAP and goat anti-rabbit IgG, Oregon Green 488 for SMA for 2 h in the blocking solution diluted 1:3 in PBS, with 1 μg/mL DAPI to stain the nuclei. The cells were rinsed 3 times with PBS and then mounted with fluorescence

mounting medium (Dako, Agilent, USA). The slides were imaged with a fluorescence microscope (Axio Imager Z1, Zeiss).

II.3. VIABILITY ASSAY AGAINST CAF CT5.3HTERT CELLS AND COLORECTAL HCT116 AND CT26 CELLS

For the crystal violet assay, the CT5.3hTERT, HCT116, and CT26 cell lines were seeded (7,000/5,000/3,000 cells per well, respectively) in 100 µL of complete culture medium in a 96-well plate (NunclonTM Delta Surface, Thermo Fisher Scientific). The next day, 100 µL of a serial dilution of the evaluated drug was added to each well, including a condition with cells but no drug ("Medium") and a condition of medium without cells ("Blank"). All conditions were run in quadruplicate (n=4). After 48 h of incubation, the medium was removed; cells were fixed in 4% PFA for 30 min and stained with 0.5% crystal violet (Merck, Germany) in a 1:4 methanol:water solution for 30 min. After two washes with deionized water and a cotton bud, 120 µL of methanol was added to dissolve the crystal violet, and the plates were agitated for 30 min. The absorbance was measured at 545 nm with a Multiskan EX plate reader (Thermo Fisher Scientific). The percent cell viability at each concentration was calculated with the equation 1

$$\textit{Equation 1: } \%viability_{Ci} = \frac{A_{Ci} - A_{Blank}}{A_{Medium} - A_{Blank}}$$

With AMedium as the "Medium" mean absorbance (considered as 100% cell viability) and ACi as the mean absorbance at the tested concentration. Cell viability as a function of drug concentration was plotted using GraphPad Prism 8, and the 50% inhibitory concentration (IC_{50}) of each experiment was calculated using the "absolute IC50" function.

II.4. FORMULATION OF LNCS LOADED WITH PTX AND ACF

The percent (w/w) excipients in the LNC formulation loaded with PTX or ACF is reported in Table 1. LNC formulations were scalable from a final weight of 2.5 g to 15 g. LNC formulation was divided into 3 steps[17]: i) weighing of the ingredients, mixing and solubilization; ii) defined heating and cooling cycles under magnetic stirring around the observed phase-inversion temperature (PIT), from PIT+10°C to PIT-10°C; and iii) addition of cold 0.9% NaCl for injection, precisely at the PIT, under high speed stirring. The unloaded LNCs were obtained using the same method without the addition of the active compound. All LNCs were filtered through a 0.2 µm filter and stored at 4°C until use.

The LNC-PTX formulation was adapted from the LNC formulation described by Bastiancich et al.[18]. To obtain LNC-PTX, PTX was dispersed in Labrafac® and sorbitane monooleate in a water bath at 50°C until complete dissolution of the drug (approximately 30 min - 1 h). Then, Solutol®, sodium chloride and water for injection were added to the formulation. Three temperature cycles were performed with a PIT of approximately 60°C.

LNC-ACF with reverse micelle formulation was prepared according to Montigaud et al.[19], but slightly modified. Briefly, Lipoid S-100 was mixed with Solutol®, Labrafil®, sodium chloride and water for injection and heated at 40°C. Four temperature cycles were performed with a PIT of approximately 65°C. In parallel, a reverse emulsion of ACF was prepared in an excess amount as follows: a solution of ACF in water at 200 mg/mL was added to a mixture of polysorbate 80 and Labrafil® at a proportion of 3:4:20 (ACF:polysorbate-80:Labrafil®). The reverse emulsion was vortexed and then stirred at high speed (>500 RPM) until use. Once the formulation reached the top temperature in the fourth cycle, the reverse micelle solution was added.

Table 1. Percent (w/w) of the ingredients in both LNC formulations.

Excipient	LNC-PTX	LNC-ACF
API	Paclitaxel 0.20%	ACF in reverse micelles 3:4:20 (ACF 200 mg/mL solution:polysorbate 80:Labrafil®) 9.6%
Oil	Labrafac® 14.1%	Labrafil® 5.5%
Hydrophobic surfactant	Sorbitane monooleate 2.8%	Lipoid S100 0.63%
Solutol®	10.9%	9.3%
Sodium chloride	0.40%	0.57%
Water for injection	11.6%	14.3%
0,9% Sodium chloride for injection	60%	60%

II.5. PHYSICOCHEMICAL CHARACTERIZATION OF THE LNC FORMULATIONS

LNC formulations were characterized for their size and ζ potential by a Zetasizer Ultra (Malvern, UK). The size was measured as the mean intensity peak of multi-angle DLS, and the polydispersity index was extracted from backscatter angle measurements. The ζ potential was measured by electrophoretic mobility in 3 different batches.

Quantification of the ACF and PTX payload and encapsulation efficiency was performed by HPLC on a Shimadzu Prominence system (Shimadzu, Japan). To measure the formulation drug payload, formulations were diluted 1:100 in methanol for ACF and in acetonitrile for PTX. To measure encapsulation efficiency, formulations were ultrafiltered with 30 kDa centrifugal filtration units (Vivaspin® 500, VWR, Belgium). The ultrafiltrate was then diluted and analyzed by the same HPLC method. Stability assays were performed on the formulation, kept at 4°C, and filtered again with a PVDF 0.45 µm filter before each measurement to remove potential drug precipitates. For ACF, analytical separations were performed by using an Xbridge® C18 grafted phenyl column (4.6×150 mm; 3 µm). The HPLC method was carried out at 50°C with a mobile phase of TFA 0.05%/methanol (30/70) at a flow rate of 0.8 mL/min, with a detection wavelength of 262 nm[19]. PTX quantification was performed by using a BDS Hypersil C18 column (Thermo Fisher Scientific) (100 × 4.6 mm; particle size 3 µm), carried out at 40°C with a mobile phase of acetonitrile/water (50/50) at a flow rate of 1 mL/min, with a detection wavelength of 227 nm[20]. The encapsulation efficiency was calculated according to the equation 2:

$$\textit{Equation 2: } EE\% = \frac{[drug]_{total} - [drug]_{free}}{[drug]_{total}}$$

Drug payload was evaluated as the ratio between the total amount of drug and the LNC dispersion (w/w)

$$\textit{Equation 3: } drug\ payload = \frac{amount\ of\ total\ drug\ (mg)}{amount\ of\ all\ components\ (g)}$$

II.6. 3D SPHEROID MODEL

Spheroids were prepared by seeding 1500 cells/well of either HCT116 or a 1:1 mix of HCT116 and CT5.3hTERT ("co-culture") in an ultra-low attachment 96-well plate (Corning, USA) in DMEM supplemented with 10% heat-inactivated FBS, containing 25 mM D-glucose and 6 mM L-glutamine. Selected drugs were added three days after seeding (day 0) by renewing half of the culture medium. Spheroid growth was monitored for 4 days, during which the medium was not changed, using an Axiovert S100 microscope (Zeiss, Germany). The spheroid area was measured using ImageJ software at different time points. Spheroid growth was quantified by normalization of each spheroid area on day 0.

Cell organization in the 3D structure was studied on 7-day-old cocultured spheroids composed of HCT116-m-cherry and CT5.3hTERT (1:1). Spheroids were fixed with 4% (w/v) PFA – 0.5% Triton X-100 at RT for 1 h, blocked for 1 h with 5% BSA and immunolabeled. An anti-vimentin antibody (D21H3, Cell Signaling, The Netherlands) and an anti-rabbit antibody coupled with Alexa

Fluor 647 (Thermo Fisher Scientific) were used successively for 24 h; nuclei were counterstained with Hoechst. After immunolabeling, spheroids were cleared following the CUBIC protocol. The acquisition was performed using a Z1 Lightsheet microscope (Zeiss) using a 5× detection objective (RI = 1.45) and the 3D view obtained by Arivis imaging software.

To measure viability, 20 µL of Alamar Blue cell viability reagent (Thermo Fisher Scientific) was introduced into each well, and the fluorescence (λex: 555 nm; λem: 585 nm) was measured in the spheroid culture plate using a SpectraMax M3 instrument (Molecular Devices, USA) after 16-18 h of incubation. Fluorescence values were normalized with the 100% viability given by the untreated wells and the 0% given by wells without spheroid and no treatment. All experiments were performed with 6 replicates, and N≥3 reproduced experiments.

Cell death was assessed by immunohistology on spheroid sections after 48 h of treatment[21]. The spheroids were incubated with propidium iodide (PI) (Sigma-Aldrich) solution at 20 µg/mL for 5 min at RT. After two washes with PBS, the spheroids were fixed with 4% PFA, cryoprotected in sucrose 30%, and embedded in OCT (VWR). Frozen sections (5 µm) were stained with a 1:500 diluted rabbit anti-vimentin antibody (D21H3) and then with a 1:250 diluted anti-rabbit antibody coupled with Alexa Fluor 647, and nuclei were counterstained with DAPI. Slides were mounted with fluorescence mounting medium (Dako, Agilent, USA), and staining was visualized with a Zeiss Axio Imager Z1 microscope equipped with an Apotome module. To evaluate HCT116 and fibroblast cell death in spheroid sections, whole tissue sections and fibroblast-enriched regions were manually delineated based on DAPI or vimentin staining with an additional one cell nucleus width around it, respectively. In these regions, the PI-stained area above a fixed threshold was measured with AxioVision 4.8 software. The results were expressed as PI-stained percentage areas inside or outside CAF-enriched regions, with the mean and deviation weighted by the areas of each zone.

II.7. IN VIVO EFFICACY EVALUATION OF LNC-ACF & LNC-PTX

The in vivo experiments were performed under the guidelines of the Belgian national regulation, with approval from the animal care ethical committee of the Université Catholique de Louvain (2017/UCL/MD/034).

Five-week-old female BALB/C mice were obtained from Janvier (France). The mice were anesthetized with 13 mg/kg and 100 mg/kg xylazine and ketamine, respectively, and injected subcutaneously (s.c.) with 5×104 CT26 cells. On day 10 following tumor inoculation, when the tumors reached approximately 50 mm3, the mice were randomly divided into the following 3

groups: group 1: untreated (N=6); group 2: i.v. LNC-PTX 7.5 mg/kg every three days (N=5); group 3: i.v. combination of LNC-PTX 7.5 mg/kg + LNC-ACF 7.5 mg/kg, every three days (N=7). Four cycles of treatments were administered before the end of the experiment, 12 days after the first administration. The tumor volume was measured with a caliper and calculated with the following equation: length × width × height.

II.8. STATISTICAL ANALYSIS

GraphPad Prism software was used to conduct the statistical analysis, and p-values<0.05 were considered statistically significant (*$p < 0.05$, **$p < 0.01$ and ***$p < 0.001$). Spheroid growth curve comparisons were performed by two-way ANOVA (mean ± SEM, N=4). The proportion of PI-positive areas was analyzed by a two-way ANOVA test, with Sidak's multiple comparisons test between %PI(CAF) and %PI(tumor) from each condition. Spheroid relative growth and viability were compared to a 100% value corresponding to the control condition by a one-way t-test for each condition, and free and encapsulated drug were compared using unpaired t test. For in vivo efficacy, two-way ANOVA was performed with Dunnett's multiple comparisons test at each measured time.

III. RESULTS

III.1. DRUG SCREENING AGAINST CAFS (CT5.3HTERT CELLS)

To determine whether anticancer drugs could be active against colorectal CAFs, we used the CT5.3hTERT cell line, a human colorectal CAF, immortalized with hTERT gene transfection[22] expressing smooth muscle actin and fibroblast activation protein, two selective markers of CAFs vs normal fibroblasts or cancer cells[6] (figure S1). We evaluated the proliferation inhibition potency of classical CRC chemotherapy (oxaliplatin, 5-FU, IRI), alternative chemotherapy (SN38, PTX), multiple kinase inhibitors including fibroblast growth factors targeting (sunitinib, nintedanib), and ACF, an antibiotic known to inhibit HIFs and EMT, to activate p53, and to induce mitochondrial or endoplasmic reticulum apoptosis and autophagy[19,23–25]. To assess the relative inhibition against cancer cells, the most active molecules were also screened against the human HCT116 and murine CT26 CRC cell lines. We observed a relative insensitivity of CAFs to antiproliferative agents in general and to current CRC standards of care chemotherapies in particular (Table 2 and Figure S2), with IC_{50} values of 8.4, 12 and 15 μM for oxaliplatin, IRI and 5-FU, respectively. CAF sensitivity to PTX was higher, with an IC_{50} of 1.7 μM, but lower than CRC cell sensitivity, with an IC_{50} of 330 and 140 nM for HCT116 and CT26 cells, respectively. Conversely, the kinase inhibitor sunitinib and ACF presented an inhibition pattern that was similar in all cell lines, approximately 2-4 μM for sunitinib and 1-2 μM for ACF, probably due to their targeted activity against some common signaling pathways. ACF and PTX had the smallest IC_{50} against CAFs. Therefore, we selected both drugs as candidates to inhibit CAFs and/or CRC.

Table 2. IC_{50} values (μM) of proliferation inhibition over 48 h (mean ± SEM, N≥3 for comparisons and N≥2 for drugs tested only with CT5.3hTERT).

Drug	CT5.3hTERT	HCT116	CT5.3hTERT/ HCT116 ratio	CT26	CT5.3hTERT/ CT26 ratio
Acriflavine	1.1 ± 0.3	0.80 ± 0.20	1.4	1.8 ± 0.1	0.61
Sunitinib	3.6 ± 0.8	2.2 ± 0.4	1.6	3.9 ± 0.4	0.92
Paclitaxel	1.7 ± 1.2	0.33 ± 0.33	5.2	0.14 ± 0.10	12
SN38	2.2 ± 1.4	0.10 ± 0.04	22	0.11 ± 0.05	20
Nintedanib	5.2 ± 0.6				
Oxaliplatin	8.4 ± 1.0				
IRI	12 ± 8				
5-FU	15 ± 8				

III.2. LNC FORMULATION

To improve their pharmaceutical properties, PTX and ACF were encapsulated in LNCs. LNC-ACF has been shown to reduce toxicity and enhance the circulation time of ACF, whereas LNC-PTX has been associated with enhanced delivery of PTX to tumors in vivo[19,26]. PTX and ACF were encapsulated in two separate formulations optimized depending on the individual drug properties. Their physicochemical characterization (Table 3) indicated that a high encapsulation efficiency of PTX and drug payload of 2 mg/g formulation were achieved. The PTX formulation was stable for at least 4 weeks with no significant drug loss (Figure S3). Increasing the drug payload to over 2 mg/mL led to a reduction in stability with drug precipitation in the following days (data not shown). ACF formulations were reproduced from a previous study[19], with an enhanced drug payload to 1.6 mg/mL achieved by increasing the ACF concentration into reverse micelles. Its stability showed a significant and continuous drug loss leading to an 18 ± 4% ACF reduction at 4 weeks (Figure S2).

Table 3. Physicochemical characterization of LNC formulations (mean ± SD, N=3).

Characteristic	Diameter (nm)	Polydispersity index	ζ potential (mV)	Drug payload (mg/g)	Encapsulation efficiency
Blank LNC-PTX	64.2 ± 0.3	0.050 ± 0.024	-6.4 ± 1.3		
LNC-PTX	60.3 ± 5.8	0.055 ± 0.005	-7.9 ± 1.3	1.98 ± 0.07	100%
Blank LNC-ACF	31.4 ± 0.1	0.041 ± 0.005	-5.4 ± 0.7		
LNC-ACF	32.7 ± 3.5	0.058 ± 0.015	-4.8 ± 1.0	1.6± 0.3	81 ± 7%

III.3. CAF INHIBITION EVALUATION IN A SPHEROID MODEL

III.3.1. Development of a cocultured spheroid

HCT116 cells or cocultured CAFs (CT5.3hTERT) and CRC cells (HCT116) were grown as spheroids in ultra-low attachment plates. On day 0 of the experiments, the HCT116 spheroid and the cocultured spheroids measured 530 ± 120 µm and 480 ± 200 µm in diameter, respectively. CAF contributed to a slightly increased growth rate since cocultured spheroids exhibited a relative area of 270% on day 4, compared to 227% for HCT116 spheroids (p=0.071, figure 1). 3D histology showed that CAFs migrated to make a few dense clusters close to the center of the spheroids (see video performed after the clearing of the spheroid at https://ars.els-cdn.com/content/image/1-s2.0-S0378517320303215-mmc2.mp4).

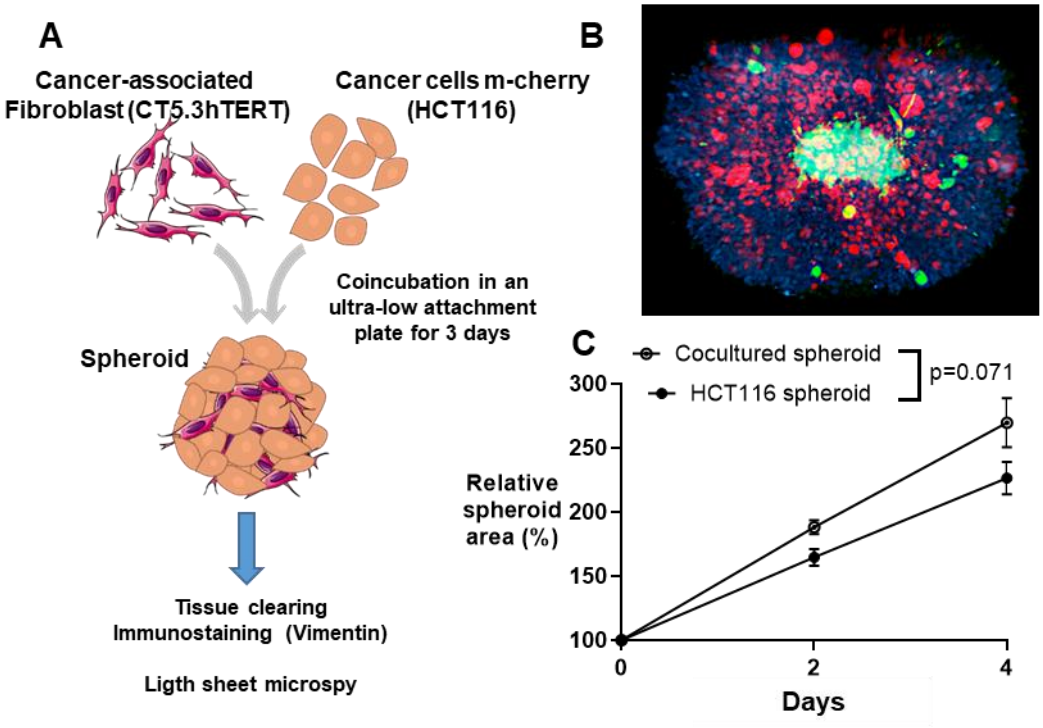

Figure 1. Cocultured spheroid model
Cell culture scheme depicting cocultured spheroid formation and characterization. B) Histological image of cocultured spheroids after clearing. Green: vimentin staining associated with CAFs; red: cancer cell fluorescence (m-cherry). C) Relative spheroid growth from day 0 to day 4, with each area normalized by its area on day 0. Comparison of curves by two-way ANOVA (mean ± SEM, N=4).

III.3.2. Drug-loaded LNC effects on spheroids

In order to evaluate the selective cytotoxicity of PTX and ACF on the two cell types of the cocultured spheroids, we incubated the spheroids with drug-loaded LNCs. Drug concentrations of 2 µM for PTX and 1 or 3 µM for ACF were established based on the literature and preliminary pilot assays, with the objective of finding a significant effect at a minimal concentration[27,28]. After 48 h, as in the monoculture drug screening, we evaluated cell death by histology using PI staining. The CAF areas were delineated by vimentin expression. LNC-PTX is associated with the highest cell death, with 3.7% of the spheroid area stained by PI and a spread of cell death across the whole spheroid with CAF over tumor cell ratios of 0.84 and 2.1, respectively (Figure 2). In contrast, LNC-ACF at 1 µM and 3 µM was associated with PI staining 18.8 and 6.3 times higher in the CAF area compared to the rest of the spheroid, respectively. This observation was confirmed by a significant interaction effect in the two-way ANOVA test ($p<0.05$). This demonstrated that in the coculture, only ACF selectively inhibited the CAF population. However, the ACF and PTX combination did not enhance cytotoxicity in either of the 2 cell populations compared to ACF for CAFs and PTX for tumor cells.

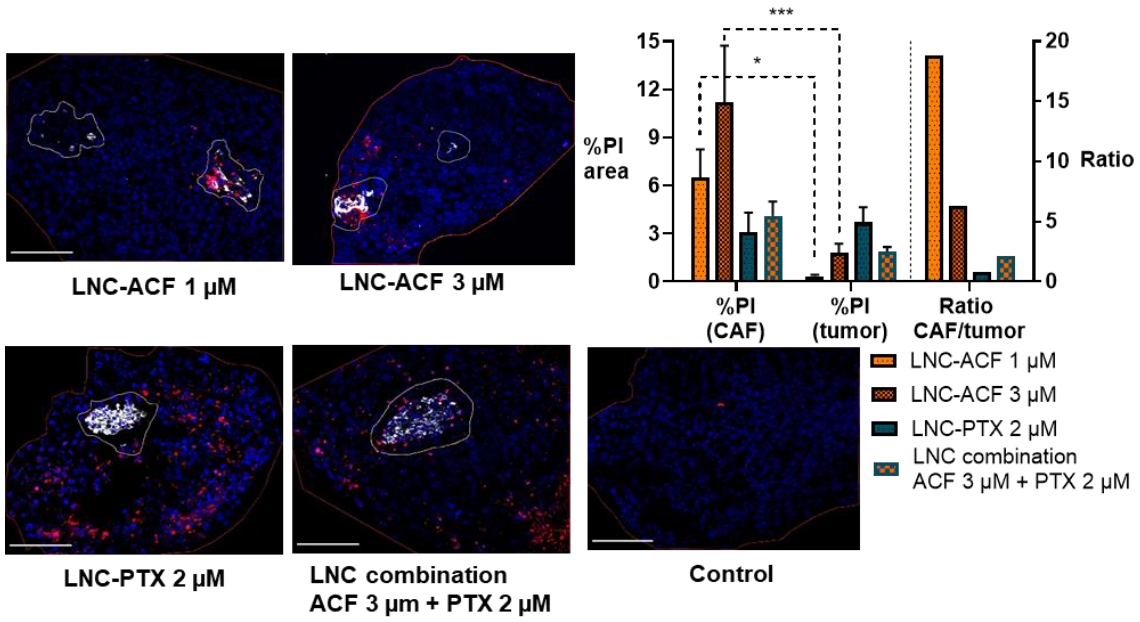

Figure 2. Histology of cocultured spheroids with cytotoxicity quantification
Left: representative spheroid pictures. Red: PI (dead cells), white: vimentin (CAF), blue: DAPI, red line: spheroid area, and white line: CAF area. Scale bar = 100 µm. Right: quantification of PI area expressed as the percent of the CAF area in the remaining part of the spheroid and the ratio of the two values (area-weighted mean ± SEM; N=7 to 12).

To evaluate the effects of drug-loaded LNCs on the whole spheroid, the spheroid area was followed for four days of treatment by phase-contrast microscopy, and final viability was assessed by resazurin fluorescence. For all treatment conditions, HCT116 spheroids did not show a significant difference from the cocultured spheroids (Figure S4). Both ACF and PTX displayed an inhibitory effect on spheroid growth (Figure 3A) and viability (Figure 3B). PTX at 2 µM induced 35% spheroid growth inhibition on day 2 and destruction of the spheroid on day 4, which was replaced by a halo of dead cells around a small core, with only 7% living cells compared to the control. ACF at 1 µM induced lower growth inhibition, with cell viability of approximately 50% and a preserved spheroid shape with less cellular debris. Encapsulation did not change spheroid growth inhibition and induced slightly increased viability compared to the free drug. The combination of LNC-PTX and LNC-ACF did not show synergistic or additive effects, and the growth area, as well as viability, were not changed compared to monotherapy (Figure 3C-E).

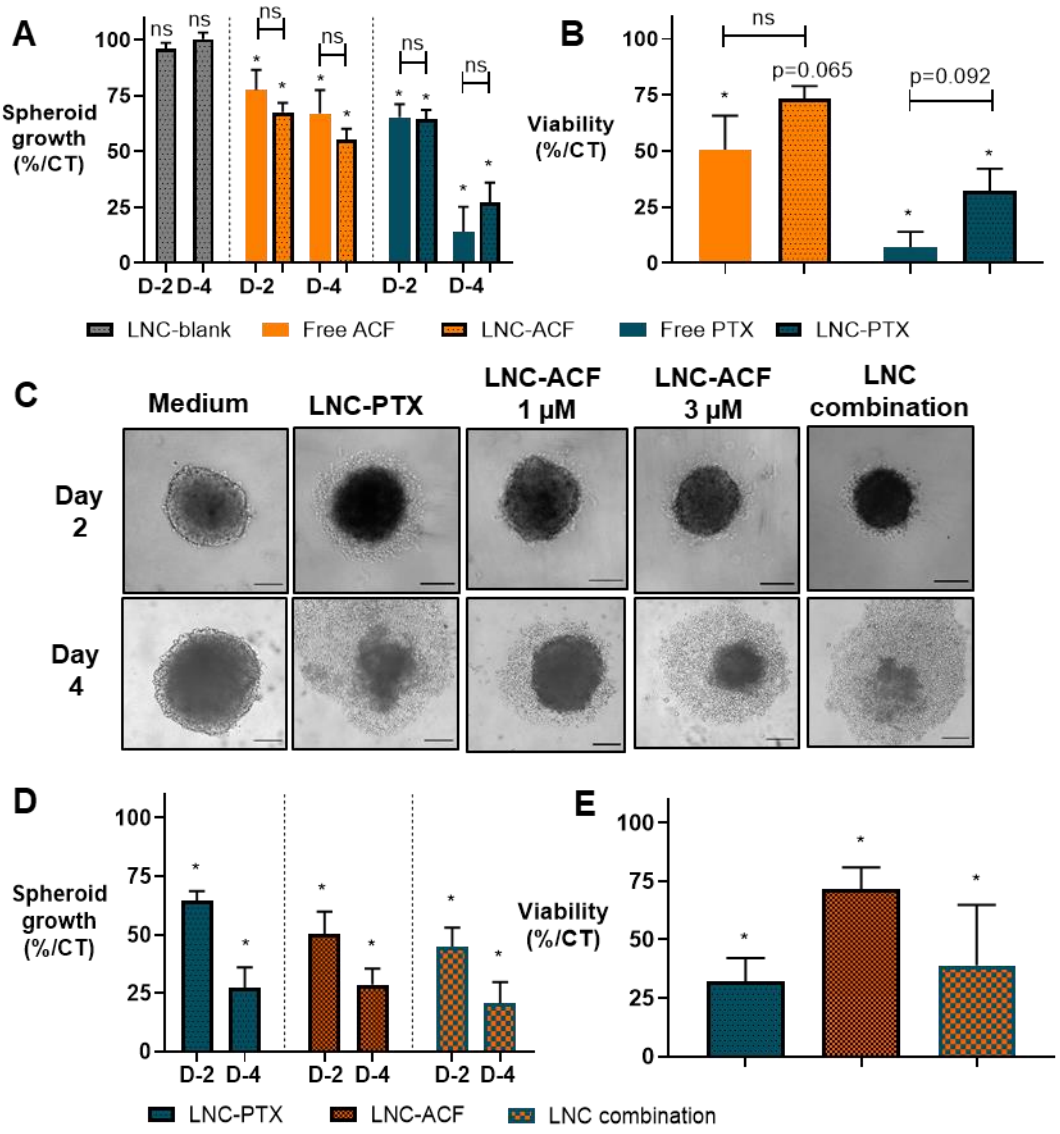

Figure 3. Cocultured spheroid growth inhibition and viability by ACF and PTX.
(A) Comparison of cell growth on days 2 and 4 and (B) viability on day 4 between the free and encapsulated drug for each condition; ACF at 1 µM, PTX at 2 µM and LNC-blank, a combination of the two blank formulations at the concentration equivalent to LNC-PTX 2 µM and LNC-ACF 1µM. C) Representative pictures of a spheroid with the different treatment conditions. Scale bar = 200 µm. D) and E) Combination effect of LNC-PTX and LNC-ACF on (D) cell growth and (E) viability; PTX at 2 µM and ACF at 3 µM. A) and D) Growth inhibition is expressed as the area ratio over control (CT) spheroids (mean ± SD; N≥3). B) and E) Viability measured by Alamar Blue assay and expressed as the ratio over control (CT) (mean ± SD; N≥2). Spheroid relative growth and viability were compared to a 100% value corresponding to the control condition by a one-way t-test for each condition. Free and encapsulated drug were compared using unpaired t test.

IV. DISCUSSION

As CAFs show tumor-promoting characteristics, the aim of this work was to design drug-loaded NPs that act not only on cancer cells but also on CAFs. The findings of this study indicated that CAFs were inhibited by several drugs that are not currently used in CRC therapy. Despite the demonstration of CAF in vitro inhibition, the in vivo translation was blocked by the lack of a model allowing CAF quantification in the TME.

The observed drug effects in the monocultured and monolayered 2D cell lines and the cocultured 3D spheroid were different. Screening the panel of drug candidates in 2D allowed the comparison of 8 potential anti-CAF drugs, selected from a preliminary wider panel (data not shown). Tumor spheroids are usually considered as more resistant to therapy, due to for instance an increased proportion of quiescent cells, ECM and interstitial fluid pressure, hypoxia or overexpression of efflux pumps, all hallmarks from in vivo tumors[11]. Surprisingly, CAFs were more sensitive than HCT116s to the molecules evaluated in the spheroid, whereas it was the reverse in the 2D results. Moreover, ACF and PTX induced the same effect in homotypic or heterotypic spheroids (Figure S4). It validated the rational choice from the 2D screening, as cocultured spheroids have demonstrated resistance to several CRC therapy such as 5-FU, Oxaliplatin, cetuximab and their combination[29], and also to PTX[30]. Tumor-stroma cocultured spheroids have also demonstrated attracting translational information for tumor response to classical or targeted therapies[11,31], and to be predictive of NP penetration, accumulation, and antitumor effect[32]. For these reasons, even if CAFs had a limited impact on spheroid growth and drug response, the strong spheroid inhibition was an evidence of the formulations activity before animal experiments. More complexity should be envisioned, such as the inclusion of immune or endothelial cells into heterotypic spheroids[12,31].

PTX was selected because it displayed the best IC_{50} against CT5.3hTERT cells among all tested drugs. However, it was not CAF selective, as its IC_{50} against HCT116 was 5-fold lower. As a mitotic blocker, PTX efficacy has been dependent on the proliferation state of the cells[33,34]. This could explain the positive tumor/CAF IC_{50} ratio. In the spheroid model, we tested PTX concentrations from 0.67 to 30 μM, and no concentration-dependent effect was observed above 2 μM (data not shown). In two other studies, higher drug concentrations of 5 μM[28] or 30 μM or more[30] were evaluated. The PTX activity was considered cytotoxic, as it destroyed the spheroid after 4 days. Spheroids have been associated to an increased expression of some efflux pumps such as the P-glycoprotein (P-gp)[11], and LNC-PTX has demonstrated P-gp inhibition[35], suggesting a potential benefit of using LNC which was not observed. PTX action on CAFs has been evaluated with controversial results: nab-PTX has demonstrated the depletion of some CAFs in pancreatic cancer

patients[10,36]. However, nab-PTX failed in phase II clinical trial with previously treated metastatic CRC, ending current clinical efforts to introduce it in CRC therapy[37]. In vitro, primary breast and lung CAFs have shown reduced PTX sensitivity compared to tumor cells, as we observed in our 2D screening[38].

ACF was selected due to the higher tumor/CAF IC_{50} ratio in the 2D culture. Its selectivity increased in the spheroid, with high cytotoxicity observed only close to or into the CAF. However, the impact of ACF on spheroid growth was limited and not only associated with CAF cytotoxicity, as HCT116 spheroids also showed an apparently cytostatic effect. Selective efficacy against CRC among several screened cancers with ACF has already been observed, without a demonstrated explanation[27]. ACF has been closely associated with hypoxia, a characteristic of the TME, as HIF-1α and HIF-1β dimerization is inhibited by ACF[23]. Hypoxia has been considered as a driver of fibroblast activation, and HIF-1α has demonstrated to shift CAF metabolism towards protumor metabolism with lactate shuttle[39,40]. However, ACF or other hypoxia inhibitors have never been considered as potential CAF inhibitors, even if CAF, hypoxia, and angiogenesis are strongly related. ACF was detected in our drug screening under nonhypoxic conditions, but the spheroid model presented hypoxia in its core[21]. It would be relevant to study lactate consumption in the spheroid depending on ACF treatment, as a drug that would prevent the metabolism reprogramming under hypoxia would be of high interest.

The PTX and ACF combination was not synergistic in the spheroid model at the tested concentrations. Indeed, cytotoxicity in tumor cells was reduced compared to PTX monotherapy, and CAFs were less sensitive to the combination compared to ACF monotherapy. Overall spheroid growth also did not change. In vivo, preliminary experiments confirmed that combination treatment was well tolerated but only slightly efficient and not significantly better than PTX monotherapy in slowing tumor growth (Figure S5). For this reason, a co-encapsulation was not intended, and monotherapy was further investigated. ACF has been shown to sensitize CRC cells to 5-FU in pretreatment but not in combination[41]. Therefore, combinations with ACF may associate cytotoxic agents, but with a focus on the schedule of each drug administration and of the cytotoxic drug choice.

V. CONCLUSION

In this study, we described a drug repurposing to inhibit CAFs in CRC, with the originality of the translation from a free drug screening in a monocultured 2D cell culture to an assessment of the combination of drug-loaded LNCs in a cocultured 3D spheroid model. 2D drug screening with a CAF cell line identified ACF and PTX as potential CAF inhibitors, with efficacy for tumor cell inhibition. These two molecules were encapsulated in tailored LNCs to benefit from their properties for future in vivo studies. The 3D cocultured spheroids allowed us to distinguish their effect on each cell population and on whole tumor growth. LNC-PTX showed strong efficacy in the inhibition of cocultured spheroids, whereas LNC-ACF inhibited CAFs. However, the combination of both drugs did not show synergy, at least at the tested concentrations. From that perspective, LNC-ACF would be promising to be combined in the future with standard colorectal chemotherapy drugs and evaluate colorectal TME evolution under this therapeutic strategy.

VI. SUPPLEMENTARY MATERIAL

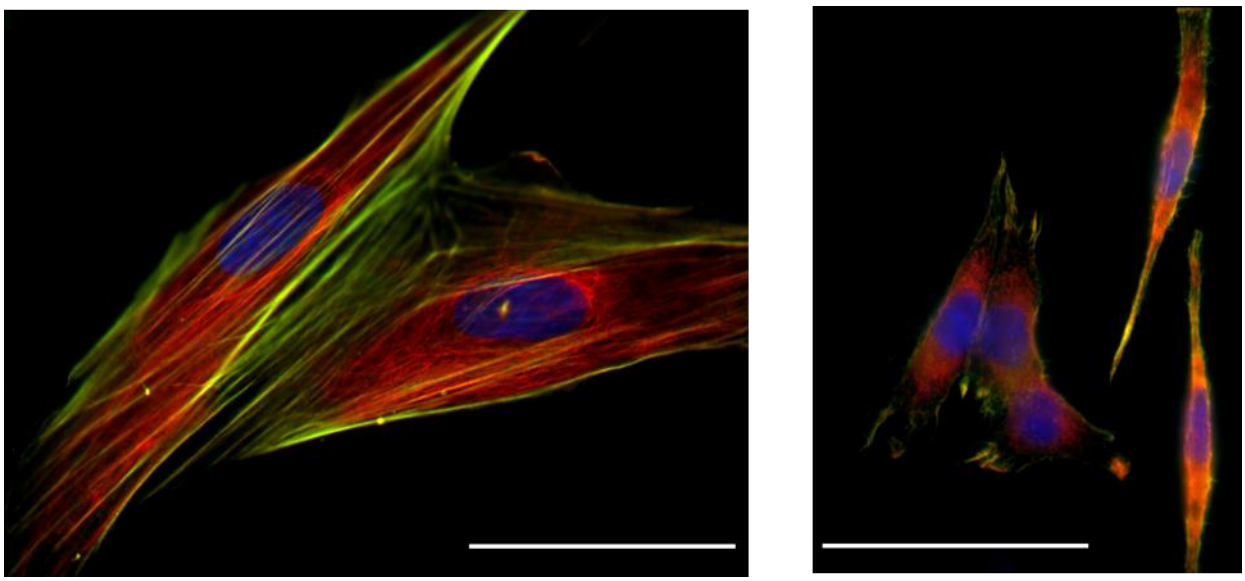

Figure S1. Cytofluorescence of CT5.3hTERT cells (left) and HCT116 cells (right). Red: FAP, green: SMA, blue: DAPI. Scale bar=50 µm.

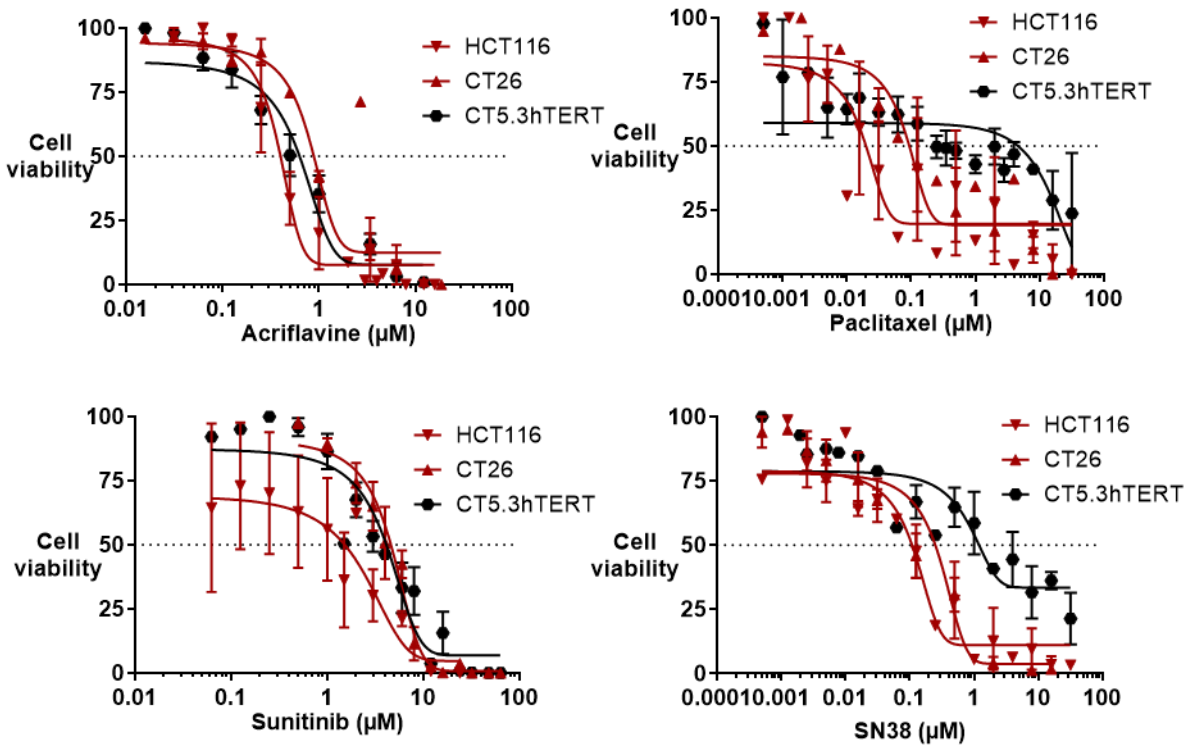

Figure S2. Survival curves of CAF (CT5.3hTERT, black) and tumor (HCT116 and CT26, red) cells after 48 h of incubation with cytotoxic drugs. Mean ± SEM.

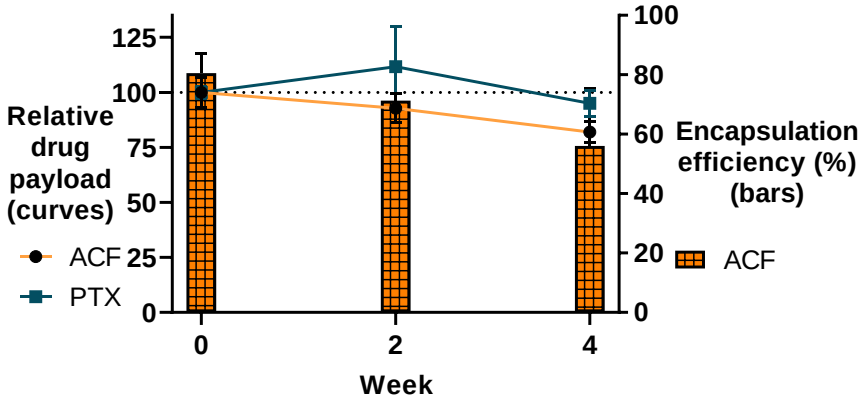

Figure S3. Stability of the LNC formulations based on their drug payload and encapsulation efficiency (mean + SD of N=3 distinct formulations).

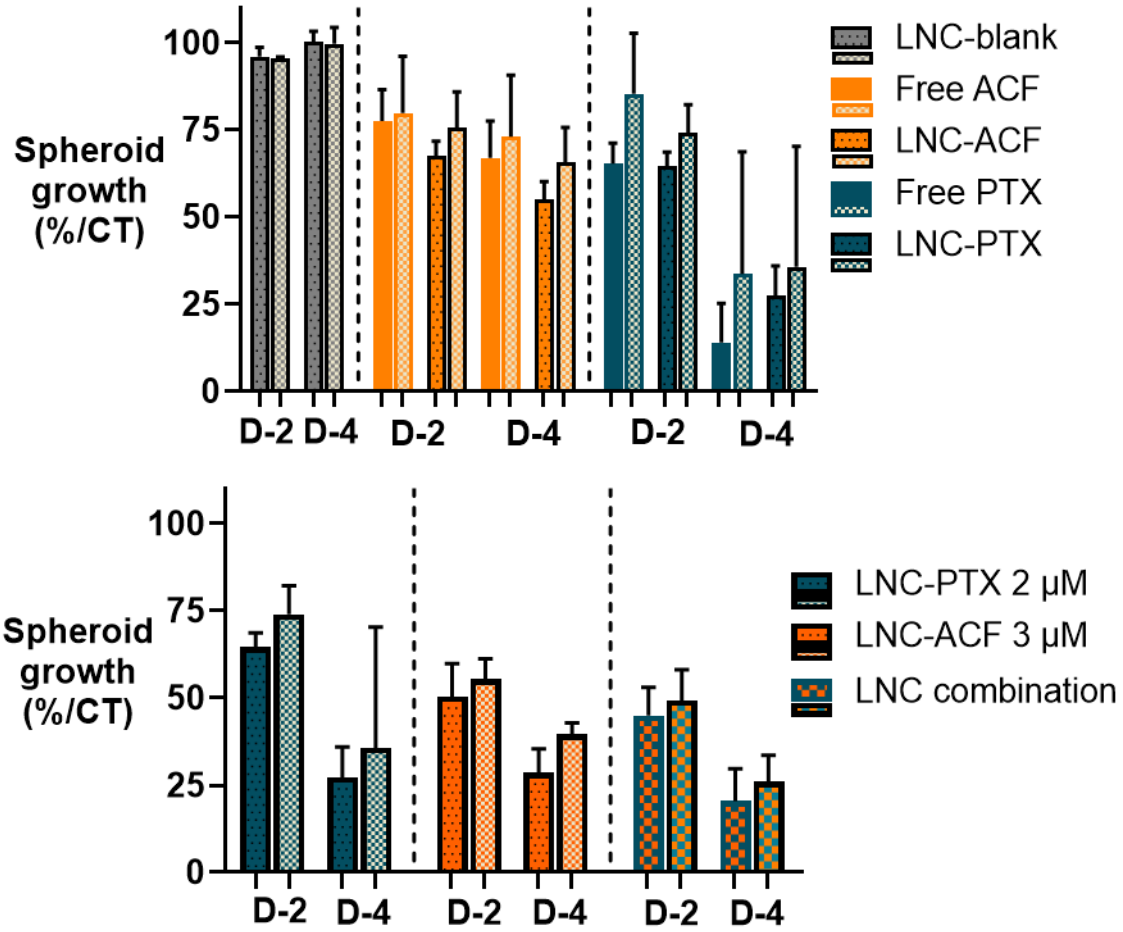

Figure S4. Comparison of cell growth into the cocultured (left) or HCT116 (right) spheroid between the free and encapsulated drug for each condition. Top, free and encapsulated drug for each condition, with ACF at 1 µM and PTX at 2 µM. Bottom, combination effect of LNC-PTX and LNC-ACF. Growth inhibition is expressed as the area ratio over the control spheroid (mean ± SD; N≥3).

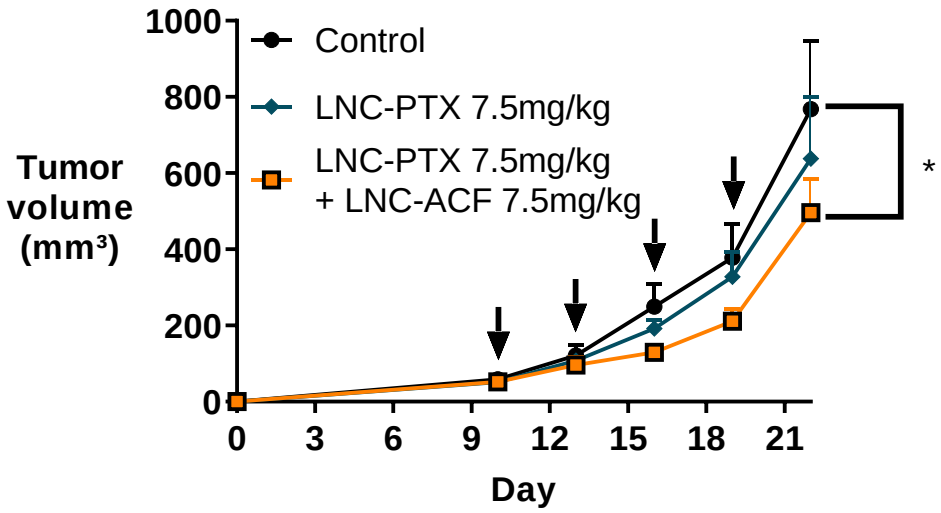

Figure S5. Antitumor efficacy studies in a s.c. CT26 model (mean ± SEM, N= 5 or 6).

VII. REFERENCES

1. Calon, A. *et al.* Stromal gene expression defines poor-prognosis subtypes in colorectal cancer. *Nat. Genet.* **47**, 320–329 (2015).
2. Becht, E. *et al.* Immune and stromal classification of Colorectal cancer is associated with molecular subtypes and relevant for precision immunotherapy. *Clin. Cancer Res.* **22**, 4057–4066 (2016).
3. Gonçalves-Ribeiro, S. *et al.* Carcinoma-associated fibroblasts affect sensitivity to oxaliplatin and 5FU in colorectal cancer cells. *Oncotarget* **7**, 59766–59780 (2016).
4. Öhlund, D., Elyada, E. & Tuveson, D. Fibroblast heterogeneity in the cancer wound. *J. Exp. Med.* **211**, 1503–1523 (2014).
5. Tommelein, J. *et al.* Cancer-Associated Fibroblasts Connect Metastasis-Promoting Communication in Colorectal Cancer. *Front. Oncol.* **5**, 1–11 (2015).
6. Chen, X. & Song, E. Turning foes to friends: targeting cancer-associated fibroblasts. *Nat. Rev. Drug Discov.* **18**, 99–115 (2019).
7. Siegler, E. L., Kim, Y. J. & Wang, P. Nanomedicine targeting the tumor microenvironment: Therapeutic strategies to inhibit angiogenesis, remodel matrix, and modulate immune responses. *J. Cell. Immunother.* **2**, 69–78 (2016).
8. Chen, B. *et al.* Comprehensively priming the tumor microenvironment by cancer-associated fibroblast-targeted liposomes for combined therapy with cancer cell-targeted chemotherapeutic drug delivery system. *J. Control. Release* **241**, 68–80 (2016).
9. Yang, Q., Li, L., Sun, W., Zhou, Z. & Huang, Y. Dual Stimuli-Responsive Hybrid Polymeric Nanoparticles Self-Assembled from POSS-Based Starlike Copolymer-Drug Conjugates for Efficient Intracellular Delivery of Hydrophobic Drugs. *ACS Appl. Mater. Interfaces* **8**, 13251–13261 (2016).
10. Alvarez, R. *et al.* Stromal disrupting effects of nab-paclitaxel in pancreatic cancer. *Br J Cancer* **109**, 926–933 (2013).
11. Nunes, A. S., Barros, A. S., Costa, E. C., Moreira, A. F. & Correia, I. J. 3D tumor spheroids as in vitro models to mimic in vivo human solid tumors resistance to therapeutic drugs. *Biotechnol. Bioeng.* **116**, 206–226 (2019).
12. Herter, S. *et al.* A novel three-dimensional heterotypic spheroid model for the assessment of the activity of cancer immunotherapy agents. *Cancer Immunol. Immunother.* **66**, 129–140 (2017).
13. Nowak-Sliwinska, P., Scapozza, L. & Ruiz i Altaba, A. Drug repurposing in oncology: Compounds, pathways, phenotypes and computational approaches for colorectal cancer. *Biochim. Biophys. Acta - Rev. Cancer* **1871**, 434–454 (2019).
14. Tsakiris, N. *et al.* Combinational drug-loaded lipid nanocapsules for the treatment of cancer. *Int. J. Pharm.* **569**, 118588 (2019).
15. Huynh, N. T., Passirani, C., Saulnier, P. & Benoit, J. P. Lipid nanocapsules: A new platform for nanomedicine. *Int. J. Pharm.* **379**, 201–209 (2009).
16. Fischer, E. *et al.* Radioimmunotherapy of fibroblast activation protein positive tumors by rapidly internalizing antibodies. *Clin. Cancer Res.* **18**, 6208–6218 (2012).
17. Heurtault, B., Saulnier, P., Pech, B., Proust, J. E. & Benoit, J. P. A novel phase inversion-based process for the preparation of lipid nanocarriers. *Pharm. Res.* **19**, 875–880 (2002).
18. Bastiancich, C. *et al.* Lauroyl-gemcitabine-loaded lipid nanocapsule hydrogel for the treatment of glioblastoma. *J. Control. Release* **225**, 283–293 (2016).

19. Montigaud, Y. *et al.* Optimized acriflavine-loaded lipid nanocapsules as a safe and effective delivery system to treat breast cancer. *Int. J. Pharm.* **551**, 322–328 (2018).

20. Zhao, M. *et al.* Post-resection treatment of glioblastoma with an injectable nanomedicine-loaded photopolymerizable hydrogel induces long-term survival. *Int. J. Pharm.* **548**, 522–529 (2018).

21. Corbet, C. *et al.* Interruption of lactate uptake by inhibiting mitochondrial pyruvate transport unravels direct antitumor and radiosensitizing effects. *Nat. Commun.* **9**, 1–11 (2018).

22. De Vlieghere, E. *et al.* Tumor-environment biomimetics delay peritoneal metastasis formation by deceiving and redirecting disseminated cancer cells. *Biomaterials* **54**, 148–157 (2015).

23. Shay, J. E. S. *et al.* Inhibition of hypoxia-inducible factors limits tumor progression in a mouse model of colorectal cancer. *Carcinogenesis* **35**, 1067–1077 (2014).

24. Lee, K. *et al.* Acriflavine inhibits HIF-1 dimerization, tumor growth, and vascularization. *Proc. Natl. Acad. Sci.* **106**, 17910–17915 (2009).

25. Lim, M.-J. *et al.* Acriflavine enhances radiosensitivity of colon cancer cells through endoplasmic reticulum stress-mediated apoptosis. *Int. J. Biochem. Cell Biol.* **44**, 1214–1222 (2012).

26. Groo, A. C. *et al.* In vivo evaluation of paclitaxel-loaded lipid nanocapsules after intravenous and oral administration on resistant tumor. *Nanomedicine* **10**, 589–601 (2015).

27. Hassan, S. *et al.* Novel activity of acriflavine against colorectal cancer tumor cells. *Cancer Sci.* **102**, 2206–2213 (2011).

28. Sha, H. *et al.* A tumor-penetrating recombinant protein anti-EGFR-iRGD enhance efficacy of paclitaxel in 3D multicellular spheroids and gastric cancer in vivo. *Eur. J. Pharm. Sci.* **77**, 60–72 (2015).

29. Hoffmann, O. I. *et al.* Impact of the spheroid model complexity on drug response. *J. Biotechnol.* **205**, 14–23 (2015).

30. Jeong, S. Y., Lee, J. H., Shin, Y., Chung, S. & Kuh, H. J. Co-culture of tumor spheroids and fibroblasts in a collagen matrix-incorporated microfluidic chip mimics reciprocal activation in solid tumor microenvironment. *PLoS One* **11**, e0159013 (2016).

31. Zoetemelk, M., Rausch, M., Colin, D. J., Dormond, O. & Nowak-Sliwinska, P. Short-term 3D culture systems of various complexity for treatment optimization of colorectal carcinoma. *Sci. Rep.* **9**, 1–14 (2019).

32. Millard, M. *et al.* Drug delivery to solid tumors: The predictive value of the multicellular tumor spheroid model for nanomedicine screening. *Int. J. Nanomedicine* **12**, 7993–8007 (2017).

33. Haschka, M., Karbon, G., Fava, L. L. & Villunger, A. Perturbing mitosis for anti-cancer therapy: is cell death the only answer? *EMBO Rep.* **19**, 1–20 (2018).

34. Mitchison, T. J. The proliferation rate paradox in antimitotic chemotherapy. *Mol. Biol. Cell* **23**, 1–6 (2012).

35. Garcion, E. *et al.* A new generation of anticancer, drug-loaded, colloidal vectors reverses multidrug resistance in glioma and reduces tumor progression in rats. *Mol. Cancer Ther.* **5**, 1710–1722 (2006).

36. Miyashita, T. *et al.* Neoadjuvant Chemotherapy with Gemcitabine Plus Nab-paclitaxel Reduces the Number of Cancer-associated Fibroblasts Through Depletion of Pancreatic Stroma. *Anticancer Res* **38**, 337–343 (2018).

37. Ducreux, M. *et al.* Efficacy and safety of nab-paclitaxel in patients with previously treated metastatic colorectal cancer: a phase II COLO-001 trial. *Cancer Chemother. Pharmacol.* **79**, 9–16 (2017).

38. Sonnenberg, M. *et al.* Highly variable response to cytotoxic chemotherapy in carcinoma-associated fibroblasts (CAFs) from lung and breast. *BMC Cancer* **8**, 364 (2008).

39. Semenza, G. L. Cancer-stromal cell interactions mediated by hypoxia-inducible factors promote angiogenesis, lymphangiogenesis, and metastasis. *Oncogene* **32**, 4057–4063 (2013).

40. Chiavarina, B. *et al.* HIF1-alpha functions as a tumor promoter in cancer associated fibroblasts, and as a tumor suppressor in breast cancer cells: Autophagy drives compartment-specific oncogenesis. *Cell Cycle* **9**, 3534–3551 (2010).

41. Zargar, P., Ghani, E., Jalali Mashayekhi, F., Ramezani, A. & Eftekhar, E. Acriflavine enhances the antitumor activity of the chemotherapeutic drug 5-fluorouracil in colorectal cancer cells. *Oncol. Lett.* **15**, 10084–10090 (2018).

In the first study, we focused on the ability of LNCs to improve the stroma-targeting in CRC, demonstrating good encapsulation of various drugs with customized formulations. However, due to limited stroma-high *in vivo* models and to the necessary validation of the therapeutic strategy *in vitro*, we did not evaluate properly the different LNC properties on tumor-bearing animal models.

Therefore, we planned a reverse approach in the second experimental chapter. LNC potential was evaluated using a drug that has already concentrated a strong interest due to its innovative therapeutic target. JQ1, the first-in-class of bromodomain and extra-terminal domain inhibitors, has seen its clinical translation hampered due to poor drugability: its high hydrophobicity prevented its intravenous solubilization, its short half-life required very high doses daily, causing chronic toxicity and limited antitumor efficacy. For these reasons, we considered that JQ1 was a very good candidate for LNC nanoencapsulation. With the objective to evaluate the advantages of LNC formulations on the previously mentioned drug challenges, we added another established nanoformulation as a comparator, pluronic polymeric micelles. Finally, as the whole BETi class was recently criticized for its unclear downstream targets leading to a misunderstood efficacy, it looked important to investigate, in our CRC model, the mechanism of action of JQ1 independently of its pharmacokinetics, presently controlled by the nanoformulations.

CHAPTER IV
COMPARISON OF TWO NANOFORMULATIONS OF BET INHIBITOR JQ1 FOR TREATMENT OF COLORECTAL CANCER

Adapted from Thibaut Fourniols, Valentina Maggio, Diana Fernandes de Sousa Rafael, Ariana Colaco, Elia García Vidal, Alessandra Lopes, Águeda Martinez Barriocanal, Veronique Preat, Diego Arango

In preparation

ABSTRACT

Bromodomain and extraterminal domain protein (BET) is a family of chromatin regulator proteins whose inhibition induces antitumor mechanisms through *MYC* transcription downregulation and potential impact on the tumor microenvironment. Two new nanoformulations of the BET inhibitor JQ1 have been established and compared for intravenous administration. JQ1-loaded in lipid nanocapsules (LNC-JQ1) was formulated by phase-inversion temperature, while pluronic F127-based micelles (PM-JQ1) at the same payload was produced using the thin-film hydration technique. In order to better understand the mechanism of action of JQ1 related to the colorectal tumor microenvironment and *MYC* downregulation, the two nanoformulations and a control cyclodextrin (CD-JQ1) suspension were incubated with human HT29 and Hutu80, and murine CT26 and MC38 cell lines. Nanoformulations and CD-JQ1 were equally effective to inhibit tumor cell growth and to downregulate *MYC* only in HT29 and MC38. Twelve-time longer blood mean residence time of DiR-LNC was observed compared to theoretical JQ1 mean residence time. Tumor accumulation was significantly higher than into the liver and lungs and similar to the spleen. CT-26 bearing mice were daily administered with the three formulations at 25 mg/kg JQ1 with or without a combination with irinotecan. Tumor growth was significantly delayed with all formulations except PM-JQ1, and only CD-JQ1 demonstrated synergy with irinotecan. This effect was *MYC*-independent. PD-L1 expression and the tumor infiltrated innate immune cells were not affected by JQ1 treatment. For the first time, high doses of JQ1 were intravenously administered and increased colorectal tumor-bearing mice survival.

KEYWORDS

BET inhibitor, colorectal cancer, JQ1, lipid nanocapsule, polymeric micelle.

TABLE OF CONTENTS

I. INTRODUCTION

Despite important progress in diagnostic and therapy, colorectal cancer (CRC) is the second most deadly and third most commonly diagnosed cancer in the world[1]. Metastatic CRC, 20% of primary and 50% of recurrent CRC, has kept a poor overall survival at 5 years of 13%[2].

Bromodomain and extraterminal domain protein inhibition (BETi) are currently in early clinical trials[3]. Bromodomain, present on 42 different human proteins, is responsible for interactions with acetylated lysines present on DNA histones and many proteins[4]. BET is a family of chromatin regulator proteins, including bromodomain proteins BRD2, BRD3, and BRD4. Their expression and function patterns are extensively overlapping each other, and their interactions with numerous transcription factors define a complex set of actions. BET proteins roles in cancer have been investigated together with the BETi development, of which JQ1 is the first-in-class.

One of the most commonly described antitumor mechanisms of BETi is *MYC* transcription downregulation[5]. C-myc is a transcription factor, able to induce the activation of numerous downstream effectors. *MYC* and its target genes are involved in almost 100% of CRC, with a central role in CMS2 subtype[6–8]. It has been demonstrated than BRD4 inhibition reduces selectively gene expression in some super-enhancer regions, more sensitive to transcription factor concentration. This is the case of *MYC* oncogene[9]. In human CRC, the long noncoding RNA CCAT1 has demonstrated a prognostic value to BETi inhibition related to *MYC*, and inhibition of Wnt/β-catenin and miR-21 have also been reported[10,11].

The tumor microenvironment (TME) is a crucial factor in tumor response to anticancer drugs[12]. The activation of an antitumor immune response is especially crucial to elicit deep inhibition and long-term survival in CRC[13]. Several studies highlighted BETi impact on the TME. BRD4 inhibition has demonstrated activity on immune checkpoint PD-L1 expression in B cell lymphoma and ovarian cancer, described as independent of c-myc inhibition[14,15]. In addition, JQ1 has been associated to immunogenic cell death or IFNγ downregulation in multiple immune cells[16,17]. But MYC is also related to the TME. In CRC, MYC has been associated to HIF-1a stabilization, responsible for further angiogenesis[18]. MYC expression in KRAS-mutant lung cancer cells produces IL-23, responsible for NK and B cells suppression, and CCL9, attracting M2 macrophages with VEGF-production associated to angiogenesis and PD-L1 production associated to T cell anergy and suppression[19].

Finally, other important mechanisms have been discovered in various tumor models, which are due to the pleiotropic action of BET. JQ1 induced autophagy-related tumor growth inhibition via

the upregulation of LKB1/p-AMPK in bladder cancer. Besides, DNA damage and direct apoptosis were obtained in a model of cholangiocarcinoma. JQ1 demonstrated lung cancer inhibition via the induction of Bim-dependent apoptosis without MYC level reduction[20]. This confirmed the intrinsic complexity of BETi, that is probably the cause that the first reported results with BETi in clinical trials have shown inconsistent activity associated with unpredictable toxicity and resistance depending on the targeted cancer[4].

Beside misunderstood mechanisms, JQ1 clinical translation has failed due to its short half-life[3,21]. This is why only JQ1 analogs and other BETi are currently in clinical trials[22]. Drug-loaded nanoparticles (NPs) have been developed to enhance drug solubility, improve its PK and biodistribution, enhance its efficacy and/or reduce its toxicity. Many nanomedicine technologies, such as polymer-based or lipid-based NPs, have allowed single or combinatorial strategies in CRC treatment[23]. Because JQ1 is hydrophobic (LogP 4.9) and poorly soluble, has a short half-life (54 min[24]), and toxicity due to its pan-BET activity, JQ1 could benefit from an encapsulation in a nanocarrier. JQ1-loaded NP has demonstrated good efficacy *in vivo* in glioblastoma in combination with temozolomide[25]. In this study, we compared two nanoformulations used for intravenous (i.v.) administration of antitumoral drugs: i) lipid nanocapsules (LNCs) and ii) polymer-based micelles (PMs)[26–28]. We aimed: i) to improve the translational potential of JQ1 as a BETi model, by the use of 2 independent nanoformulations and ii) to better understand BETi impact on CRC microenvironment and c-myc.

II. MATERIALS AND METHODS

II.1. MATERIALS

(+)-JQ-1 (JQ1) and IRI were purchased from MedChemExpress (Sweden). 1,1'-Dioctadecyl-3,3,3',3'-tetramethylindotricarbocyanine iodide (DiR), RNAlater stabilization solution, and TRIzol™ Reagent were purchased from Invitrogen™ (ThermoFisher Scientific, Belgium). High-capacity cDNA kit was purchased from Applied Biosystems™ (ThermoFisher Scientific). Trichloroacetic acid (TCA) was purchased from Fisher scientific (ThermoFisher Scientific). Labrafac™ lipophile WL 1349 (caprylic/capric triglycerides) was gifted by Gattefossé S.A (Saint-Priest, France). Lipoid® S-100 (soybean, approximately 100% phosphatidylcholine) was kindly provided by Lipoid Gmbh (Ludwigshafen, Germany). Solutol® HS15 (a mixture of free polyethylene glycol 660 and polyethylene glycol 660 hydroxystearate), polysorbate 80, (2-Hydroxypropyl)-β-cyclodextrin, deoxyribonuclease I from bovine pancreas, dispase II, collagenase from Clostridium histolyticum, sulforhodamine B (SRB) and xylazine were purchased from Sigma-Aldrich (St. Louis, USA). OCT compound was purchased from VWR (Leuven, Belgium). BALB/cJRj mice were purchased from Janvier (France). Ketamine (Nimatek®) was purchased from Dechra (Nederlands). Pluronic® F127 was purchased from Merck (Spain). Rotilabo™ Syringe filters Polyvinylidene fluoride (PVDF) 0.22 µm and L-lactic acid were purchased from Carl Roth (Karlsruhe, Germany). NZYol was purchased from NZYtech (Lisboa, Portugal).

Anti-CD11b, anti-GR1, and anti-CD274, antibodies were purchased from BD Pharmingen (BD Biosciences, Franklin Lakes, New Jersey). Anti-F4/80 antibody was purchased from Ebioscience (Thermo Fisher Scientific). Anti-CD335, anti-CD206, anti-CD49b, and anti-CD45 antibodies were purchased from Biolegend (San Diego, California).

II.2. JQ1 FORMULATIONS

LNC-JQ1 formulation was prepared according to the original LNC protocol[29], slightly modified. LNC formulation was scalable from a final weight of 1 g to 10 g. Briefly, for a 1mL LNC-JQ1 formulation at 10 mg/mL, JQ1 (10 mg) was mixed with Labrafac (59 mg) and lipoid S-100 (4.2 mg) and heated at 40°C until JQ1 dissolution. Then, Solutol® (48 mg), injectable water (169 mg), and Sodium chloride (5 mg) were added. The mix was submitted to three heating and cooling cycles between 60 and 85°C. During the third cooling cycle, at the observed phase-inversion temperature (70-75°C), cold 0.9% NaCl injectable solution (706 mg) was added to the formulation under high speed stirring. LNCs were stored at 4°C until use. The unloaded LNC and LNC-DiR were prepared with the same protocol, without JQ1 and at 120µg/mL of DiR.

10 mg/mL PM-JQ1 was produced using the thin-film hydration technique[30,31]. First, amphiphilic polymer Pluronic® F127 was diluted in ethanol:methanol (1:1) mixture, and JQ1 was added. Then, the solvent was removed under vacuum in a rotary evaporator (bath temperature 60°C, 200 rpm). The resulting thin-film was hydrated with PBS into a final 1% (m/v) polymer concentration and vortexed for 5 minutes at full speed. The obtained product was freeze-dried using a VirTis BenchTop Freeze-Dryer (SP Scientific, Spain). After reconstitution in water, the product was stored at RT.

Both formulations were pH-adjusted to the physiological range by a drop of sodium phosphate buffer and filtered through a 0.22μm PVDF syringe filter to sterilize the final formulation before use.

CD-JQ1 formulation was extemporaneously prepared: a solution of JQ1 at 100 mg/ml in dimethylsulfoxide (DMSO) was added dropwise to a 10% (2-Hydroxypropyl)-β-cyclodextrin (βCD), 0.2% polysorbate 80 solution in saline under high-speed mixing (5mg/ml final concentration)[32].

II.3. FORMULATION CHARACTERIZATION

The mean NP size, ζ potential, and polydispersity index of the formulations were measured by using a Zetasizer Ultra (Malvern, UK). LNC formulations were diluted 1/100 (v/v), PM-JQ1 formulations 1/5 and 1/100, and CD-JQ1 1/6 in PBS:water 1:19 (N≥3 distinct batches) before measurement. Diameter is given as the mean intensity using multi-angle DLS, whereas the polydispersity index is the mean at 175° (back) scatter angle.

PM formulation shape and morphology were also observed by transmission electron microscopy (TEM). For the analysis, a drop of the sample was placed on a carbon 400-mesh copper grid, treated with uranyl acetate, and then assessed in a JEM-1400 Electron Microscope (JEOL Ltd., Tokyo, Japan) with an applied voltage of 120kV.

Quantification of JQ1 was performed with an HPLC system (Shimadzu Prominence HPLC, Japan). The analytical separation was performed on an Xbridge® C18 grafted phenyl column (4.6×150 mm; 3 μm). HPLC analyze was carried out at 40°C with a mobile phase of acetonitrile:water (70:30) at a flow rate of 0.8 mL/min. Absorbance wavelengths were set at 250 and 295 nm. Linearity was obtained from 0.5 to 200 μg/mL with a limit of detection of 0.13 μg/mL and a limit of quantification of 0.434 μg/mL. JQ1 and its thermal degradation product retention times were 3.4 min and 2.4 min, respectively. Drug payload was the full JQ1 content of the final formulation (mg/g), measured by HPLC after dilution 1:100 in Acetonitrile. To measure the free drug,

formulations were ultrafiltered with 30 kDa Centrifugal filtration units (Vivaspin® 500, VWR) at 15,000 g for 10 min and the ultrafiltrate was diluted in acetonitrile then measured by HPLC.

II.4. CELL EXPERIMENTS

CT26, HT29, Hutu80, and MC38 cell lines were purchased from ATCC (Manassas, USA). The cell lines were cultured in DMEM medium, high glucose, supplemented with 10% of fetal bovine serum (FBS), 1% of a 200mM L-glutamine solution, 1% of a 10,000 U/mL penicillin, 10,000 µg/mL streptomycin solution, at 37°C in a 5% CO_2 incubator. All cell culture reagents were purchased from Gibco (Thermo Fisher Scientific, Belgium). All cells were cultured at 37°C in an atmosphere of 5% CO2.

II.4.1. Proliferation assays

Briefly, 4,000 HT29 cells, 2,000 HuTu80 cells, 1,000 CT26 cells, or 2,500 MC38 cells were seeded in 96-well plates and allowed to attach to the substratum for 24h. Cells were then exposed in quadruplicate with the JQ1 formulations at concentrations varying between 15 nM and 16 µM for 72 h. One plate was harvested at time 0 and the remaining plates 72 h post-treatment, fixed by adding 30% TCA overnight at room temperature. Plates were stained with 0.4% SRB in 1% acetic acid for 30 min, rinsed three times with 1% acetic acid and air-dried. SRB was solubilized in 200 µl/well of 10 mM Tris pH 10, and the absorbance at 595 nm recorded using a Benchmark Plus microplate spectrophotometer (BioRad Laboratories, Hercules, CA). Measurements were adjusted for background and the absorbance of the corresponding time 0 plates was subtracted. The concentrations corresponding to 50% of the Emax (EC_{50}) were calculated using Prism 5.0 software.

For further extraction of total RNA or proteins, 24h after cell seeding in 6 wells, HT29, CT26 (2.5 x 10^5), HuTu80 (1.25 x 10^5), and MC38 (6 x 10^5) cells were treated with JQ1 formulations (1 µM) or control formulations (DMSO 0.1% or the equivalent empty NP) for 24h.

II.4.2. Real-time qPCR

Total RNA was extracted using NZYol. 1 µg of RNA was retrotranscribed into cDNA using the High-capacity cDNA kit. Real-time PCR reactions were performed on an ABI PRISM 7500 Real-Time System (Applied Biosystems) using the SYBR green method or TaqMan Gene Expression Assay for the 18S house-keeping gene. All primers are in table S1. Data were analyzed with the 7500 System SDS Software. To estimate relative transcript levels, we used the comparative

Threshold cycle (Ct) method. 18S was used as the endogenous control gene. Three independent experiments with technical triplicates were performed.

II.4.3. Western Blot (WB) of c-myc protein

For protein detection, cells were washed once with ice-cold PBS, collected with a rubber scraper, and transferred into a pre-cooled microfuge tube. Cell pellets were obtained by centrifugation at 1500 g for 5 min at 4°C and resuspended in RIPA lysis buffer supplemented with protease inhibitors (Complete™, Mini, EDTA-free Protease Inhibitor Cocktail, Roche). After 30 min of incubation on ice, cells were sonicated for 10 seconds at 20-50 kHz on ice. Lysates were centrifuged 15 minutes at 12,000 g at 4°C. Supernatants were collected in a new tube kept on ice and stored at -80°C for later use.

To determine protein concentration, we used the BCATM Protein Assay Kit (Thermo Scientific). Bovine serum albumin (BSA) was used as a standard. The absorbance was read at 620 nm on the EpochTM Microplate Spectrophotometer (BioTek). The values obtained for the BSA standards were used to construct a standard curve used to compare the sample values to know their concentration.

Separation of proteins was performed by one-dimensional SDS-PAGE electrophoresis assay as follows. Protein samples were denatured in loading Laemmli buffer at 95°C for 5 minutes. 50 µg of protein lysate per lane were loaded into a polyacrylamide gel (4% stacking gel, 8% to 12% gradient running gel). The electrophoresis was run in running buffer for approximately 1.5 hours or until the migration front reached the bottom of the gel. After the electrophoresis, the electrophoretic wet transfer setup was run at 100 V for 120 min at 4°C in a chamber filled with ice-cold 1x transfer buffer. Specific proteins in the membranes were detected by incubation with antibodies. The blocking solution was a 5% not-fat milk solution prepared in PBS Buffer Saline Tween 0.1% (PBST) buffer for 1 h incubation. The membrane was then incubated overnight at 4°C with the primary antibody at the concentration of 1 µg/mL (Vinculin and c-myc antibody were purchased in Cell Signaling Technology). Unbound antibodies were removed by washing. The membrane was then incubated for 1 hour at room temperature with a secondary antibody conjugated with horseradish peroxidase (Polyclonal Swine Anti-Rabbit or anti-mouse Immunoglobulins/HRP, Dako) diluted 1:5000 in blocking buffer. After three washes with PBST, specific reactivity to antibodies was detected using the ECL Western Blotting Detection reagent (GE Healthcare). An X-ray film (AGFA) was exposed to the membrane to detect the chemiluminescent signal, and after automated film development, the bands were visualized.

Densitometric analysis of WB signals with antibody to c-myc was performed using ImageJ software. Vinculin signal was used as a loading control and for quantification.

II.5. ANIMAL EXPERIMENTS

II.5.1. Tumor implantation

Animal studies were performed according to the ethical committee of Université Catholique de Louvain (N°UCL/MD/2017/034). Six-week-old female BALB/cJRj mice were subcutaneously (s.c.) injected into the right flank with 5 x 10^4 CT26 cells in 50 µL of PBS. Tumor growth was monitored once palpable tumors developed by caliper measurement of its 3 dimensions. Tumor volume was determined using the following formula: V= d1 x d2 x d3.

II.5.2. Biodistribution

Once the tumor reached a mean volume of 90 mm^3, mice were randomly administered with a unique dose of either LNC labeled with fluorescent dye DiR (N=6) or free DiR (N=3) at 0.3 mg DiR/kg by i.v. administration route. 25µL blood samples were collected from the tail extremity at t=15 min, 3 h, 24 h, 48 h, and 72 h after i.v. injection. At 3, 24, 44, and 72 h, tumor-accumulation and whole-body biodistribution were measured non-invasively by DiR fluorescence imaging (FLI) from the ventral mouse view, using the IVIS® Spectrum *in vivo* imaging system (PerkinElmer, USA) analyzed using Living Image® 4.7.3 software (PerkinElmer). In addition, at 24h for the LNC-DiR group and 72 h for both groups, 3 animals were sacrificed. Their blood, tissue, and tumor samples were collected, weighed, and processed for ex vivo imaging. The fluorescence signal in all measurements was quantified in radiant efficiency. The blood DiR fluorescence was measured similarly by the IVIS® Spectrum and analyzed by PKSolver add-in for Microsoft Excel, using the non-compartmental IV bolus analysis[33]. The mean residence time "MRT_{0-t}" from the software was obtained by the linear trapezoidal method from 0 to the last measurement point (72 h). For the graphical representation, data was fitted using two phases decay regression using GraphPad Prism, with the fluorescence at 15 min after injection considered as 100% of the injected dose.

II.5.3. Anti-tumor efficacy study

Once tumor volume exceeded 20 mm^3, mice were randomized into the following groups receiving an equivalent daily dose of 25 mg/kg JQ1: i) intraperitoneal (i.p.) CD vehicle (5% DMSO, 10% (2-Hydroxypropyl)-β-cyclodextrin, 0.2% polysorbate 80 in saline) (n=6); ii) i.p. injection of CD-JQ1 (n=6); iii) i.v. injection of LNC-JQ1 (n=7); iv) i.v. injection of PM-JQ1 (n=6). Tumor volume and

weight were followed every other day, with the endpoint of V > 1500 mm^3 or tumor bloody necrosis.

For the mechanistic experiment, the previous experiment was repeated with the same groups. The only change was that 5 x 10^4 CT26 cells were injected s.c. into both flanks. i) vehicle n=7; ii) CD-JQ1 n=6; iii) LNC-JQ1 n=8; and iv) PM-JQ1 n=7. Nine days after randomization, mice were sacrificed, and both tumors were collected and weighted. The smallest tumor was fixed in 4% PFA overnight, then frozen in OCT. The biggest tumor was cut in two asymmetrical parts. One part was minced and incubated 30min in a solution of DMEM with dispase II (3 mg/ml), collagenase (1 mg/ml) and DNAse I (0.2 mg/ml) at 37°C. Then, the cell dispersion was filter trough a 70µm cell strainer (Greiner), centrifuged, resuspended in pure FBS and stored at -80°C until use for FACS. The other fragment was stored at -80°C in RNAlater solution until use for RNA extraction.

For the combination with IRI, the experiment was performed in parallel and with the same protocol as the anti-tumor efficacy. IRI was prepared at 2 mg/mL in a 6 mg/ml lactic acid solution and administered IP every other day at a dose of 10 mg/kg. Mice were randomized between 4 groups: i) IRI monotherapy n=7; ii) IRI + CD-JQ1 n=6; iii) IRI + LNC-JQ1 n=6; iv) IRI + PM-JQ1 n=6. DMSO + CD vehicle group was shared between both anti-tumor efficacy experiments.

II.5.4. RT-qPCR

To extract total RNA, the tumor part was mixed with TRIzol™ Reagent, and RNA was obtained following the manufacturer protocol. The quality and quantity of RNA were evaluated using a nano spectrophotometer (NanoDrop 2000, Thermo Fisher Scientific). RNA was converted into cDNA using the GoScript™ kit (Promega, USA). For *MYC*, the same PCR protocol than for cell experiments was used. For PD-L1 and PD-1, the resulting cDNA was used as a template for 40 cycles of PCR amplification with an annealing temperature of 62.4°C. SYBR™ green real-time qPCR (GoTaq qPCR MasterMix kit, Promega) was conducted on a StepOne Plus Real-Time PCR System (Thermo Fisher Scientific). Analysis of the melting curves was performed to ensure the purity of the PCR products. The results were analyzed with StepOne Software V2.1. mRNA expressions of the targeted genes were calculated relative to the corresponding expression of β-actin and GAPDH (housekeeping gene) according to the delta-delta Ct method. Samples with house-keeping genes Ct values exceeding 20 were removed from the analysis. The results were normalized compared to the DMSO + CD control group. Primers are indicated in table S1.

Table S1. PCR primers

Gene	Forward	Reverse
MYC (human)	CAG CTG CTT AGA CGC TGG ATT	GTA GAA ATA CGG CTG CAC CGA
PDCD1 (PD-1)	GTG TCA GAG GGA GCA AAT G	CGG TTC CAG TTC AGC ATA AG
PDL1	TAA TCA GCT ACG GTG GTG CG	AAA CAT CAT TCG CTG TGG CG
MYC	GCC CCC AAG GTA GTG ATC CT	TGC TCG TCT GCT TGA ATG GA
18S	AGT CCC TGC CCT TTG TAC ACA	GAT CCG AGG GCC TCA CTA AAC
beta-actin	ACT CCT ATG TGG GTG ACG AG	CAT CTT TTC ACG GTT GGC CTT AG
GAPDH	ATC ACC ATC TTC CAG GAG CGA GAC	ATG CCA GTG AGC TTC CCG TTC AGC

II.5.5. Flow cytometry (FACS)

PDL1 positive cells, tumor-associated macrophages (TAMs), and myeloid-derived suppressor cell (MDSC) populations were analyzed by FACS. The tumor cell suspension was thawed, diluted in PBS, and counted using an automatic cell counter (Invitrogen, California). Then, the cell suspension was incubated with Fixable viability dye eFluor™ 506 (ebioscience, ThermoFisher) according to the manufacturer. Unspecific staining was prevented using a blocking solution with an anti-CD16/CD32 antibody for 10 min on ice (clone 93, Biolegend). Cells were then directly incubated for 60 min at 4 °C with the following antibodies (clone name): CD11b-FITC (M1/70), GR1-PE (RB6-8C5), F4/80-APC (BM8), CD335-BV421 (29A1.4), CD206-PE-Cy7 (C068C2), CD49b-PerCP-Cy5.5 (HMα2) for the innate immune cells panel; CD274-APC (MIH5) and CD45-Pe-Cy7 (30-F11) for the PDL1 panel. Sample data were acquired with FACS Verse (BD biosciences) and analyzed with FlowJo software (FlowJo LLC, Ashland, Oregon). The number of cells was normalized by the tumor weight (mg).

II.5.6. Immunohistochemistry

4 µm sections were placed on poly-L-Lysine coated microscope slides, incubated at 54 ºC for 1 h, and deparaffined by immersion in xylene and hydrated by serial immersion in ethanol and distilled water prior staining. Nuclear and cytoplasmic staining were achieved with hematoxylin and eosin respectively. was achieved incubating slides for 30-40s with filtered hematoxylin. Cytoplasmic staining with eosin incubation for 1min. Immunostaining for c-myc (Antibody Abcam 1952907, 1:50) was carried after antigen retrieval with 10 mM citrate buffer pH 6.0 in a pressure cooker for 4 min. Slides were finally mounted with DPX mounting medium (Panreac Quimica). Three representative pictures were taken for each immunostained tumor. DAB mean intensity in positive cells was measured using QuPath software[34].

II.6. STATISTICS

Statistical analyses were performed using GraphPad Prism 8 for Windows. *In vitro MYC* RNA expressions were compared by unpaired t-test with Welch's correction when the variances were significantly different by F test. A one-way ANOVA was performed for *in vitro* growth inhibition experiments. Dunnett's T3 multiple comparisons test was performed to compare the LNC-DiR accumulation (FLI/g) between tumor and each other organ. Tumor growths and mouse weight evolutions comparisons were performed by a two-way ANOVA analysis, with Geisser-Greenhouse correction for sphericity, comparing each treatment effect with the vehicle group, with the Bonferroni multiple corrections, from day 0 to day 16, with a fixed tumor volume of 1500 or a constant weight for those who achieved the end-point before. Mouse survival comparison was performed using Log-rank (Mantel-Cox test) comparing each curve to the vehicle group curve. Infiltrated populations by FACS comparisons and ΔΔCT gene expression comparisons were performed by Dunnett's T3 multiple comparisons test against the vehicle group. Correlation curves were established to associate for each mouse its tumor growth rate and some biological parameter. Pearson correlation was performed to determine the correlation strength.

III. RESULTS & DISCUSSION

III.1. JQ1 FORMULATIONS

Translation of JQ1 to the clinics is limited by the low aqueous stability and short half-life. Therefore, JQ1 was encapsulated in lipid- or polymer-based nanoformulations. To allow i.v. administration at the therapeutic dose (minimum 10 mg/ml to inject 50 mg/kg in mice), LNC-JQ1 was formulated at 10 mg/ml, by phase-inversion temperature process. JQ1 was also encapsulated in the inner core of polymeric micelles formed by amphiphilic polymer Pluronic® F127 by a thin-film hydration technique (Figure 1A). PM-JQ1 contained 100 mg/mL pluronic, to remain above its critical micelle concentration value of 0.09 mg/mL upon dilution in blood[35].

LNC-JQ1 showed a size of 46.4 nm with low polydispersity, whereas PM-JQ1, after freeze-drying and reconstitution, showed a smaller size of 26.2 nm with a bigger polydispersity (Figure 1B). This data was confirmed by TEM, where it was possible to observe micelles of small size in the region of 20-25 nm with a spherical morphology (Figure 1C). PM-JQ1 diameter was not fully stable through dilution, as a 100-time dilution increased its diameter to 59.0 nm. Both formulations showed slightly negative ζ-potential (Table 1). A JQ1 payload around 10 mg/mL was confirmed for both formulations, including <1% and 4% of free JQ1 outside LNCs and PMs, respectively.

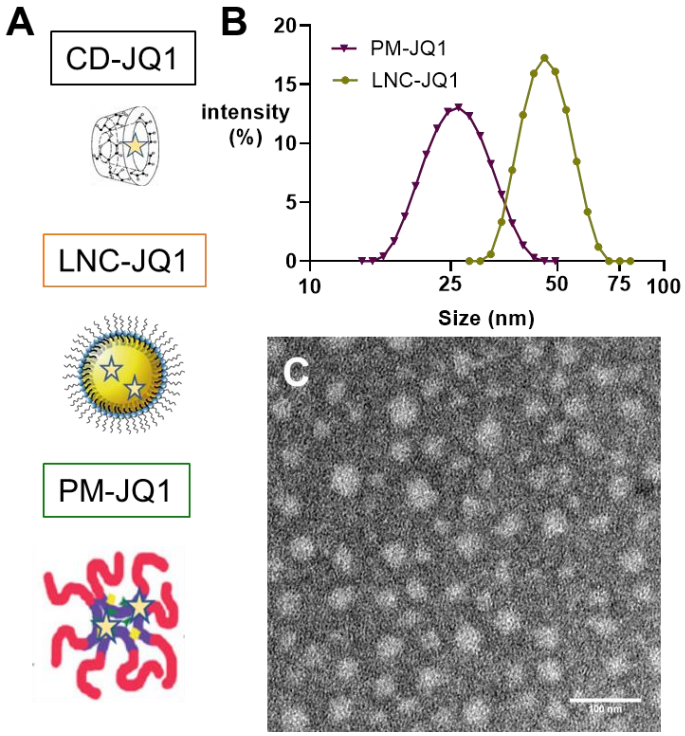

Figure 1. Physico-chemical characterization of JQ1 formulations.
A) Schematic representation of the 3 formulations. B) Diameter intensity of the two nanoformulations. C) TEM image of the PM-JQ1.

As JQ1 is thermosensitive, JQ1 thermal degradation product was quantified by HPLC. LNC-JQ1 manufacturing induced less than 0.5% of the degradation product (Table S2).

Table S2. JQ1 thermosensitivity (N=3)

Conditions	Degradation product (%)
100°C 30 min	13.1
90°C 30 min	4.3
LNC-JQ1	0.43 ± 0.15

As a control formulation of JQ1, an i.p. injection formulation was developed based on the literature review. The standard formulations of JQ1 contain DMSO (5-10%), (2-Hydroxypropyl)-β-cyclodextrin (5-20%), polysorbate 80 (0.2-5%) or captisol (10%) in saline[24,25,36–38]. The control formulation used in this study was to dilute JQ1 at 5 mg/ml in a final 5% DMSO, 10% β-cyclodextrin, and 0.2% polysorbate 80 solution (CD-JQ1). Even so, there were still unsoluble particles, preventing its i.v. administration.

Table 1. Physicochemical characterization of JQ1 formulation. (mean ± SD, N=3).

Formulation	Diameter (nm)	Polydispersity index	ζ potential (mV)	Drug payload (mg/ml)
LNC-JQ1	46.4 ± 1.6	0.032 ± 0.019	-6.9 ± 2.1	11.2 ± 2.2
PM-JQ1	26.2 ± 0.8	0.146 ± 0.022	-7.7 ± 1.5	9.7 ± 2.1

III.2. *IN VITRO* CHARACTERIZATION OF JQ1-LOADED FORMULATIONS ON *MYC* EXPRESSION AND GROWTH INHIBITION

To evaluate the impact of JQ1 encapsulation on its activity on c-myc as a surrogate marker of efficacy, four cell lines were incubated with the three formulations. HT29 and Hutu80 have been selected for their opposite sensitivity to JQ1, HT29 being described as sensitive to JQ1 and HuTu80 as resistant[36]. Murine cell lines CT26 and MC38 were assessed to select one for *in vivo* experiments in immunocompetent mice. *MYC* expression was evaluated by qPCR (Figure 2A) and by WB (Figure 2B) after incubation with the formulations at 1 µM. *MYC* gene expression was inhibited with the 3 JQ1 formulations in human HT29 and murine MC38 cell lines, with a 35% and 54% mean reduction, respectively. Hutu80 and CT26, on the contrary, showed low or no inhibition. The inhibition of protein expression looked more robust with an effective reduction from 30% to 90% depending on cell line and formulation.

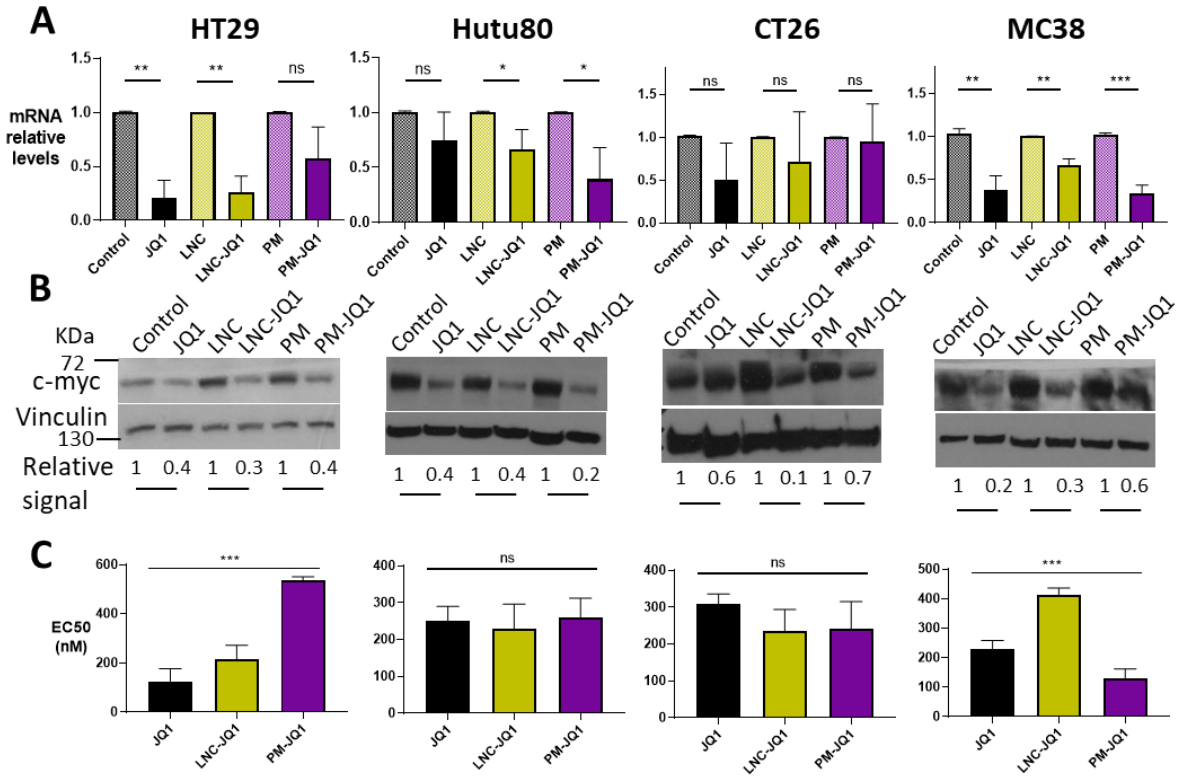

Figure 2. JQ1 effect on 4 CRC cell lines
A) JQ1 downregulates *MYC* mRNA in some cell lines only. Relative mRNA levels of *MYC* by RT-PCR after 24 h with 1 µM JQ1 (Mean ± SD, N=3). B) JQ1 reduces c-myc protein expression in all cell lines. Western blot of c-myc and vinculin. C) EC_{50} of JQ1 growth inhibition determined by SRB assay (Mean ± SD, N=3). One-way ANOVA test was used to determine if the different formulations have a significantly different EC_{50}.

Finally, cell proliferation inhibition was evaluated during 72 h incubation. At the low concentrations tested (~10 nM to 10 μM), JQ1 exhibited a similar cytostatic effect on all cell lines, with an EC_{50} amplitude from 126 nM for free JQ1 to 539 nM for PM-JQ1 on HT29. The sensitivity difference found in previous studies was not reproduced[36]. Hutu80 and CT26 were inhibited independently from the formulation and *MYC* inhibition, with mean EC_{50} around 250 nM for Hutu80 and 260 nM for CT26. The JQ1 formulations showed reduced growth and *MYC* inhibition for PM-JQ1 in HT29 and for LNC-JQ1 in MC38. The CT26 cell line was selected for further animal experiments for the following reasons: i) as a syngeneic model, it allowed assessing a complete immune TME, ii) the three JQ1 formulations showed the same activity, and iii) JQ1 activity appeared to be less related to *MYC* inhibition, leaving room for other mechanisms to be explored.

III.3. BIODISTRIBUTION OF LNC

To evaluate the biodistribution and blood circulation of LNCs, DiR-loaded LNC (LNC-DiR) or free DiR were i.v. administered to CT26 tumor-bearing mice. The s.c. tumor was localized close to the mammary gland in the right caudal area. We measured DiR accumulation in the tumor and the liver and the spleen localized in the upper abdominal part (Figure 3A). The fluorescence ratio between the two regions of interest showed an accumulation of the DiR encapsulated in LNC into the tumor, in comparison to free DiR. LNC relative accumulation in the tumor increased from 3 h to 48 h then plateaued until 72 h (Figure 3B). *Ex vivo* organ fluorescence analysis confirmed that LNCs promoted accumulation in the tumor. After normalization based on organ mass, LNC concentrated first in lymph nodes, then in the tumor (Figure 3C). The accumulation in mesenteric lymph nodes could encourage the use of LNC for tumor lymph node invasion. A similar study has been performed with PM-JQ1, with another tumor model[28]. PM-JQ1 was associated with a lower tumor concentration compared to liver uptake. Blood circulation of LNC-DiR showed 6.2 ± 1.6% of the initial concentration remaining after 24 h. The blood fluorescence was analysed by a non-compartmental model and the mean residence time was estimated to 10.9 h (Figure 3D). Therefore, this biodistribution study suggested that LNCs should improve both free JQ1 mean residence time that was estimated to 52 min[24] and JQ1 availability into the tumor compared to PM-JQ1.

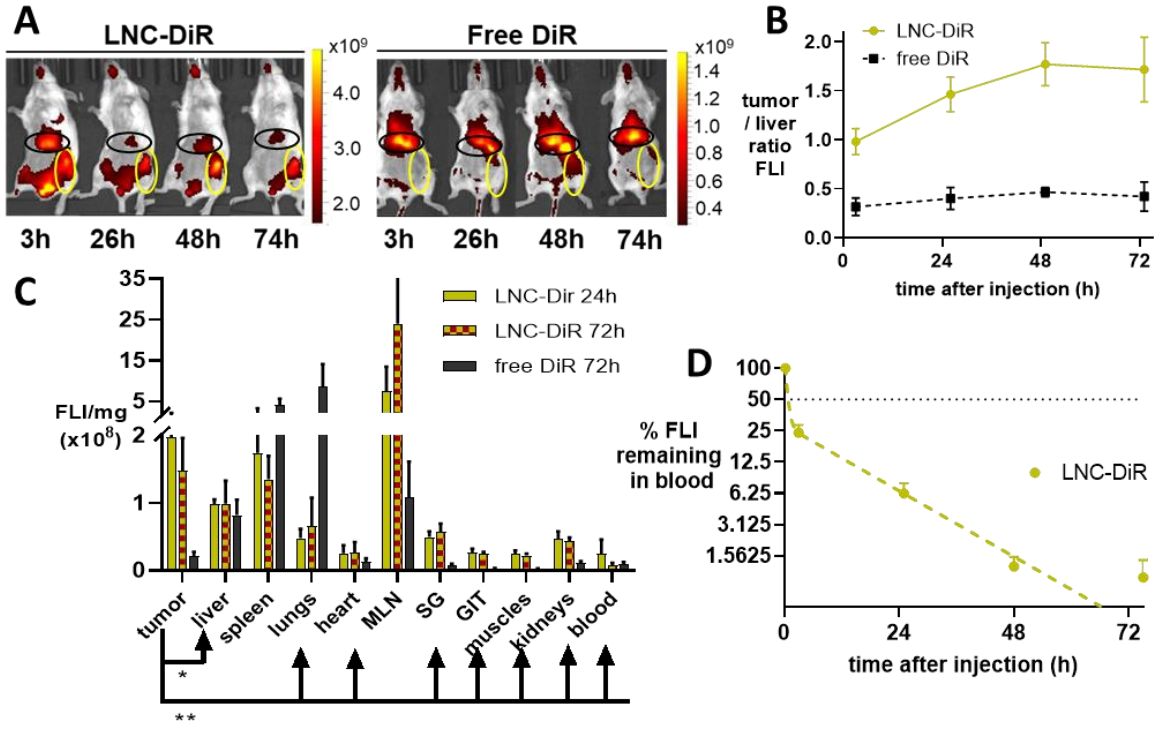

Figure 3. LNC biodistribution of LNC
A) Illustrative pictures of *in vivo* ventral fluorescence intensity over time after a single i.v. injection of LNC-DiR or free DiR. The region of interests of liver & spleen (black) and of tumor (yellow) are represented. B) Ratio of average fluorescence intensity between tumor area and liver & spleen area as a function of time. C) *Ex vivo* quantification of total fluorescence intensity of mice organs, normalized by organ weight. The tumor LNC-DiR accumulation is compared with each other organ (Dunnett's T3 multiple comparison). D) Pharmacokinetic of blood fluorescence intensity, expressed as a % of initial dosing, with a two-phase decay fit in dotted line. All fluorescences are measured as the radiant efficiency. Mean ± SD, N=3 (or 6 until 24h). FLI: fluorescence intensity; MLN: Mesenteric lymph nodes; SG: salivary glands; GIT: gastro-intestinal tract (from stomach to caecum).

III.4. ANTI-TUMOR EFFICACY OF JQ1-LOADED FORMULATIONS

To assess the potential of JQ1 therapy, CT26 tumor-bearing mice were treated daily until the endpoint, i) i.p. with the vehicle DMSO + CD; ii) i.p. with CD-JQ1; iii) i.v. with LNC-JQ1 or iv) i.v. with PM-JQ1. A low number of studies reported iv injections of JQ1. It was performed at 2 mg/kg in NPs[25], at 5 mg/kg in unknown vehicle[24,39], and two studies claimed to have made multiple i.v. injections at 50 mg/kg using only DMSO[11,16]. A pilot experiment with a 50 mg/kg dose demonstrated acute toxicity, visible by convulsive seizures induced by both i.v. nanoformulations. A dose reduction to 25 mg/kg prevented almost completely this toxicity, with only five low-grade observed events over more than 200 injections for LNC-JQ1 and none for PM-JQ1. We observed a tumor growth delay with both LNC-JQ1 (p=0.004) and CD-JQ1 (p=0.027), but not with PM-JQ1 (Figure 4A). The overall median survival after treatment initiation was increased from 15 days to 20 days with PM-JQ1 (p=0.0376), 20.5 days with CD-JQ1 (p=0.0142), and 23 days with LNC-

JQ1 (p=0.0019) (Figure 4C). LNC-JQ1 did not demonstrate significantly better antitumor efficacy than i.p. CD-JQ1. No tumor volume reduction was obtained and the treatment effect was visible after more than a week of treatment when the tumors already reached 200-300 mm³. Mice weight gain was stopped only by LNC-JQ1 treatment (Figure 4B). This moderate toxicity may be partially explained by the occurrence of rare acute toxicity during the injection and the presence of free surfactant. The superiority of LNC-JQ1 over PM-JQ1 could be explained by a fast release of JQ1 by PMs, that are not thermodynamically stable once diluted, or by a higher liver uptake observed in the biodistribution study[28].

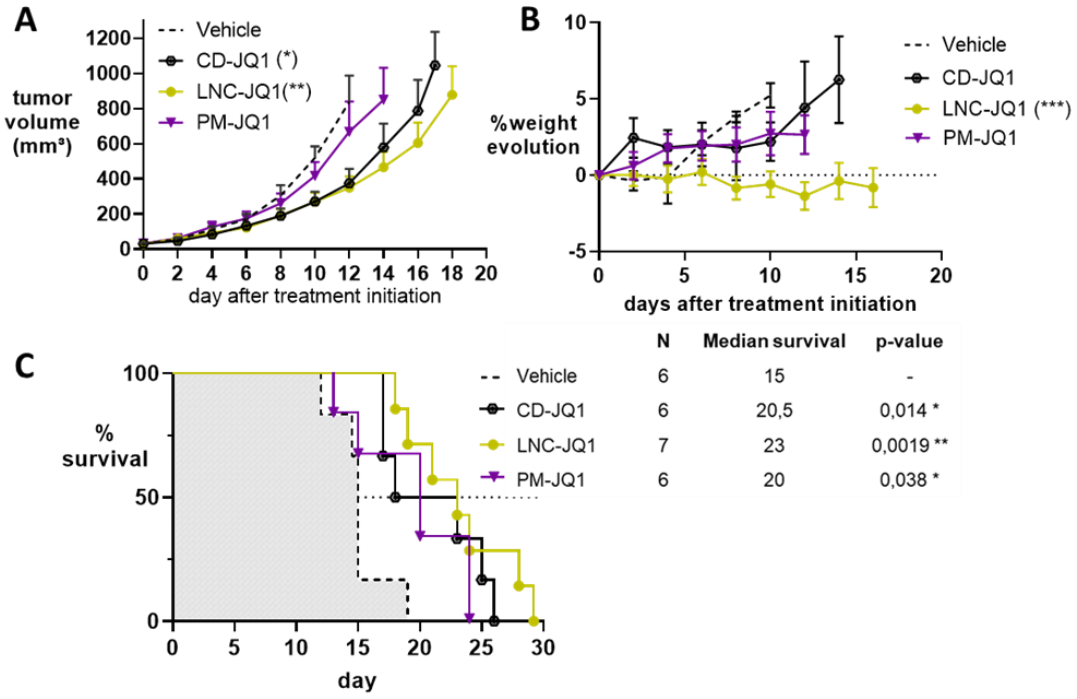

Figure 4. Anti-tumor efficacy study
Administered drug dose: 25 mg/kg/day i.p. for CD-JQ1 and i.v. for LNC-JQ1 and PM-JQ1. A) Tumor volume as a function of time (mean ± SEM). Statistical analysis (two-way ANOVA) refers to comparisons with the vehicle group. B) Toxicity evaluated by weight evolution. Statistical analysis by two-way ANOVA concerns the LNC-JQ1 group against any other group. C) Kaplan-Meier survival curves for all animal groups. Statistical analysis refers to the comparisons with the vehicle group by the Mantel-Cox test. A) & C) The curves are stopped at the end-point of the first animal of the group. (*) p-value < 0.05, (**) p-value < 0.01, (***) p-value < 0.001 (N ≥ 6 animals per group).

III.5. *IN VIVO* JQ1 MECHANISM OF ACTION

In order to explain the observed tumor growth delay, the in vivo experiment was repeated with a shorter end-point. 9 days after JQ1 treatment initiation, the tumors were collected and analyzed by FACS, qPCR, and immunohistology. At this time point, there was a tendency of tumor growth slow-down but their volume was not significantly different, allowing comparisons unbiased by the tumor size.

III.5.1. JQ1 effect on MYC expression

MYC downregulation is described as one of the main therapeutic effects of BETi. This potential *MYC* inhibition by JQ1 was investigated on the tumor samples. *MYC* expression evaluated on the whole tumor level did not show any downregulation (Figure 5A). Immunostaining of the contralateral tumor demonstrated also a uniform c-myc presence in percent positive cells and cell staining intensity (Figure 5B&C). Therefore, the combined cell and animal investigations demonstrated the CT26 cell line sensitivity to JQ1 by a *MYC*-independent mechanism. Similar observations have been described in B cell lymphomas[15] or osteosarcomas[40]. *MYC* inhibition by BETi has also not been considered as the main antitumor mechanism in glioma cells[25,41,42].

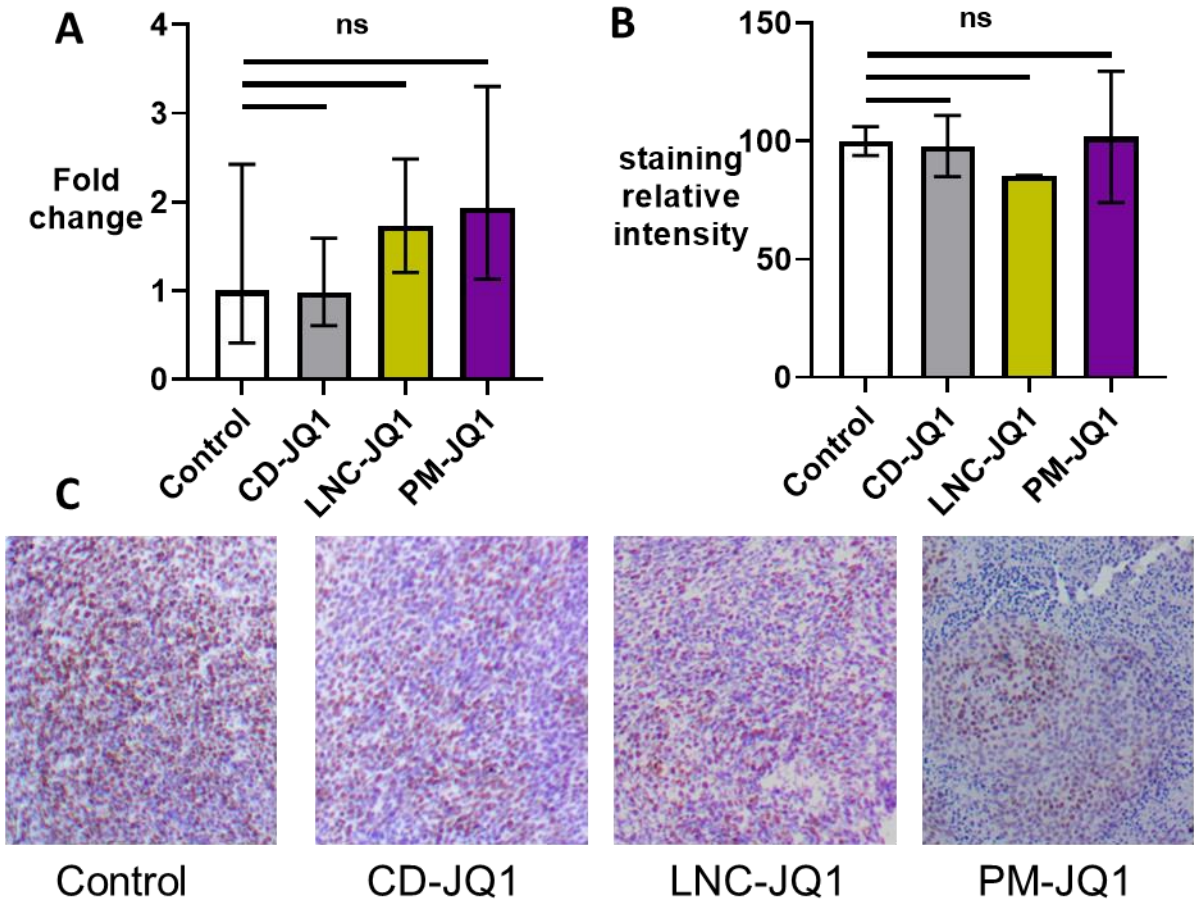

Figure 5. *MYC* expression by CT26 tumors after JQ1 treatment. A) Relative *MYC* gene expression of the tumor of JQ1-treated mice, expressed in fold change compared to the control group ($2^{-\Delta\Delta Ct \pm SEM}$). B) C-myc mean immunostaining intensity relative to control (N=3 tumor samples, n=3 pictures per sample; Mean ± SD). C) Representative picture of c-myc immunostaining for each condition (zoom x4).

III.5.2.Investigation on immune TME impact of JQ1 treatment

Previous studies reporting a link between JQ1 and PD-L1[14,15] have driven our focus on the immune TME. The underlying hypothesis was that JQ1 treatment causes a shift in the immune TME leading to PD-L1 reduction and enhanced antitumor immunity. By FACS, PD-L1 positive immune and tumor cells were counted (Figure 6A). There was high heterogeneity in terms of PD-L1 expression into each group, but no difference between groups (Figure 6B). Likewise, the *PD-L1* gene expression was not reduced. Interestingly, *PDCD1* (PD-1 gene) expression was slightly increased for CD-JQ1 (x2.5, p-value 0.57) and LNC-JQ1 (x2.1, p-value 0.35), that could result from an increased of infiltrated CTLs (Figure 6C). Infiltration of innate immune cells was contradictory (Figure 6D). On the one hand, the TAM polarization determined by CD206 expression showed a tendency towards M2 polarization in LNC-JQ1 and CD-JQ1 (Figure 6E), normally associated with a worse outcome, and on the other hand, MDSC populations were almost significantly reduced in these 2 groups (Figure 6F), which is associated to reduced immunosuppression[23,43]. Correlations between individual tumor growth rate and either MDSC cells or *PD-1* expression were plotted (Figure 6G). While there was no correlation between MDSC content and tumor growth, the PD-1 gene expression associated significantly PD-1 increase to a reduced tumor growth rate. The investigation of the number of CTLs by immunofluorescence or FACS has been delayed and is still planned. At the time of this writing, there is still no demonstrated immune change following JQ1 treatment. Recently, a study demonstrated JQ1-induced immunogenic cell death and increased CD3/CD8+ lymphocytes recruitment in a squamous cell carcinoma model[16], while another study showed IFNγ downregulation in multiple immune cells treated by JQ1[17]. These two mechanisms will be explored in our next experiments.

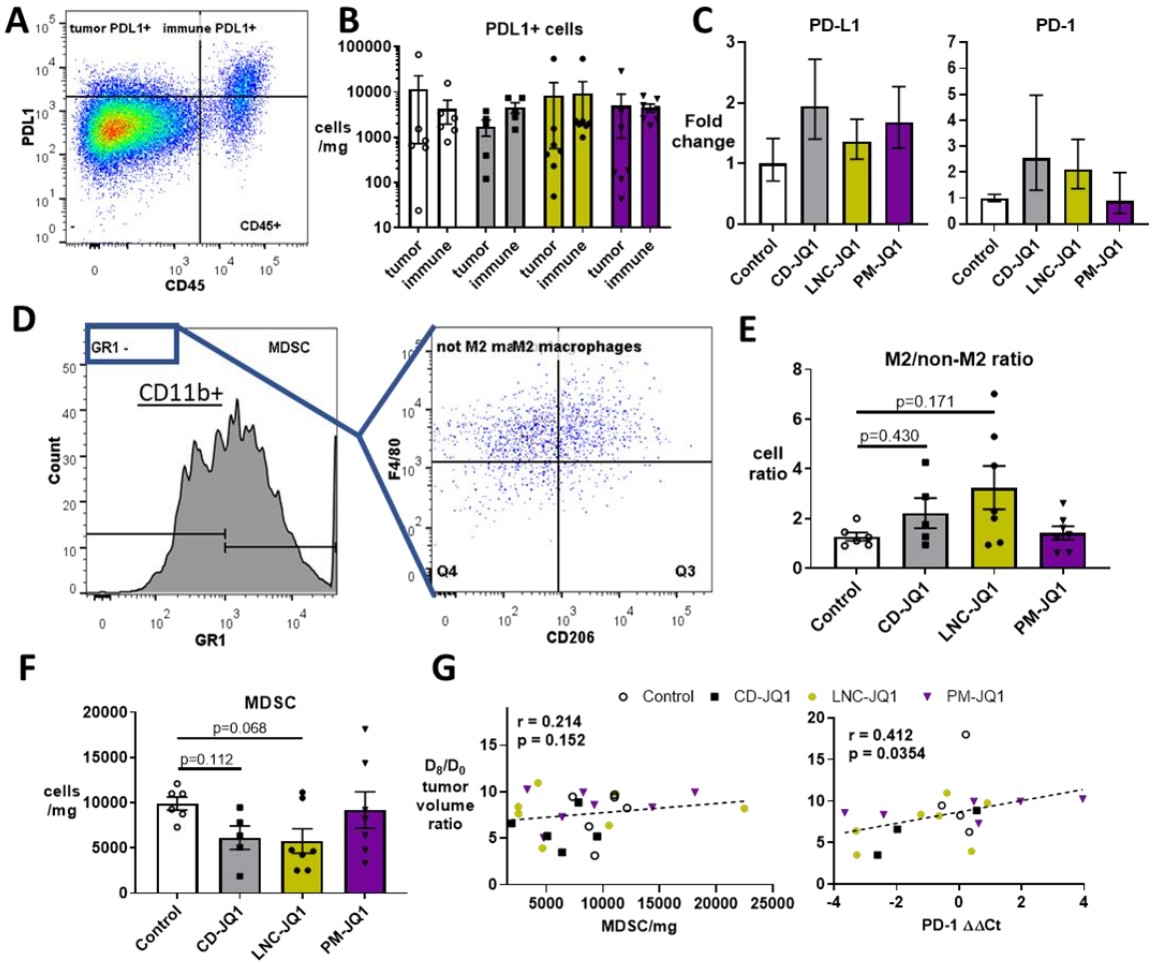

Figure 6. Immune TME of JQ1-treated CT26 tumors. Gating strategy for (A) PD-L1 expression and (D) myeloid cells. Normalized (B) PD-L1 positive cells, (E) M2/non-M2 TAMs ratio and (F) MDSCs per mg of tumor (N=5-7). Cell densities were compared to the control group using Dunnett's T3 test. (C) Fold change of PD-L1 and PD-1 gene expressions compared to the control group ($2^{-\Delta\Delta Ct \pm SEM}$). Control (n=4); CD-JQ1 (n=3); LNC-JQ1 (n=7); PM-JQ1 (n=6). (G) Correlation curves for individual tumors between their growth, expressed as the volume ration between day 0 and day 8 of treatment, and either their MDSC cell density or their PD-1 (ΔΔCt). Pearson r factor and p-value are shown.

III.6. JQ1 COMBINATION WITH IRINOTECAN

BETi has been early envisioned in combination with other antitumor agents[36]. Indeed, BETi monotherapy is associated to a high probability of resistance, which has been confirmed in clinical trials[4,44]. To improve the anti-tumor effect of JQ1, a combination with IRI, a cytotoxic agent used clinically for CRC and with a demonstrated IC_{50} of 2.4 µM on CT26[45], was assessed. IRI monotherapy was not effective to slow down tumor growth, and its combination with our 3 formulations showed a synergy only with the i.p. CD-JQ1, with an improved median survival up to 27 days (Figure 7). The common route of administration between IRI and CD-JQ1 may help to act together, and suggesting that JQ1 should be co-encapsulated with IRI to improve its synergy by i.v. administration.

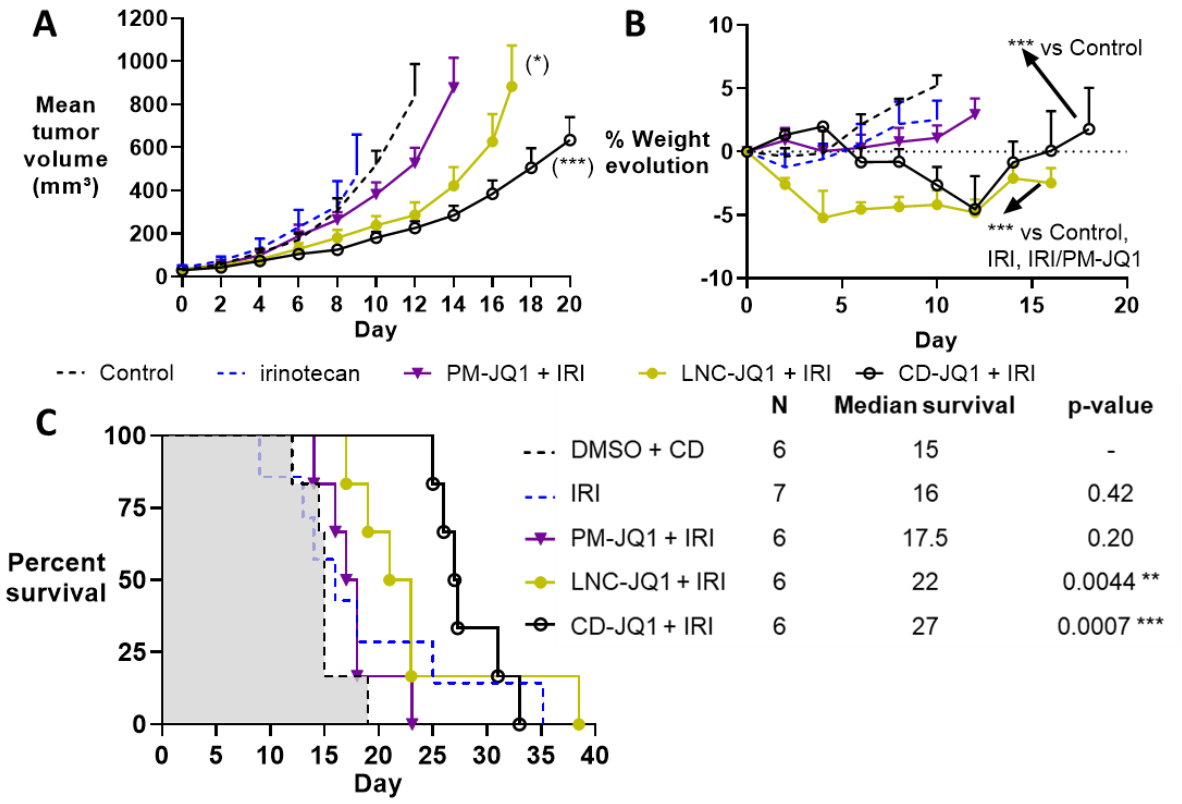

Figure 7. Anti-tumor efficacy study of IRI in combination with JQ1. Administered drug dose: 10mg/kg every other day for IRI and 25mg/kg/day for JQ1. A) Tumor volume as a function of time (mean ± SEM). Statistical analysis (two-way ANOVA) refers to comparisons with the vehicle group. B) Toxicity evaluated by weight evolution from the beginning of treatment. C) Kaplan-Meier survival curves for all animal groups. Statistical analysis refers to the comparisons with the vehicle group by the Mantel-Cox test. The curves are stopped at the end-point of the first animal of the group. (*) p-value<0.05, (**) p-value<0.01, (***) p-value<0.001.

IV. CONCLUSION AND PERSPECTIVES

In this study, we investigated the mechanism of action of the pan-BETi JQ1 in inhibiting CRC, and the possibility of increasing the efficiency and translational use of JQ1 by nanoencapsulation. A high drug payload of 10 mg/mL was obtained with PM-JQ1 and LNC-JQ1. Several CRC cell lines were sensitive to JQ1 formulations at the same level as free JQ1 in terms of growth inhibition. The overall cell growth inhibition was not dependent on *MYC* inhibition in the Hutu80 and CT26 cell lines. *In vivo*, the biodistribution of LNC-DiR suggested a 13-time increase of blood mean residence time compared to free JQ1, and a better tumor over liver ratio accumulation than PM-JQ1. JQ1 treatment delayed tumor growth except for PM-JQ1, in a s.c. CT26 tumor model. The antitumor effect was not related to *MYC* expression inhibition. A preliminary study of the immune environment did not show significant changes by JQ1 treatment. JQ1 combination with IRI showed an effective synergy only with free JQ1. The statement of this study is not to minimize *MYC* downregulation, as BRD4 is a demonstrated *MYC* transcription facilitator[9]. However, the complexity of BETi epigenetic mechanisms of action is well beyond *MYC* inhibition, and its rational in antitumor therapies has been questioned for this reason[21]. A deeper understanding of JQ1 and other selective BETi is necessary for selecting better combinations that could allow long-lasting tumor regressions. Nanoformulations, such as LNC-JQ1, should be considered for further studies to allow i.v. administration and co-encapsulation or co-administration with other molecules.

V. REFERENCES

1. Bray, F. *et al.* Global cancer statistics 2018: GLOBOCAN estimates of incidence and mortality worldwide for 36 cancers in 185 countries. *CA. Cancer J. Clin.* **68**, 394–424 (2018).
2. Miller, K. D. *et al.* Cancer treatment and survivorship statistics, 2019. *CA. Cancer J. Clin.* **69**, 363–385 (2019).
3. Alqahtani, A. *et al.* Bromodomain and extra-terminal motif inhibitors: a review of preclinical and clinical advances in cancer therapy. *Futur. Sci. OA* **5**, FSO372 (2019).
4. Bechter, O. & Schöffski, P. Make your best BET: The emerging role of BET inhibitor treatment in malignant tumors. *Pharmacol. Ther.* **208**, 107479 (2020).
5. Delmore, J. E. *et al.* BET bromodomain inhibition as a therapeutic strategy to target c-Myc. *Cell* **146**, 904–917 (2011).
6. Muzny, D. M. *et al.* Comprehensive molecular characterization of human colon and rectal cancer. *Nature* **487**, 330–337 (2012).
7. Elbadawy, M., Usui, T., Yamawaki, H. & Sasaki, K. Emerging Roles of C-Myc in Cancer Stem Cell-Related Signaling and Resistance to Cancer Chemotherapy: A Potential Therapeutic Target Against Colorectal Cancer. *Int. J. Mol. Sci.* **20**, 2340 (2019).
8. Qiao, L. & Wong, B. C. Y. Role of notch signaling in colorectal cancer. *Carcinogenesis* **30**, 1979–1986 (2009).
9. Lovén, J. *et al.* Selective inhibition of tumor oncogenes by disruption of super-enhancers. *Cell* **153**, 320–334 (2013).
10. McCleland, M. L. *et al.* CCAT1 is an enhancer-templated RNA that predicts BET sensitivity in colorectal cancer. *J. Clin. Invest.* **126**, 639–652 (2016).
11. Zhang, Y. *et al.* JQ-1 Inhibits Colon Cancer Proliferation via Suppressing Wnt/β-Catenin Signaling and miR-21. *Chem. Res. Toxicol.* **31**, 302–307 (2018).
12. Senthebane, D. A. *et al.* The role of tumor microenvironment in chemoresistance: To survive, keep your enemies closer. *Int. J. Mol. Sci.* **18**, 1586 (2017).
13. Mlecnik, B. *et al.* Comprehensive intrametastatic immune quantification and major impact of immunoscore on survival. *J. Natl. Cancer Inst.* **110**, 97–108 (2018).
14. Zhu, H. *et al.* BET Bromodomain Inhibition Promotes Anti-tumor Immunity by Suppressing PD-L1 Expression. *Cell Rep.* **16**, 2829–2837 (2016).
15. Hogg, S. J. *et al.* BET-Bromodomain Inhibitors Engage the Host Immune System and Regulate Expression of the Immune Checkpoint Ligand PD-L1. *Cell Rep.* **18**, 2162–2174 (2017).
16. Wang, M. *et al.* BET bromodomain inhibitor JQ1 promotes immunogenic cell death in tongue squamous cell carcinoma. *Int. Immunopharmacol.* **76**, 105921 (2019).
17. Gibbons, H. R. *et al.* Bromodomain inhibitor JQ1 reversibly blocks IFN-γ production. *Sci. Rep.* **9**, 10280 (2019).
18. Chen, C. *et al.* C-Myc enhances colon cancer cell-mediated angiogenesis through the regulation of HIF-1α. *Biochem. Biophys. Res. Commun.* **430**, 505–511 (2013).
19. Kortlever, R. M. *et al.* Myc Cooperates with Ras by Programming Inflammation and Immune Suppression. *Cell* **171**, 1301-1315.e14 (2017).

20. Zong, D. *et al.* BRD4 Levels Determine the Response of Human Lung Cancer Cells to BET Degraders That Potently Induce Apoptosis through Suppression of Mcl-1. *Cancer Res.* **80**, 2380–2393 (2020).

21. Andrieu, G., Belkina, A. C. & Denis, G. V. Clinical trials for BET inhibitors run ahead of the science. *Drug Discov. Today Technol.* **19**, 45–50 (2016).

22. Tanaka, M., Roberts, J. M., Qi, J. & Bradner, J. E. Inhibitors of emerging epigenetic targets for cancer therapy: a patent review (2010–2014). *Pharm. Pat. Anal.* **4**, 261–284 (2015).

23. Matos, A. I. *et al.* Nanotechnology is an important strategy for combinational innovative chemo-immunotherapies against colorectal cancer. *Journal of Controlled Release* **307**, 108–138 (2019).

24. Filippakopoulos, P. *et al.* Selective inhibition of BET bromodomains. *Nature* **468**, 1067–1073 (2010).

25. Lam, F. C. *et al.* Enhanced efficacy of combined temozolomide and bromodomain inhibitor therapy for gliomas using targeted nanoparticles. *Nat. Commun.* **9**, 1991 (2018).

26. Groo, A. C. *et al.* In vivo evaluation of paclitaxel-loaded lipid nanocapsules after intravenous and oral administration on resistant tumor. *Nanomedicine* **10**, 589–601 (2015).

27. Montigaud, Y. *et al.* Optimized acriflavine-loaded lipid nanocapsules as a safe and effective delivery system to treat breast cancer. *Int. J. Pharm.* **551**, 322–328 (2018).

28. Gener, P. *et al.* Zileuton™ loaded in polymer micelles effectively reduce breast cancer circulating tumor cells and intratumoral cancer stem cells. *Nanomedicine Nanotechnology, Biol. Med.* **24**, 102106 (2020).

29. Heurtault, B., Saulnier, P., Pech, B., Proust, J. E. & Benoit, J. P. A novel phase inversion-based process for the preparation of lipid nanocarriers. *Pharm. Res.* **19**, 875–880 (2002).

30. Andrade, F. *et al.* Pharmacological and toxicological assessment of innovative self-Assembled polymeric micelles as powders for insulin pulmonary delivery. *Nanomedicine* **11**, 2305–2317 (2016).

31. Rafael, D. *et al.* AKT2 siRNA delivery with amphiphilic-based polymeric micelles show efficacy against cancer stem cells. *Drug Deliv.* **25**, 961–972 (2018).

32. Zuber, J. *et al.* RNAi screen identifies Brd4 as a therapeutic target in acute myeloid leukaemia. *Nature* **478**, 524–528 (2011).

33. Zhang, Y., Huo, M., Zhou, J. & Xie, S. PKSolver: An add-in program for pharmacokinetic and pharmacodynamic data analysis in Microsoft Excel. *Comput. Methods Programs Biomed.* **99**, 306–314 (2010).

34. Bankhead, P. *et al.* QuPath: Open source software for digital pathology image analysis. *Sci. Rep.* **7**, 16878 (2017).

35. Gyulai, G. *et al.* Preparation and characterization of cationic pluronic for surface modification and functionalization of polymeric drug delivery nanoparticles. *Express Polym. Lett.* **10**, 216–226 (2016).

36. Tögel, L. *et al.* Dual Targeting of Bromodomain and Extraterminal Domain Proteins, and WNT or MAPK Signaling, Inhibits c-MYC Expression and Proliferation of Colorectal Cancer Cells. *Mol. Cancer Ther.* **15**, 1217–1226 (2016).

37. Sánchez-Ventura, J., Amo-Aparicio, J., Navarro, X. & Penas, C. BET protein inhibition regulates cytokine production and promotes neuroprotection after spinal cord injury. *J. Neuroinflammation* **16**, 1–12 (2019).

38. Tanaka, M. *et al.* Design and characterization of bivalent BET inhibitors. *Nat. Chem. Biol.* **12**, 1089–1096 (2016).

39. Zhao, B., Cheng, X. & Zhou, X. The BET-bromodomain inhibitor JQ1 mitigates vemurafenib drug resistance in melanoma. *Melanoma Res.* **28**, 521–526 (2018).

40. Baker, E. K. *et al.* BET inhibitors induce apoptosis through a MYC independent mechanism and synergise with CDK inhibitors to kill osteosarcoma cells. *Sci. Rep.* **5**, 10120 (2015).

41. Berenguer-Daizé, C. *et al.* OTX015 (MK-8628), a novel BET inhibitor, displays in vitro and in vivo antitumor effects alone and in combination with conventional therapies in glioblastoma models. *Int. J. Cancer* **139**, 2047–2055 (2016).

42. Cheng, Z. *et al.* Inhibition of BET Bromodomain Targets Genetically Diverse Glioblastoma. *Clin. Cancer Res.* **19**, 1748–1759 (2013).

43. Komohara, Y., Fujiwara, Y., Ohnishi, K. & Takeya, M. Tumor-associated macrophages: Potential therapeutic targets for anti-cancer therapy. *Adv. Drug Deliv. Rev.* **99**, 180–185 (2016).

44. Berthon, C. *et al.* Bromodomain inhibitor OTX015 in patients with acute leukaemia: A dose-escalation, phase 1 study. *Lancet Haematol.* **3**, e186–e195 (2016).

45. Tsakiris, N. *et al.* Combinational drug-loaded lipid nanocapsules for the treatment of cancer. *Int. J. Pharm.* **569**, 118588 (2019).

CHAPTER V
DISCUSSION AND PERSPECTIVES

TABLE OF CONTENTS

I. SUMMARY OF THE KEY FINDINGS

The field of nanomedicines is at a moment of truth. After having demonstrated multiple functionalities in drug delivery in preclinical investigations, most of the clinical translation left specialists disappointed. Expert opinions calling for a paradigm shift have multiplied since the beginning of this thesis project[1–3]. The nanocarriers should be simple, robustly produced at different scales, adaptable to several drugs, and fully characterized for their formulation, *in vitro*, and *in vivo* behavior. It is in this context that we decided to develop nanoformulations based on LNCs. Indeed, previous work with this technology had already investigated in detail the formulation process with its design space, the adaptation to many molecules and multiple preclinical applications[4].

The CRC CMS classification has identified the desmoplastic CMS4 CRC as a current challenge for therapy[5,6]. There is still no tailored therapeutic for this cancer presenting an abundant immune and stromal infiltration. Based on the growing evidence about TME protumorigenic roles, it was decided to develop LNC formulations to treat CRC by modulating its TME.

In this thesis, three drugs have been rationally selected. LNC-ACF, LNC-PTX, and LNC-JQ1 have been formulated, characterized, and evaluated. In vitro models with several cell lines have been used to elucidate their effect on CAFs and JQ1 impact on c-myc expression. *In vivo,* the CT26 tumor model has allowed the evaluation of LNC-JQ1 impact on mice survival.

The key findings of this thesis include:

- A rational choice of the drugs: twelve drugs have been screened against CT5.3hTERT, including unpublished regorafenib, another CRC standard treatment that could inhibit several CAF pathways, tranilast, an anti-fibrotic drug, salinomycin, and TAS-102. Among the twelve drugs, ACF was the only one that demonstrated a lower IC50 for CT53 than for CT26, showing that its mechanism of action was particularly harmful to CAFs.
- The evaluation of ACF on a cocultured spheroid model closer from the real tumor: CAF selective sensitivity to ACF at 1 µM was confirmed, with propidium iodide immunostaining showing eighteen-fold more cytotoxicity in the CAF areas compared to tumor cells.
- JQ1 effectively inhibited CT26 growth in vitro and in vivo at submicromolar concentration. This effect was independent of c-myc inhibition.
- LNC-ACF and LNC-PTX drug payloads were slightly increased compared to previous studies7,8. JQ1 was encapsulated for the first time in LNCs, at a high drug payload (10 mg/mL) allowing intravenous (i.v.) injection of the desired dose.

- *In vitro*, drug-loaded LNCs showed a similar effect than free drug.
- *In vivo*, repeated i.v. administrations for LNC-JQ1, LNC-ACF, and LNC-PTX showed i) a general safety and good tolerance, with the limit of a mouse weight growth delay for LNC-JQ1, and some acute adverse reactions for LNC-JQ1 and LNC-ACF; ii) a biodistribution with more accumulation into the tumor than the liver and equal to the spleen, with bicompartmental blood circulation with half-lives around 1 and 11h, respectively; iii) a significant CT26 tumor growth delay and extended survival vs untreated but no tumor volume reduction with the combination LNC-ACF+LNC-PTX or with the monotherapy LNC-JQ1.

Finally, we could answer to the initial aim to check whether new LNC-based strategies have better anti-CRC efficacy than classical administration or other nanotechnologies. While customized LNCs have adapted properties for a tumor drug delivery, the selected drug cargo and tumor models did not allow us to demonstrate a significant superiority of LNC use over classical administration.

II. DISCUSSION ON LNC FORMULATIONS FOR I.V. ADMINSTRATION

The LNC formulation was described in 2002[9]. Since then, it has been used in 252 scientific publications[1], but the first administration in humans has not been made yet. The main questions around LNCs translation will be discussed in regard to the thesis results. It particularly concerns LNC cargo loading, PK, safety, efficacy along with their ability to be industrialized[10,11].

II.1. CARGO LOADING AND GENERAL CHARACTERISTICS OF LNC FORMULATIONS

Of the three drugs encapsulated in LNCs, only ACF and PTX had been already loaded in numerous NPs in previous studies, including LNCs (Tables 1-2). However, the comparison with previous LNCs demonstrated the benefits of the efforts put on the customization. Indeed, our LNC-ACF displayed improved drug loading associated to a significantly reduced Solutol content, the most potentially toxic excipient. Our LNC-PTX also showed slightly increased PTX loading compared to the classical LNC-PTX formulation but lower than the high-concentration formulation only used in one publication. In both cases, the Solutol concentrations were higher. Concerning the comparison with other nanotechnologies, ACF had been formulated with a higher drug loading with liposomes and core-shell silica NPs, even if the injected payload was lower or unknown. PTX nanoformulations market is very competitive[9]. Albumin-bound PTX has the characteristics of an NP but in this case, PTX is not encapsulated. This could explain the very high drug loading with Nab-PTX. JQ1 hydrophobicity allowed a very effective encapsulation in LNCs, leading to a high drug loading of 9%, achieved also by the polymeric micelles (Table 3). For all formulations, LNCs size is lower than the liposomes or polymeric NPs, and corresponds to the recommendations (10-100 nm) for NPs blood circulation and tumor extravasation[10].

Table 1. Comparison between different acriflavine-loaded nanocarriers of the literature.

Formulations	LNC-ACF	LNC-ACF[1]	Liposome-ACF[2]	Organosilica core-shell ACF[3]
Encapsulation efficiency (%)	81	83	94	18.5
Drug loading (% excipients)	0.72	0.2	8.6	3.2
Injected drug payload (mg/mL)	1.6	1	1	?
Solutol (%)	9.3	16		
Size (nm)	33	30	139	260
Zeta potential (mV)	-4.8	-2.5	-15	4

Table 2. Comparison between different paclitaxel-loaded nanocarriers of the literature.

Formulations	LNC-PTX	LNC-PTX[4]	LNC-PTX high-concentration[5]	PLGA-PTX[6]	Nab-PTX[7]
Encapsulation efficiency (%)	100	94	99	72	NA
Drug loading (% excipients)	0.72	0.57	1.06	0.72	11
Injected drug payload (mg/mL)	2.0	1.79	2.99	0.35	5
Solutol (%)	10.9	14.0	12.6		
Size (nm)	60	53	70	114	130
Zeta potential (mV)	-7.9	-7.2	-7.6	-0.36	-31

Table 3. Comparison between different JQ1-loaded nanocarriers of the literature.

Formulations	LNC-JQ1	PM-JQ1	Liposome-JQ1[8]
Encapsulation efficiency (%)	100	96	35
Drug loading (% excipients)	9	10	2.1
Injected drug payload (mg/mL)	11	9.7	0.44
Size (nm)	46	26	137
Zeta potential (mV)	-6.9	-7.7	-12

II.2. LNCs PHARMACOKINETICS

In this project, LNC distribution after i.v. administration was studied by the fluorescence tracking of LNC-DiR in the blood, and in the main organs *ex vivo*. Long blood circulation after i.v. administration is considered as a crucial parameter to let time to the NP to extravasate to the tumor. This paradigm has been established after the success of Doxil® liposome, the first approved nanocarrier, which demonstrated a mean residence time (MRT) of 38 h in rat and 4 days in human patients[12,13]. Nevertheless, this long MRT has also been considered as the source of a new toxicity profile, characterized by stomatitis and palmoplantar erythrodysesthesia. Lipodox®, another formulation with even longer circulation time, further exaggerates these symptoms[12]. In our case, a bicompartmental model fitted the measures, as a distribution half-life during the three first hours was estimated to 1 h, significantly faster than an elimination half-life of 11 h. The combined blood MRT of 10 h was longer than previously described MRTs of 54 min for LNC-PTX[14] and 4.5 h for LNC-(C12)-Decitabine[15], both in rats. The tested LNC-DiR formulation was similar to LNC-JQ1,

whose formulation followed the original excipient proportions[9], and it would be interesting to compare its biodistribution with more tailored LNC-PTX and LNC-ACF, to see the effect of the different sizes and PEGylated surfactant concentrations. The organ distribution has shown an accumulation of LNC-DiR in the CT26 tumor at a higher fluorescence/organ weight than in the liver or the lungs, and comparable to the spleen, the three organs associated with reticuloendothelial system uptake. Among all the organs studied (tumor, liver, spleen, lungs, heart, mesenteric lymph nodes, salivary glands, gastrointestinal tract, a thigh muscle, kidneys, and blood) representing 4-5 g of the 20 g mouse total weight, tumor fluorescence represented 9% at 24h and 11% at 72 h. Two other biodistribution studies have been realized with LNCs, but the first one measured only short time points on healthy rats[16], while the other used healthy mice and did not quantify the signal[17]. The comparison with a study realized with Pluronic F127-based micelles with a similar protocol showed a better tumor accumulation of our formulation[18].

Altogether, the biodistribution predicted a high drug delivery to the tumor. But NP biodistribution by fluorescence imaging is semi-quantitative and presents important biases, such as possible signal quenching or fluorescence variations depending on the organ[19]. It cannot replace a biodistribution with the drug and liquid chromatography/mass spectrometry to get quantitative measurements. Therefore, the question of the percentage of LNCs which reached the tumor remained, in comparison with the median value of 0.7% of the total injected dose in the whole nanocarriers field[20]. In my opinion, a real biodistribution study with dosage by mass spectrometry of the drug content in the tumor and in the blood at several time points would be necessary to understand the similar activity of i.p. free JQ1 and i.v. LNC-JQ1, and their different interaction with irinotecan treatment.

II.3. LNCs SAFETY

Previous work already established the LNC safety profile, both in vitro[21] and in vivo[22]. It was shown that 40% of Solutol HS15, i.e. a mix of PEGylated hydroxystearate and free PEG, was released during the first days of LNC use[23]. Thus, Solutol was identified as the ingredient responsible for *in vitro t*oxicity, with an LC_{50} of 0.427 mg/mL on murine macrophages[21]. In some of our *in vitro* 2D experiments, the control condition with blank LNCs demonstrated significant toxicity. *In vivo*, the Solutol effect should be less significant but it may be partly responsible for the observed chronic toxicity of repeated injections of LNC-JQ1. The tailored formulations of LNC-ACF and LNC-PTX were both using twice as much Solutol than LNC-JQ1, and include other surfactants: sorbitane monooleate in LNC-ACF and polysorbate 80 in LNC-PTX, used at 3.9 and 6.5 lower concentration than Solutol, respectively. Their toxicity profile looks also safer, with published 50%

viability on human fibroblasts at only 50 mg/mL for polysorbate 80, for instance[24]. Solutol should be reduced in optimized formulations.

In this thesis, the safety of LNC formulations has been measured during *in vivo* experiments by following weight evolution and observing any acute toxicity symptoms. During the three animal experiments with JQ1 treatment, we have experienced the possibility of injecting up to 20 daily repeated doses of LNC per animal. The LNC-JQ1 formulation demonstrated some manageable level of toxicity. Repeated injections of LNC-ACF, LNC-PTX, or the combination of both have also been performed with up to five injections. LNC-PTX was very well tolerated, in accordance with the first studies of LNC-PTX[22]. On the contrary, LNC-ACF demonstrated unpredictable acute toxicity with some mice's death, potentially due to ACF precipitation or aggregation.

Tolerability is crucial for nanomaterials, as nanoencapsulation claims to reduce toxicity. Nanocarrier by itself can be safe, but the PK change of the encapsulated drug can drive new toxicities, as described with Doxil®. In my opinion, for a given drug-loaded nanoformulation, each of the side-effects attributed to the free drugs should be measured with the LNC formulation, in addition to general clinical condition monitoring and weight. It could be more complex for investigational new drugs with unknown toxicity patterns, such as JQ1 or ACF. LNC-PTX toxicity evaluation has been performed previously with another LNC formulation, demonstrating no acute or subacute toxicity after up to 48 mg/kg of PTX[22]. Such a study is important to optimize the drug schedule and doses, to maximize its efficacy.

Complete preclinical toxicity studies need true expertise and are often entrusted to contracted research organizations. Once an LNC formulation would have demonstrated sufficient benefits, it would be an important step before first-in-human.

II.4. LNCs EFFICACY

Even though many studies have addressed LNC characterization, few data have been collected concerning the *in vivo* antitumor efficacy of i.v. administered of LNC formulations. We have gathered the published results and our studies, all with s.c. tumors or in the mammary fat pad:

- LNC-PTX induced
  - An initial mean tumor regression of 50% in 6/9 mice and a 9-days longer median survival time (vs 25% in 3/9 mice and 5 days with Taxol) in mice bearing a 100 mm^3 NCI-H460 large cell lung tumor at daily 12 mg/kg during 5 days[22];

  - A 5-days (57%) growth delay vs control or Taxol at day 18 in rats bearing a 200 mm³ 9L glioma isograft of tumor resistant to PTX after 3 weekly treatments of LNC(NH2)- PTX at 5 mg/kg[14];
- LNC-ACF induced a 2-days (39%) growth delay vs control (1-day and 22% for daily free ACF) at day 12 in mice bearing an unpalpable orthotopic 4T1 breast tumor after 2 weekly injections at 5 mg/kg7.
- LNC-ACF and LNC-PTX induced a 3-days (43%) growth delay vs control (1-day and 17% for LNC-PTX only) at day 12 in mice bearing a 55 mm³ CT26 colon tumor after 4 injections at 7.5 mg/kg of both PTX and ACF every three days.
- LNC-SN38 and LNC-Regorafenib induced a 12-days (80% growth delay at day 13) longer median survival time vs control (4-days longer and 34% for free SN-38) in mice bearing a 25 mm³ CT26 colon tumor after 3 weekly cycles of two injections at 1 mg/kg SN38 and 10 mg/kg regorafenib[25].
- LNC-JQ1 induced an 8-days (58% growth delay at day 12) longer median survival time vs control (5.5-days longer and 55% for free JQ1) in mice bearing a 30 mm³ CT26 colon tumor after daily injections at 25 mg/kg until endpoint

If we look honestly to the results, i.v. administered drug-loaded LNCs did not outperform free drugs (when data is available), with the only exception of PTX, for which LNC-PTX demonstrated efficacy in PTX-resistant cell lines due to P-gp inhibition. Tumor regression was obtained when a maximum tolerated dose was previously established, allowing the administration of a maximal dose. In all models, no long-term cures were obtained. Therefore there is a need for new strategies with new molecules or combinations if one would hope a translation of LNCs. It was one of the main objectives of my thesis with the targeting of the TME. But the gap of improving antitumor efficacy has not been bridged.

LNCs formulations may have a better future in alternative routes of administrations, such as oral or local routes. LNC-PTX has demonstrated equivalent efficacy after oral or i.v. administration, with the limit of a 5-times higher dose p.o.[14]. Orally-administered LNCs have also demonstrated impressive activity in peptide delivery for diabetis[26]. Finally, injectable lauroyl-gemcitabine loaded LNCs-based hydrogel for local treatment of resected glioblastoma has also demonstrated the interest of alternative strategies without i.v. administrations[27].

II.5. LNCs ACTIVE TARGETING

LNC-ACF and LNC-PTX have demonstrated antitumor activity in the spheroid model, but the LNC-PTX effect was not CAF-selective, and preliminary *in vivo* treatment showed low efficacy. The active targeting is currently challenged in the literature, but numerous preclinical assays have demonstrated an enhanced antitumor activity, including in our lab with RGD[28]. The grafting of a targeting part to LNCs has been previously described by two methods, i.e. post-insertion of DSPE-PEG or transacylation of the PEG moieties of solutol®[29–31].

The selection of FAP for CAF targeting has been validated since the first clinical trials using anti-FAP sibrotuzumab that was associated to a good biodistribution[32]. In addition, FAP+ CAFs have been recognized as potentially responsible for the immunosuppressive actions of CAFs, at least in breast cancer[33]. During this thesis, in order to graft anti-FAP targeting agent at the surface of the developed LNC, we aimed to i) validate the feasibility of the grafting method, ii) compare two ligands in term of grafting and efficacy (full-size antibody and single-chain variable fragment), and iii) establish a method of characterization of this grafting.

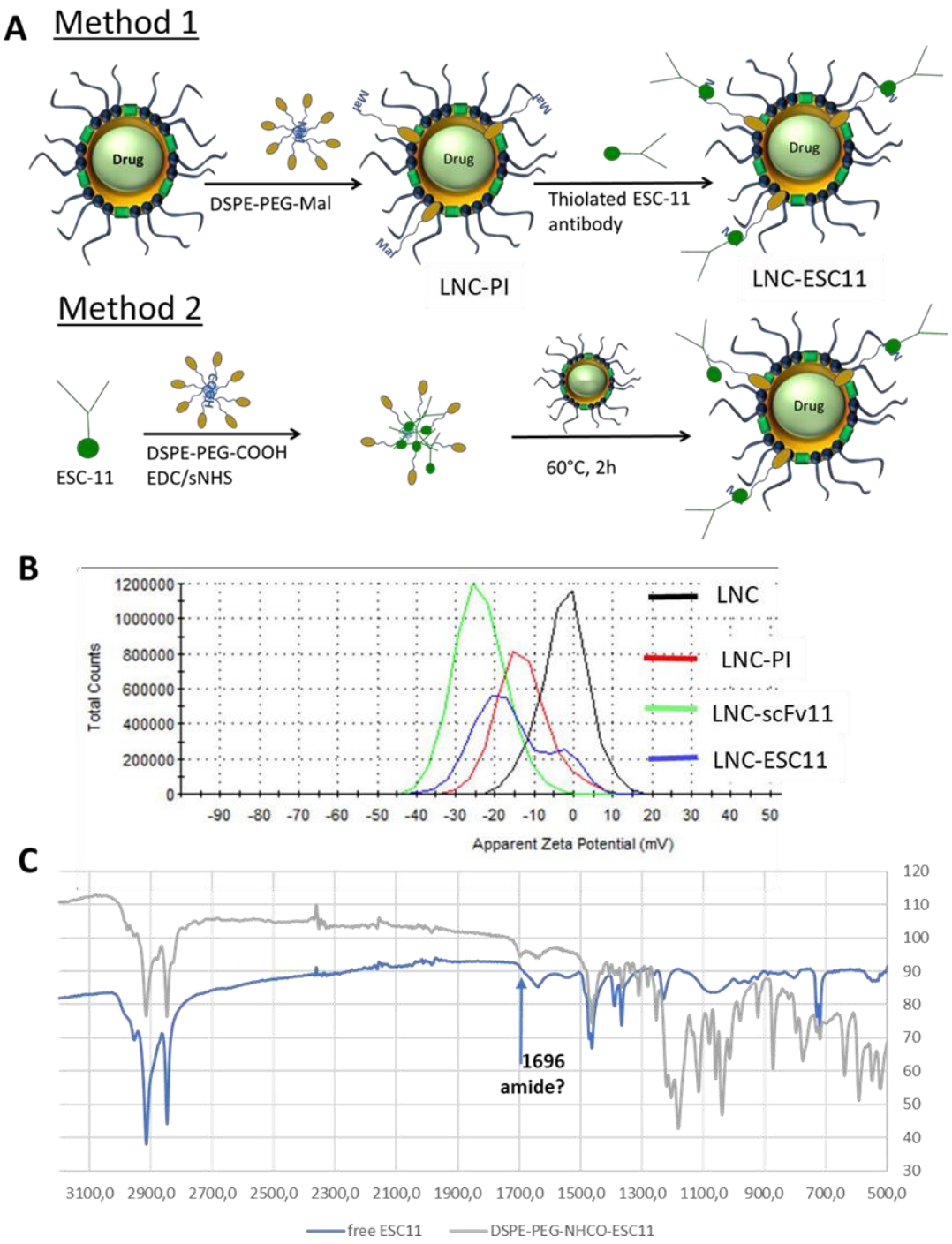

Figure 1. Post-insertions methods and characterization of the products. A) Scheme of the two grafting methods. B) ζ-potential of the formulation at the different steps (method 1). C) Infrared analysis of the coupling between ESC11 and DSPE-PEG-COOH (method 2). Mal: maleimide; EDC: 1-ethyl-3-(3-dimethylaminopropyl)carbodiimide;

Two targeting ligands were used for grafting, ESC11 and scFv11. The anti-FAP antibody ESC11 was developed by the Olivia Newton-John cancer research Institute of Melbourne as an improved version of the F19 antibody[34]. Free ESC11 aliquots were kindly provided by Dr Andrew Scott. ScFv11 was produced by Technophage SA (Lisbon, Portugal) and provided in a collaboration. ScFv11 shared the variable fragments with ESC11 and the protein sequence was modified to express a terminal cysteine and a His-tag. Two coupling methods have been investigated (Figure 1A). In method 1, DSPE-PEG-Maleimide was post-inserted into LNCs, then coupled with a thiolated ligand. In method 2, DSPE-PEG-COOH was coupled to the ligand, then the product was post-inserted. In both cases, unbound ligands were removed by dialysis.

The physical characterization of the product was performed using several methodologies. Post-inserted and coupled LNCs were compared to the original formulation by using size and ζ-potential. We observed a non-significant increase of the size (data not shown), and a large reduction of the ζ-potential toward negative values during post-insertion and coupling (method 1, Figure 1B). However, this shift was mostly due to the reaction media, as controls without the targeting ligands also induced some negative shift. For method 2, the coupling product between ESC11 and DSPE-PEG-COOH was dialyzed and analyzed by infrared spectrometry. The coupling was probably validated by the appearance of a band at 1696 cm^{-1}, in the range of amide bond (Figure 1C).

The FAP-targeting LNCs were also biologically characterized for their activity. The evaluation of CT5.3hTERT cell uptake by confocal microscopy was reproduced twice. The first experiment showed the presence of signal clusters only in control LNCs, whereas the second one was associated to an homogeneous staining with each condition (Figure 2A). FACS allowed us to follow the cell uptake over time. There was a time-dependent uptake that was not enhanced by the grafted ligand (Figure 2B). Finally, cocultured spheroids were exposed to ESC11-grafted LNCs, and the growth inhibition was slightly lower with targeted LNCs vs the non-targeted control (Figure 2C). Taken together, these results gave a clear tendency of reduced cellular uptake of FAP-targeting LNCs. The hypothesis to explain this reduced effect could be a loss of cargo during grafting and purification or a change in the ζ- potential that could reduce the interactions with the cell membrane. The characterization was not enough advanced to quantify the ligand at the surface or to check if it kept its whole integrity.

In perspective, LNCs are facing the same challenges for cell targeting than the whole nanomedicine field (cf Introduction-V.5). To allow potential translation of targeted NPs, a detailed characterization of both the physicochemical properties after ligand grafting and the targeting ability with adapted *in vitro* and *in vivo* models is required. For instance, the *in vitro* study of targeting

with different serum concentrations would indicate potential behavior over the blood stream[11]. In our case, the different targeting evaluations demonstrated that there were issues with the nanocarrier itself. Another approach to improve targeting would be the bioinspiration from physiological targeting with extracellular vesicles, containing multiple transmembrane proteins such as tetraspanins, able to finely tune the cell-targeting properties[12].

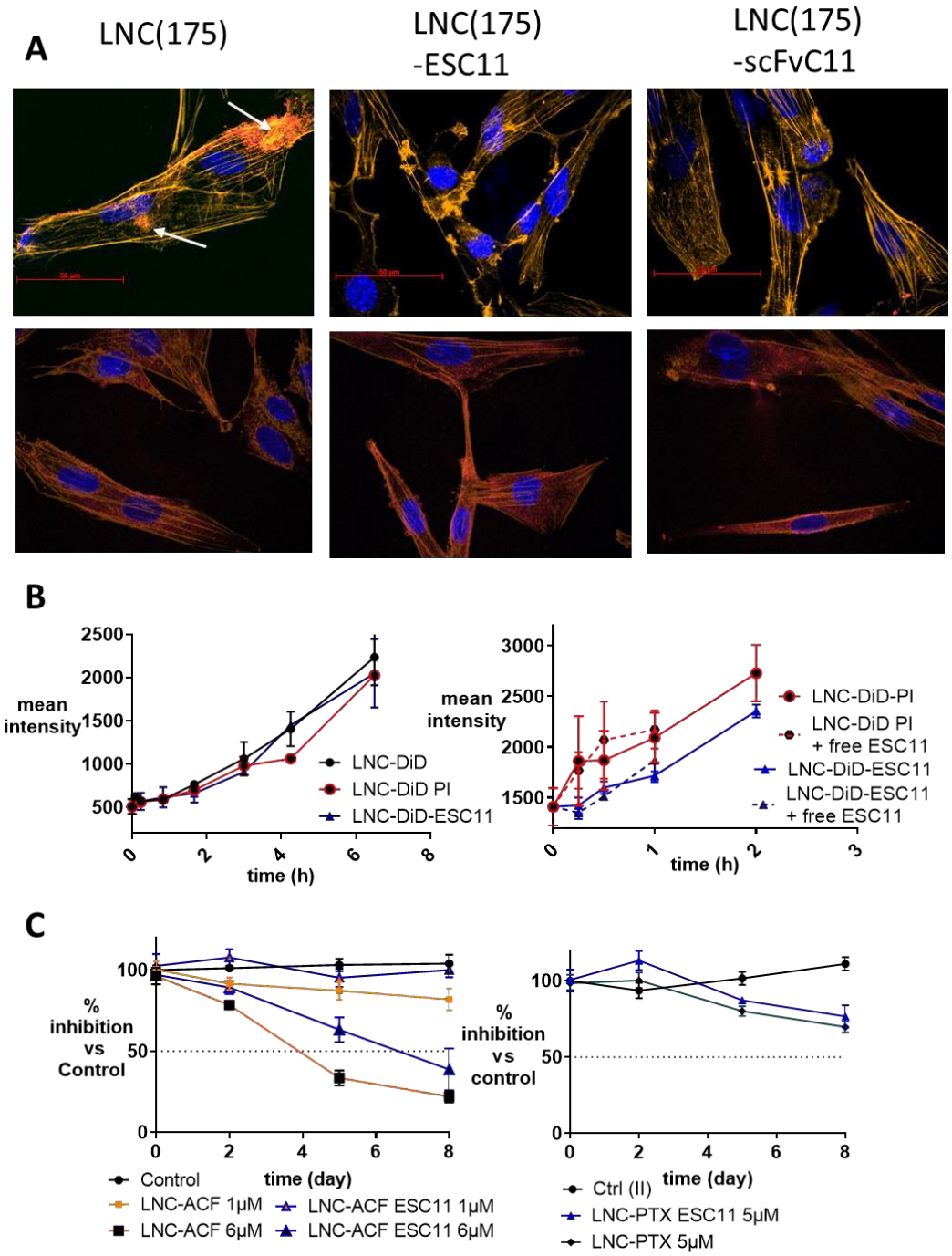

Figure 2. Biological characterization of FAP-targeting LNCs. A) Confocal microscopy of CT5.3hTERT cell uptake after 1h incubation, using 175nm LNCs (to increase the fluorescence signal) with or without targeting agent (method 1). Yellow: phalloidin; red: LNC-DiD, blue: DAPI. The two pictures for each condition are from two experiments. B) CT5.3hTERT cell uptake of ESC11-grafted LNC-DiD (method 2). Each graph represents a single experiment (n=3 replicates). The right graph includes conditions with free ESC11. C) Cocultured spheroid inhibition by ESC11-grafted ACF or PTX-loaded LNCs (method 2) (n=6) replicates).

II.6. LONG-TERM PERSPECTIVE: LNCS INDUSTRIALIZATION & COST

On a long-term perspective, if one succeeds to formulate improved LNC with better antitumor efficacy, the potential translation of LNC would begin. And as explained previously, a lot of works has already been performed to prepare the scale-up process and long-term stability, limiting its potential cost[35–37]. The critical parameters of the LNC PIT process are temperature control over time and space, i.e. warming, cooling, and temperature homogenization. The viscosity of LNC formulation during the PIT process depends on the selected lipids. At 50-80°C, it would be low enough to allow low-energy stirring. Depending on the strategy, for any batch volume, LNC formulation could be performed in one-pot or two-pot for the last dilution, as selected in the published scale-up pilot[35]. The major issue would be storage capacity. During this thesis, the colloidal LNC dispersions have been used for two to four weeks at 4°C. Beyond this period, the main stability issue encountered during this thesis was micro-organism contaminations caused by the process and especially multiple samples, which were not performed in aseptic conditions, and the lack of preservatives in the formulation. An aseptic LNC preparation has been validated by a colleague without further modifications of the PIT process. Then, another stability issue was drug precipitation. Stability studies at different drug loadings and lipids should be performed to find the best consensus between drug loading and stability. Once these two issues would be solved, LNCs would probably be stable at least 18 months at 6°C, as described in the LNC first study[9]. The cost of nanocarriers is often considered too expensive for the low improvements offered[38]. LNC formulation may have a probably higher cost than a comparable free drug, but its simple manufacture would maintain the production cost at a minimal value. Finally, its potential use as a platform for multiple drugs or sizes could allow sharing the development costs between several drug products.

III. DISCUSSION ON THE STROMAL TARGETING STRATEGY

As described in the introduction, plenty of anti-CAF strategies have been developed[39]. Among then, FAP targeting, CAF depletion, inhibition of CAF activation or functions have all shown preclinical efficacy. Even if CAF reprogramming or targeted inhibition of some CAFs functions are becoming more popular, there is currently no evidence of the negative impact of whole CAF inhibition in desmoplastic CRC, contrary to PDAC. For this reason, we have screened anti-CAF molecules, tested them in cocultured spheroids, and preliminary in an animal model. In this section, we will discuss the results of the thesis with the current CAF therapy field, before proposing a program to succeed in the clinical translation of such therapies.

III.1. DRUG SCREENING

To discover anti-CAF properties of already investigated molecules, we have developed a drug screening assay with two primary outcomes: the 50% viability molar concentration (IC_{50}) at 48 h against CT5.3hTERT, and the relative IC_{50} vs cancer cell lines CT26 and HCT116. The absolute IC_{50} went from 1.1 to 15 μM. The CAF over tumor cell IC_{50} ratios went from 0.61 to 22. These two values were sufficient to observe different profiles, such as the cytotoxic compounds, much more active on cancer cell (e.g. PTX, SN38), the FGFR/VEGFR/PDGFR kinase inhibitors (sunitinib, nintedanib), which were less active in the tested conditions, and acriflavine, combining potency with a low IC_{50} and selectivity with the best IC_{50} ratio. This particular profile of acriflavine was further confirmed by the 3D model.

The methodology of drug screening has a major impact on the obtained results. Indeed, cell viability assays often face poor inter-experimentation reproducibility. A number of biological (cell line, medium composition and volume, seeding density) and technical (edge effect, drug type, dose, storage, treatment time, assay duration time, and dose-response metric) factors have been confirmed to interfere with the quality of the results and reproducibility by a recent paper[40]. With a final mean SEM/IC_{50} ratio at 42% for all the drug tested, there was a quite high variation between our reproductions of the viability experiments. In my opinion, it mainly came from IC_{50} dependence on the cell growth rate. Thus, the percentage of confluence, passage number, and time since the last passage drastically influence this proliferation speed, even though they cannot be kept identical over the experiment repeats. In the three laboratories where I performed viability assays, the technical parameters were different, including cell culture automation in one case, removing the possibility of experimenter variation, and biological variation remained high.

Though the variability was high, the comparison remained still valid as most of the drugs were tested in parallel within the same experiments, showing real sensitivity differences.

The selected cell viability assay method was aspecific of action, as cristal violet counts DNA content. Therefore, it did not inform on molecule mechanisms but allowed standard comparison between molecules from various therapeutic classes. The IC_{50} (50% of the cell quantity compared to the control condition) metric choice vs EC_{50} (50% of the Emax of the experiment), GI_{50} (50% less cell growth than the control, compared to a reference point before treatment), or AUC (area under the dose-response curve) is not neutral. EC_{50} and GI_{50} are recognized as less sensitive to the differences in cellular division rates (biological variation)[41]. But EC_{50} is not adapted to various compounds that could have different E_{max}. And GI_{50} was tested but its set up was not satisfactory.

Another recent study performed high-throughput screening (HTS) of sixty-five different drugs on nine primary CAF cell lines[42]. Their outcome was AUC, and they identified bortezomib, carfilzomib, and panobinostat as CAF inhibitors. Like us, they found oxaliplatin, IRI, and 5-FU as low CAF inhibitors. It highlighted one limit of our assay, which is the single cell line used to model CAF. CT5.3hTERT, established and kindly provided by Pr O. De Wever, was derived from a colorectal adenocarcinoma resection specimen, but we don't know if the tumor was particularly desmoplastic, or if the patient was pretreated by neoadjuvant therapy, for instance[43]. Immortalization allowed using the same cell line for all experiments, which is beneficial, but some authors raised the point of the CAF features stability over immortalization and passages[44]. The heterogeneity of CAF has been raised in the introduction[45,46], and the validity of acriflavine inhibition of CAF should be validated on other primary CAFs.

III.2. 3D MODELS FOR DRUG TESTING

Cells cultured on a flat plastic surface have allowed the expansion of the cell biology field. However, the 2D-cultured cells have shown properties that are not reproduced during 3D-culture[47]. Indeed, the tissue stiffness, the physical and chemical environment constituted by the ECM, and the network of homo and heterocellular interactions modulate cell behavior and response to stimuli, including drug response[48]. This is even more important for CAF than other cell types. In the investigation on CAFs, various 3D cocultured models have taken great importance to study CAF-tumor cell interactions and their response to anticancer agents[49]. Compared to animal models, 3D co-cultures offer better control of the CAF content, higher throughput to test multiple conditions, and the possibility to follow by microscopy multiple features. We collaborated with the laboratory from Pr O. Feron to work with a cocultured spheroid constituted from a mix of CT5.3hTERT and

HCT116, at an optimized ratio of 1:1, which allowed keeping visible CAF clusters until the end of the experiment.

With this model, we have observed the effect of ACF and PTX at micromolar concentration. It allowed us to distinguish the effect produced by the two molecules. ACF effect depended on its concentration. While at 1 μM ACF slowed down spheroid growth and killed almost exclusively CAFs, at 3 μM the inhibition was less specific and induced spheroid regression. In a range of concentrations, PTX killed both cell populations and induced a spheroid regression until complete disaggregation. Surprisingly, the cocultured spheroid was 10-15% more sensitive for every condition compared to the simple spheroid without CAF. As CAF presence increased the spheroid growth rate from 15-20%, it could explain this increased sensitivity. In the literature, CAF presence is more often associated to increased drug resistance[50,51]. We could postulate that the selected drugs, due to their CAF inhibition, exert more effect on the co-culture. But the lack of difference between PTX and ACF on this over-inhibition and the lack of control with standard chemotherapy prevent to draw more conclusions.

Spheroids are considered as interesting models to evaluate NPs penetration and accumulation into tumors[52]. Nevertheless, we did not observe changes in the spheroid sensitivity with LNC nanoencapsulation. ACF being fluorescent, we have observed its uniform distribution across spheroid cells. But ACF has a strong burst release from LNCs, and its dispersion is not likely to represent the LNC one. The use of LNC-DiR would be a good option to follow by fluorescence the spheroid cell uptake of LNCs. The stroma has been described to form a barrier between the blood vessels and the tumor cells[53]. In our model, CAFs localize at the center of the spheroid, which does not mimic this stromal barrier effect of desmoplastic tumors.

The 3D model could be further improved to fill the remaining gap until the animal model. New and more robust information on spheroids and treatment interactions would have been provided by a 3D imaging of the spheroids by light-sheet microscopy, as it was performed on untreated spheroids. To validate the ACF specific profile, the experiment should be reproduced with other spheroids with a different genetic profile. There are fewer examples of the use of multiple CAF cell lines to evaluate drugs in 3D models than multiple cancer cell lines and a single CAF[51,54]. From one example where primary CAF from different tissue origins where tested, the sensitivity to several inhibitors were variable[48]. The question of the heterogeneity of CAFs between patients in the same cancer localization is not solved. Otherwise, the possibility of expanding personalized 3D patient-derived models is attractive and has already demonstrated good prognostic values, even with the use of primary CAF from another patient[51]. It will require higher throughput of spheroid production

with homogeneity, but many efforts are going to pay back in this field[48,55,56]. Finally, the cocultured spheroid could be more complex by the addition of other TME populations like endothelial or immune cells[54,57], increasing the time of culture, or study spheroid regrowth after treatment[52,58].

III.3. THE CT26 ANIMAL MODEL FOR TME INVESTIGATION

Despite the increased complexity of *in vitro* models, including 3D modalities, animal experiments remain crucial for testing anticancer therapy. In the domain of CRC, several alternatives exist: the syngeneic CT26 and MC38 models, human-derived cell lines including HCT116, HT29, and Hutu80 in immunocompromised mice, and genetically engineered mouse models[59].

The CT26 cell line implanted on Balb/c mice has been the main model used in this thesis. CT26 cell line was obtained from a carcinoma induced by mouse exposition to N-nitroso-N-methylurethane[60]. Among the canonical CRC mutations, CT26 is $KRAS^{MUT}$ and $Tp53^{WT}$ or APC^{WT}. Due to N-nitroso-N-methylurethane carcinogen, CT26 presents a mutational load 10 times superior to the median CRC, with a high number of tumor antigens[61]. Immune infiltration in CT26 tumors was described as rich, with numerous NK cells, with a global high cytolytic activity[61]. Finally, CT26 was considered having a mesenchymal-like phenotype, with vimentin expression and no E-cadherin. In our analysis of immune infiltration, the infiltrate was found as rich in MDSCs, macrophages, and lymphocytes, but no NKs were stained.

Several studies have used CT26-bearing mice to target CAF, all using FAP-associated strategies. The results of these studies are contrasted. First of all, the level of FAP in the s.c. tumor is variable, when measured by qPCR or by IHC[62–65]. FAP enzymatic activity inhibition by PT-100 or PT-630 induced CT26 tumor to slow down, affected the ECM, the angiogenesis, and the sensitivity to chemotherapy such as Oxaliplatin[64,65]. FAP DNA vaccine induced anti-tumor efficacy at various degrees in three independent studies[62,66,67]. A whole CT26-tumor vaccine therapeutic efficacy was increased by using FAP-transfected CT26 cells[68]. Therefore, these studies suggested an important role of FAP and FAP^{+}cells. The only warning came from a single study with anti-FAP CAR-T cells that showed no expression of FAP by CT26 tumors, no efficacy of the CAR-T cell therapy, and strong toxicity due to FAP expression by bone marrow MSCs. Since several tumor models presented the same response, it suggests that the designed CAR-T was probably not FAP specific[63]. These studies brought enough evidence to select the CT26 tumor model as a FAP positive tumor sensitive to anti-CAF treatment. In addition, the choice of this syngeneic and thus immunocompetent model allows the study of the immune effect of CAFs. Indeed, immune T cells

inhibition by CAFs has been demonstrated in the literature and CAF inhibition is potentially able to increase their action[69,70]. In CT26, this hypothesis has been confirmed by CT26 isolated FAP$^+$ CAF having the capacity of inhibiting anti-PD-1 therapy by immunosuppression effect[71].

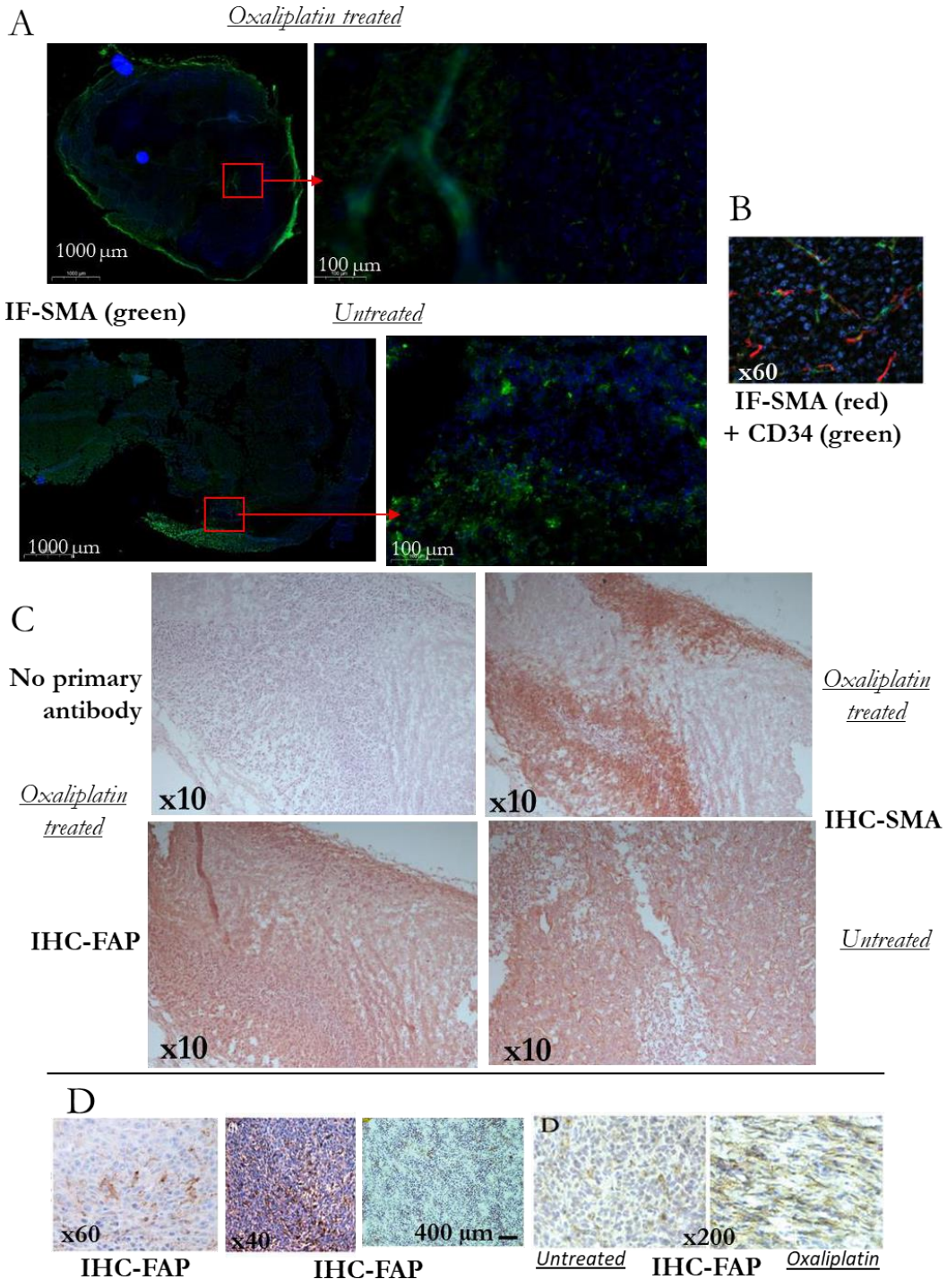

Figure 3. Immunostaining on s.c. CRC CT26 tumors. (A & C) CT26-bearing mice were treated or not with i.p. oxaliplatin at 5 mg/kg, 3/week, for two weeks. A) Two magnifications after SMA immunofluorescence. At low magnification, the tumor is split between highly and scarcely stained areas. The high magnification is selected at the transition between the two areas. C) Three immunostaining conditions (control, SMA, FAP) of the same oxaliplatin- treated tumor, and an SMA-stained untreated tumor. (B & D) Pictures from the literature [63–65,67].

We intended to understand the evolution of CAF presence in CT26 tumors. We used FACS and immunohistochemistry, and tried to affect CAF by treating tumors with oxaliplatin, or by developing orthotopic tumors. Histology staining of FAP demonstrated aspecific spread staining, different from the punctual FAP staining described in the literature (Figure 3). SMA staining was a mix of highly stained areas and areas with dispersed stained cells. These immunostainings were heterogeneous, and the intended quantification of SMA was not enough precise. Another approach was the single-cell analysis from the digested tumors by FACS. Using ESC11 anti-FAP antibody, SMA, or PDGFRβ, it was not possible to isolate a stromal population from CT26. Interestingly, CAFs analysis by FACS is not frequently described, there are very few commercially available antibodies, and only one paper described the isolation of CT26 CAF by FACS, using PDGFRα antibody[71]. It could rely on the heterogeneity of surface markers expressed by CAFs.

Two main and compatible hypothesis could explain the remaining gap of CT26 CAF quantification. The CT26 tumors could have low infiltration of CAFs, as suggested by the low FAP immunostaining and the absence of a defined stroma, due to the rapid growth of CT26 cells as a bulk tumor. Or CT26 cells could express at some level CAF markers in vivo, as they have demonstrated vimentin expression, causing our spread and not cell-specific staining.

Other *in vivo* modalities than subcutaneous injection of CT26 cells do exist. Orthotopic injections of CT26 cells in the caecum have been realized during my thesis. The microenvironment should be more relevant in this case. But two drawbacks have limited its use: first, the laparotomy needed to access to the caecum is responsible for an increased inflammation that must have an impact on the TME. Orthotopic establishment by endoscopy-guided microinjection has been described to solve this issue[13]. Then the tumor progression followed by bioluminescence remains less precise than subcutaneous manual measurements, making its use for therapeutical evaluation inconvenient. Another CT26-based model is their injection in FAP-KO mice[14]. It could provide adapted negative control for FAP or CAF directed therapies, but does not represent the clinical situation or does not help to characterize TME.

Better in vivo models including CAFs have been described and should be used instead of CT26. We can cite co-implantation models, injecting primary CAFs with tumor cells, mostly in nude mice, or patient-derived xenograft, including CAF from the initial samples, mostly in SCID mice. Nude and SCID mice are two immunodeficient mice, lacking respectively T or B+T lymphocytes, practical for human xenografts[72]. However, the lack of an adaptive immune system altered an important aspect of CAF functions, reducing the translation of therapeutic assays. Genetically engineered mouse models, with the full recapitulation of tumor development, do not have this

disadvantage. In colon cancer, they are not frequently used for CAF study due to their complex setup. But the already described LAKTP model (Lgr5e$^{GFP\text{-}creERT2}$, Apc$^{fl/fl}$, Kras$^{LSL\text{-}G12D}$, Tgfbr2$^{fl/fl}$, and Trp53$^{fl/fl}$)[73], the Apc$^{2lox14/+}$ Kras$^{LSL\text{-}G12D}$ Fabpl-Cre adenocarcinoma model, or the Villin-Cre/ Msh2^{LoxP} model[74] should be further evaluated for their stroma, to allow their use for stromal targeting.

III.4. LONG-TERM PERSPECTIVE: A STEP-BY-STEP PROGRAM TOWARDS THE APPROVAL OF STROMAL COMPARTMENT TARGETING STRATEGIES

The stromal strategies to treat solid cancer are at a turning point. Several reviews have highlighted the multiplication of strategies with very promising preclinical proofs-of-concept, while the first clinical trials have been at some point disappointing, with even detrimental effects of stroma ablation in PDAC[39,75–77]. The following section has the ambition to propose some steps necessary to go towards the potential approval of stromal therapies (Figure 4).

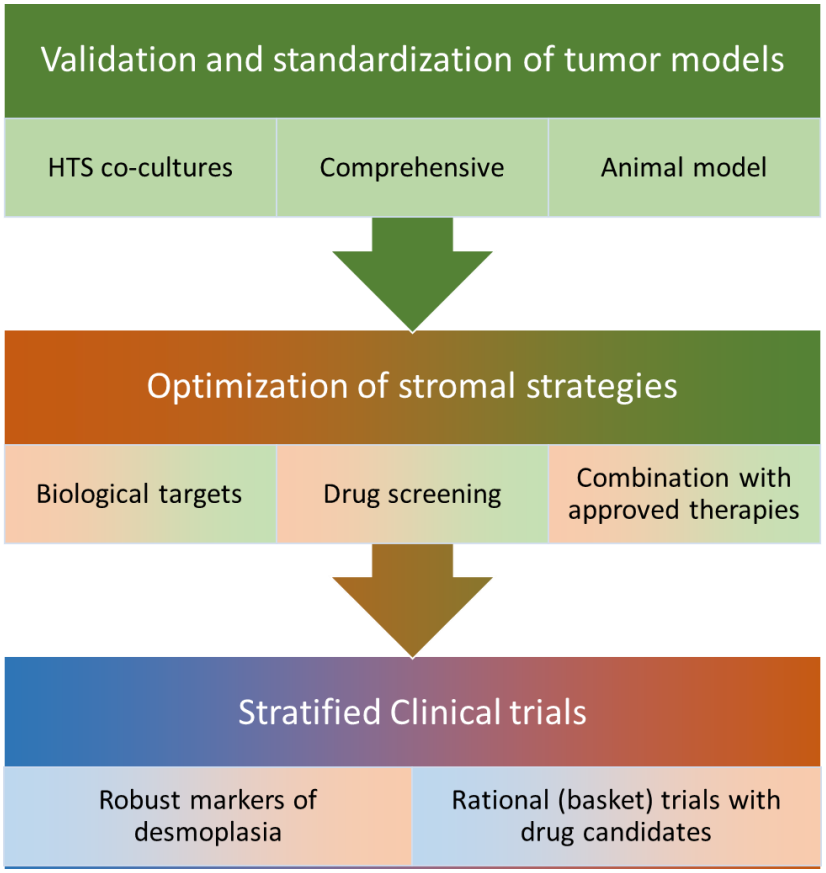

Figure 4. 3 steps towards clinical use of optimized anti-stromal therapies. The different actors are explicated by the colors academic, industry, hospital

III.4.1. Standardization of anti-CAF drug testing

As described previously, models to test anti-stromal therapies are not lacking but suffer from being not validated. The diversity of *in vitro* and *in vivo* models is very high, with frequent co-development of the model and the therapeutic. It complicates the comparison between the different strategies. In the case of this thesis, the time has been divided between the development of both, which has slowed down the potential advancements. Therefore, in accordance with several recent calls to better characterize primary CAF material and to better understand their heterogeneity[44,78], more efforts should be put on the validation of representative models of desmoplastic tumors. Such work has been already initiated with pancreatic desmoplasia but is still lacking in other cancers[79]. The development and most importantly the validation of these models would ideally be performed by an open consortium including mostly academic partners.

In vitro models should use co-cultured 3D models with CAFs. Immortalized well-characterized CAFs should be preferred, if they demonstrate their equivalence with primary CAFs, especially for their response to treatment. At default, a precise methodology for CAF isolation and characterization should be established, allowing quality controls for CAFs collected by each team.

The models should include an HTS modality to test chemical libraries and optimized series on representative desmoplastic cancer cell lines. In addition, more complex models should let access to the respective mechanism of action on CAF, cancer cells, and their dialog. Specific models to assess CAF interaction with immune infiltrated cells and angiogenesis could be added.

In vivo animal models are mandatory to assess benefit/risk ratio and dose-effect PK/PD relationship. In the case of desmoplastic tumors, a single model of at least pancreatic, breast, colorectal, and lung cancer should be included. More rare cancers presenting desmoplastic properties, such as bladder, melanoma, or cholangiocarcinoma, could be added. In my opinion, existing or new genetically engineered mouse models would offer a compromise between high reproducibility and natural TME. But the management of therapeutic experiments is tricky as each animal develops a tumor at different time points. Validated medical imagery at a fixed frequency could help their enrollment for survival studies. Another possibility is the orthotopic or s.c. surgical implantation of tumor spheroids, or the CAF and cancer cell co-implantation. In each case, the time point of treatment initiation and the end-point should be fixed and related to clinical reality. The models should include the quantification of CAF presence and activity on the immune system and the ECM. Metastatic settings being the first cause of cancer mortality, it should be included in animal models. Finally, the translation capacity from selected *in vitro* to *in vivo* models must be validated.

III.4.2. Optimization of current stromal strategies

Even if basic research on new anti-stromal strategies has to continue, there are already numerous described biological targets. FAP, hyaluronic acid, vitamin D receptor, or SHH are some examples that have benefited from clinical trials. The potential of each target should be compared on the same standard models. Each strategy could determine its impact as monotherapy at early, advanced, and metastatic stages of the different cancer diseases. Based on these results, the industry would have robust data to go on drug development. The optimization of the lead compounds would be helped by *in vitro* HTS and validated animal models. At this step, the advantages brought by nanocarriers should be evaluated. The development of potential combination strategies of stromal therapies with standard or innovative cytotoxic chemotherapy, targeted inhibitors, immunotherapies, radiotherapy, cell or gene therapy, would also be paramount. Open and collaborative research from several industries and academic partners would finally give birth to a limited number of anti-stromal therapeutic strategies, with a clear view of their potential activity and on the conditions required to be effective.

III.4.3. Rational clinical trials

The anti-stromal therapy clinical trials have recently focused on PDAC. This is due to the major medical need in this pathology and the high percentage of desmoplasia, hiding an important heterogeneity in stroma density and SMA expression[80]. Therefore, all cancer types would benefit from a desmoplastic-dependant stratification to offer personalized anti-stromal therapies. Systematic studies should fill the remaining gaps about tumor classification, based on biopsy immunohistological staining of stromal markers like FAP, SMA, or PDGFRα/β, together with collagen or other ECM parameters, as performed in numerous publications[33,71,81–83]. The ongoing generalization of gene-based analysis should complete this classification, only if it is applicable for patient stratification in hospital clinical trial routine. The future clinical trial designs should match the drug candidate profile determined by validated preclinical assays with patient stroma characteristics. Based on this knowledge, patient inclusion and candidate drug indication should be proposed. It could potentially include different cancer diseases, with a common stromal phenotype, joining the current trend of oncology basket trials and indications.

IV. REFERENCES

1. Park, K. The drug delivery field at the inflection point: Time to fight its way out of the egg. *J. Control. Release* **267**, 2–14 (2017).
2. Lagarce, F. Nanomedicines: promises and reality. *Drug Discov. Today* **00**, 1–2 (2020).
3. Bisso, S. & Leroux, J.-C. Nanopharmaceuticals: A focus on their clinical translatability. *Int. J. Pharm.* **578**, 119098 (2020).
4. Huynh, N. T., Passirani, C., Saulnier, P. & Benoit, J. P. Lipid nanocapsules: A new platform for nanomedicine. *Int. J. Pharm.* **379**, 201–209 (2009).
5. Becht, E. *et al.* Immune and stromal classification of Colorectal cancer is associated with molecular subtypes and relevant for precision immunotherapy. *Clin. Cancer Res.* **22**, 4057– 4066 (2016).
6. Guinney, J. *et al.* The consensus molecular subtypes of colorectal cancer. *Nat. Med.* **21**, 1350– 1356 (2015).
7. Montigaud, Y. *et al.* Optimized acriflavine-loaded lipid nanocapsules as a safe and effective delivery system to treat breast cancer. *Int. J. Pharm.* **551**, 322–328 (2018).
8. Bastiancich, C. *et al.* Drug combination using an injectable nanomedicine hydrogel for glioblastoma treatment. *Int. J. Pharm.* **559**, 220–227 (2019).
9. Heurtault, B., Saulnier, P., Pech, B., Proust, J. E. & Benoit, J. P. A novel phase inversion- based process for the preparation of lipid nanocarriers. *Pharm. Res.* **19**, 875–880 (2002).
10. Tran, S., DeGiovanni, P.-J., Piel, B. & Rai, P. Cancer nanomedicine: a review of recent success in drug delivery. *Clin. Transl. Med.* **6**, 44 (2017).
11. Ventola, C. L. Progress in nanomedicine: Approved and investigational nanodrugs. *P T* **42**, 742–755 (2017).
12. Pillai, G. Nanotechnology toward treating cancer: a comprehensive review. in *Applications of Targeted Nano Drugs and Delivery Systems* (eds. Shyam Ranjan, M. S., Dasgupta, N., Kumar, R. & Thomas, S.) 221 (Elsevier, 2019). doi:10.1016/C2017-0-00274-4
13. Working, P. K. *et al.* Pharmacokinetics, Biodistribution and Therapeutic Efficacy of Doxorubicin Encapsulated in Stealth® Liposomes (Doxil®). *J. Liposome Res.* **4**, 667–687 (1994).
14. Groo, A. C. *et al.* In vivo evaluation of paclitaxel-loaded lipid nanocapsules after intravenous and oral administration on resistant tumor. *Nanomedicine* **10**, 589–601 (2015).
15. Briot, T. *et al.* Di-O-lauroyl-decitabine-lipid nanocapsules: Toward extending decitabine activity. *Int. J. Nanomedicine* **14**, 2091–2102 (2019).
16. Lacoeuille, F. *et al.* In vivo evaluation of lipid nanocapsules as a promising colloidal carrier for paclitaxel. *Int. J. Pharm.* **344**, 143–149 (2007).
17. Lainé, A. L. *et al.* Conventional versus stealth lipid nanoparticles: Formulation and in vivo fate prediction through FRET monitoring. *J. Control. Release* **188**, 1–8 (2014).
18. Gener, P. *et al.* Zileuton^{TM} loaded in polymer micelles effectively reduce breast cancer circulating tumor cells and intratumoral cancer stem cells. *Nanomedicine Nanotechnology, Biol. Med.* **24**, 102106 (2020).

19. Meng, F., Wang, J., Ping, Q. & Yeo, Y. Quantitative Assessment of Nanoparticle Biodistribution by Fluorescence Imaging, Revisited. *ACS Nano* **12**, 6458–6468 (2018).

20. Wilhelm, S. *et al.* Analysis of nanoparticle delivery to tumours. *Nat. Rev. Mater.* **1**, 16014 (2016).

21. Le Roux, G. *et al.* Cytotoxicity and genotoxicity of lipid nanocapsules. *Toxicol. Vitr.* **41**, 189– 199 (2017).

22. Hureaux, J. *et al.* Toxicological study and efficacy of blank and paclitaxel-loaded lipid nanocapsules after i.v. administration in mice. *Pharm. Res.* **27**, 421–430 (2010).

23. Garcion, E. *et al.* A new generation of anticancer, drug-loaded, colloidal vectors reverses multidrug resistance in glioma and reduces tumor progression in rats. *Mol. Cancer Ther.* **5**, 1710–1722 (2006).

24. Czajkowska-Kośnik, A., Wolska, E., Chorazewicz, J. & Sznitowska, M. Comparison of cytotoxicity in vitro and irritation in vivo for aqueous and oily solutions of surfactants. *Drug Dev. Ind. Pharm.* **41**, 1232–1236 (2015).

25. Tsakiris, N. *et al.* Combinational drug-loaded lipid nanocapsules for the treatment of cancer. *Int. J. Pharm.* **569**, 118588 (2019).

26. Xu, Y. *et al.* Novel strategy for oral peptide delivery in incretin-based diabetes treatment. *Gut* **69**, 911–919 (2020).

27. Bastiancich, C. *et al.* Injectable nanomedicine hydrogel for local chemotherapy of glioblastoma after surgical resection. *J. Control. Release* (2017). doi:10.1016/j.jconrel.2017.08.019

28. Danhier, F. *et al.* Tumor Targeting by RGD-Grafted PLGA-Based Nanotheranostics Loaded with Paclitaxel and Superparamagnetic Iron Oxides. in *Methods in Pharmacology and Toxicology* (ed. Press, H.) 1–17 (2015). doi:10.1007/7653_2015_43

29. Perrier, T. Modifications de nanocapsules lipidiques par des procédés post-formulation : {Elaboration} de vecteurs multifonctionnels de médicaments. (Angers, 2009).

30. Perrier, T., Saulnier, P., Fouchet, F., Lautram, N. & Benoît, J. P. Post-insertion into Lipid NanoCapsules (LNCs): From experimental aspects to mechanisms. *Int. J. Pharm.* **396**, 204– 209 (2010).

31. Bourseau-Guilmain, E. *et al.* Development and characterization of immuno-nanocarriers targeting the cancer stem cell marker AC133. *Int. J. Pharm.* **423**, 93–101 (2012).

32. Welt, S. *et al.* Antibody targeting in metastatic colon cancer: a phase I study of monoclonal antibody F19 against a cell-surface protein of reactive tumor stromal fibroblasts. *J. Clin. Oncol.* **12**, 1193–1203 (1994).

33. Costa, A. *et al.* Fibroblast Heterogeneity and Immunosuppressive Environment in Human Breast Cancer. *Cancer Cell* **33**, 463-479.e10 (2018).

34. Fischer, E. *et al.* Radioimmunotherapy of fibroblast activation protein positive tumors by rapidly internalizing antibodies. *Clin. Cancer Res.* **18**, 6208–6218 (2012).

35. Thomas, O. & Lagarce, F. Lipid Nanocapsules: A Nanocarrier Suitable for Scale-Up Process. *J. Drug Deliv. Sci. Technol.* **23**, 555–559 (2013).

36. Dulieu, C. & Bazile, D. Influence of lipid nanocapsules composition on their aptness to freeze-drying. *Pharm. Res.* **22**, 285–292 (2005).

37. Hureaux, J. *et al.* The adaptation of lipid nanocapsule formulations for blood administration in animals. *Int. J. Pharm.* **379**, 266–269 (2009).

38. Hua, S., de Matos, M. B. C., Metselaar, J. M. & Storm, G. Current trends and challenges in the clinical translation of nanoparticulate nanomedicines: Pathways for translational development and commercialization. *Front. Pharmacol.* **9**, 1–14 (2018).

39. Valkenburg, K. C., De Groot, A. E. & Pienta, K. J. Targeting the tumour stroma to improve cancer therapy. *Nature Reviews Clinical Oncology* **15**, (2018).

40. Larsson, P. *et al.* Optimization of cell viability assays to improve replicability and reproducibility of cancer drug sensitivity screens. *Sci. Rep.* **10**, 1–12 (2020).

41. Hafner, M., Niepel, M., Chung, M. & Sorger, P. K. Growth rate inhibition metrics correct for confounders in measuring sensitivity to cancer drugs. *Nat. Methods* **13**, 521–527 (2016).

42. Lee, H.-M. *et al.* Drug repurposing screening identifies bortezomib and panobinostat as drugs targeting cancer associated fibroblasts (CAFs) by synergistic induction of apoptosis. *Invest. New Drugs* **36**, 545–560 (2018).

43. De Vlieghere, E. *et al.* Tumor-environment biomimetics delay peritoneal metastasis formation by deceiving and redirecting disseminated cancer cells. *Biomaterials* **54**, 148–157 (2015).

44. Sahai, E. *et al.* A framework for advancing our understanding of cancer-associated fibroblasts. *Nat. Rev. Cancer* **20**, 174–186 (2020).

45. Ishii, G., Ochiai, A. & Neri, S. Phenotypic and functional heterogeneity of cancer-associated fibroblast within the tumor microenvironment. *Adv. Drug Deliv. Rev.* **99**, 186–196 (2016).

46. Bu, L. *et al.* Biological heterogeneity and versatility of cancer-associated fibroblasts in the tumor microenvironment. *Oncogene* **38**, (2019).

47. Shamir, E. R. & Ewald, A. J. Three-dimensional organotypic culture: experimental models of mammalian biology and disease. *Nat. Rev. Mol. Cell Biol.* **15**, 647–664 (2014).

48. Chitty, J. L. *et al.* The Mini-Organo: A rapid high-throughput 3D coculture organotypic assay for oncology screening and drug development. *Cancer Rep.* **3**, 1–15 (2020).

49. Langhans, S. A. Three-dimensional in vitro cell culture models in drug discovery and drug repositioning. *Front. Pharmacol.* **9**, (2018).

50. Lee, J., Shin, D. & Roh, J.-L. Development of an in vitro cell-sheet cancer model for chemotherapeutic screening. *Theranostics* **8**, 3964–3973 (2018).

51. Onion, D. *et al.* 3-Dimensional Patient-Derived Lung Cancer Assays Reveal Resistance To Standards-of-Care Promoted By Stromal Cells But Sensitivity To Histone Deacetylase Inhibitors. *Mol. Cancer Ther.* **15**, 753–763 (2016).

52. Millard, M. *et al.* Drug delivery to solid tumors: The predictive value of the multicellular tumor spheroid model for nanomedicine screening. *Int. J. Nanomedicine* **12**, 7993–8007 (2017).

53. Miao, L., Lin, C. M. & Huang, L. Stromal barriers and strategies for the delivery of nanomedicine to desmoplastic tumors. *J. Control. Release* **219**, 192–204 (2015).

54. Zoetemelk, M., Rausch, M., Colin, D. J., Dormond, O. & Nowak-Sliwinska, P. Short-term 3D culture systems of various complexity for treatment optimization of colorectal carcinoma. *Sci. Rep.* **9**, 1–14 (2019).

55. Sun, Q. *et al.* Microfluidic Formation of Coculture Tumor Spheroids with Stromal Cells As a Novel 3D Tumor Model for Drug Testing. *ACS Biomater. Sci. Eng.* **4**, 4425–4433 (2018).

56. Lee, J. M. *et al.* Generation of uniform-sized multicellular tumor spheroids using hydrogel microwells for advanced drug screening. *Sci. Rep.* **8**, 1–10 (2018).

57. Herter, S. *et al.* A novel three-dimensional heterotypic spheroid model for the assessment of the activity of cancer immunotherapy agents. *Cancer Immunol. Immunother.* **66**, 129–140 (2017).

58. Aw Yong, K. M., Li, Z., Merajver, S. D. & Fu, J. Tracking the tumor invasion front using long-term fluidic tumoroid culture. *Sci. Rep.* **7**, 10784 (2017).

59. Golovko, D., Kedrin, D., Yilmaz, Ö. H. & Roper, J. Colorectal cancer models for novel drug discovery. *Expert Opin. Drug Discov.* **10**, 1217–1229 (2015).

60. Castle, J. C. *et al.* Immunomic, genomic and transcriptomic characterization of CT26 colorectal carcinoma. *BMC Genomics* **15**, (2014).

61. Zhong, W. *et al.* Comparison of the molecular and cellular phenotypes of common mouse syngeneic models with human tumors. *BMC Genomics* **21**, 1–17 (2020).

62. Xia, Q. *et al.* Anti-tumor effects of DNA vaccine targeting human fibroblast activation protein α by producing specific immune responses and altering tumor microenvironment in the 4T1 murine breast cancer model. *Cancer Immunol. Immunother.* **65**, 613–624 (2016).

63. Tran, E. *et al.* Immune targeting of fibroblast activation protein triggers recognition of multipotent bone marrow stromal cells and cachexia. *J Exp Med* **210**, 1125–1135 (2013).

64. Santos, A. M., Jung, J., Aziz, N., Kissil, J. L. & Puré, E. Targeting fibroblast activation protein inhibits tumor stromagenesis and growth in mice. *J. Clin. Invest.* **119**, 3613–3625 (2009).

65. Li, M. *et al.* Targeting of cancer-associated fibroblasts enhances the efficacy of cancer chemotherapy by regulating the tumor microenvironment. *Mol. Med. Rep.* (2016). doi:10.3892/mmr.2016.4868

66. Loeffler, M., Krüger, J. A., Niethammer, A. G. & Reisfeld, R. A. Targeting tumor-associated fibroblasts improves cancer chemotherapy by increasing intratumoral drug uptake. *J. Clin. Invest.* **116**, 1955–1962 (2006).

67. Wen, Y. *et al.* Immunotherapy targeting fibroblast activation protein inhibits tumor growth and increases survival in a murine colon cancer model. *Cancer Sci.* **101**, 2325–2332 (2010).

68. Chen, M. *et al.* A whole-cell tumor vaccine modified to express fibroblast activation protein induces antitumor immunity against both tumor cells and cancer-associated fibroblasts. *Sci. Rep.* **5**, (2015).

69. Ziani, L., Chouaib, S. & Thiery, J. Alteration of the antitumor immune response by cancer- associated fibroblasts. *Front. Immunol.* **9**, Article 414 (2018).

70. Kraman, M. *et al.* Suppression of antitumor immunity by stromal cells expressing fibroblast activation protein-α. *Science (80-.).* **330**, 827–830 (2010).

71. Chen, L., Qiu, X., Wang, X. & He, J. FAP positive fibroblasts induce immune checkpoint blockade resistance in colorectal cancer via promoting immunosuppression. *Biochem. Biophys. Res. Commun.* **487**, 8–14 (2017).

72. Jin, K. *et al.* Patient-derived human tumour tissue xenografts in immunodeficient mice: A systematic review. *Clinical and Translational Oncology* (2010). doi:10.1007/s12094-010-0540-6

73. Tauriello, D. V. F. *et al.* TGFβ drives immune evasion in genetically reconstituted colon cancer metastasis. *Nature* **554**, 538–543 (2018).

74. Mcintyre, R. E., Buczacki, S. J. A., Arends, M. J. & Adams, D. J. Mouse models of colorectal cancer as preclinical models. *BioEssays* **37**, 909–920 (2015).

75. Chen, X. & Song, E. Turning foes to friends: targeting cancer-associated fibroblasts. *Nat. Rev. Drug Discov.* **18**, 99–115 (2019).

76. Gieniec, K. A., Butler, L. M., Worthley, D. L. & Woods, S. L. Cancer-associated fibroblasts—heroes or villains? *Br. J. Cancer* **121**, 293–302 (2019).

77. Han, X. *et al.* Emerging nanomedicines for anti-stromal therapy against desmoplastic tumors. *Biomaterials* **232**, 119745 (2020).

78. De Jaeghere, E. A., Denys, H. G. & De Wever, O. Fibroblasts Fuel Immune Escape in the Tumor Microenvironment. *Trends in Cancer* **5**, 704–723 (2019).

79. Suklabaidya, S. *et al.* Experimental models of pancreatic cancer desmoplasia. *Lab. Investig.* **98**, 27–40 (2018).

80. Wang, L. M. *et al.* The prognostic role of desmoplastic stroma in pancreatic ductal adenocarcinoma. *Oncotarget* **7**, 4183–4194 (2016).

81. Özdemir, B. C. *et al.* Depletion of carcinoma-associated fibroblasts and fibrosis induces immunosuppression and accelerates pancreas cancer with reduced survival. *Cancer Cell* **25**, 719–734 (2014).

82. Duperret, E. K. *et al.* Alteration of the tumor stroma using a consensus DNA vaccine targeting Fibroblast Activation Protein (FAP) synergizes with antitumor vaccine therapy in Mice. *Clin. Cancer Res.* **24**, 1190–1201 (2018).

83. Kwak, Y. *et al.* The clinical implication of cancer-associated microvasculature and fibroblast in advanced colorectal cancer patients with synchronous or metachronous metastases. *PLoS One* **9**, 1–8 (2014).